

**Late Quaternary climate variability from western
Mediterranean lake archives by multi-proxy data**

Von der Fakultät für Georessourcen und Materialtechnik der
Rheinisch– Westfälischen Technischen Hochschule Aachen

zur Erlangung des akademischen Grades einer
Doktorin der Naturwissenschaften
genehmigte Dissertation

vorgelegt von **M.Sc.**

Nicole Höbig

aus Bardenberg (Würselen)

Berichter:

Univ.-Prof. Dr. Klaus Reicherter
Prof. Dr. Juan Ignacio Santisteban Navarro

Tag der mündlichen Prüfung: 29.04.2016

Diese Dissertation ist auf den Internetseiten der Hochschulbibliothek online verfügbar

“... y muchas veces le vino deseo de tomar la pluma, y darle fin al pie de la letra como allí se promete; y sin duda alguna lo hiciera, y aun saliera con ello, si otros mayores y continuos pensamientos no se lo estorbaran.”

– Miguel de Cervantes Saavedra (1605)
El ingenioso hidalgo Don Quijote de la Mancha

“... oftmals kam ihm der Wunsch, die Feder zu ergreifen und dem Buch einen Schluß zu geben, buchstäblich so, wie es dort versprochen wird; und ohne Zweifel hätte er es getan, ja er wäre damit zustande gekommen, wenn andere größere und ununterbrochen ihm beschäftigende Ideen es ihm nicht verwehrt hätten.”

(translated by Susanne Lange)

“... and many a time was he tempted to take up his pen and finish it properly as is there proposed, which no doubt he would have done, and made a successful piece of work of it too, had not greater and more absorbing thoughts prevented him.”

(translated by John Ormsby)

“Rompi, corté, abollé, y dije y hice”

– Miguel de Cervantes Saavedra (1605)
El ingenioso hidalgo Don Quijote de la Mancha

“Ich brach, hieb, sprach, schlug Beulen, hab vollbracht”

(translated by Susanne Lange)

“In slashing, hewing, cleaving, word and deed”

(translated by John Ormsby)

Abstract

Climate change is under global debate, due to increasing occurrence of extreme weather events affecting the present-day life. Predicting future climate is challenging, because of the complex interactions in the climate system. Only full understanding of past climate processes and forcing mechanisms allows us to understand and evaluate on-going changes. Some regions are more vulnerable than others. The Western Mediterranean, due to the transitional location between complex atmospheric and marine circulation systems, is highly sensitive to climatic changes.

This work is affiliated to a Collaborative Research Centre (CRC 806 “Our Way to Europe”) dealing with history of human mankind and is in particular a contribution to the sub-project investigating the disappearance of Neanderthals in the Iberian Peninsula, which is supposed to be connected to high frequent climate variability.

Three different sites, aligned on a SW-NE-axis from Southern Spain to Northern Italy, have been under investigation for Late Quaternary palaeoenvironmental reconstruction. Aiming on terrestrial records, which are scarce for the Western Mediterranean, sediment cores from three lakes revealed palaeoinformation: i) Laguna de Fuente de Piedra (LFP; SW-Spain), ii) Lake Banyoles (NE-Spain), and iii) Lake Como (N-Italy). LFP a shallow endorheic saline lake, whereas Lake Banyoles is a tectono-karstic open fresh-water lake, and Lake Como is a large 450 m-deep, semi-closed lake, all three are obviously of particularly difference in their characteristics. Multi-proxy data acquisition has been carried out and palaeoclimatic records at different temporal resolution with different temporal range have been achieved. Due to the different control mechanisms on sedimentation processes, the selection of climate-sensitive proxies for each site was challenging.

For the hydro-sensitive LFP, optical description of sediment cores (max. 14 m long), elemental data (Ti, Ca, S, Sr, ratios, and time series analyses), mineralogical data including crystal habits and stable isotopic signatures of carbonates and gypsum have been acquired. This dataset leads for lithofacies-based palaeohydrological reconstruction. The obtained age control has been achieved by radiocarbon dating. But the low TOC content, bacterial sulfate reduction processes as well as saline groundwater circulation (with long mean residence times) increased the complexity of this site and probably affected datings. The identified lake level changes have been correlated with North Atlantic cold events for the past approximately 28,000 years.

The Lake Banyoles sediment core (66 m long) characterization contains optical description, elemental data, and sediment-physical properties, isotopic data, and diatom analyses leading to different lithofacies. Robust age control has been achieved by U/Th dating, which has been re-assessed by stable isotope record correlation for the upper 30,000 years. Radiocarbon ages were used cautiously, due to an approx. 5,000 year reservoir effect. The high content of endogenic carbonates in Banyoles sediments makes this site highly sensitive to terrigenous influx, as observed in elemental data and their ratios, particularly K/Ca ratio. Potassium-rich material has been correlated to North Atlantic cold events (Heinrich Events 1-5), which are supposed

to originate in clay minerals transported either fluvial or aeolian to the lake. The impact of North Atlantic circulation has also been proven by stable isotopic signatures, which rather show an Atlantic than Mediterranean signal.

From a sedimentary record (65 m long) from Lake Como, different lithofacies have been revealed by optical description, elemental and sediment-physical properties (core logging). The radiocarbon chronology encompasses to upper 32 m and two age-depth models have been discussed for the entire record. Implications for palaeoclimate have been obtained from the younger chronology, assuming ca. 17,000 years at the base. This site also recorded effects from North Atlantic cold events, for the Holocene and have been further discussed for the Deglaciation. Two event layers composed of significantly coarser material are most probable related to climatic forcings as they coincide with warming phases, but seismotectonic triggers cannot be fully excluded.

This work narrows the gap in terrestrial long-term records from the Western Mediterranean. It is shown that the sites are affected by North Atlantic Circulation, but all three show certain differences in their response to past North Atlantic Cold Events, which needs further work for detailed causative analyses.

Kurzfassung

Aufgrund der steigenden Anzahl extremer Wetterereignisse, die unseren Alltag beeinflussen, ist Klimawandel von globalem Interesse. Vermehrtes Auftreten extremer Wetterereignisse beeinflusst unseren Alltag. Klimaprognosen sind eine Herausforderung, aufgrund der komplexen Interaktionen, die unser Klima auszeichnet. Erst das nahezu vollständige Verständnis der ablaufenden Prozesse und treibenden Kräfte wird es uns ermöglichen, die derzeitigen Veränderungen zu verstehen und zu evaluieren. Einige Regionen sind verletzlicher gegenüber Veränderungen als andere. Der westliche Mittelmeerraum ist, aufgrund seiner geographischen Lage, zwischen unterschiedlichen, interagierenden atmosphärischen und marinen Zirkulationssystemen, sensibel bezüglich Klimaveränderungen.

Diese Arbeit ist an einen Sonderforschungsbereich angegliedert (SFB 806 "Our Way to Europe"), welcher sich mit Fragestellungen der Menschheitsgeschichte beschäftigt und ist ein Beitrag zu insbesondere einem Teilprojekt, das das Verschwinden des Neandertalers auf der Iberischen Halbinsel erforscht, welches unter anderem mit hochfrequenten Klimaveränderungen in Verbindung gebracht wird.

Drei unterschiedliche Lokationen, die entlang einer SW-NE Achse von Südspanien nach Norditalien angeordnet sind, wurden zur Rekonstruktion der spätquartären Paläoumwelt untersucht. Terrestrische Klimaaufzeichnungen aus dem westlichen Mittelmeerraum sind bisher in geringer Anzahl erforscht. Deshalb wurden im Rahmen dieser Arbeit Sedimentbohrkerne aus drei verschiedenen Seen auf ihre Paläoumweltinformationen untersucht: i) Laguna de Fuente de Piedra (LFP; Südspanien), ii) Banyoles See (Nordostspanien), und iii) Comer See (Norditalien). LFP ist ein flacher, endorheischer, saliner See, wohingegen der Banyoles See ein hydrologisch offener Süßwassersee ist, der sich in einem Becken tektonisch-karstischen Ursprungs befindet. Der Comer See ist ein großer, 450 m tiefer, hydrologisch halb geschlossener See. Somit unterscheiden alle sich signifikant in ihren Eigenschaften. Die durchgeführten Multiparameterstudien haben Klimaaufzeichnungen in variierender, zeitlicher Auflösung und Reichweite ergeben. Aufgrund der unterschiedlichen Prozesse, die Sedimentation kontrollieren, ist die Identifizierung individueller klimaempfindlicher Parameter eine Herausforderung.

Bohrkernanalysen an der LFP (max. 14 m lang) umfassen optische Charakterisierung, elementare Zusammensetzung (Ti, Ca, S, Sr, Verhältnisse, Zeitreihenanalyse), mineralogische Analyse einschließlich Kristallmorphologie und Analyse stabiler Isotope von Karbonaten und Gips. Auf Grundlage dieser Daten wurden Lithofazies charakterisiert und paläohydrologische Veränderungen rekonstruiert und mit Hilfe von Radiokohlenstoffdatierungen ein Altersmodell entwickelt. Aber die geringen Gehalte an organischem Kohlenstoff, Sulfatreduktion durch Bakterien, und die Zirkulation von salinen Grundwässern (mit langen mittleren Verweilzeiten) erhöhen die Komplexität dieses Archivs und haben möglicherweise die Altersdaten beeinflusst. Die rekonstruierten Seespiegelschwankungen der vergangenen 28.000 Jahre konnten mit kurzzeitigen Kältephasen im Nordatlantikraum korreliert werden.

Die Charakterisierung unterschiedlicher Lithofazies anhand des Sedimentbohrkerns (66 m lang) vom Banyoles See umfasst optische Beschreibung, Elementzusammensetzung, sedimentphysikalische Eigenschaften, Daten zu Isotopensignaturen und eine Analyse der Diatomeen. Ein robustes Altersmodell wurde mittels U/Th Datierungen erstellt und im Weiteren durch die Korrelation mit der Isotopenkurve für die letzten 30.000 Jahre verifiziert. Radiokarbonalter können am Banyoles See einen Reservoirereffekt von ca. 5.000 Jahren aufweisen und sind deshalb als weniger zuverlässige Altersdaten betrachtet worden. Aufgrund des hohen Anteils endogenen Karbonats in den Banyoles-Sedimenten, ist das System hoch sensibel für terrestrischen Eintrag. Dies ist in der elementaren Zusammensetzung und den berechneten Verhältnissen, insbesondere K/Ca, zu erkennen. Der Eintrag kaliumreichen Materials, wobei es sich wahrscheinlich um fluviatil oder äolisch eingetragene Tonminerale handelt, korreliert mit kurzzeitigen Kältephasen im Nordatlantikraum (Heinrich Events 1-5). Die Analyse der stabilen Karbonatisotopie zeigt eher einen primär Atlantischen Einfluss als eine mediterrane Signatur, was den Einfluss der nordatlantischen Zirkulation auf den Banyoles See bestätigt.

Die Bohrkernanalyse der ca. 65 m langen Sedimentsequenz des Comer Sees beinhaltet die optische Beschreibung, elementare Zusammensetzung, sedimentphysikalische Messungen und verschiedene Lithofazies wurden charakterisiert. Altersdatierungen des Radiokohlenstoffs erfassen die oberen 32 m der Sedimentabfolge, weshalb zwei unterschiedliche Altersmodelle für den gesamten Bohrkern diskutiert werden. Unter Annahme der jüngeren Chronologie reicht der Bohrkern 17.000 Jahre zurück und Hinweise auf Paläoklimaschwankungen wurden diskutiert. Auch für dieses Archiv konnte zumindest für das Holozän ein nordatlantischer Einfluss gezeigt werden und für das Spätpleistozän extrapoliert werden. Zwei Ereignislagen, welche sich durch deutlich gröberes Material auszeichnen, konnte wahrscheinlich mit Klimaereignissen in Verbindung gebracht werden, da sie mit Warmphasen zusammenfallen. Allerdings können seismische Auslöser nicht vollständig ausgeschlossen werden.

Diese Arbeit ist ein Beitrag, um die Lücke langer terrestrischer Paläoklimaarchive im westlichen Mediterranraum zu schließen. Es konnte gezeigt werden, dass alle untersuchten Archive von der nordatlantischen Zirkulation beeinflusst werden. Da die Reaktionen teilweise unterschiedlich sind, sind weitere Untersuchungen der kausalen Zusammenhänge notwendig.

Acknowledgements

This work would not have been possible without my supervisors. I would like to thank Prof. Dr. Klaus Reicherter for his continuous support, inspiration, motivation and advice. I'm grateful to Prof. Dr. Juan Santisteban (Complutense University of Madrid, Spain) for his support and keeping the focus, when I was lost in details. The scientific support and warm words from Dr. Rosa Mediavilla (IGME – Instituto Geológico y Minero de España, Madrid, Spain) were essential for this work and are gratefully acknowledged (Muchísimas gracias, Rosa! Yeso, todo yeso!). The coincidence to meet Prof. Dr. Luís Gibert (University of Barcelona, Spain) during a field trip was another milestone in understanding lacustrine evaporites, which was triggered by extensive discussions at various Baza outcrops. I'm also grateful to Dr. Dioni Cendón (Australian Nuclear Science and Technology Organisation; University of New South Wales, Sydney, Australia), whom's help was significant to overcome one of the main troubles: age models. I want to thank Prof. Dr. Rafiq Azzam (RWTH Aachen) for chairing my oral examination. To all afore mentioned: Even spontaneous and last minute I could count on you. Furthermore the thesis, containing articles, benefited greatly from critical comments and suggestions from different reviewers, which are greatly acknowledged either.

Many thanks also go to...

...Prof. Dr. Martin Melles (University Cologne, Germany) for giving me access to his lab facilities and his straightforwardness.

...Prof. Dr. Melanie Leng (British Geological Survey, NERC Isotope Geosciences Laboratory) and Dr. Jack Lacey (University of Nottingham, Great Britain) for introducing me to the world of stable isotopes.

...Prof. Dr. Gerd-Christian Weniger (Neanderthal Museum Mettmann, Germany) in particular for his patience with geologist's questions on archaeological issues and the traditional Neanderthal-BBQ.

...the best cave painter alive, Dr. Pedro Cantalejo (Museo Municipal de la Historia y las Tradiciones de Ardales, Spain) for his confidence and sharing Ardales Cave.

...Team Como: Prof. Dr. Alessandro Michetti (University of Insubria Como, Italy), Dr. Franz Livio, Dr. (Maria) Francesca Ferrario, and Dr. Elisa Martinelli for the pleasant wintertime in Como and thank you, for making me addicted to good Italian coffee.

...Prof. Dr. em. Ramon Julià for committing me the Banyoles drill core.

...Team Cologne: Dr. Michael Weber and Johannes Jakob for the MSCL support, Dr. Daniela Sprenk for the FTIRS analyses, and Dr. Volker Wennrich for the support in XRF scanning, and Nicole Mantke for helping me with any lab-issue.

...Prof. Dr. Frank Lehmkuhl (RWTH Aachen University) and Marianne Dohms for easy access to the FPXRF.

...Prof. Dr. Helge Stanjek (CIM, RWTH Aachen), Dr. Sven Sindern (IML, RWTH Aachen), and Uwe Wollenberg (GIA, RWTH Aachen) for several support with analytics.

...Dr. Norbert Nowaczyk (GFZ, Deutsches GeoForschungszentrum, Potsdam, Germany)

for his introduction in palaeomagnetism and analysis.

...Dr. Javier García-Veigas (University of Barcelona, Spain) for access and support at the SEM and Dr. Jordi Ibáñez (ICTJA – Institut de Ciències de la Terra Jaume Almera, Barcelona, Spain) for numerous XRD analyses.

...Prof. Dr. Jane Reed (University of Hull, Great Britain) for introducing me to diatoms.
...numerous students during field work.

...Prof. Dr. Flavio Anselmetti (University of Bern, Switzerland) for the great EAWAG Summer School, which was an excellent kickstart into limnogeology.

...the Collaborative Research Centre 806, in particular the C-Cluster team and the IRTG colleagues

...my NUGGED-colleagues for the outstanding time together, having inexhaustible discussions, great fieldtrips, and detailed investigations of the unique *Kuckucksnest*.

...Werner Kraus (NUG, RWTH Aachen) for his help in keeping our lab running and his warm words in stormy times.

...Max, my family and friends.

The support by the following is furthermore gratefully acknowledged:

- RWTH Graduiertenförderung (PhD scholarship)
- CRC 806 “Our Way to Europe” (Affiliation)
- ERASMUS (4 months research in Como, Italy)

I'm pretty sure that there are many more, who deserve my gratefulness ...

Contents

Abstract

Kurzfassung

Acknowledgements

I

1. Introduction

1

- 1.1. Motivation and societal relevance 1
- 1.2. Palaeoclimate archives 1

2. Scope and motivation

3

- 2.1. Main objectives 3
- 2.2. Multi-proxy approach 3
- 2.3. Study sites 5
- 2.4. Thesis outline 7

3. Palaeohydrological evolution and implications for palaeoclimate since the Late Glacial at Laguna de Fuente de Piedra, southern Spain

9

- Abstract 9
- 3.1. Introduction 10
- 3.2. Study area 12
- 3.3. Materials and methods 14
 - 3.3.1. Coring 14
 - 3.3.2. Core-log data (XRF & MS) 15
 - 3.3.3. Total (in)organic carbon (TOC & TIC) 15
 - 3.3.4. Mineralogical data (SEM, EDS & XRD) 15
 - 3.3.5. Stable Isotopes 17
 - 3.3.6. Radiocarbon dating 17
 - 3.3.7. Empirical Mode Decomposition 17
- 3.4. Results and interpretation 18
 - 3.4.1. Lithofacies characterization 18
 - 3.4.2. Facies and lake margin model 20
 - 3.4.3. Radiocarbon data 23
 - 3.4.4. Isotopic signatures 25
- 3.5. Discussion 27
 - 3.5.1. Chronology 27
 - 3.5.2. Lithostratigraphy and palaeohydrology 29
 - 3.5.3. Implications for palaeoclimate 31
- 3.6. Conclusions 33
 - 3.6.1. Lithostratigraphy and lake margin model 33
 - 3.6.2. Chronology 34

3.6.3. Palaeoclimate	34
3.7. Acknowledgements	34
4. Lake Banyoles (northeastern Spain): A Last Glacial to Holocene multi-proxy study with regard to environmental variability and human occupation	37
Abstract	37
4.1. Introduction	37
4.1.1. Previous studies	39
4.1.2. Physical lake characteristics	41
4.1.3. Geology of Lake Banyoles	41
4.2. Methods	42
4.2.1. Sediment-physical properties	42
4.2.2. Total organic and inorganic carbon (TOC, TIC)	43
4.2.3. Geochemical composition by XRF analyses	43
4.2.4. Additional sedimentological observations	43
4.2.5. Dating	43
4.3. Results	44
4.3.1. Facies	44
4.3.2. Age models	49
4.4. Interpretation and Discussion	50
4.4.1. Variabilities of depositional environments during the last 55 ka BP	50
4.4.2. Implications for settlement patterns and cultural change in NE Iberia	53
4.5. Conclusions	55
4.6. Acknowledgements	55
4.7. A 60 ka Multi-Proxy Record from Lake Banyoles (Northeastern Spain): Extended data	57
Abstract	57
4.7.1. Introduction	57
4.7.2. Situation	58
4.7.3. Methods	58
4.7.4. Data	59
4.7.5. Interpretation	60
4.7.6. Conclusions	60
5. Western Mediterranean climate and environment since Marine Isotope Stage 3: a 50,000 year record from Lake Banyoles, Spain	63
5.1. Introduction	63
5.2. Study site	65
5.3. Material and Methods	67
5.3.1. Core recovery and sedimentology	67
5.3.2. Mineralogy	69
5.3.3. Stable isotope analysis of calcite	69
5.3.4. Diatom analysis	70
5.4. Results	72
5.4.1. Geochemical and isotope analysis	72
5.4.2. Diatom analysis	72
5.5. Re-assessment of the chronology	74

5.6. Discussions	75
5.6.1. Modern lake-water isotope composition and controls	75
5.6.2. Oxygen isotope composition of calcite from Lake Banyoles	76
5.6.3. Carbon isotope composition of calcite from Lake Banyoles	77
5.6.4. Isotope covariance and facies variability	80
5.6.5. Lake Banyoles climate and hydrology: MIS 3-1	81
5.7. Conclusions	82
5.8. Acknowledgements	83
6. Late Quaternary environmental evolution of the Como urban area (Northern Italy): A multidisciplinary tool for risk management and urban planning	85
Abstract	85
6.1. Introduction	85
6.2. Geological and environmental framework	90
6.3. Modeling the urban subsurface: multidisciplinary data collection	90
6.3.1. Stratigraphy	91
6.3.2. Geotechnical data	92
6.3.3. Chronological constraint: ^{14}C dates and archeology	94
6.3.4. Lake flooding and subsidence	96
6.3.5. Hydrogeology	97
6.4. Modeling the urban subsurface: results	100
6.4.1. Stratigraphic correlations	100
6.4.2. Landscape evolution	101
6.5. Applying the model: lake-shore area	104
6.5.1. In situ and laboratory tests	106
6.5.2. Geotechnical stratigraphy	106
6.5.3. Model reliability and insights on the historical evolution of the town . . .	108
6.6. Conclusions	108
6.7. Acknowledgements	110
7. Lithofacies and geochemical characterization of post-LGM sediments at Lake Como, North Italy	111
7.1. Introduction	111
7.2. Setting	111
7.3. Materials and methods	112
7.4. Results and interpretation	113
7.4.1. Lithofacies characterization	113
7.4.2. Lithostratigraphy	115
7.5. Discussion	116
7.5.1. Slope overloading	118
7.5.2. Seismic events	118
7.5.3. Lake level fluctuations	119
7.5.4. Wind action	119
7.5.5. Run-off peaks	119
7.5.6. Implications for palaeoclimate	120
7.6. Conclusions	120

8. Resume	121
8.1. Re-evaluation and synthesis	121
8.2. Outlook	126
References	128
A. Appendix	157

List of Figures

2.1.	Scheme: multi-proxy approach of studied lake palaeoenvironments	4
2.2.	Studied lake archives: overview map & lake characteristics	6
3.1.	Fuente de Piedra: site map & present-day lake environment	11
3.2.	Map Fuente de Piedra: geology, morphology, lake levels & core locations	13
3.3.	Multi-proxy data of core 2013-04 at Fuente de Piedra	16
3.4.	Lithofacies characterization of Fuente de Piedra sediments	18
3.5.	Conceptual lake margin model of Fuente de Piedra	21
3.6.	Plots: $\delta^{18}\text{O}$ against $\delta^{34}\text{S}$ (gypsum) & $\delta^{13}\text{C}$ against $\delta^{18}\text{O}$ (Fe-dolomite)	26
3.7.	Age-depth plot of Laguna de Fuente de Piedra	28
3.8.	Lake level reconstruction at Laguna de Fuente de Piedra	30
3.9.	Palaeorecord correlation of Fuente de Piedra & other archives	32
4.1.	Map Lake Banyoles: location, geology, bathymetry & core locations	39
4.2.	Lithofacies characterization of Lake Banyoles sediments	46
4.3.	Slumping & faulting in facies J of the Banyoles core	48
4.4.	Multi-proxy data of the Banyoles core	49
4.5.	Age-depth plots of Lake Banyoles & key proxy data	50
4.6.	Correlation of palaeoenvironments from other archives with Lake Banyoles	54
4.7.	Extended multi-proxy data of the Banyoles core	59
4.8.	Age-depth plots of Lake Banyoles & extended key proxy data	61
5.1.	Map Lake Banyoles: shaded relief, bathymetry, lake levels & core locations	64
5.2.	Annual atmospheric data from Banyoles & isotopic signature of rainfall	66
5.3.	Multi-proxy data & ^{13}C & ^{18}O (calcite) cross-core correlation at Lake Banyoles	68
5.4.	Diatom assemblage at Lake Banyoles	71
5.5.	Revised age-depth model of Lake Banyoles	74
5.6.	Global, W- & E-Mediterranean d-excess values and precipitation at Girona	75
5.7.	$\delta^{18}\text{O}$ record correlation of Lake Banyoles and other archives	79
6.1.	Map Lake Como: morphology, geology & locations of data acquisition	86
6.2.	Map of Como urban area	87
6.3.	Piezocone test results and calculated friction ratio	88
6.4.	Multi-proxy data of SV1 core at Lake Como	89
6.5.	Recorded lake levels of Lake Como	95
6.6.	Piezometric level reconstruction of the phreatic aquifer in Como	98
6.7.	Plots: Comparison of lake and ground water levels in Lake Como	99
6.8.	SW-NE & NW-SE geological cross sections including borehole locations	100
6.9.	Lake Como basin landscape evolution since the last glacial maximum	102
6.10.	Structural map (base unit 3) and vertical thickness of unit 3	103
6.11.	Map Como area: evolution of hydrological setting and alluvial fans	104

6.12. Data from the 2013 coring campaign in the Como area	105
6.13. Flow chart: conceptual research workflow for flood hazard mitigation in Como . .	109
7.1. Map Lake Como: palaeoenvironmental evolution since LGM & Sv2 coring site . .	112
7.2. Lithofacies characterization of Lake Como sediments	114
7.3. Multi-proxy data of Sv2 core at Lake Como	116
7.4. Age-depth plots of Lake Como	117
7.5. Palaeorecord correlation of Lake Como and other archives	118
8.1. Key proxy comparison and correlation of the studied lakes & other records	122
8.2. Western Mediterranean climate settings at the Pleistocene/Holocene transition .	124
A.1. Previous version of Figure 3.9 including nearby terrestrial archives	158

List of Tables

3.1.	Fuente de Piedra: core locations, core lengths & settings	14
3.2.	^{14}C ages of Fuente de Piedra sediments	24
3.3.	Isotopic composition of gypsum ($\delta^{34}\text{S}$, $\delta^{18}\text{O}$) & Fe-dolomite ($\delta^{13}\text{C}$, $\delta^{18}\text{O}$)	25
4.1.	^{14}C & U-series ages of Lake Banyoles sediments	45
6.1.	^{14}C ages of Lake Como sediments	94
6.2.	Physical and mechanical parameters of the Como stratigraphic units	107
7.1.	^{14}C ages of Lake Como: updated calibration	115

1. Introduction

1.1. Motivation and societal relevance

The understanding of palaeoclimate change forcing mechanisms is essential for several reasons: (1) Climate change has affected life in the past, (2) climate change is affecting our present-day life and (3) climate change will affect future life. The past changes answer questions dealing with major impact on life on earth, for example the Permo-Triassic mass extinction or the disappearance of dinosaurs at the Cretaceous-Cainozoic boundary. Such remarkable events are not mono-causative, and thus forcing mechanisms and secondary interactions must be identified. The disappearance of Neanderthals in the Late Pleistocene is of particular interest with respect to history of mankind (e.g., [Higham et al., 2014](#)). It has to be clarified, whether orbital forcing, natural hazards or individual/societal interaction are the driving mechanisms. What nowadays seems obvious for the dinosaur-case is still under debate for the Neanderthals. Climate-ecosystem-human interactions are within the scope of recent investigations (e.g., [Birks et al., 2015](#); [Bradtmöller et al., 2012](#); [Schmidt et al., 2012](#)). Understanding of past climatic fluctuations is crucial to fully anticipate (and possibly forecast) climate change in the future ([Bradley and Eddy, 1991](#)). Integration of different climate records highlighted synchronous global climate changes, which may show regional variabilities ([Blockley et al., 2012](#)). The temporary coincidence indicates similar, higher level forcing mechanisms (e.g., Holocene: [Mayewski et al., 2004](#)). As regions like the Mediterranean are more sensitive to effects of climate change, it is important to understand cause-effect relationships in detail for those key sites. The Mediterranean is already prone to intense seasonal rainfall (e.g., [Lionello et al., 2006](#)) and extreme weather events like floods and droughts (e.g., [Vannière et al., 2011](#)). This highly vulnerable region needs detailed reconstructions of the past in order to develop sustainable strategies for potential future climate change scenarios.

1.2. Palaeoclimate archives

Palaeoclimatology is generally based on a simple chain of cause and effect ([Bradley, 1999](#)). An external forcing (e.g., changes in orbital parameters) induces an internal response (e.g., climate change), which affects earth surface processes. Natural archives may record changes in these processes and are later investigated by palaeoclimatologists. To reveal a palaeoclimate record so called proxy data is necessary. Measured properties (analytical data) need to be integrated with fundamental understanding of site specific processes resulting in individual proxy data sets. These data sets deliver information on palaeoenvironmental conditions during the time of formation.

Different types of archives contain palaeoclimatic information at different temporal resolution and temporal range ([Bradley, 1999](#)). Besides glaciological (ice cores; e.g., NGRIP; [Andersen et al., 2004](#)), biological (tree rings; e.g., [Esper et al., 2012](#)), and historical (written documents),

geological archives (marine sediments; e.g., [Hodell et al., 2013](#); terrestrial archives; [Moreno et al., 2012](#)) contain valuable palaeorecords. Terrestrial archives are raising attention in palaeoclimatology. Various environments, like lakes, caves, rivers, and deserts provide palaeoinformation at high temporal resolution. In the entire Mediterranean lots of work has been performed on these kinds of climate archives (e.g., lakes: [Roberts et al., 2008](#), and references therein) to obtain continuous long-term records for correlation between marine or global ice core records (NGRIP; [Andersen et al., 2004](#)). But in particular for Spain it is challenging to find large lacustrine archives ([Valero-Garcés and Moreno, 2011](#)). Thus the W-Mediterranean is still in need of long, continuous, terrestrial records covering Quaternary climate history.

2. Scope and motivation

2.1. Main objectives

- I “Individual proxy data sets” – Identify controls on lacustrine deposits for the studied sites and develop proxy data sets for complex terrestrial archives
- II “Closing the gap” – Establish terrestrial climatic records in the W-Mediterranean reaching back to the Late Pleistocene
- III “Site comparison” – Re-evaluation of the studied lakes (different sensitivities)
- IV “Inter-archive correlation” – Direct comparison with other archives
- V “Extreme climate events” – Identify major changes in palaeoenvironment and propose forcing mechanisms with respect to hazardous potential

2.2. Multi-proxy approach

By multi-proxy analyses the histories of the archives are reconstructed and the most valuable proxies have to be chosen for palaeoinformation. In this study, due to the complexity of terrestrial archives and the different settings of the studied sites, various proxies have been taken into account (Figure 2.1). As most analyses require sediment cores from the archive, the best sedimentary sequences (e.g., most continuous sedimentation) have to be recovered. For site pre-investigation basic remote sensing techniques, like GIS-based morphological analyses, have been performed. Based on the results coring sites have been selected. Non-destructive and destructive analyses have been performed on the sediment cores. For non-destructive analyses Multi-Sensor Core Loggers (MSCL), X-Ray fluorescence scanners (XRF scanner), and Field Portable X-Ray Fluorescence devices (FPXRF) have been used. The destructive analyses contain primarily standard procedures and measurement devices, but for total organic carbon (TOC) and total inorganic carbon (TIC) a relatively new approach in palaeolimnology has been chosen. The TOC and TIC content has been detected by Fourier Transform Infrared Spectroscopy (FTIRS, see [Rosén et al., 2009](#)). For crystal habit characterization Scanning Electron Microscopy (SEM) and Energy-Dispersed Spectroscopy (EDS) have been used. Further details for each case study are described in the site-specific methodology chapters.

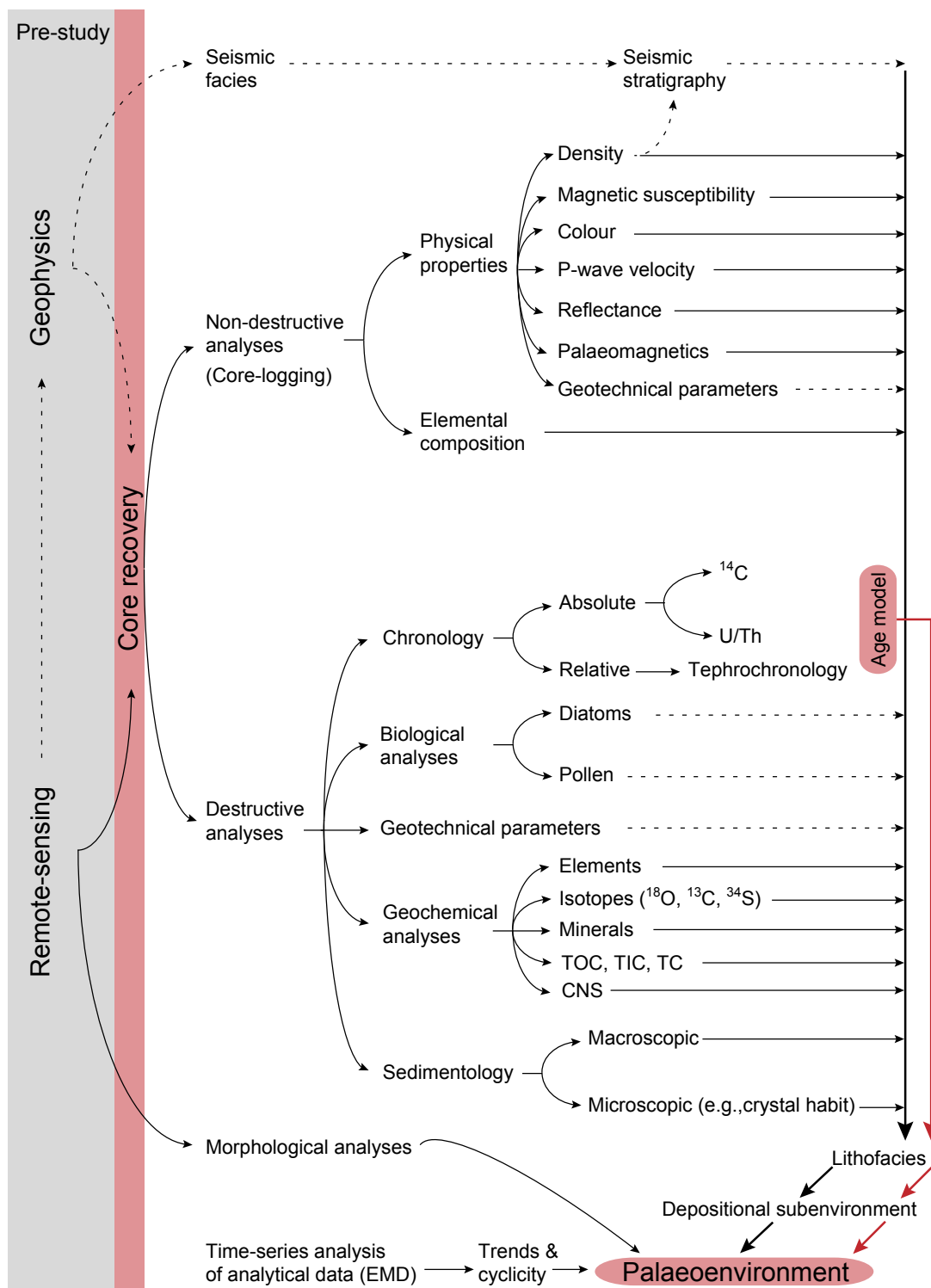


Figure 2.1.: Scheme illustrating the multi-proxy approach used in this work to reconstruct the palaeoenvironment at the three studied lake archives (modified from [Moreno et al., 2012](#)). Solid lines: applied in this study; dashed lines: relevant for the sites in this study. TOC: total organic carbon; TIC: total inorganic carbon; TC: total carbon; CNS: carbon, nitrogen, sulphur; EMD: empirical mode decomposition.

2.3. Study sites

Three lacustrine sites have been studied within this work (see Figure 2.2):

- I. Laguna de Fuente de Piedra, southwestern Spain
- II. Lake Banyoles, northeastern Spain
- III. Lake Como, North Italy

These lakes are aligned on NE-SW axis across the Western Mediterranean, thus hosted in different climatic settings. Present-day climate varies from thermo-/meso-mediterranean climate in the south ($< 40^{\circ}\text{N}$) to meso-/supra-mediterranean ($40\text{--}45^{\circ}\text{N}$), and sub-mediterranean climate in the north (Roberts et al., 2008, 2004). These Mediterranean climate zones are primarily distinct because of the different duration of the dry season (North: three months; South: > 5 months; Quézel and Médail, 2003). The elevation should be of minor importance for the chosen sites, which are located between ca. 170–400 m asl. As already revealed from other close-by studies, the chosen lakes have been most likely affected by large-scale climatic patterns and regional climatic variability (S-Spain: Vegas et al., 2010, NE-Spain: Morellón et al., 2009; N-Italy: Wirth, 2013).

All basins contain a sedimentary infill, predisposing them as suitable lacustrine recorders. In general, wet mudflats/ephemeral saline lakes (I.), and open water lakes, which are prone to re-suspension (II.) have a fair to good potential for palaeolimnological records. Deep lake basins (III.) even have good to excellent conditions depending on the pre-conditions for re-depositional events, (e.g., Cohen, 2003).

Glacier activity and steep slopes might cause difficulties. Furthermore, two of three sites (I and II) are geographically closely related to archaeological sites in order to assure best conditions for correlation with archaeological data as contribution to the Collaborative Research Centre 806.

- I. The southernmost site, Laguna de Fuente de Piedra (LFP), is also the shallowest (0.7 m mean depth) of the three studied sites. The basin has evolved by dissolution-induced subsidence in relation to the local lithology, which is mainly composed of evaporitic formations. As an endorheic basin with low water depth this setting is hydro-sensitive and is supposed to show quick responses to variability in the water balance. The southern lakeshore, chosen for this study, is supposed to give the most continuous sequence, as the major fluvial inflow takes place at the north shore of the lake. The longest recovered core composed of 14 m lacustrine sediments has been used to compile the main palaeohydrological record from LFP.

The multi-proxy dataset at LFP contains optic sediment core description, elemental composition from X-ray fluorescence scan (XRF), mineralogical information from X-ray diffraction (XRD) energy-dispersed spectrometry (EDS). Additionally the crystal habit has been studied by scanning electron microscopy (SEM). Long-term trends have been identified by Empirical Mode Decomposition (EMD). Isotopic signatures from gypsum (^{18}O , ^{34}S) and Fe-dolomite (^{18}O , ^{13}C) were measured. As radiocarbon age control revealed limitations, major challenges of dating this discharge playa have been determined. By sequence stratigraphy a marginal lake model highlights changes in palaeolake level and the complexity in this particular setting with saline groundwater circulation is addressed.

- II. In contrast to LFP, Lake Banyoles is a permanent lake and comprises the smallest water surface of the three sites (compared to LFP at high waterlevel stage). Lake Banyoles is

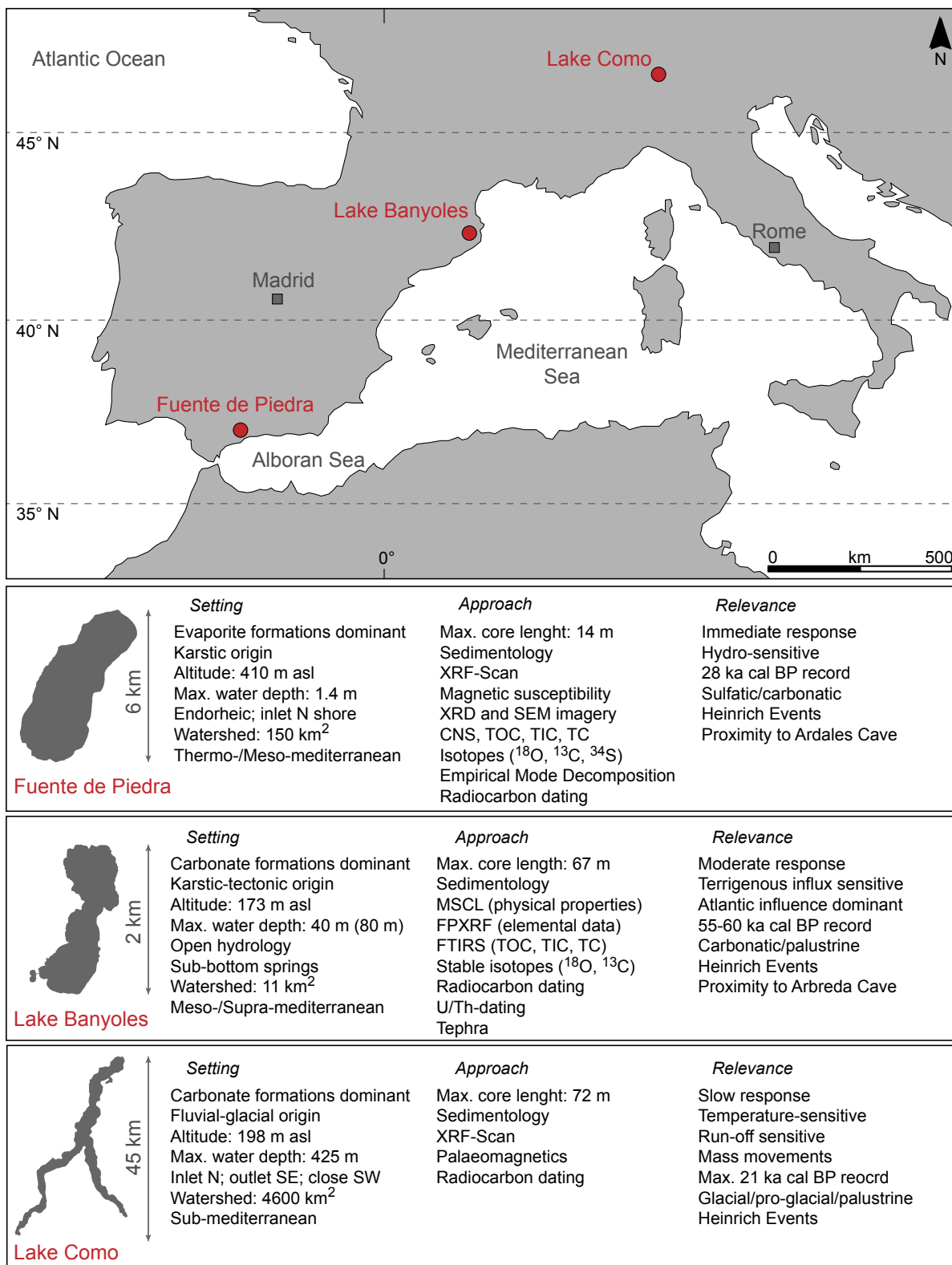


Figure 2.2.: Locations of three sites investigated within the scope of this thesis: (1) Laguna de Fuente de Piedra, (2) Lake Banyoles, and (3) Lake Como. Overview of the characteristics of each lake: (i) setting, (ii) approach, and (iii) relevance.

build-up of several merged collapsed dolines, which host a fresh-water, through-flow setting. The main recharge occurs at the bottom of the lake by hydrothermal subbottom springs in a karstic aquifer, connected to the La Garrotxa volcanic field.

From optic sediment core description, multi-sensor core-logging (MSCL), field portable X-ray fluorescence (FPXRF) analyses, total (in)-organic carbon (TOC/TIC) by Fourier Transform Infrared Spectroscopy (FTIRS), and stable isotope signatures from endogenic carbonates (^{18}O , ^{13}C) a palaeorecord has been reconstructed. The temporal control has been achieved by radiocarbon dating, U/Th dating, tephra, and has been furthermore re-assessed by correlation of the new stable isotope record with a shorter prior published isotope record from Lake Banyoles (Valero-Garcés et al., 1998).

- III. Lake Como - the largest lake investigated within this work. The deeply incised valley has its origin in fluvial downcutting during the Messinian and glacial overprint has taken place during the Pleistocene. The hosting geology is mainly composed of carbonates and minor siliciclastic formations in the southern and northern vicinity of the lake. A sediment infill of more than 180 m has been identified in the Como basin from former seismic survey and drillings (Ferrario et al., 2015, and references therein). The recovered 65 m long sedimentary sequence has been studied optically and by non-destructive logging of u-channels. Elemental composition and sediment-physical parameters including palaeomagnetic properties have been measured.

Como is located in the Southern Alps, which is the northern edge of the Mediterranean. This area is climatically sensitive due to the transition of the subtropical North African and temperate Central European climate (e.g., Finsinger et al., 2008). Furthermore, the proximity to the Alps is interesting for climate reconstructions since the last Deglaciation and there are not many continuous records in the southern Alpine region covering this time span.

2.4. Thesis outline

This thesis contains chapters, which already have been published peer-reviewed or are supposed to be published, which makes a partial overlap of the content inevitable.

Chapter 3 – This chapter is based on one peer-reviewed publication.

Höbig et al. (2016) Palaeohydrological evolution and implications for palaeoclimate since the Late Glacial at Laguna de Fuente de Piedra, southern Spain.

Self-assessment: NH contributed > 80% to this article.

Chapter 4 – This chapter is based on two peer-reviewed publications.

Höbig et al. (2012) Lake Banyoles (northeastern Spain): A Last Glacial to Holocene multi-proxy study with regard to environmental variability and human occupation.

Self-assessment: NH contributed > 70% to this article.

Höbig et al. (2013) A 60 ka multi-proxy record from Lake Banyoles (Northeastern Spain): extended data.

Self-assessment: NH contributed > 90% to this extended abstract.

Chapter 5 – This chapter is based on one peer-reviewed publication.

Lacey et al. (2015) Western Mediterranean climate and environment since Marine Isotope

Stage 3: a 50,000 year record from Lake Banyoles, Spain.

Self-assessment: NH contributed > 30% to this article.

Chapter 6 – This chapter is based on one peer-reviewed publication.

[Ferrario et al. \(2015\)](#) Late Quaternary environmental evolution of the Como urban area (Northern Italy): A multi-disciplinary tool for risk management and urban planning.

Self-assessment: NH contributed ca. 10% to this article.

Chapter 7 – Geochemical characterization of sediments since the Late Glacial at Lake Como, North Italy.

Self-assessment: NH contributed > 90% to this section.

Chapter 8 – This chapter contains a resume of the investigated sites, including a site correlation, main conclusions, problems, and further research questions are addressed.

Self-assessment: NH contributed 100% to this section.

3. Palaeohydrological evolution and implications for palaeoclimate since the Late Glacial at Laguna de Fuente de Piedra, southern Spain

This chapter is a slightly modified version of a published article:

Höbig, N., Mediavilla, R., Gibert, L., Santisteban, J.I., Cendón, D.I., Ibáñez, J., Reicherter, K. (2016). Palaeohydrological evolution and implications for palaeoclimate since the Late Glacial at Laguna de Fuente de Piedra, southern Spain. *Quaternary International* 407: 29–46.

Abstract

Here, we present a terrestrial multi-proxy record of Late Quaternary environmental changes in the southern Iberian Peninsula covering approximately 30 ka. This sedimentary record originates from a saline playa lake (*Laguna de Fuente de Piedra*) hosted within a complex geological setting dominated by Triassic claystones and evaporites, Jurassic carbonates and Miocene deposits leading to a complex hydrogeological setting. Dissolution of evaporites in the catchment and intense evaporation are responsible for saline waters fluctuating in the basin. Thus, salinity as palaeohydrological proxy, requires a decoupling of internal and external hydrogeochemical processes. The greatest accumulation of evaporites in the LFP late Pleistocene–Holocene record coincides with a more humid or, at least, less evaporative, period. Based on multi-proxy data we describe five lithofacies (fluvial: 1; lacustrine: 2–5) from sediment cores. The proposed conceptual lake margin model contains three main lake water stages repeated within the sedimentary succession and building up the characteristic lithofacies. Lake water stages refer to a flooding stage (influx > outflux), high water stage (influx = outflux), and low water stage (influx < outflux). The lithostratigraphy reveals a palaeohydrological record suggesting climate changes and associated lake level fluctuations. Lake level oscillations of different amplitudes have been identified. Low amplitude changes have been revealed for the periods from 28 ka cal BP to 17.5 ka cal BP and from 8.2 ka cal BP to present, whereas in between (17.5 ka cal BP to 8.2 ka cal BP) the Late Pleistocene/Holocene transition shows high amplitude lake level changes. The latter coincides with an increased influence of saline subsurface waters, due to groundwater level rising (sulfate signature). In contrast, the Holocene, records the low amplitude oscillations and a drop of the groundwater levels, which creates a less saline or fresher footprint in the sediments (carbonate signature). Thus, the periods of low amplitude lake level oscillations, low inputs of clastics and low groundwater levels (drier) coincide with periods of minimal seasonal insolation difference. In contrast, the period of higher amplitude lake level oscillations, higher input of clastics and higher groundwater table (wetter) is correlative to periods of maximum difference between summer and winter insolation.

3.1. Introduction

The Iberian Peninsula, due to its mid-latitude location constitutes an excellent region for Quaternary climate variability studies (e.g. [Moreno et al., 2005](#); [Valero-Garcés and Moreno, 2011](#)). Complex atmospheric circulation patterns (e.g., North Atlantic Oscillation) resulting in either humid Atlantic or dry Mediterranean conditions in Iberia are matter of debate and have been documented in various archives (e.g., [Combourieu-Nebout et al., 2002](#); [Martin-Vide and Lopez-Bustins, 2006](#); [Naughton et al., 2009](#); [Rodrigo-Gámiz et al., 2011](#); [Sánchez-Goñi et al., 2008](#)). Although terrestrial environments like lakes are often complex and influenced by several external factors (e.g., hosting geology, hydrological setting), the study of their accumulated sediments is still advantageous. Lacustrine sedimentary sequences can provide continuous records of local and global signals at relatively high-resolution with reliable chronologies (e.g., [Moreno et al., 2012](#)). Recent palaeoclimatic terrestrial records derived from fluvial deposits (MIS1– Late Glacial, [Wolf and Faust, 2015](#)), and saline lakes (e.g., Laguna Medina, 8 ka BP, [Reed et al., 2001](#); Salines, 70 ka, SE Spain, [Giralt and Julia, 2003](#), Zon ar Lake, 4 ka BP, [Martin-Puertas et al., 2008](#)) have been derived for southern Spain. However, terrestrial records covering the last Glacial cycle are still scarce compared to other European locations ([Roberts et al., 2008](#)). Most lacustrine settings in Spain are shallow saline lakes hosted in endorheic basins ([Alonso, 1998](#); [Comín and Alonso, 1988](#)). Due to the typically low water depth, endorheic ephemeral lakes can have limitations as palaeoclimate archives, because of potential hiatuses caused by desiccation. However, this highlights their high sensitivity to climate variability. Even minor differences in the hydrological regimes can cause significant changes in lake level and therefore affect proxies recorded in the lake sediments.

The studied ephemeral lake, linked to ancient evaporite formations, constitutes a challenge for the hydrogeochemical and sedimentological reconstruction. While various studies use crystal morphology of saline lake precipitates to reconstruct palaeohydrology ([Casas and Lowenstein, 1989](#); [Cody and Cody, 1988](#); [Gibert et al., 2007](#); [Hovorka, 1992](#); [Magee, 1991](#); [Magee et al., 1995](#); [Schubel and Lowenstein, 1997](#)), a decoupling of internal and external palaeohydrological influences on the sediment deposits is necessary ([Mees et al., 2012](#)).

In this paper, we examine the palaeohydrological history of the second largest ephemeral saline lake in Spain–Laguna de Fuente de Piedra. We apply several methods to identify proxies sensitive to palaeoenvironmental changes. The general aims are to i) describe lithofacies to reconstruct the palaeohydrological evolution, ii) evaluate salinity as palaeohydrological proxy in evaporite dominated setting hosting lakes, iii) to propose a tentative chronology for the lake sediments after careful characterisation of influencing parameters, iv) discuss insolation as forcing mechanisms of lake level changes, and v) compile a terrestrial palaeoclimatic record for south Spain covering the Holocene and last glacial cycle that can be used to correlate between other regional or global records.

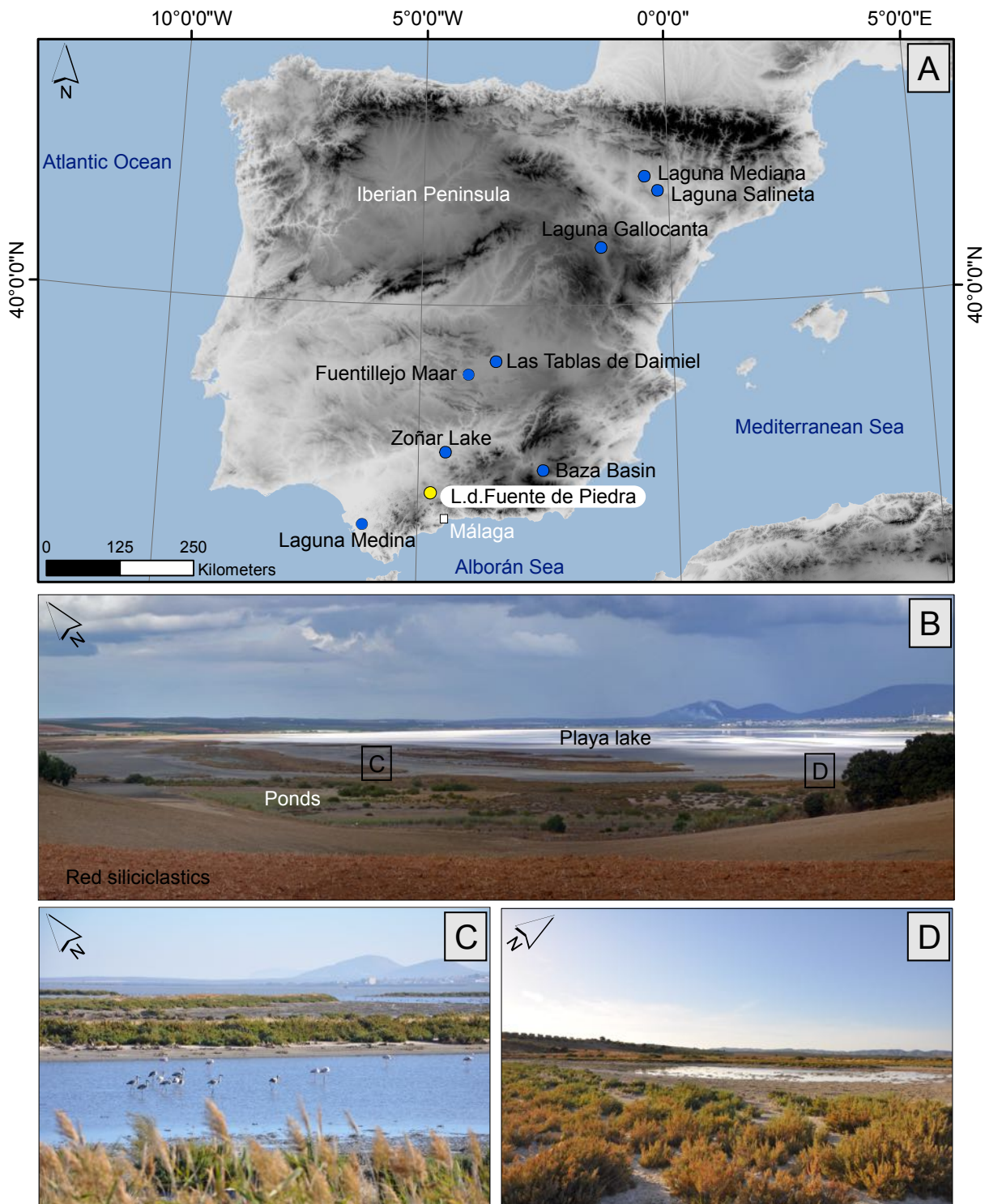


Figure 3.1.: (A) Overview of the Iberian Peninsula with location of the studied site Laguna de Fuente de Piedra (LFP) and relevant sites used for comparison in this study. (B) Image of the shallow LFP basin with the playa lake and ponds, note Fuente de Piedra town in the background. (C & D) Image of small ponds shielded by vegetation at the SW-rim of the basin.

3.2. Study area

The catchment of saline lake Laguna de Fuente de Piedra (LFP) is situated in the water divide of the Atlantic Ocean (Guadalquivir river) and Mediterranean Sea (Guadalhorce river) near Antequera (Málaga, Spain) (Fig. 3.3). The lake covers an area of approximately 13.5 km² (NE-axis: 6.8 km; SE-axis: 2.5 km) and is situated within an endorheic basin with a catchment of ~ 150 km². The present-day lake has an average water depth of 70.5 cm (Rodríguez-Rodríguez, 2002) and several small ponds around the margin (see Fig. 3.3). The main fluvial supply is located in the north, and minor streams in the east and west. The south is less disturbed by fluvial activity and deeper, constituting a depocenter with the most continuous sediment deposition. Due to its shallow water, the site is an ideal habitat for migrating and non-migrating birds (e.g., pink flamingos; Rendón et al., 2014) and therefore it is protected as one of the most important wetlands in the western Mediterranean.

From a geological point of view, LFP is located in an intramontane basin in the external zone of the Betic Cordillera (Subbetic), which developed during Neogene times. The geological substratum of the basin is characterised by (1) mainly Triassic rocks (claystone, dolomites, evaporites, ophites) and Miocene, (2) Jurassic limestones, (3) post-orogenic Miocene rocks and Quaternary deposits. The surrounding mountain ranges, like Sierra Mollina/Sierra de la Camorra (NE), Sierra de Humilladero (E) and Sierra de Yeguas (NW) are built up of karstified Jurassic (and minor Cretaceous) limestones and dolostones. The Triassic consists mainly of reddishgreen marl-/claystones and evaporites (Keuper facies). The nature of LFP basin is more of erosional/subrosional origin than tectonic, as major faults are missing. These underlying Triassic evaporites and their karstification promote saline lake genesis by migrating subsurface-waters and the associated subsidence (Gutiérrez et al., 2002). Karstification favours preferential groundwater flow paths as well as mixing of water sources. Several flow systems, due to contrasting water densities exist in the Fuente de Piedra basin and make the hydrological setting complex (Heredia et al., 2004). Miocene, Jurassic units, and Quaternary alluvium build up important local aquifers. LFP as a classical discharge playa is fed by groundwater inflow ($8.6\text{--}10.6 \cdot 10^6 \text{ m}^3/\text{a}$) as well as rainfall ($6 \cdot 10^6 \text{ m}^3/\text{a}$) and surface runoff ($5.6\text{--}7 \cdot 10^6 \text{ m}^3/\text{a}$) from ephemeral rivers (N:Arroyo Santillán, W:Arroyo Arenales and Arroyo Charcón; Heredia et al., 2004; Linares, 1990). Both, subterranean and surficial contributions are of similar amount and add up to approximately $2 \cdot 10^7 \text{ m}^3/\text{a}$ under modern average climatic conditions. LFP desiccates frequently during summer (e.g., 1997/1998, Rodríguez-Rodríguez et al., 2006, and recently 2012/2013).

Groundwater varies between moderately fresh to saline (1 – 300 g/L; Heredia et al., 2004; Rodríguez-Rodríguez et al., 2005) with water types ranging from calcium-magnesium-bicarbonate type and in some parts calcium-sulfate waters to sodium-chlorine brines. Three main groundwater types with a decline of total dissolved solids in groundwater from north (high) to the south (low) are present in LFP (Kohfahl et al., 2008). The zoning suggests the southern basin receives more freshwater. Surface waters at the LFP are saline and generally of the Na-Cl-type with SO₄ as secondary anion and Mg or Ca as secondary cations. Evaporation of lake waters increases salinity seasonally and causes a convective subbottom density flow. Dissolution of Triassic evaporites controls groundwater salinity, the discharge into the lake is mixing with evaporated surface water. The resulting mixed component of ground, surface plus overprinted evaporation controls the major ion composition of the lake. Previous water stable isotope work reveals the evaporative enrichment of surface waters ($\delta^{18}\text{O} = -3.6 \text{ ‰}$ to 7.0 ‰), whereas relatively light isotopic signatures along the south shore and Arroyo Santillán ($\delta^{18}\text{O} = -5.19 \text{ ‰}$) indicate freshwater inputs (Kohfahl et al., 2008; Rodríguez-Rodríguez et al., 2006). In general a

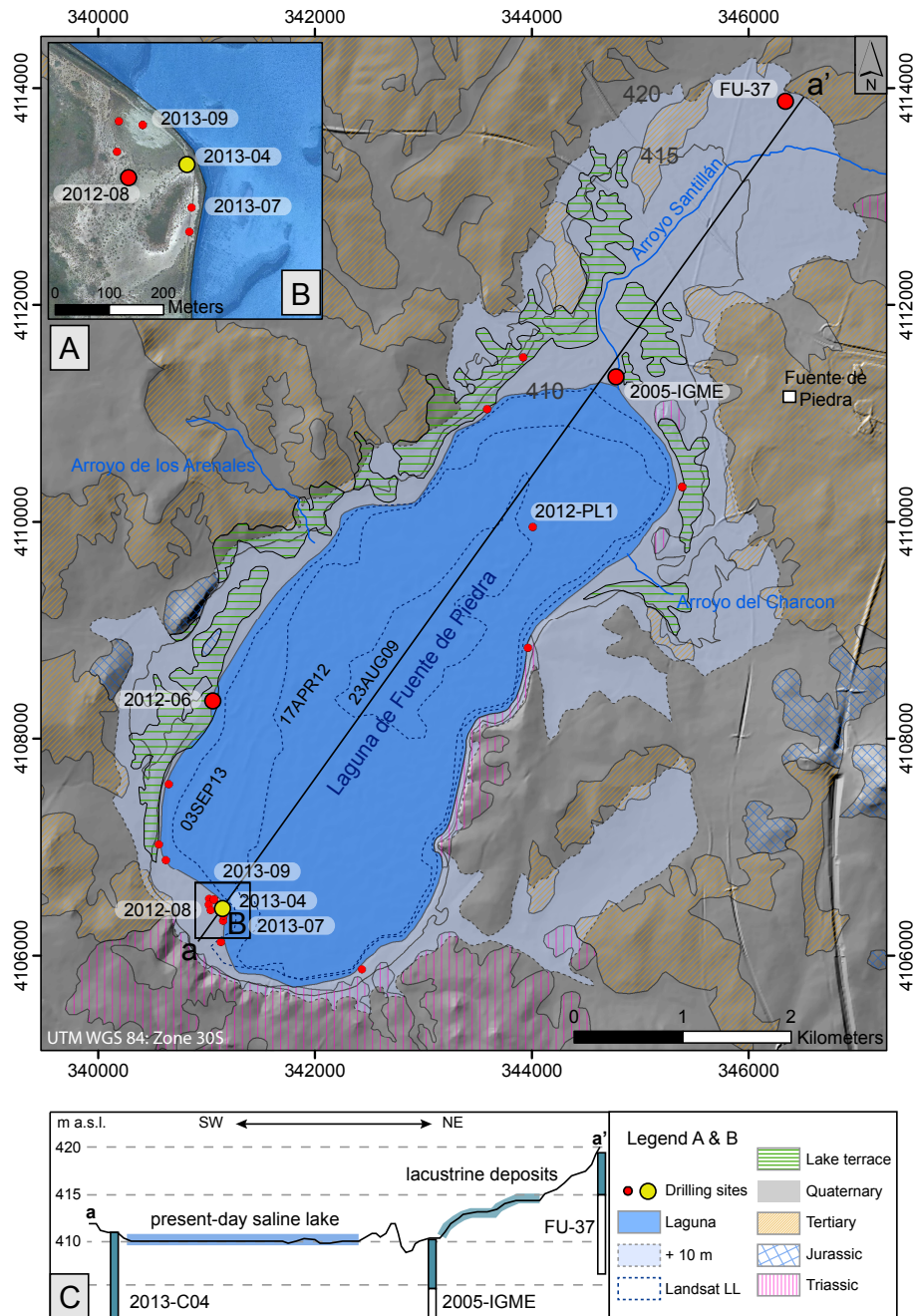


Figure 3.2.: (A) Map of Laguna de Fuente de Piedra with main stratigraphic units (based on geological map 1:50,000, [Martin-Serrano García 1982](#)), drilling locations and potential palaeolake levels (+ 5 m and + 10 m, after [Menz and Fenk 2007](#)) from morphological GIS-analyses (based on a digital elevation model, 5 m cell size, [CNIG 2015](#)) From Landsat images ([USGS Earth Explorer, 2012, 2013](#)) digitised lake levels (LL) in August 2009 (site reconnaissance) and during the drilling campaigns (April 2012; September 2013). (B) Location of the 14 m-long record (2013-04) presented in this study and other relevant cores. (C) Cross-section (a-a') of the Fuente de Piedra basin SW-NE oriented including the core 2013-04, core 2005-IGME ([Heredia et al., 2009](#)), and core FU-37 ([Menz and Fenk, 2007](#)).

trend to a less evaporative signal with increasing distance from the lake centre is observed. Radioactive isotope analysis (^3H and ^{14}C) from groundwater samples (Heredia et al., 2004) reveals diverse groundwater flowpaths with residence times ranging from modern to several thousand years.

The average mineral assemblage of the Fuente de Piedra deposits consists mainly of phyllosilicates/clay minerals, quartz, feldspars, calcite, dolomite, and gypsum (Rodríguez-Jiménez et al., 1993). However, Kohfahl et al. (2008) described an organic layer with a salt crust on the top few centimetres of cores recovered along the shoreline. According to Heredia et al. (2004) salts form during summer, when water reaches halite saturation, but they dissolve during the rainy season (October/November).

Ancient lacustrine deposits, composed of organic-rich marls, have been mapped as Late Pleistocene lacustrine terraces around the present-day lake shore (Martin-Serrano García, 1982, see Fig. 3.3). These deposits are situated at 415–420 m a.s.l., whereas the recent lake is at 410 m a.s.l. A drill core recovered north of the lake contains lacustrine deposits in a comparable elevation (see Fig. 3.3: FU-37; Menz and Fenk, 2007). As a remnant of Quaternary lake level fluctuations at LFP those deposits constitute evidence in large palaeohydrological changes at LFP.

3.3. Materials and methods

3.3.1. Coring

Table 3.1.: *Relevant sediment cores taken at LFP with location in UTM coordinates, recovered core length, and depositional setting.*

Core	UTM coordinates			Depth (m)	Setting
2012-06	30S	341,035	4,108,357	8.0	Margin
2012-08	30S	341,019	4,106,470	7.0	Margin
2012-PL1	30S	344,005	4,109,951	1.4	Centre
2013-04	30S	341,155	4,106,446	14.0	Margin
2013-07	30S	341,156	4,106,367	9.0	Margin
2013-09	30S	341,066	4,106,519	12.0	Margin

During two field campaigns 20 drill cores were recovered at LFP (Fig. 3.3). The coring sites are distributed along the lakeshore and the longest core, of 14 m length (core 2013-04) was recovered in the southwest. The cores, used for this study (see Table 3.1) were taken with a core sampler in PVC-tubes (5 cm in diameter) in meter sections. Non-destructive analyses were performed on core halves. Samples for X-ray diffraction (XRD), scanning electron microscopy (SEM), stable isotopes analysis and radiocarbon dating have been recovered from different layers at varying resolution. In this study, we present three cores from the southern and western margin. The core from the lake centre (2012-PL1, see Table 3.1; Fig. 3.3) has been used for stable isotope analyses for comparison with the present day setting. The longest (14 m) and most continuous marginal record (2013-04) has been used for lake level reconstruction and comparison with other

palaeoclimate records. A conceptual lake margin model has been proposed from multi-proxy data and the subsequent lithofacies succession.

3.3.2. Core-log data (XRF & MS)

Elemental composition of sediment cores from LFP (2012-06, 2012-08, 2013-04) have been studied with an ITRAX core scanner (COX Ltd.). An X-ray Cr-tube was selected to enhance light element sensibility. The core was scanned at 30 kV and 30 mA, with 5 mm intervals and with a detection time of 20 s per measurement. 35 elements have been provided by the scanner, but not all of those are used for palaeoenvironmental interpretation. A similar compositional behaviour is shown by titanium, silicon, aluminium, potassium, iron, and manganese, which are often related to clay minerals and siliciclastic group (Cohen, 2003). An opposing trend is revealed by calcium, primarily derived from either sulfates or carbonates. Due to the watershed geology both authigenic and allogenic origins are possible. The sulfur and strontium trends show a different behaviour.

Magnetic susceptibility (MS) was measured with a Bartington MS2K device at 1 cm resolution in dimensionless SI units on core halves. The MS data matches well with the siliciclastic group (Ti etc.), as it is controlled by the mineral magnetic properties (ferro- magnetic, paramagnetic, diamagnetic; Dearing, 1994).

3.3.3. Total (in)organic carbon (TOC & TIC)

The total carbon (TC), total inorganic carbon (TIC), and total carbon content (TOC) have been measured for 85 samples in total, equidistant at 16 cm resolution, for the long core (2013-04). The samples were pulverised and 30–40 mg sediments suspended in 10 g purified water, before detecting the released CO₂ during combustion in a Dimatoc 2000 (by Dimatec). TC and TIC have been quantified and TOC calculated based on measured parameters.

3.3.4. Mineralogical data (SEM, EDS & XRD)

SEM analyses were performed on several samples from a marginal core (2013-04). Prior to carbon coating, high soluble salts have been removed from the sediments by washing with de-ionised water. SEM-images were used for characterization of crystal habits and specific grains were investigated for elemental composition using energy-dispersed spectroscopy (EDS).

For XRD analyses samples were pulverised and carefully homogenised to produce randomly-oriented powders. The XRD measurements were carried out with a Bruker D8-A25 diffractometer, equipped with a Cu X-ray source (Cu K α radiation) and a LynxEye position sensitive detector (PSD). The scans were acquired between 3° and 70° in 2 Θ with a 0.015° steps. Phase identification was performed with the DIFFRAC.EVA software together with the Powder Diffraction File PDF-2 and the Crystallography Open Database (COD). Quantitative phase analyses (QPA) were carried out with the Rietveld method (Young, 1993) by using the TOPAS 4.2 program from Bruker. Pseudo-Voigt peak shape functions were employed to calculate the theoretical diffraction peaks.

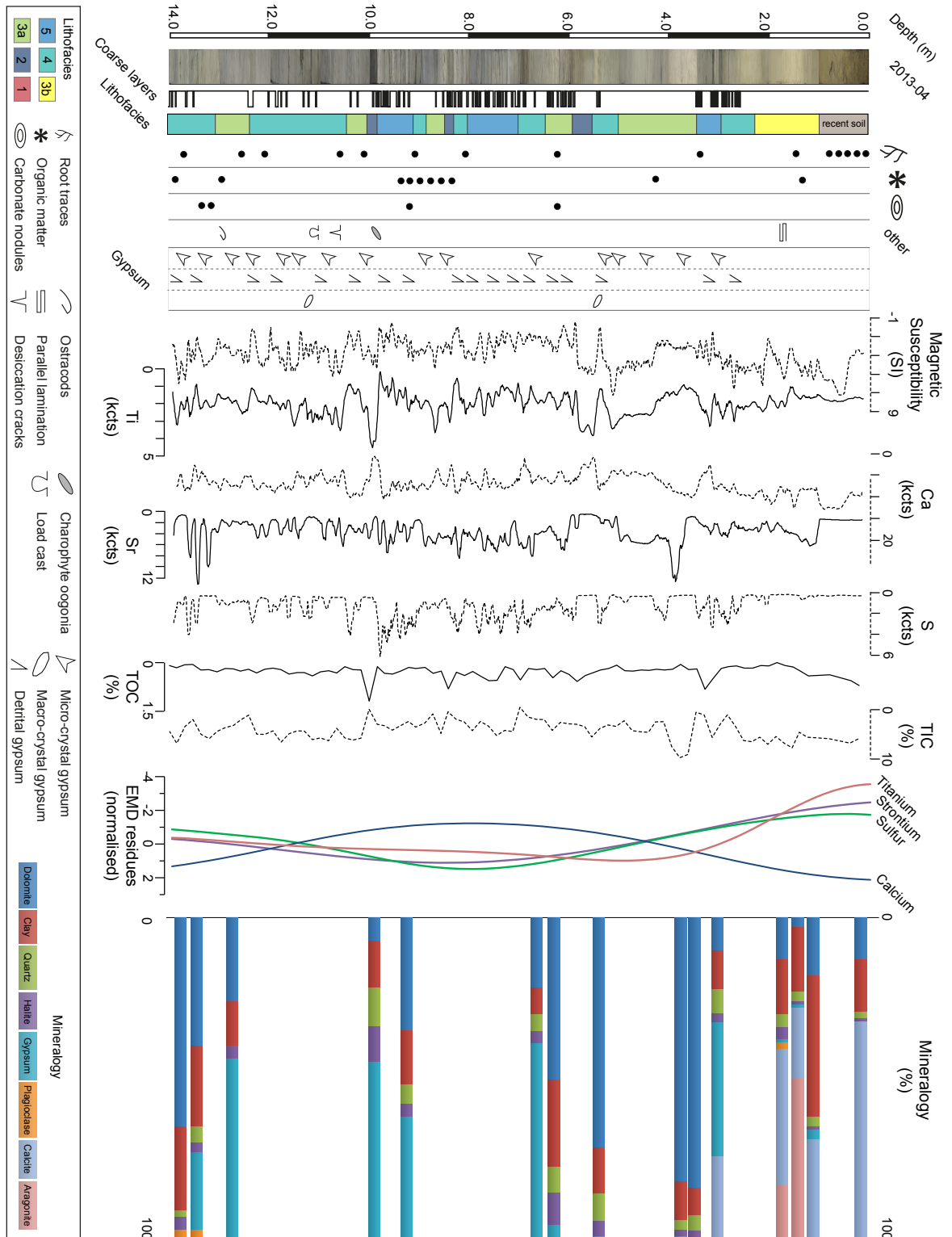


Figure 3.3.: see facing page.

(facing page) Figure 3.3.: Photo of the 14 m long marginal core (2013-04; see Fig. 3.2), coarse layers, lithofacies (see Fig. 3.4 for further description), sedimentological features, magnetic susceptibility (10 mm resolution), elemental composition (XRF scan; 5 mm resolution), total organic carbon (TOC) and total inorganic carbon (TIC). Empirical Mode Decomposition (EMD) residues of Ti, Sr, S, Ca data normalised by mean and standard deviation. Mineralogical composition (dolomite, calcite, gypsum, aragonite, clays, quartz, plagioclase, halite).

3.3.5. Stable Isotopes

Stable isotope analyses of sulfates ($\delta^{34}\text{S}$) and carbonates ($\delta^{13}\text{C}$ and $\delta^{18}\text{O}$) have been performed on gypsum and carbonates from the lake centre (2012-PL1) and margin (2013-04). The carbonate fraction was split into calcite and dolomite, in order to eliminate potential mineral specific fractionation and/or non-synchronous mineral precipitation effects. Separation of dolomite from calcite/aragonite was achieved by reaction with phosphoric acid. The resulting CO_2 formed during the first minute is related to calcite/aragonite and the subsequent CO_2 evolves from dolomite.

In order to obtain approximate groundwater residence times in the LFP basin, we performed calculations with NETPATH (Plummer et al., 1994). The inverse geochemical model calculations are based on available groundwater hydrochemical analysis from the LFP basin published by Heredia et al. (2004) and Rodríguez-Rodríguez et al. (2005). The data utilised includes major ion composition, $\delta^{13}\text{C}$, ^{14}C activity, pH, and temperature. Values for pH and temperature were estimated from mean values in various water samples from LFP (Rodríguez-Rodríguez et al., 2005).

3.3.6. Radiocarbon dating

A total of 29 samples were dated by AMS ^{14}C in three different laboratories (Beta Analytic, CologneAMS, and GADAM Centre). Bulk organic matter, pollen extracts and manually picked oogonia from charophytes, seeds, and charcoal were chosen. Pollen extracts have been created by acid digestion (see e.g., Rull and Abbott, 2010). Six samples from the 2012-08 core, 17 samples from the 2013-04 core, and six samples from the 2005-IGME core were measured in the labs. The obtained conventional radiocarbon ages (2012-08, 2013-04) were calibrated by OxCal v. 4.2 (Ramsey, 2009) using the IntCal 13 curve (Reimer et al., 2013), whereas results from the 2005-IGME core were calibrated by CALIB 7.1 (Stuiver and Reimer, 1986), using the IntCal 13 curve (Reimer et al., 2013).

3.3.7. Empirical Mode Decomposition

Data obtained by XRF-scanning (see subsection 3.3.2) might contain noise, hiding small amplitude oscillations, which are difficult to recognize by eye. But those signals are often helpful in terms of palaeoclimate reconstruction. Identification of those oscillations can be revealed by the Empirical Mode Decomposition method (EMD; Huang et al., 1998; Solé et al., 2007). This approach gives intrinsic signals from non-stationary and nonlinear data by empirical decomposition. EMD creates envelopes along local extreme values and calculates the mean that is subtracted from the original data, creating intrinsic mode functions, which provide a non-

linear filtering of the original data. Iteratively, by spline interpolation the residual close to zero describes the first intrinsic mode function. This is repeated until the overall trend of the time series (residues) remains. Those residues have been normalized by mean and standard deviation $(\text{Element} - \text{Mean})/\text{Deviation}$ for better comparability.

3.4. Results and interpretation

3.4.1. Lithofacies characterization

Visual core description, microscopic observation and analytical data of cores 2013-09, 2012-08, 2013-07 and 2013-04 (for core 2013-04 see Fig. 3.3) revealed several lithofacies (1–5; Fig. 3.4) at the southwest shore of LFP representing different environments within the lacustrine basin. These lithofacies are described attending their bedding, composition, color and internal structures.

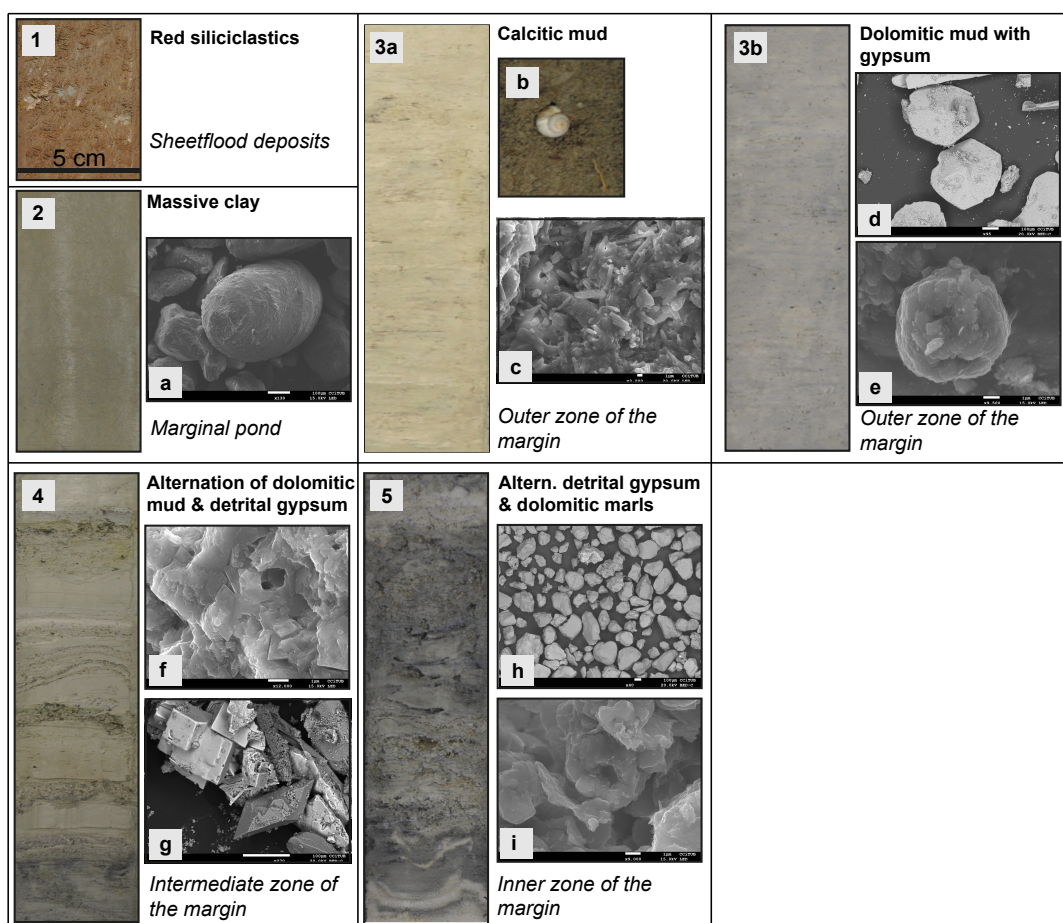


Figure 3.4.: Lithofacies (1–5) identified at LFP (**bold:** lithofacies name; *italic:* genesis). Pictures (a–i) show details of each facies; (a) charophyte oogonia, (b) gastropoda, (c) aragonite needles, (d) lenticular gypsum, (e) dolomite sphere, (f) dolomite rhombohedra, (g) prismatic gypsum, (h) detrital gypsum, (i) dolomite spheres.

Lithofacies 1 (Red siliciclastics)

Massive, poorly sorted gravels (fine to medium size) and silty clays in beds of some centimetres up to a meter in thickness with sharp boundaries. They are composed mainly of quartz and re-worked carbonates from the catchment. Clay minerals are also of detrital origin (illite, smectite, kaolinite). They show red colour with greyish to blueish spots in relation to rootlets or grouped in patches.

Lithofacies 2 (massive clay)

Massive clays in layers of 5–17 cm in thickness with sharp boundaries. They are composed by phyllosilicates (illite, smectite, kaolinite), quartz, sparse dolomite and, occasionally, interstitial microlenticular gypsum. They show dark colour (black, green) but bleached areas are common in relation to root traces. Organic content is high in comparison to other facies but maximum TOC is 1.5%. Well-preserved oogonia of Charophyceae (Fig. 3.4a) and vegetal remains are frequent.

Lithofacies 3a (Calcitic mud)

Pale (beige) carbonated muds in beds with sharp boundaries, from 70 cm up to 140 cm in thickness, located in the uppermost 3 m of the cores. They are composed by carbonates (49–80%), silicates (18–47%), and evaporites (1–5%). Main carbonates are calcite and needle-shape aragonite (Fig. 3.4b) while dolomite is accessory. Main silicates are clay minerals (illite, kaolinite, smectites), quartz and, as accessory, plagioclase. Evaporites are represented by micro-lenticular gypsum and halite. Scarce gastropoda fossils are present. These sediments can show a faint parallel lamination that is masked, to the top of the beds, by edaphic features (root traces, nodulization).

Lithofacies 3b (Dolomitic mud with gypsum)

Pale (beige or green) massive carbonated muds in beds from 50 up to 80 cm in thickness with sharp boundaries. They are composed by carbonate (26–82%), silicates (12–17%), and evaporites (2–60%). Carbonate is represented only by dolomite (Fig. 3.3) which can be both spherical (Fig. 3.4i) or rhombohedral (Fig. 3.4f). Main silicates (12–14%) are clay minerals (illite, smectite, kaolinite) while quartz is accessory (0–3%). Evaporites are dominated by gypsum (1–56%) and halite is a minor component (1–4%). Gypsum appears as lenticular crystals, maximum observed length between 1 mm and 5 cm, single or twinned along the (101) plane. These crystals are embedded into the dolomitic mud, show sharp boundaries and growth zonation pointed by included dolomite crystals. Fossils, some ostracod valves, and organic matter mottles are scarce. Pedogenic features, such as root traces, nodulization, brecciation, are common along the beds and abundant to the top of them.

Lithofacies 4 (Alternation of dolomitic mud and detrital gypsum)

Beds varying from 30 to 70 cm in thickness built up by an alternation of centimetre-scale thickness layers of dolomitic mud and layers of detrital gypsum, the later giving a thinning-upwards sequence. Both dolomitic mud and detrital gypsum layers show interstitial crystals of microlenticular gypsum (0.5–2 mm crystal size), sparse or grouped in discontinuous levels, and, rarely, prismatic crystals of gypsum and single or twinned macrocrystals of lenticular gypsum of centimetre-scale like those described for lithofacies 3b.

Detrital gypsum layers are composed by subangular to rounded grains of lenticular gypsum of sand-to silt-size with scarce dolomitic matrix and less than 3% in quartz and plagioclase grains. The layers of dolomitic mud show a composition similar to those described for lithofacies 3b, and they show subaerial exposure features (root traces, desiccation cracks, nodulization) that are more frequent towards the top of the bed.

Lithofacies 5 (Alternation of detrital gypsum and dolomitic mud)

Beds varying from 30 to 70 cm in thickness built up by an alternation of centimetre-thick layers of dolomitic mud and layers of detrital gypsum, the later giving a thinning-upwards sequence. It's similar to lithofacies 4 but detrital gypsum layers are more abundant in lithofacies 5 and subaerial exposure features and interstitial gypsum crystals are rare.

3.4.2. Facies and lake margin model

The interpretation of the observed lithofacies is based on the similitude of present day sediments and those coming from cores, examples found in the literature and the reasoning that can derived from them. So, processes inferred from facies are first proposed, followed by an interpretation of environments. It should be noticed that minor fluctuations within shallow environments, like LFP, affect wide areas of the system. Interpretations focus on materials recovered along the lake margin therefore this is not a model for the entire lake basin. Due to the resolution of this study, the lithofacies described and interpreted represent the accumulation during several years or decades and are not representative of shorter time-scales.

Clastic composition, poor sorting and massive structure of red siliciclastic deposits (**Lithofacies 1**) are very similar to that of present day sheetflood deposits that cover the slopes of the hills surrounding the lake basin (Fig. 3.1B). They are sedimented from high energy currents with high viscosity that suddenly decelerate after short transport. Red colour is typical of Quaternary Mediterranean soils in South Spain (Schulte and Julià, 2001), but root traces, testifying quick vegetal colonization, and bleaching (greyish, blueish mottles), indicative of hydromorphic processes, are weakly developed (Kraus and Aslan, 1993; Retallack, 1988). This is indicative of immature paleosoils developed in active alluvial systems (Bown and Kraus, 1981; Mack et al., 1993). These sedimentary and postsedimentary features point to a sheetflood sedimentation with subaerial exposure and a shallow groundwater table.

Silicon-dominated composition of the massive clay deposits (**Lithofacies 2**) and the detrital nature of these minerals (clays and quartz) point to sedimentation from running waters but in a standing freshwater body, as testified by the presence of well-preserved oogonia of Charophyceae and vegetal remains. The low TOC content (maximum: 1.5%) and the presence of Charophyceae points to well-oxygenated waters, despite the dark color and well-preserved vegetal remains. The presence of root traces and hydromorphic features point to an environment

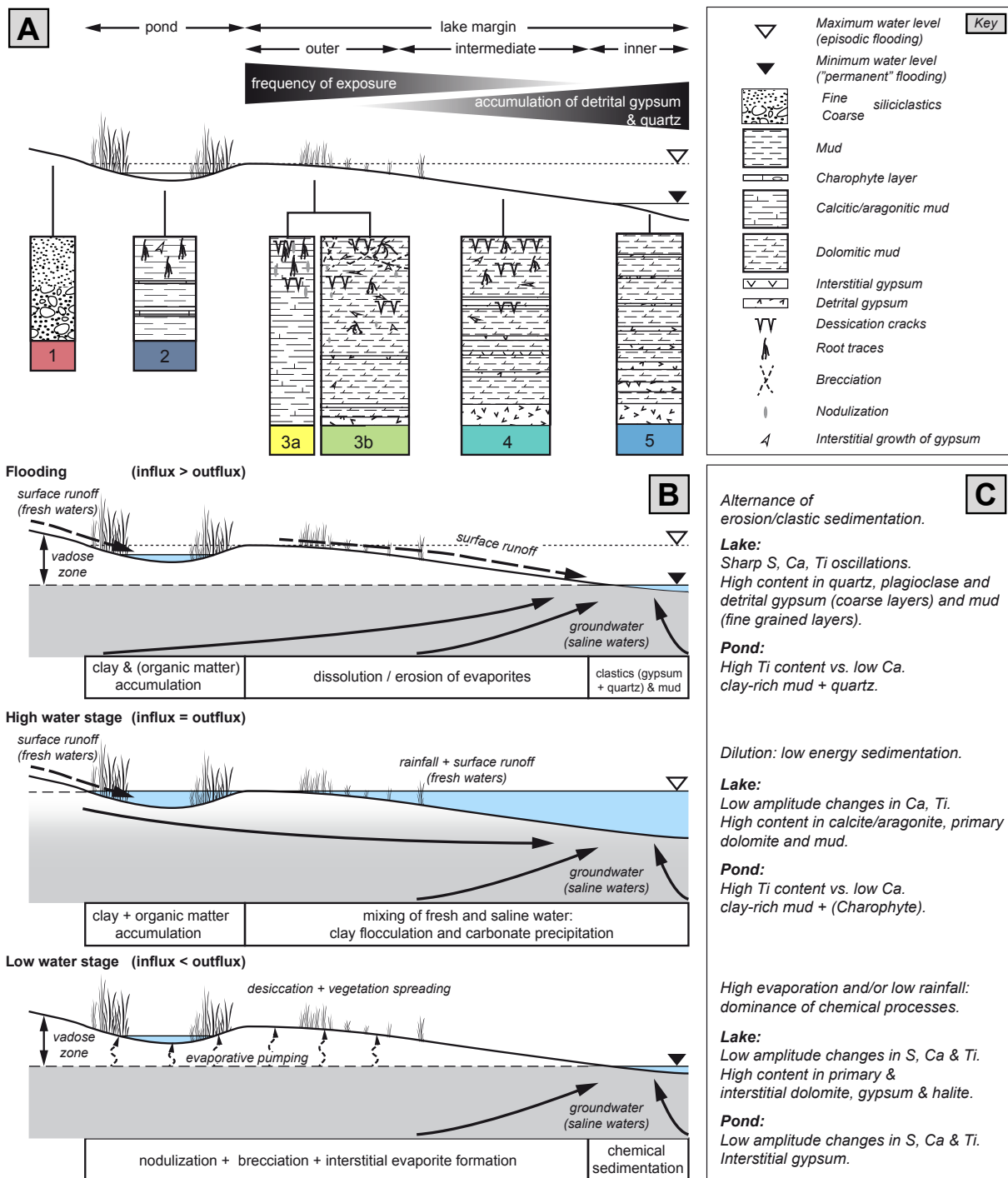


Figure 3.5.: A) Conceptual lake model (modified from Mediavilla, 2001) with the observed five main lithofacies and their depositional environments (pond, outer marginal lake, intermediate marginal lake, inner marginal lake). (B) Depositional processes during three specific lake stages (flooding stage, high water stage, low water stage). Lithofacies are built of repetition of those stage deposits. (C) Proxies: Characteristic behaviour of elemental and mineralogical composition in relation to the depositional environment.

with a fluctuating water table (Kraus and Aslan, 1993; Retallack, 1988). Similar deposits have been interpreted as pond sediments by Reeves (1968); Wetzel (1981); Mediavilla et al. (2003). Such ponds can be identified in the present-day basin surrounding the lake area (Fig. 3.1C and D).

The mixture of chemical precipitates (calcite-aragonite) with detrital components (inherited clay minerals) of calcitic muds (**Lithofacies 3a**) is indicative of processes of precipitation and flocculation in a standing water body with surface waters input and mixing of fresh and saline waters. The formation of interstitial halite and gypsum is indicative of processes of pore water saturation by evaporation. Root traces and nodulization are indicative of an ephemeral water table and subaerially exposure for prolonged periods of time (Freytet and Plaziat, 1982). Thus, these deposits are representative of an environment undergoing episodic flooding and prolonged episodes of desiccation. Similar deposits have been described in shallow saline lakes in Spain by Valero-Garcés et al. (2000a); Pérez et al. (2002); Mayayo et al. (2003).

Similar conditions and environment can be interpreted for the dolomitic mud with gypsum (**Lithofacies 3b**). The interstitial nature of gypsum and the presence of remains of the sediment inclusions into the crystals are indicative of a shallow origin by evaporation and concentration of interstitial brines in the vadose zone and/or in the upper part of the phreatic zone (Murray, 1964). Under these conditions, the bigger crystals are the last to form (Shearman, 1966; Cody and Cody, 1988). The presence of spherical aggregates of dolomite can be indicative of some bacterial activity (Vasconcelos and McKenzie, 1997; Warren, 2000) that could be linked to the sulfur cycle. Root traces and nodulization are indicative of an ephemeral water table and prolonged periods of subaerial exposition (Freytet and Plaziat, 1982). Similar deposits have been described by Ortí et al. (2003); Gibert et al. (2007).

The alternation of dolomitic mud and detrital gypsum (**Lithofacies 4**) comprises (i) periods of calm, during which precipitation of carbonate and flocculation of clay took place in the lake water body, (ii) periods of agitation, during which interstitial gypsum, formed in the more marginal areas of the lake, was reworked by waves and transported into deeper areas by waves and currents, and (iii) periods of dryness, during which the interstitial gypsum and the subaerial exposure features developed. Deposits of detrital gypsum like those presented here are common in the literature (Schreiber, 1987; Truc, 1978; Fort et al., 1982; Ortí et al., 2003) and similar lithofacies have been described in the Iberian Peninsula by Sanz et al. (1994); Mediavilla (2001). The similar features between the alternation of detrital gypsum and dolomitic mud (**Lithofacies 5**) and lithofacies 4 point to a common origin. However, the scarcity of subaerial exposure features in lithofacies 5 is indicative of a deeper environment only occasionally exposed.

Thus, based on lithofacies characteristics and their environmental interpretation, we can arrange them according to their position and relation to the lake level (Fig. 3.5A). In the subaerial domain, out of the lake, we can identify gentle slopes along which runoff can supply detrital material as sheetfloods (Lithofacies 1). These clastics can reach the lake or be trapped in ponds that surround the lake (Lithofacies 2). Three processes take place in the lake. The clastics that reach the lake (mostly clay but also some sand) are mixed with the chemical precipitates of the lake (carbonate) giving carbonated muds during the calm periods. As waters evaporates, the lake shrinks and concentration of pore waters leads to precipitation of interstitial salts (mostly gypsum) along marginal areas. Agitation periods during high water level stages causes reworking of interstitial crystals into deeper areas of the lake.

The relative dominance of these processes allows to define three subenvironments in the margin of the lake (Fig. 3.5A): an outer area characterized by frequent exposure and formation of interstitial gypsum or carbonate (Lithofacies 3a, 3b), an inner area where the products of the erosion of the outer zone are accumulated and rarely is exposed (Lithofacies 5) and an intermediate area

that shares features of the previous ones (Lithofacies 4).

The formation processes of the characteristic sediments for the five lithofacies have been simplified in three main lake stages, which are controlled by local hydrology, i.e. (1) flooding, (2) high water level, and (3) low water level (Fig. 3.5B). The lithofacies result from repetition of these short-term stages and their piling up built the filling trend of the lake (e.g. [Lowenstein and Hardie, 1985](#); [Mediavilla, 2001](#)).

The flooding lake stage describes a short period of intense precipitation after/during a dry period, when recharge exceeds discharge (influx >outflux) The phreatic level is initially relatively low and saline groundwater mainly feeds the lake. The direct runoff erodes the lake margin, whereas within shielded ponds fresh water conditions are preserved. The sediments are characterized by alternation of erosion and/or clastic sedimentation. In the pond clay minerals accumulate, at the lake margin/intermediate zone dissolution and erosion of evaporites occur and in the inner lake zone the detrital gypsum accumulates. The proxy data (Fig. 3.5C) reveal pronounced oscillations in S, Ca, and Ti content and high content in quartz (also plagioclase is present), detrital gypsum (coarse layers), and carbonate mud (fine grained layers) within the lake. In the ponds we observe generally a high Ti content with low Ca values, indicative of a clay-rich mud with a certain amount of quartz.

The high water-level lake stage is characterized by dilution processes and low energy sedimentation. Discharge and recharge are similar with a rise of the phreatic level (influx = outflux). Increased surface water influx creates mixing of fresh and saline waters or dilution of the brines. This implies good preservation conditions for the in-washed detrital gypsum layers that increase towards the lake centre. Those deposits are buried by precipitated calcite/aragonite, primary/biogenic dolomite. In the pond (lithofacies 2) besides clay accumulation, sparse organic matter and Charophyceae oogonia are observed.

The low water-level lake stage indicates persistent dry conditions with intense evaporation and/or low amounts in rainfall. The lakes water loss exceeds the recharge, which forces lake level and phreatic level to decrease (influx <outflux). Under extreme conditions the lake desiccates and vegetation spreads. Root traces and desiccation cracks are observed increasing with distance from the lake centre. Evaporative pumping is acting in either subenvironments (lake and pond). Thus, chemical mineral formation processes dominate at this lake stage. Nodulization, brecciation and interstitial evaporitic growth is present. For the pond we observe interstitial gypsum and towards the lake centre, besides interstitial gypsum, dolomite and halite, primary evaporites (e.g., prismatic gypsum) are present. Due to the more dispersed occurrence of interstitial formation of evaporites, low amplitude changes characterize the S, Ca, and Ti content data (Fig. 3.3).

3.4.3. Radiocarbon data

Analysis of six samples from core 2012-08 (#01 – #06, Table 3.2 provided three results in chronological order. Linear interpolation between those results shows an offset for the other samples towards older ages. From the drilling campaign in 2013 a 14 m-long core (2013-04) next to core 2012-08 was recovered. The 17 radiocarbon dating analysis (#07 – #23) revealed a large variety in the age-depth plot (see Fig. 3.8). A very little amount of recovered carbon from a small charcoal piece (#14, Table 3.2), provided an age of 3865 cal a BP at ca. 11 m depth. Contamination of the small carbon target, close to instrumental capabilities, could not be ruled out, therefore this sample was excluded from further interpretation. The dates for the 2005-IGME core at the Arroyo de Santillán in the North (#24 – #29, Table 3.2) revealed all

Table 3.2.: Radiocarbon dates from two sediment cores (samples 01–06 from core 2012-08 and samples 07–23 from core 2013-04) from Laguna de Fuente de Piedra reported as conventional age and as calibrated ages with a 2σ uncertainty by OxCal (Ramsey, 2009) and IntCal 13 curve (Reimer et al., 2013). Six samples from 2005-IGME core have been used for age model validation.

No.	Laboratory ID	Core	Depth (m)	Material	Conv. Age (a BP)	Cal. Age (a BP)	2σ (cal. a BP)
01	Beta-353780	2012-08	1.50-1.52	bulk sediment	9220±40	10380	10510 to 10250
02	Beta-353782	2012-08	2.84-2.86	bulk sediment	28510±170	32890	33310 to 32470
03	Beta-353784	2012-08	3.12-3.14	bulk sediment	24240±130	29035	29420 to 28650
04	Beta-353786	2012-08	4.79-4.81	bulk sediment	15300±60	18590	18640 to 18540
05	Beta-353788	2012-08	5.68-5.70	bulk sediment	30540±200	34965	35190 to 34740
06	Beta-353790	2012-08	6.78-6.80	bulk sediment	17560±90	20895	21280 to 20510
07	Beta-366926	2013-04	7.71-7.72	bulk sediment	24810±150	29790	30160 to 29420
08	Beta-365743	2013-04	8.38-8.39	bulk sediment	38170±420	42625	43180 to 42070
09	Beta-365744	2013-04	9.93-9.94	bulk sediment	39690±500	43735	44500 to 42970
10	Beta-365745	2013-04	10.72-10.73	bulk sediment	32450±240	36980	37420 to 36540
11	Beta-365746	2013-04	11.45-11.46	bulk sediment	31450±220	35870	36510 to 35230
12	Beta-365747	2013-04	13.69-13.70	bulk sediment	22290±100	26800	26970 to 26630
13	Beta-386843	2013-04	9.91-9.93	oogonia+seeds	37750±360	42063	42520 to 41605
14	Beta-386844	2013-04	10.99-11.00	charcoal	3570±30	3865	3835 to 3895
15	COL2742.1.1	2013-04	1.82-1.83	plant/wood	212±53	1763	1884 to 1642
16	COL2740.0.1	2013-04	3.19-3.20	pollen	29053±154	31598	31919 to 31277
17	COL2737.0.1	2013-04	5.79-5.80	pollen	25464±345	28499	29016 to 27982
18	COL2735.0.1	2013-04	7.50-7.52	pollen	16825±163	18092	18415 to 17769
19	COL2734.0.1	2013-04	8.38-8.40	pollen	43510±515	45122	46719 to 43525
20	COL2733.0.1	2013-04	9.20-9.22	pollen	15008±226	16290	16573 to 16007
21	COL2731.0.1	2013-04	9.93-9.96	pollen	31999±190	34113	34472 to 33754
22	COL2730.0.1	2013-04	10.12-10.14	pollen	12491±123	12822	13187 to 12457
23	COL2729.0.1	2013-04	11.44-11.45	pollen	19159±173	21007	21317 to 20697
24	GdA-1445	2005-IGME	0.048	bulk sediment	106.01±0.34 pMC	-7	-7.51 to -6.84
25	GdA-1446	2005-IGME	0.0625	bulk sediment	4015±35	4482	4569 to 4417
26	GdA-1447	2005-IGME	1.891	bulk sediment	4970±40	5695	5753 to 5603
27	GdA-1449	2005-IGME	4.636	bulk sediment	9620±60	10952	11178 to 10760
28	GdA-1449	2005-IGME	5.967	bulk sediment	39340+/-720	43165	44383 to 42147
29	GdA-1450	2005-IGME	7.123	bulk sediment	42000±1000	45359	47273 to 43467

samples in chronological order, but two sedimentary unconformities are likely. They are placed around 100 a cal BP and approximately 12.5 ka cal BP. The first one is an erosive surface that can be of natural (river activity) or of man action. The second one is located between sample #27 and #28 would coincide with the Pleistocene/Holocene transition.

3.4.4. Isotopic signatures

Table 3.3.: Sulphur isotopic composition from eight selected gypsum samples (01-08), and carbon and oxygen isotopic composition (09-14) of Fe-dolomite. Note that samples are from two different cores (i) central core 2012-PL1 and (ii) the marginal core 2013-04. All values are reported in ‰.

No.	Core	Mineral	Depth (m)	$\delta^{34}\text{S}$ (CDT)	$\delta^{18}\text{O}$ (V-SMOW)	$\delta^{13}\text{C}$ (PDB)	$\delta^{18}\text{O}$ (PDB)
01	2012-PL1	Gypsum	0.53	18.3	23.0		
02	2012-PL1	Gypsum	1.33	20.9	20.6		
03	2013-04	Gypsum	1.9	15.9	20.1		
04	2013-04	Gypsum	5.37	18.3	20.8		
05	2013-04	Gypsum	6.63	16.5	21.8		
06	2013-04	Gypsum	9.95	15.6	19.1		
07	2013-04	Gypsum	11.37	16.5	20.6		
08	2013-04	Gypsum	13.45	18	19.8		
09	2012-PL1	Fe-dolomite	0.47			-4.2	7.8
10	2012-PL1	Fe-dolomite	0.65			-3.3	7.9
11	2013-04	Fe-dolomite	3.58			-3.9	6.4
12	2013-04	Fe-dolomite	5.49			-4.6	5.7
13	2013-04	Fe-dolomite	12.65			-6.1	6.7
14	2013-04	Fe-dolomite	13.73			-5.4	6.3

Isotopic composition of gypsum ($\delta^{34}\text{S}$ and $\delta^{18}\text{O}$)

Eight samples in total, taken from a marginal and a central core, range between 15.6‰ and 20.9‰ for sulphur and between 19.1‰ and 23.0‰ for oxygen (see Table 3.3 and Fig. 3.6A). The LFP-gypsum seems to be enriched in $\delta^{34}\text{S}$ compared to Triassic gypsum (Ortí et al., 2014). The values trend from those close to Triassic recycled sulfate (14.8‰ in the Antequera area, Ortí et al., 2014) to higher values similar to dissolved sulfate in modern seawater. Assuming all SO_4 is from Triassic sources, the 20.9‰ may suggest internal recycling of evaporites. The “recycled samples” (if the hypothesis of recycling is correct) should be from the deeper area where

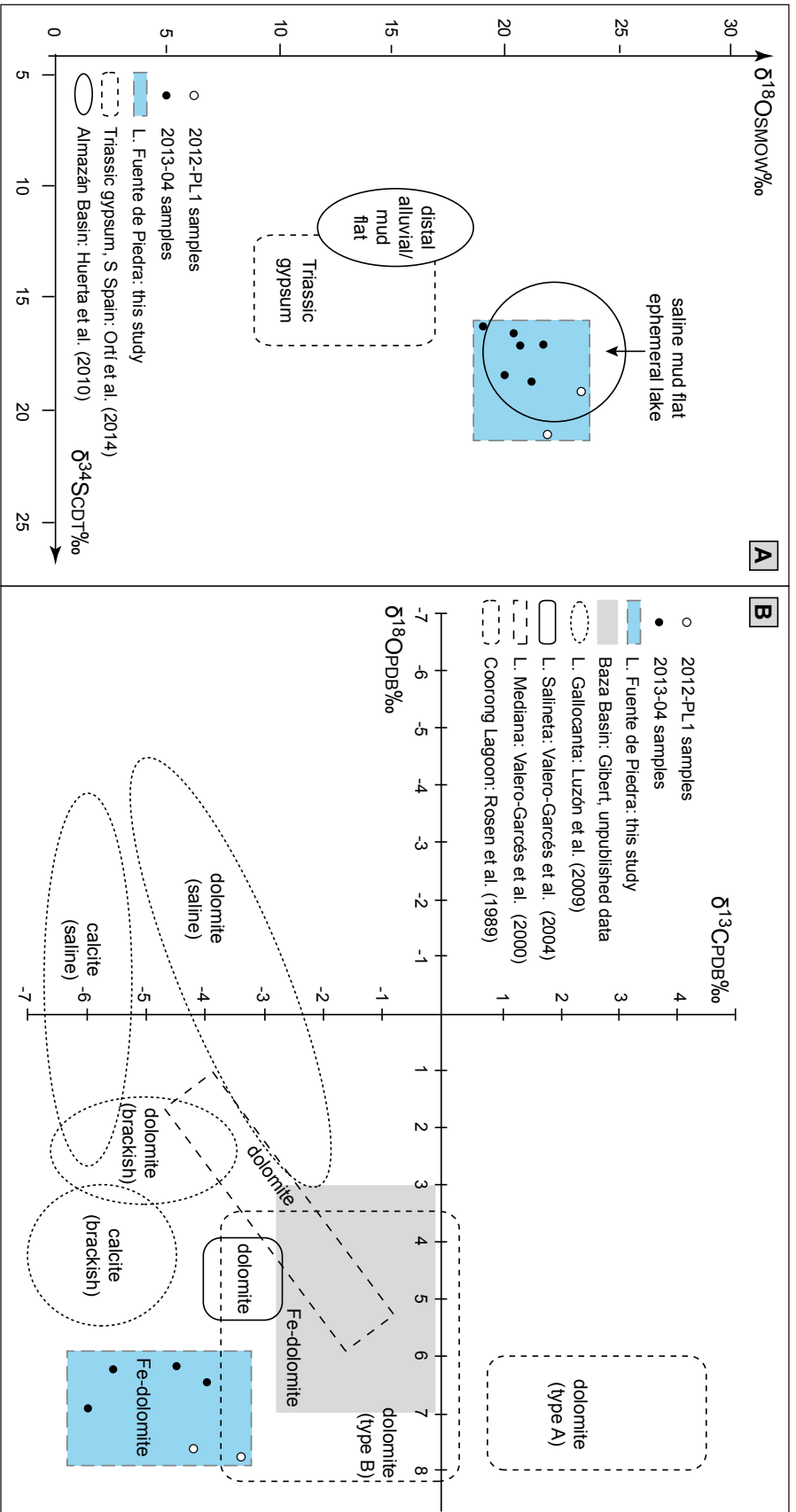


Figure 3.6.: (A) $\delta^{18}\text{O}$ and $\delta^{34}\text{S}$ plot including sulfur values of gypsum from Fuente de Piedra, data from the Almazán basin in northern Spain (Huerta et al., 2010), and the range of Triassic gypsum from the Betic Cordillera, south Spain (Ortí et al., 2014). (B) Crossplot of $\delta^{13}\text{C}$ and $\delta^{18}\text{O}$ values of Fe-dolomite from Fuente de Piedra in correlation to isotopic ranges of other saline lake deposits (Laguna Gallocanta, Spain: Luzón et al. 2009; Laguna Mediana, NE Spain: Valero-Garcés et al. 2000a; La Salineta, NE Spain: Valero-Garcés et al. 2004; Coorong Lagoon, S Australia: Rosen et al. 1989; Baza Basin: Gibert, unpublished data).

accumulation is possible and the possibility of desiccation decreases. Another explanation for the $\delta^{34}\text{S}$ enrichment is the Rayleigh distillation effect (reservoir effect) when all sulfate inputs stops, while evaporation and gypsum precipitation progresses, leading to an increase of the heavier isotope. Both hypotheses coincide with the results obtained from the central core, which are slightly heavier than those from the margin and show a clear signature of saline mudflat/ephemeral lake deposits (Huerta et al., 2010). Bacterial sulfate-reduction in pore waters of the anoxic bottom at shallow LFP might be responsible further for the higher $\delta^{34}\text{S}$ values of LFP-gypsum compared to Triassic gypsum.

Isotopic composition of Fe-dolomite ($\delta^{13}\text{C}$ and $\delta^{18}\text{O}$)

After calcite/aragonite separation, $\delta^{13}\text{C}$ and $\delta^{18}\text{O}$ (Table 3.3) of Fe-dolomite are also analysed. The Fe-dolomite values range between -3.3‰ and -6.1‰ for $\delta^{13}\text{C}$, and from 5.7‰ to 7.9‰ for $\delta^{18}\text{O}$. The carbon isotopic values for LFP Fe-dolomite are relatively light compared to results from nearby similar environments, like Laguna Gallocanta or the Baza Basin (see, Fig. 3.6B). This is probably a result of mixtures of carbonates from different sources. Weathering of marine carbonates in the catchment would have values around 0‰ for $\delta^{13}\text{C}$ and could cause a shift to light values (Clark and Fritz, 1997). At LFP the climate is more arid and warmer than in northern Spain (Laguna Mediana, Valero-Garcés et al., 2000a; Laguna Salineta, Valero-Garcés et al., 2004), which should cause a more intense evaporation at LFP compared to the other sites. The kinetic fractionation of oxygen is mainly driven by evaporation (Talbot, 1990), which is in agreement with the observed heavy $\delta^{18}\text{O}$ values in LFP Fe-dolomite. Fe-dolomite from the Baza Basin (South Spain Gibert et al., 2011) plots in a similar range as LFP Fe-dolomite. As mineral specific fractionation effects can be excluded for those two ranges, one may conclude the Baza Basin deposits as ancient analogue environmental setting on a bigger scale to LFP.

Isotopic signatures of waters

Calculations with NETPATH (Plummer et al., 1994) in this paper, based on available ground-water analysis (Heredia et al., 2004) show potential groundwater residence times spanning from modern (presence of tritium) to 27 ka. This suggests a potential maximum groundwater reservoir effect of around 27 ka for the LFP basin.

3.5. Discussion

3.5.1. Chronology

Obtaining reliable chronologies has been a challenge in many previous saline lake studies (e.g., Dutkiewicz et al., 2000; Giralt et al., 1999). In the literature many processes have been described to take account for shifts in ages, either to younger ages (e.g., humic acids, bioturbation, root penetration; e.g., Kaland et al., 1984) or older ages (e.g. reworked material from the catchment, water enriched in old CO_2 or DIC; e.g., Münnich, 1975; Olsson, 1979; Sutherland, 1980; Valero-Garcés et al., 2000a). Furthermore, the sampling procedure, amount of material, and the storage may affect the results and cause errors (e.g., Wohlfarth et al., 1998).

The high variety of such lacustrine sediments may contain numerous sources of error. However,

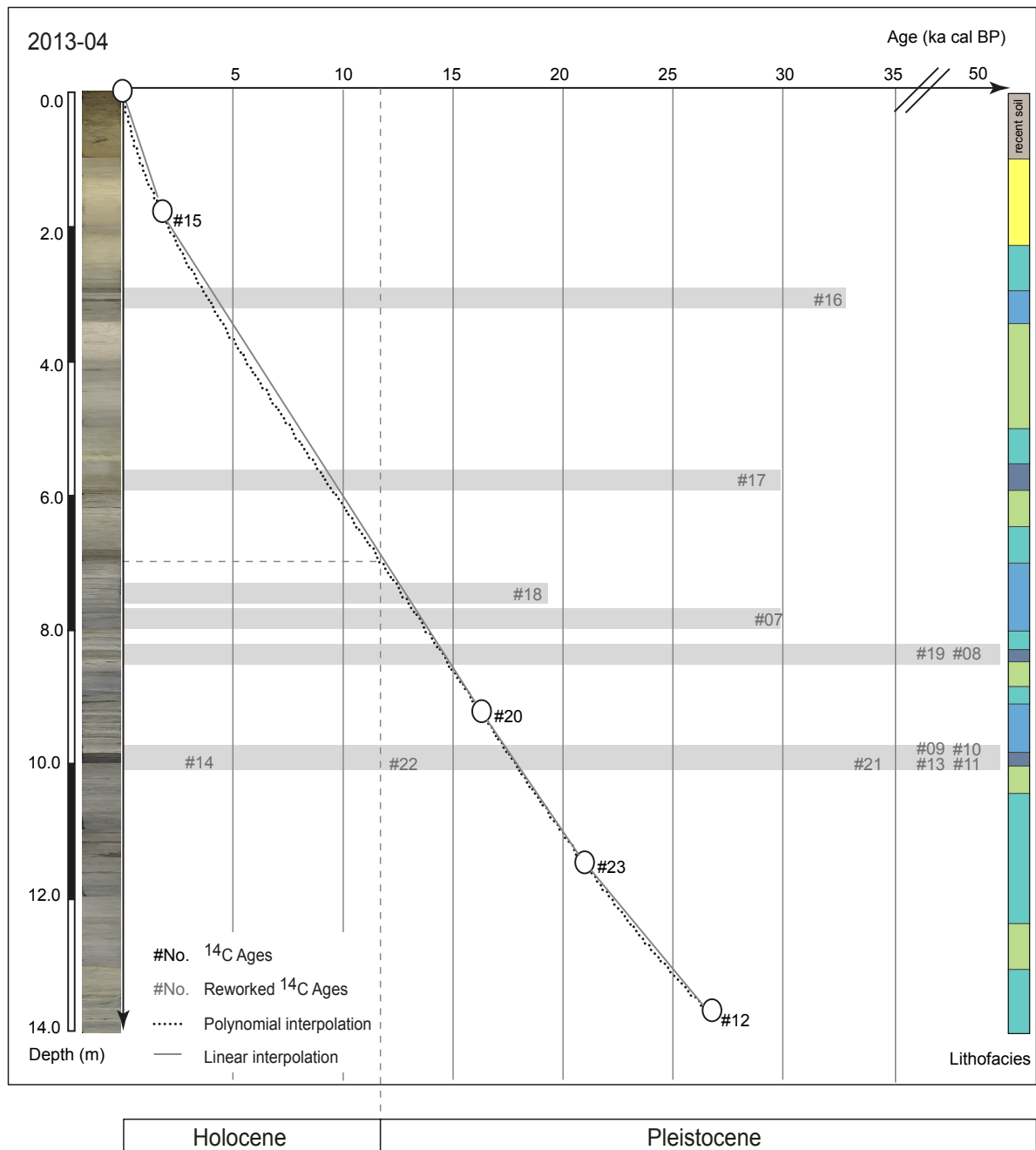


Figure 3.7.: Age-depth plot of radiocarbon ages from 2013-04 sediment core (SW-rim of the basin, see Table 3.2 for age data) with lithostratigraphy (see Figs. 3.3 and 3.4 for further description).

regardless which material has been dated at LFP (pollen, bulk sediment etc., see Table 3.2), data shows a large variance along the records. The geological setting and the highly dynamic response of LFP to any change in environmental conditions forces a cautious interpretation of radiocarbon dates. Cores 2012-08 and 2005-IGME were affected by fluvial activity, which most probably caused hiatuses in those two records. Thus, their chronologies have not been incorporated in the presented age depth model (Fig. 3.7). Although all three showed similar sediment accumulation it is difficult to correlate between the cores via lithostratigraphy. Thus, the developed age model is based on the 2013-04 sediment core, which is supposed to be the most continuous record recovered from the depocentre where fluvial imprint is absent.

At LFP three general potential aspects affecting radiocarbon dating attracted our attention: i) bacterial sulphate reduction (BSR), ii) internal water circulation and iii) reworking in the catchment.

Active BSR during dolomite formation enhances the recycling of organic material and the production of HCO_3^- and it likely has affected the dated materials. Isotopic water analysis reveal residence times as high as ~ 27 ka (from deep brine waters), so it cannot be discarded that the internal water circulation affected the radiocarbon dating. But as this sector of the lake is dominated by shallower and younger groundwaters (Heredia et al., 2009) we assume a minor role of reservoir effect in the samples. Most evidences point to reworking as the main factor responsible of shifting of dates in LFP record. The presence of hiatuses in relation to river activity (cores 2012-08, 2005-IGME) and abundance of detrital layers and remains of terrestrial vegetation in core 2013-04 testify the presence of reworked organic material into the lake.

All three described processes at LFP will cause a shift of the dates to older ages contributing to a radiocarbon reservoir effect (Geyh et al., 1999; Scheiber et al., 2015), together with the low organic carbon content ($\text{TOC} < 1.5\%$) giving further uncertainty. We identify samples #07 – #11, #13, #16 – #19, and #21 as reworked material. Pollen sample #22 has been taken from the lithofacies 3b and might be contaminated by younger plant material from root penetration, which have been observed in the sampled layer.

Age-depth data from the remaining samples (#15, #20, #23, and #12) were fitted by linear and polynomial interpolation. Differences between both models were minimal and for further discussion the polynomial age-depth model ($R^2 = 0.9$) is used. This implies an age of almost 28 ka cal BP at 14 m depth in the southwest margin.

3.5.2. Lithostratigraphy and palaeohydrology

Changes in lithofacies indicate five major oscillations in the lake water table for core 2013-04 (a–e; see Fig. 3.8). These oscillations represent an initial rapid flooding to high lake water stage, with consequent desiccation at a final stage. A tendency to calcite/aragonite in the upper part of the sediment core (lithofacies 3a) is noted, whereas with increasing depth dolomite becomes dominant. Diagenetic/interstitial overprint of calcite/aragonite can be responsible for this trend. But as ferruginous dolomite is present in sediments from the inner lake margin (at 10 cm depth) and the crystal habit indicates bio-induced crystal growth, both origins of dolomitic mud in LFP seem to be likely.

Extrapolation of the five oscillations to an overall trend, revealed a general tendency to deeper lake conditions (c, d), but higher amplitude oscillations, for the central part of the record, (peaking around 8 m) and a long-term change to shallower conditions including the uppermost two sequences (a, b). In normalised elemental residues, obtained with the EMD method, this trend is observed as well. More saline minerals have been detected in the centre of the sequence and

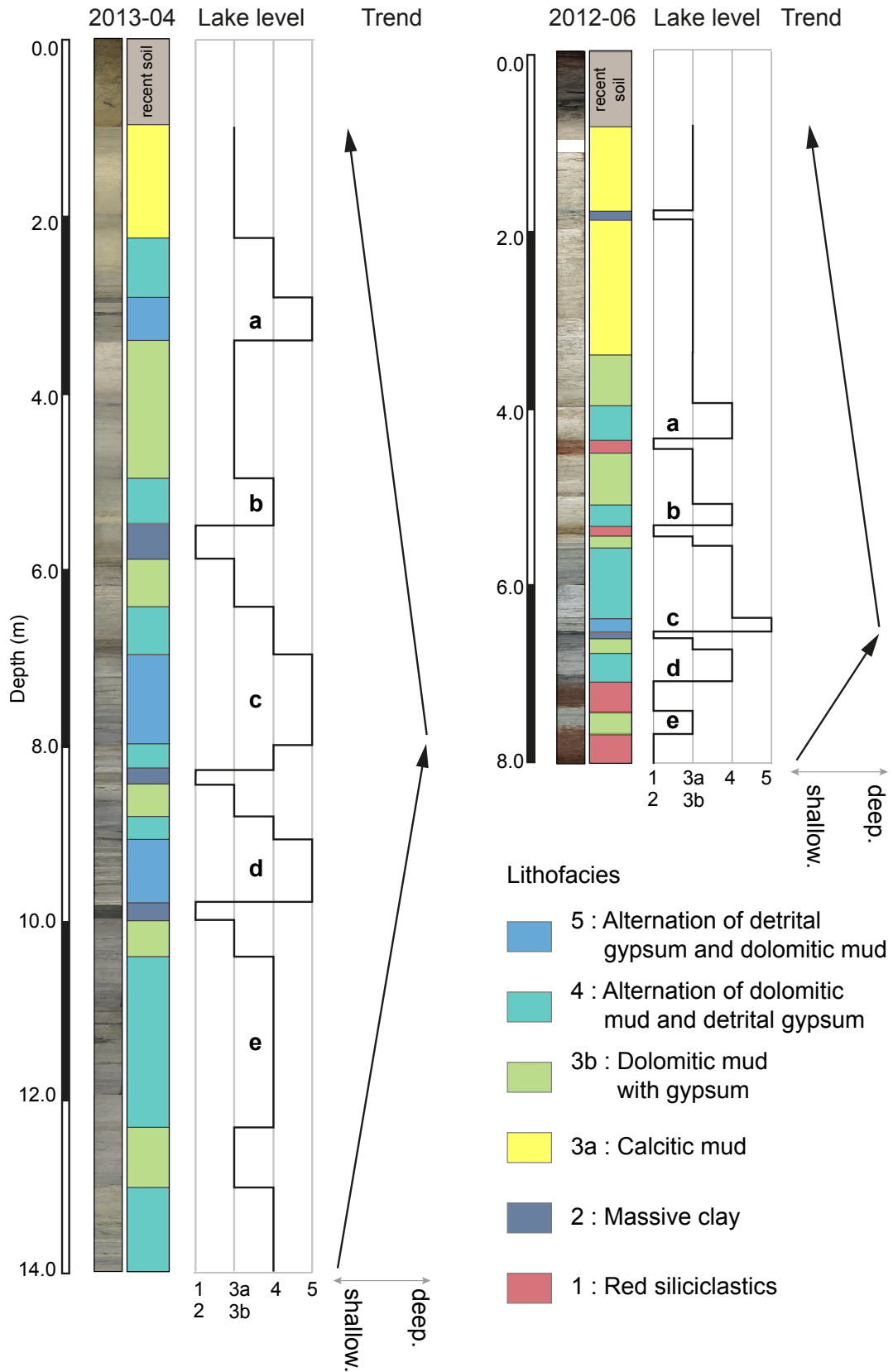


Figure 3.8.: See facing page.

a more carbonated or fresher trend to the top. This is controlled by changes in the groundwater/surface water ratio. The impact of saline subsurface waters becomes less important caused by the decreasing groundwater level during the Holocene at least since 7 ka BP, when Mediterranean conditions established in South Spain. Thus, sediments indicate fresher conditions although climate was less humid, due to reduced influence of saline groundwaters.

Comparison of the lithostratigraphy from the southwestern rim with a sediment core from the western margin (core 2012-06, see Fig. 3.8) revealed similar trends. The core contains additional fluvial deposits (lithofacies 1), deposited during the phases of low lake level. Five oscillations (a–e) have been identified, showing deepening and shallowing trends, with the deepest lake stage around 6.5 m sub-bottom depth. This correlates with the trend observed in core 2013-04. The similitude in trends around the lake margin discards local factors as controls of those observed changes. Thus, precipitation and evaporation, which is mainly influenced by solar irradiance/temperature and wind activity must be the main controls on sedimentation.

3.5.3. Implications for palaeoclimate

As already stated by prior palaeoclimate studies in the western Mediterranean, the Iberian Peninsula is prone to influence of Atlantic and Mediterranean circulation patterns and affected by climate oscillations (e.g., [Bout-Roumazeilles et al., 2007](#); [Cacho et al., 2001](#); [Martin-Vide and Lopez-Bustins, 2006](#)). Changes in lithofacies in sediment cores from LFP are showing distinct lake level oscillations. Five phases of lake level oscillations (a–e) have been identified, with c and b located at the Pleistocene to Holocene transition. Due to the tectonically inactive setting and the hydro-sensitive nature of the shallow basin, we stress out climatic variation as forcing of lake level oscillations. Thus the change in local hydrology could be induced by changes in precipitation, temperature or wind. Due to the uncertainty in the chronology, correlation with specific climatic events (e.g., North Atlantic Cold Events) is not possible. Nevertheless, those climatic events have been drawn for reference (see, Fig. 3.9 and references therein).

The history of Laguna de Fuente de Piedra shows an evolution characterized by three periods. From ca. 28 ka cal BP up to ca. 17.5 ka cal BP (oscillation e and prior to e), lake level oscillations were of low amplitude, the calcium content shows a decreasing trend, while the remaining elements rose. Correlative to these changes, the difference between summer and winter insolation reached a minimum. From ca. 17.5 ka cal BP until ca. 8.2 ka cal BP (oscillations d and c), lake level changes were of high amplitude (reaching the maximum and minimum levels for this record). Ca reaches its minimum value and the other elements their maxima. During this period, the difference between summer and winter insolation was maximum. From 8.2 ka cal BP until present (oscillations b and a), amplitude of lake level changes another time decreased. Thus, the Ca trend rises, whereas the remaining elements decrease coincidental with, a minimal difference in seasonal insolation.

There are few references covering the record since the Late Glacial Maxima in the western Mediterranean region. [Desprat et al. \(2013\)](#) concludes a cold and dry setting for the periods

(facing page) Figure 3.8.: Correlation of drill cores at the southwest shore (2013-04) based on multi-proxy observations resulting in different lithofacies (1–5) indicative for changes in lake level and for further correlation of a core from the west margin (2012-06), which shows fluvial deposits (1) as additional indicator for major changes in lake level. Variation in lake level (oscillations a–e) and the shown trend refers to overall palaeolake level evolution.

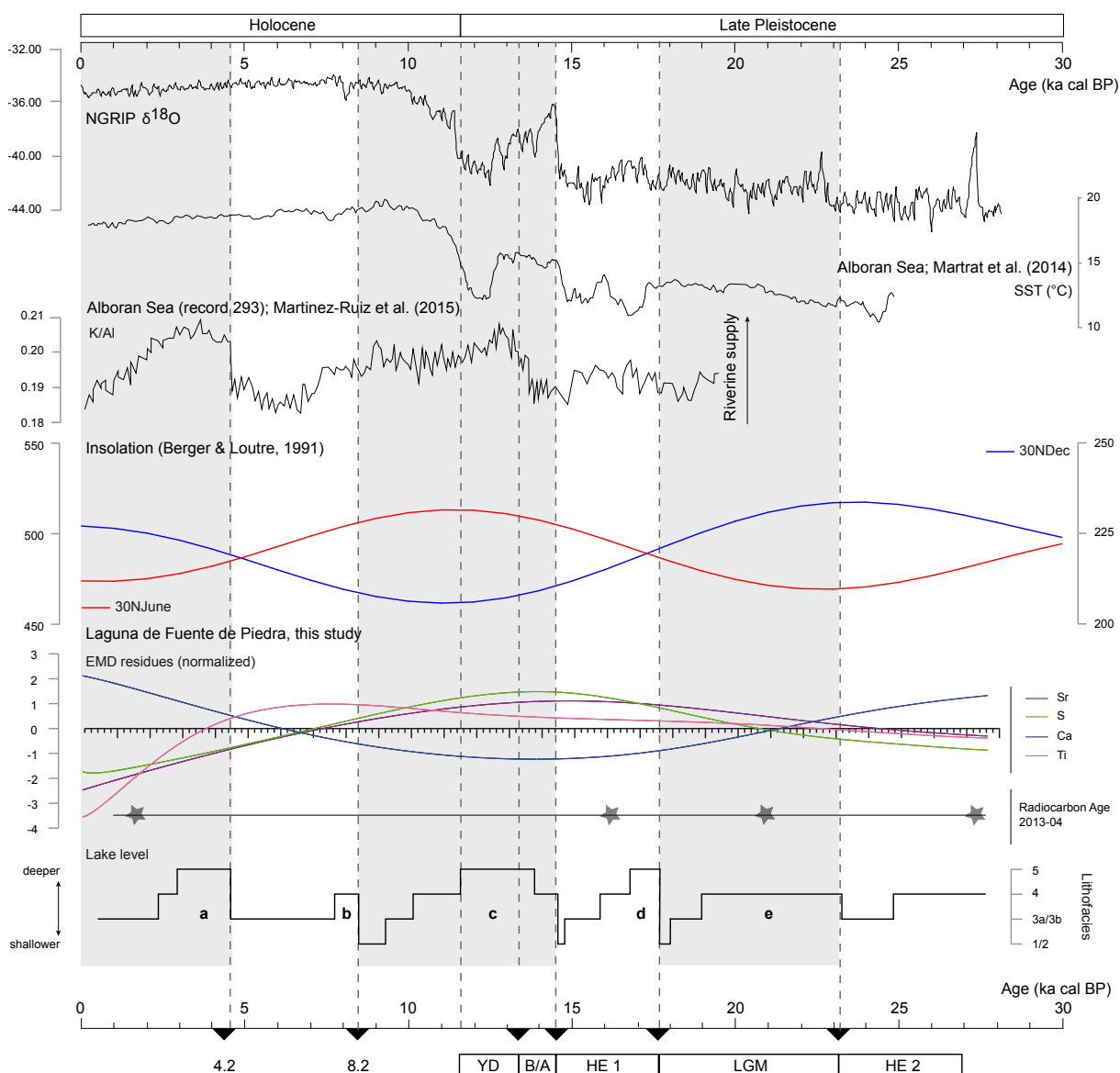


Figure 3.9.: Correlation of the Laguna de Fuente de Piedra palaeorecord with records from other studies from the western Mediterranean (see Fig. 3.1 for location) and NGRIP oxygen isotope data is plotted for reference (North Greenland Ice Core Project members [Rasmussen et al., 2008](#)). From Alborán Sea seasurface temperature ([Martrat et al., 2014](#)) and riverine input from K/Al ratio ([Martínez-Ruiz et al., 2015](#)) are shown. The insolation variability for June and December after [Berger and Loutre \(1991\)](#) are plotted (Data from IGBP PAGES/World Data Center for Paleoclimatology, NOAA/NGDC Paleoclimatology Program, Boulder, Colorado, USA.) Normalized residues of the empirical mode decomposition of elemental data (Ti, Ca, Sr, S) and reconstructed palaeolakelevel at LFP including a–e oscillations, are plotted for correlation. Radiocarbon samples used for the age model are indicated by grey asteriks. For reference climatic events like 4.2 and 8.2 ka Bond Events (([Bond et al., 1997](#)), Heinrich Events (HE; [Heinrich, 1988](#); [Hemming, 2004](#)), Last Glacial Maximum (LGM), Bølling/Allerød (B/A)), Younger Dryas (YD), etc. are plotted. Figure A.1 shows a former version this figure (see Appendix).

from 18.2 to 14.7 ka cal BP and 13.1 to 12.3 ka cal BP, while between 14.7 and 13.1 ka cal BP it is warmer and less dry. From 12.3 to 6.6 ka cal BP they interpret a more humid period that they relate to changes in winter precipitation, which are supposed to be controlled by variations in winter insolation. In particular, these authors propose that increased melting of the Laurentide Ice Sheet between 10 and 6.8 ka cal BP combined with weak winter insolation played a major role in the Mediterranean winter precipitation maxima during the early Holocene. They relate this effect to a more frequent southern position of the North Atlantic storm tracks than during the mid-to late Holocene.

Zielhofer et al. (2004) record high groundwater levels in the Medjerda basin (Tunisia) during the Bølling/Allerød, that they correlate to large-scale climate events like drifts in the polar vortex and an ‘interstadial mode’ in the North–Atlantic deep-water formation. Other high groundwater levels are reached between 11.8 and 6.6 ka cal BP. However, despite the similitude in periods, they relate this wet period to a maximum summer insolation that enhanced the contrast between land and sea. This induces an enforced influx of summer moisture into the Sahara and circumjacent regions. From that point onwards, the gradual decrease in summer solar insolation led to the aridification of the Sahara.

Brayshaw et al. (2011) simulated the climate for the last 12,000 years with special focus on the Mediterranean region attending, among other factors, to changes in insolation. The main features suggested for these experiments for the early Holocene (relative to the preindustrial climate) were an enhanced seasonality, the African Monsoon did not reach the Mediterranean coastline, and a weakening of the North Atlantic/European storm track and its associated surface westerly winds leading to a reduced precipitation in northwest Europe and increased winter precipitation over the Mediterranean. However, it must be noticed that these authors payed most of their attention to the eastern Mediterranean region. García-Alix et al. (2014) identified humid conditions for the Bølling period followed by dry and cold conditions at the Younger Dryas and a hydrologically stable phase during the early to mid-Holocene in Otiñar palaeolake (Jaén, S Spain).

In our case, the coincidence between the periods of lower amplitude variations in lake level with the minimum difference in seasonal insolation seem to point to a weaker seasonality leading to a minor hydrological contrast into the basin. However, the strongest seasonality during the transition to the Holocene could result in maximum hydrological changes as recorded in LFP. In addition, this period of stronger seasonality was also the wettest (averaged on time), when the deeper saline groundwater tables reached the surface, as evidenced by the general enrichment in sulphate and greater supply of siliciclastics.

3.6. Conclusions

3.6.1. Lithostratigraphy and lake margin model

The lacustrine infill at the southern tip of LFP is supposed to be thicker than 14 m, because the Triassic material has not been recovered during drilling. Sedimentological investigation of the sedimentary record of LFP revealed five main facies for the southern lake margin. In a conceptual lake margin model, three main repetitive lake stages (flooding, high water level, and low water level) have been introduced. Repetitions of the stages build up characteristic sedimentary successions creating the distinct lithofacies. From sedimentological analyses we conclude relative lake level changes. This variability is interpreted to represent an indicator for

the palaeohydrological history of LFP, which is a hydro-sensitive environment and any changes noted basin-wide are supposed to be controlled by climate. Due to the sensitivity, both short-term and long-term effects are stored in the LFP deposits.

3.6.2. Chronology

The age control has limitations, which can be related to three main factors: (i) complex hydrological flow patterns with influence of groundwater with variable mean residence time (modern to 27 ka), (ii) sulphate reducing bacteria activity, and (iii) reworking of old material from catchment. The maximum age shifts are correlating with allogenic-, clay-rich lithofacies that coincide with the transitional phases between lake level oscillations a–e. Those are supposed to be phases of flooding at LFP, when lake level is low and the runoff increases, dating ca. 4.5 ka cal BP, 9 ka cal BP, 14.8 ka cal BP, and 18 ka cal BP, under consideration of the suggested age model. An effect of groundwater with large mean residence times cannot be fully excluded. Other methods such as luminescence or palaeomagnetism (intensity, secular variations) have to be used in the future to crossvalidate the palaeoenvironmental findings and make the chronostratigraphic frame more robust and allow a more detailed comparison with other records.

3.6.3. Palaeoclimate

Five lake level oscillation phases have been described for the last approximately 25 ka, which have been revealed from lithofacies at the southern lakeshore. The late Pleistocene to the Holocene, in Laguna de Fuente de Piedra, is characterized by a transition from low amplitude to high amplitude lake level changes correlative to a rise in the deeper saline groundwater table. The Holocene, on its side, records the return to the low amplitude oscillations and a drop of the groundwater levels. These changes are correlative to changes in insolation as observed in other areas in the Mediterranean. So, the periods of low amplitude oscillations of lake level, low inputs of clastics and low groundwater levels (drier) coincide with periods of minimal seasonal insolation difference while the period of higher amplitude lake level oscillations, higher input of clastics and higher groundwater table (wetter) is correlative to a period of maximal difference between summer and winter insolation.

3.7. Acknowledgements

The authors thank two anonymous reviewers and the editor, Dominik Faust, for their comprehensive comments that substantially improved the manuscript. Furthermore, Manuel Rendón Martos (Director Conservador de la Laguna de Fuente de Piedra) for access to the LFP and support during field work including fruitful discussion is gratefully acknowledged. The authors greatly appreciate the cooperation of Klaus Kohfahl (Spanish Geological Survey, IGME Sevilla), who gave us access to his data and his experience with LFP was beneficial for our work. Javier Garcia Veigas is gratefully acknowledged for the introduction to the SEM at Barcelona University, as well as Martin Melles and Volker Wennrich (University Cologne) for their analytic and scientific support. Esther Sanz-Montero (Complutense Madrid), Melanie Leng (British Geological Survey, NERC Nottingham), and Blas Valero-Garcés (Instituto Pirenaico de Ecología, CSIC Saragossa) are acknowledged for the discussion during the ILIC Conference 2015. Last

but not least we thank Santiago Giralt (Institute of Earth Sciences Jaume Almera, CSIC Barcelona) for his helpful comments on the radiocarbon data. This study is a contribution to the Collaborative Research Centre 806 “OurWay to Europe”. The project CGL2011-30302-C02-01, financed by the Spanish Ministry of Economy and Competitiveness, has provided technical and scientific support to this research.

4. Lake Banyoles (northeastern Spain): A Last Glacial to Holocene multi-proxy study with regard to environmental variability and human occupation

This chapter is a slightly modified version of a published article:

Höbig, N., Weber, M. E., Kehl, M., Weniger, G.-C., Juliá, R., Melles, M., Fülöp, R. H., Vogel, H. and Reicherter, K. (2012). Lake Banyoles (northeastern Spain): A Last Glacial to Holocene multi-proxy study with regard to environmental variability and human occupation. *Quaternary International* 274: 205–218.

Abstract

Analyses of a 67-m long sediment core from Lake Banyoles (northeastern Spain) have revealed evidence for the palaeoclimate history of the northern Iberian Peninsula. Investigations have included high-resolution and non-destructive sediment-physical, geochemical, and optical methods to generate proxies indicative of sedimentologic variability and climate change. Primary stratigraphic control is based on ^{14}C and U-series dates of organic and inorganic material, as well as tephra from the Late Pleistocene Olot volcanic episode.

While preliminary ages obtained for the core base date back to approximately 60 ka, the Last Glacial Maximum (23–19 ka) interval ends at 15 m. The top 8 m of deposits accumulated in the Holocene. Several slump events were observed in the core section, as were microtectonic structures, which constrain the movement. Evidence for palaeoclimate variations in element ratios is interpreted to represent effects of Heinrich Events H0–H5. Associated changes in environmental conditions (e.g. humidity) may have affected human occupation during the Palaeolithic–Neolithic period. Implications on human occupation in northeastern Iberia due to climate changes are discussed from archeological findings and cave sediments in neighbouring areas and are analyzed with respect to the palaeolimnologic data of Lake Banyoles.

4.1. Introduction

Small and large-scale collapses of Northern Hemisphere ice sheets influenced the climate history on the Iberian Peninsula during the last glacial cycle. The associated changes in temperature, precipitation/humidity, and wind speed may have affected human occupation during the Palaeolithic–Neolithic period. Many studies focused on palaeoclimate reconstructions of the Iberian Peninsula during the Quaternary have used various sedimentary archives and proxies. Palynological studies of sequences from peat bogs or marshland e.g., Padul ([Pons and Reille](#),

1988; Peñalba, 1994) and a multi-proxy study from El Portalet peatbog (González-Sampérez et al., 2006) have shown Quaternary palaeoclimatic variability on the Iberian Peninsula may have been affected by North Atlantic and North African climate. Cave sediments like Cova de l'Arbreda (Burjachs and Renault-Miskovsky, 1992) or Carihuela Cave (e.g., Fernández et al., 2007), speleothems (e.g., Moreno et al., 2010), and travertines (e.g., Valero-Garcés et al., 2008) have also provided climatic information. Moreover, coastal environments as described from Gibraltar (e.g., Carrión et al., 2008; Cortés-Sánchez et al., 2008) and Atlantic as well as Mediterranean sediments (e.g., Bárcena et al., 2001; Cacho et al., 1999; Carrión et al., 2010; Combourieu-Nebout et al., 2002; Frigola et al., 2007; González-Donoso et al., 2000; Moreno et al., 2002; Sierro et al., 2005) have been subject of several working groups on Quaternary climate. Fluvial deposits in northeastern Spain (e.g., Fuller et al., 1996) and southeastern Spain (e.g., Schulte, 2002) have been investigated to estimate fluvial dynamics in the Mediterranean landscape. Furthermore, humidity variations during the Late Pleistocene have been deduced from loess-palaeosol sequences in southern Spain (e.g., Günster et al., 2001). Concerning lacustrine archives, several multi-proxy climatic records have been produced from palaeolakes or (saline) lakes in northern Iberia located in Ebro valley (e.g., González-Sampérez et al., 2008; Rodó et al., 2002; Valero-Garcés et al., 2000b, 2004) and Lake Estanya of the Pre-Pyrenees (e.g., Morellón et al., 2009; Moreno et al., 2012). From Lake Banyoles, palynological investigations of a 31 ka sedimentary record have been undertaken by Pérez-Obiol and Julià (1994). The vegetation changes observed during the Holocene in the Lake Banyoles core may be primarily related to changes in humidity (e.g., Valero-Garcés et al., 1998).

This paper presents a facies and an age model for Lake Banyoles for the Last Glacial and Holocene periods based on sedimentology, multi-sensor core logger (MSCL, e.g., Weber et al., 1997), X-ray fluorescence (XRF, e.g., Giralt et al., 2011), Fourier Transform Infrared Spectroscopy (FTIRS, Rosén et al., 2010, 2011; Vogel et al., 2008), and age dating (AMS ^{14}C , and U-series). A 67-m long sediment core (BAN II) from Lake Banyoles (northeastern Spain; see Fig. 4.1) was investigated to reveal the depositional and palaeoclimate history of the northern Iberian Peninsula using high-resolution and non-destructive sediment-physical, geochemical, and optical methods. Lake Banyoles is interesting, because the long-persisting lake serves as sedimentary archive, and a number of papers have been published with respect to palaeoclimate (e.g., Burjachs and Allué, 2003; Pérez-Obiol and Julià, 1994). However, the work presented in this paper is the first multi-proxy study covering the Last Glacial to Holocene. One aim is to compare the geochemical and geophysical data with palaeoclimate data of previous studies (e.g., Pérez-Obiol and Julià, 1994) and to obtain new palaeoenvironmental information from the Banyoles sequence.

The lake offers also a good geographical position for comparison with archaeological studies. Northeastern Iberia has a long and detailed archaeological record starting in the Middle Pleistocene (d'Errico and Sánchez-Goñi, 2003; Martínez et al., 2010; Saladié et al., 2008; Sepulchre et al., 2007). For instance, the rock shelter Cova de l'Arbreda records all major cultural technocomplexes from the late Middle Palaeolithic to the Magdalenian. The transitional phase from Middle to Upper Palaeolithic in Iberia is still under debate in Palaeolithic archaeology. Northeastern Iberia may have played played an important role in the arrival of anatomically modern humans on the Iberian Peninsula (e.g., Zilhao, 2006; Soler Subils et al., 2009; Maroto et al., 1996). It is generally expected that rapid climate changes affected the settlement pattern of hunter-gatherer populations in Iberia (Bradtmöller et al., 2012; d'Errico and Sánchez-Goñi, 2003; Schmidt et al., 2012; Sepulchre et al., 2007). Furthermore, impacts of climate change have been detected in cave sequences (Courty and Vallverdu, 2001) and might even have forced erosion of sediments in some archaeological sites in Portugal (Aubry et al., 2011). This paper

will discuss whether climate history as deduced from the Lake Banyoles core and other climate archives of the area is related to human settlement patterns in northeastern Iberia.

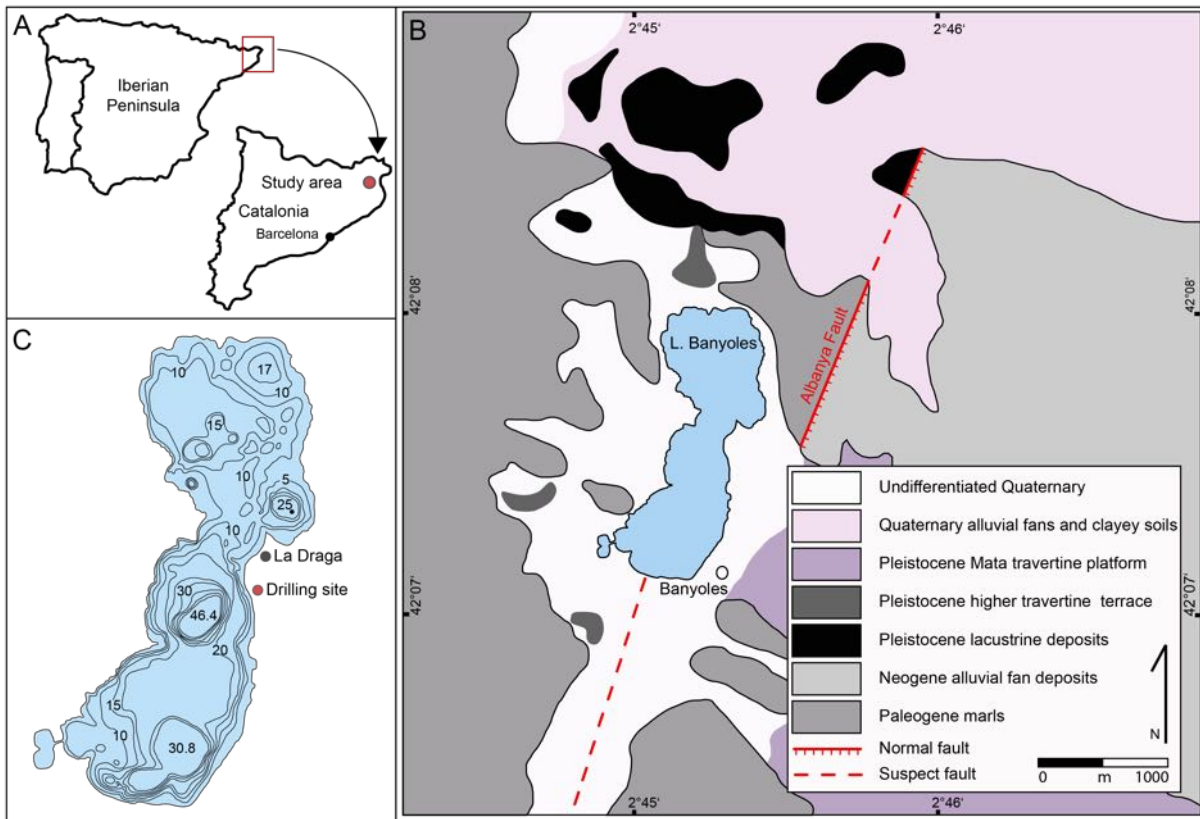


Figure 4.1.: (A) Location of the studied lake on the Iberian Peninsula in Catalonia, NE-Spain. (B) Simplified geological map of the Banyoles region (based on the geological map 1:50,000, [Barnolas 1989](#)). Lake Banyoles is situated at 172 m a.s.l. and surrounded by moderate to shallow topography. Two NNE-SSW trending normal faults influence the morphology and hydrology of the lake (after [Bischoff et al., 1994](#)). (C) Bathymetric map of Lake Banyoles (modified from [Moreno-Amich and García-Berthou, 1989](#)) shows two subbasins with several deeper lobes, which are attributed to the tectono-karst genesis ([Pérez-Obiol and Julià, 1994](#)). The depths of some dolines shown in the map are underestimated due to resuspended material from the bottom affecting seismic investigation. The maximum depth of the lake bottom reaches up to 46.4 m in the southern subbasin ([Canals et al., 1990](#)). The drilling site of the investigated sediment core is situated on the eastern margin close to the deepest lobe of the lake ($42^{\circ}07'29''$ N/ $2^{\circ}45'29''$ E). Northwards of the coring location the Early Neolithic site "La Draga" was excavated ([Tarrús, 2008](#)).

4.1.1. Previous studies

The potential of the karstic Lake Banyoles for palaeoclimatic studies in northeastern Spain has already been recognized by several geoscientific groups. [Pérez-Obiol and Julià \(1994\)](#) provided a U/Th- and ^{14}C -dated pollen record from core BAN II, showing evidence for Late Pleistocene interstadial conditions in the lowermost part (30–27 ka cal BP), followed by full glacial conditions

that ended abruptly at the beginning of the Bølling/Allerø daround 14.5 ka. These were followed by a late glacial sequence, including the Younger Dryas between 11.5 and 12.7 ka, a cold event around 11 ka, and a tree cover maximum around 6 ka. The correlation of Lake Banyoles to Lake Isli sequences (Meknes-Tafialet, Morocco; Valero-Garcés et al., 1998) contributed to the development of a palaeoclimate scenario for the wider Mediterranean mountainous area. Accordingly, major environmental changes at Banyoles correlate with the most recent Heinrich Events (H) recorded along the Portuguese Atlantic margin, namely H3 (27 ka), H2 (21–22 ka), H1 (13.5–15.9 ka), and H0 (10.5 ka; Valero-Garcés et al., 1998). Other, more general, climate reconstructions for Northern Iberian Peninsula are based on the vegetation cycle (e.g., Jalut et al., 2000; Leroy, 2008) Holocene climatic changes based on pollen ratios from several sites from SE-France to SE-Spain revealed, on several transects, evidence for six major changes in vegetation cover, corresponding to aridification phases around 9.5–9 ka, 7.5–7 ka, 4.5–4 ka, 3.7–3.3 ka, 2.6–1.9 ka BP, and 1.3–1 ka (Jalut et al., 2000). These phases correlate roughly with observations on humid and dry phases by Pérez-Obiol et al. (2011) who found evidence for a humid phase between 12 and 7 ka, a transitional phase between 7 and 5.5 ka (marked by a decreasing pollen concentration between 6.7 and 6 ka at Banyoles), and finally a phase of aridification from 5.5 ka until today. Moreno et al. (2012) studied the last glacial cycle in Iberia using multi-proxy analyses of lake sediments. Accordingly, Marine Isotope Stages (MIS) 4 was cold and humid until 60 ka; MIS 4 and 3 showed a tendency to aridity until 23.5 ka (Moreno et al., 2012), punctuated by Heinrich Events; MIS 2 was complex and highly variable at 23.5–14.6 ka, and divided into the global last glacial maximum (LGM; 23–19 ka), and the so-called "Mystery Interval" (18.5–14.6 ka), which surprisingly turned out to be the coldest and most arid investigated period. Deposits from Olot volcanic field, Lake Banyoles, and archaeological site Abric Romani cover the last 80 ka and have been studied by Burjachs and Allué (2003) for pollen and anthracological analyses. Their results tend to corroborate the results of Moreno et al. (2012) with a humid and cold MIS 4, a highly variable MIS 3 with abrupt and short climatic changes, and a dry and cold MIS 2 with steppe character. Burjachs and Allué (2003) compiled a synthetic pollen profile of the Last Glacial and Holocene for NE Iberia which indicates significant changes in arboreal pollen, Pinus, Poaceaea and Artemisia percentages during MIS 3 and 2, reflecting changes in plant assemblages including forests, riverside forests, prairies, and steppes. For MIS 3, several changes from warm to cool and from moist to dry conditions were detected. During the interval from 50 to 47 ka BP, low percentages in Pinus and arboreal pollen with concomitant increases in Asteraceae, Artemisia and Poaceae were interpreted as indicating the expansion of mixed steppe under cold and arid climate conditions. This phase was later correlated with Heinrich Event 5 (cf. to Burjachs et al., 2012). It was followed by a change to more humid and warm climatic conditions of Greenland Interstadial 12. Based on micro-mammal fossils, the mean annual temperature was estimated -5.7 to -5.4 °C lower than today, whereas the mean annual precipitation was about 150 to 60 mm higher (López-García and Cuenca-Bescós, 2010). Similar changes in pollen composition during MIS 2 at Lake Banyoles (Burjachs and Allué, 2003; Pérez-Obiol and Julià, 1994) suggest short-term vegetation changes triggered by climatic fluctuations, as for instance, the interstadial event was detected between 30 and 27 ka. A correlation of the dry and humid intervals reflected in the pollen spectra with Heinrich Events 4 to 1 remains unclear.

4.1.2. Physical lake characteristics

Lake Banyoles is situated in the Province of Girona, Catalonia, NE Spain (Figure 4.1, 42°07'N / 2°45'E, at 172 m a.s.l.) and it is part of a former wide spread Pliocene-Quaternary freshwater basin with intense carbonate precipitation (Julià Brugués, 1977). Lake Banyoles is 2130 m long and up to 750 m wide, resulting in a water-surface area of 11.80 km² (Canals et al., 1990; Casamitjana et al., 2006), which almost equals the catchment area of 11.42 km² (Fig. 4.1). The average water depth is 15 m, however, it varies significantly and shows maximum values of 46.4 m. Lake Banyoles is situated in an endorheic basin with no natural outflow; it has been characterized as a hydrologically open karstic lake (Valero-Garcés et al., 1998). Additionally, the lake basin is fault-controlled by the "Albanya Fault" (Abellà et al., 1985; Bischoff et al., 1994), which is trending N30E, and southerly situated fault segments (Fig. 4.1). The normal Albanya Fault has been further studied by Goula et al. (1999). It is situated 20 km N of Lake Banyoles and strikes NE-SW. In order to avoid confusion, the fault in Lake Banyoles has to be considered as a minor dextral strike-slip fault between two major normal faults: the Albanya Fault in the N and the Olot normal fault in the S (see Goula et al., 1999). Aligned collapsed dolines within the lake shape the lake bottom with several deeper depocenters (Fig. 4.1). A prominent collapse occurred on November 12, 1978, when a new basin called lagoon "Estanyol Nou" formed on the western shore (Abellà et al., 1985), demonstrating the active karst and collapse processes at Lake Banyoles. On account of the recent formation of sink holes, karstification is still ongoing in the study area (Julià Brugués, 1980). The N30E trending fault along the eastern shore of Lake Banyoles acts as a barrier for groundwater and induces upwelling (Abellà et al., 1985; Canals et al., 1990). Inflow into the lake primary results from 13 sub-bottom springs (Moreno-Amich and García-Berthou, 1989) that are fed by a relatively distant recharge area in the Olot volcanic field (20 km NW of Banyoles; Sanz, 1981). Both areas are connected by flows through the bedrock and therefore the water volume of the lake is regulated by precipitation in the recharge area as often typical for karstic systems.

The current humid Mediterranean climate is characterized by mean monthly temperatures of 23°C in July/August and annual precipitation of 750 mm in the study area (Pérez-Obiol and Julià, 1994). Location and intensity of the winter rain belt are the main factors controlling precipitation in this part of the Mediterranean region (Valero-Garcés et al., 1998). Modern vegetation includes evergreen oak forest and sparse beech forest at higher altitude.

4.1.3. Geology of Lake Banyoles

The formation of the lake is attributed to intense karstification, which is favoured by both the geological setting and the tectonic situation (Fig. 4.1). Northern Catalonia is a low to moderate seismic area linked to the Pyrenean Range. Some rare Holocene earthquakes have been described (Alasset and Meghraoui, 2005; Gutiérrez-Santolalla et al., 2005), which may have triggered mass flows in lakes alongside steep slopes (Morellón et al., 2009). Along the E-W trending Maladeta Fault, the Ribagorza Earthquake occurred in 1373 AD with a magnitude of M 6.2 (Olivera et al., 1994, 2006). The seismic hazard map of Catalonia shows intensities of MSK VII–VIII for the Banyoles region (Secanell et al., 2004), which may yield the potential of triggering mass wasting. Mainly three Eocene formations are important for the regional geology and karstification history. The Perafita Formation with 100–200 m thick dolomites of Late Ypresian age is overlain by the Beuda Formation, consisting of 200–300 m thick gypsum deposits that have been dated as Early Lutetian. The uppermost unit is formed by the Banyoles Formation, made up of marls of Late

Lutetian age, and covered by Quaternary terrigenous deposits (Bischoff et al., 1994; Martínez et al., 1997). Due to the contact of dolomite and gypsum, aggressive karstification takes place and the dissolution of the Beuda Formation causes several dolines that form the multi-basin lake close to the city of Banyoles. Water recharge regulates the intensity of re-suspension of lake bottom sediments. Discharge is mainly carried out by five artificial outlets on the SE-edge of Lake Banyoles (Serra et al., 2005).

The lake water is supersaturated in calcite causing precipitation, and constituting the main component of the lake sediments (Bischoff et al., 1994). An average sedimentation rate of 1 mm/a has been assumed by Pérez-Obiol and Julià (1994). According to the sedimentary facies, carbonate-rich littoral calcarenites and muds, capped by a peat layer, have been described (Valero-Garcés et al., 1998). These carbonates consist of up to 98 % of low-magnesium calcite with minor amounts of clays, quartz, and feldspar. Dominant biogenic components are charophytes, encrusting aquatic vegetation, gastropods, and ostracods.

Generally, total organic carbon (TOC) is <1 %, and total inorganic carbon (TIC) is much higher with sequences of pure calcite where TIC reaches more than 10 %. The sedimentary sequence is mostly composed of alternating coarse calcarenites and fine-grained biogenic carbonates that record changes in lake level and productivity (Valero-Garcés et al., 1998). Oxygen and carbon isotope studies on charophyte remains revealed small changes and relatively low values as would be expected in a hydrologically-open system dominated by groundwater input ($\delta^{18}\text{O}$, short residence time) and trends of vegetation changes (C3 vs. C4 plants), revealing a correlation of C3-plants with decreasing $\delta^{13}\text{C}$ (Valero-Garcés et al., 1998).

4.2. Methods

A 67 m long sediment core with a diameter of 10 cm was taken in PVC-tubes from the eastern shore of Lake Banyoles (Fig. 4.1) in the early 1990s, sliced in maximum 1.5 m long sections and stored in darkness at 6 °C. We investigated the sedimentary sequence of core BAN II continuously with non-destructive techniques and 366 equidistant samples with destructive methods, using a multi-parameter approach in order to quantify its biogeochemical and geophysical properties. In detail, we used the methods described below.

4.2.1. Sediment-physical properties

High-resolution geophysical data have been obtained on the entire BAN II core by Multi-Sensor Core Logger (MSCL) measurements. Core-logging included gamma-ray attenuation, p-wave velocity and magnetic susceptibility, LAB-colour and RGB-colour values, all measured at 1 cm increments (6000 measurements in total). From gamma-ray attenuation we calculated wet bulk density, dry bulk density and water content. Calibration and data processing was performed using MSCL software version 7 (Geotek, 2011) and the procedures described in Weber et al. (1997). Also a line-scan camera attached to the MSCL took high-resolution (ca. 500 dpi) surface images from each core and scanned also for RGB colours at the same resolution.

4.2.2. Total organic and inorganic carbon (TOC, TIC)

366 samples collected every 10 cm from core BAN II were selected for total organic carbon (TOC) and total inorganic carbon (TIC) measurements by means of Fourier Transform Infrared Spectroscopy (FTIRS; Rosén et al., 2010, 2011; Vogel et al., 2008). All FTIRS analyses were performed on a VERTEX 70 (Bruker Optics Inc.). Quantification of TOC and TIC concentrations by FTIRS is based on the latest calibration models introduced by Rosén et al. (2011). For sample treatment prior to analysis, measurement setups, and numerical analyses see Rosén et al. (2011). Groundtruthing of results obtained from FTIRS measurements is based on 20 TOC and TIC concentrations measured on selected samples with a LECO RC 412 carbon determinator. Strong correlation coefficients between FTIRS and conventionally measured concentrations for TOC ($r^2 = 0.99$) and TIC ($r^2 = 0.91$) prove the validity of the FTIRS results.

4.2.3. Geochemical composition by XRF analyses

Using a field portable X-ray fluorescence detector NITON XLt 700 series (FPXRF; Kalnicky and Singhvi, 2001), we determined geochemical properties non-destructively. In this instrument an X-ray tube with a silver target was operating for 30 seconds count time each measurement. A total of 1500 measurements were made in 2 cm intervals for approximately 30 m of the sediment core. This rapid method aimed at fast screening and identifying significant changes in geochemistry qualitatively and semi-quantitatively.

4.2.4. Additional sedimentological observations

Besides a general description of sedimentary structures for deducing depositional environments and events of re-deposition, a few random samples were inspected for the presence of ostracods, bivalves, and plant remains. In order to detect volcanic ash, smear slides were prepared with samples taken from selected layers and tested for the presence of volcanic glass shards using a polarization microscope.

4.2.5. Dating

Time control is essential for any kind of palaeoclimate reconstruction and for the calculation of sedimentation rates. The correlation of different archives, e.g., ice cores, marine or lacustrine deposits; or correlation of different proxies, e.g., pollen, geochemistry signatures, isotopic composition, archaeological findings, or tephra layers within an archive, depends on absolute dating. However, ^{14}C dating of lake sediments can have several errors, e.g. lake reservoir effect, hard-water effect and other, like inherited carbonate that we expect in Lake Banyoles. Absolute age dating of the sediments of Lake Banyoles was achieved by using Accelerator Mass Spectrometry radiocarbon (AMS ^{14}C) and U-series dating-techniques. Electron Spin Resonance (ESR) carried out by the University of Cologne did not reveal successful data, because of insufficient signals. AMS ^{14}C dating was performed at the newly-established Cologne Radiocarbon Laboratory. The peat sample (COL1089) underwent a standard AAA pre-treatment to remove contaminants, outlined in Rethemeyer et al. (2013). The shell sample (COL1088) was pre-treated using diluted H_2SO_4 whereas the bulk carbonate sediment samples (COL1159–COL1164) were analyzed without any pre-treatment (see Tab. 4.1). The carbon content of the organic samples

was released using an Elementar Analyzer, trapped on a zeolite trap, and graphitized using the newly developed AGE Graphitization System (Wacker et al., 2010b). Carbonate samples were graphitized using a newly developed hydrolysis system described in detail by Wacker et al. (2010a): carbonates are converted into CO₂ using 99 % H₃PO₄ in septum-sealed vials under helium atmosphere and directly connected to the aforementioned AGE graphitization system. Data were calibrated with CalPal (Danzeglocke et al., 2008).

The U-series dating technique was utilized in order to detect older ages, which were correlated with radiocarbon dates to generate a robust time control of the sedimentary sequence. Dates generated by U-series are reliable for sediments from Banyoles after Pérez-Obiol and Julià (1994) because of the authigenic deposition, high sedimentation rates in the system and no indicators for subaerial exposure. Hence, no secondary movement of uranium has contaminated the carbonates. The measurements were performed by α -spectroscopy, a conventional technique for this method (Bischoff and Rosenbauer, 1988).

Several identified volcanic glass shards of dispersed tephra layers, which are useful stratigraphic markers, have been incorporated in our accumulation rate calculation and correlated with tephrochronological frameworks of the Olot volcanic field (Cebrià et al., 2000).

4.3. Results

The results of the sedimentological description with core images and macrophotographies of details and the interpretation of the depositional environment are summarized in Figure 4.2. In general, two main units can be distinguished. An organic-rich layer on the top of the sequence, which is underlain by a carbonate sequence. The organic-rich bed consists of a several-cm thick peat and the carbonate sequence mainly consists of inorganic (endogenic precipitation) and biogenic (gastropods, bivalves, ostracods and encrusted Characeae) carbonates. We detected a calcite content of more than 95 %, which agrees with a low-magnesium calcite content of up to 98 % determined by Pérez-Obiol and Julià (1994) .

4.3.1. Facies

Based on detailed sedimentological core description and a few random fossil microscopic observations, ten different facies types have been identified in the Banyoles sedimentary sequence (Fig. 4.2), and are described here from bottom to top:

Facies **J** (66.1–67.07 m) consists of alternating dark and light carbonates with clay- and silt-size (Fig. 4.2, X) and is apparently laminated. A detailed view of this section is shown in Fig. 4.3. The sediments have tilted and opposite-inclining laminations, which are interpreted as a slump deposit. The core section below the sliding plane shows minor-scale normal faulting and shear planes with normal faulting (Fig. 4.3, A–C). The sliding plane is located at 66.8 m depth, both magnetic susceptibility and density values are higher underneath the slide horizon relative to the remainder of the core (apart from the peat). The calcium content is higher in light gray layers whereas the amount of titanium is lower compared to darker layers, where it is exactly opposite in the deepest part of the sedimentary sequence. These sediments might be deposited on the slope of the lake. Moreover, tephra has been found in this facies as evidenced by a few small glass shards.

The following facies **I** (56.0–61.2 m) consists of maximum 1-m thick fining-upward sequences with coarse sand- to fine gravel-size at the base and homogeneous clay containing plant remains

Table 4.1.: Conventional radiocarbon ages are reported in years before present (a BP), calculated according to *Stuiver and Polach (1977)*. The bulk peat was pre-treated by standard acid-alkali-acid extraction to remove carbonates and humic acids, shells were pre-cleaned with diluted sulphuric acid, and the bulk carbonate sediment was dated untreated. The U-series dates are reported in Isochron ages, corrected nominal ages in years before present (a BP). Calibration of radiocarbon ages was performed by CalPal (*Danzeglocke et al., 2008*).

Sample ID	Core depth (m)	Dating method	Material dated	Conventional age (a BP)	2 σ range	Calibrated age (a BP)	2 σ range
COL1089	2.8	AMS ^{14}C	C_{org} (peat)	4,593 \pm 30	4,563-4,623	5,367 \pm 66	5,301-5,433
no ID	5.00*	U-series		9,664 \pm 190	9,474-9,854	9,664 \pm 190	9,474-9,854
no ID	5.65-5.70*	U-series		11,410 \pm 100	11,310-11,510	11,410 \pm 100	11,310-11,510
COL1088	5.81	AMS ^{14}C	gastropod shell	14,341 \pm 67	14,274-14,341	17,511 \pm 253	17,258-17,764
no ID	8.70-8.78*	U-series		12,484 \pm 680	11,804-13,164	12,484 \pm 680	11,804-13,164
no ID	9.65-9.72*	U-series		14,423 \pm 410	14,013-14,833	14,423 \pm 410	14,013-14,833
COL1159	16.2	AMS ^{14}C	bulk carbonate sediment	18,503 \pm 64	18,439-18,503	22,113 \pm 311	21,802-22,424
no ID	18.54-18.61*	U-series		17,771 \pm 350	17,421-18,121	17,771 \pm 350	17,421-18,121
COL1160	20.3	AMS ^{14}C	bulk carbonate sediment	23,489 \pm 94	23,395-23,583	28,292 \pm 220	28,072-28,512
no ID	22.0-22.05*	U-series		19,878 \pm 110	19,768-19,988	19,878 \pm 110	19,768-19,988
COL1161	25.18	AMS ^{14}C	bulk carbonate sediment	30,164 \pm 175	29,989-30,339	34,370 \pm 158	34,212-34,528
COL1162	29.73	AMS ^{14}C	bulk carbonate sediment	30,315 \pm 175	30,140-30,490	34,586 \pm 195	34,391-34,781
no ID	31.70*	U-series		27,862 \pm 3000	24,862-30,862	27,862 \pm 3000	24,862-30,862
COL1163	35.36	AMS ^{14}C	bulk carbonate sediment	33,755 \pm 259	33,496-34,014	39,399 \pm 1090	38,309-40,489
no ID	43.75	U-series	bulk sediment	36,451			
no ID	55.6	U-series	bulk sediment	42,764			
COL1164	61.06	AMS ^{14}C	bulk carbonate sediment	44,643 \pm 864	43,779-45,507	47,998 \pm 1706	46,292-49,704
no ID	65.6	U-series	bulk sediment	51,448			

*from (*Pérez-Obiol and Julià, 1994*)




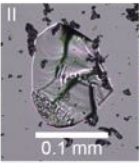


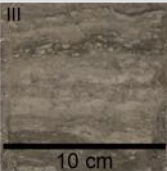



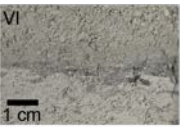

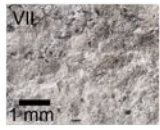



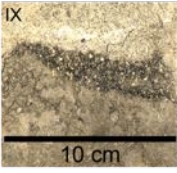
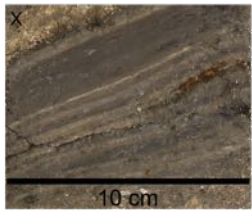
F	image	short description	details & depositional environment	
A		Palustrine wetland: Alternating peat & carbonates layers with bioturbation	subaerial swamp	
B		Bioturbated carbonates with gastropods (I) & plant remains (peat clasts)	shallow water	
C		Well layered carbonates with volcanic ashes (II), gastropods (< 1 cm), peat fragments, plant remains and a few coarser-grained (< 2 mm) carbonates		
D		Travertine developed under sublittoral spring to terrestrial conditions	terrestrial	
E		Bright and dark silty (wavy-) laminated and lenticular laminated (III) carbonates intercalated with large remains of Characeae (IV)	littoral	
F		Heterogeneous grey silty-clayey matrix with cemented angular fragments (< 10 cm) with Characeae (V), deformation feature like flame structure layers (VI) and plant remains (VII)		
G		Alternating carbonates: layered clay-size sediment and calcified Characeae	littoral	
H		Repeating thick (1-2 m) fining-upward sequences with Characeae and clay clasts at the base as deposits of low frequent changes in littoral to pelagial subenvironments		
I		Fining-upward sequences (max. 1 m with homogeneous clay with plant remains on the top) and a coarsening-upward sequence with clay clasts (redeposition?) and a sharp coarse layer	littoral vs. pelagial	
J		Fine lamination with inclined strata (X) interpreted as slump deposit	redeposition?	
			slope	

Figure 4.2.: High-resolution images of ten main facies types (A–J) composing the sedimentary sequence of Lake Banyoles.

on the top. Additionally, a coarsening upward sequence with clayey clasts indicative for re-worked sediment, and a coarse (coarse-sand size) sharp-bounded layer capping the top (Fig. 4.2, IX) has been identified in the core.

Further up in the sedimentary sequence, facies **H** (40.0–53.7 m) was developed, which includes thicker fining-upward sequences up to 2 m also intercalated with organic-rich homogeneous clays (Fig. 4.2, VIII) and Characeae remains in the coarser beds. Furthermore, facies **H** includes some clay clasts at the base, which could point to re-deposition.

Facies **G** (33.0–40.0 m) shows thin-bedded, alternating silt- and sand-sized carbonates with small Characeae remains. This facies is overlain by a heterogeneous deposit (facies **F**: 20.0–31.0 m) consisting of a clay- to silt-sized carbonate matrix with angular clasts. A sharp-bounded layer of plant remains (Fig. 4.2, VII) and flame structures (Fig. 4.2, VI) as well as inclined laminations are conspicuous in this sequence. This may indicate fast depositional/reworking events and is interpreted as slump deposit. Angular clasts are cemented sediments with abundant Characeae content (Fig. 4.2, V).

Further lake development generated facies **E** (20.0–17.0 m; 31.0–33.0 m; 53.7–56.0 m), consisting of coarse (fine gravel-size) calcified Characeae remains (Fig. 4.2, IV) in alternation with wavy-bedded or lenticular-bedded (Fig. 4.2, III) silt- to clay-size carbonates. These two main components have been developed in different sub-environments. Coarse-grained sediments were formed in a littoral setting, whereas fine-grained sediments likely developed in deeper water.

Facies **D** (17.0–16.0 m) contains travertine. This terrigenous, chemical deposit is embedded in the lacustrine carbonate sediments that show more yellowish colours above the travertine relative to the rest of this sequence. The travertine is likely generated from sub-aerial spring and of terrestrial origin. It is overlain by facies **C** (16.0–10.0 m), which consists of layered carbonate muds (silt- to sand-size). These sediments have some tephritic glass shards (Fig. 4.2, II), gastropods (Fig. 4.2, I), and plant remains. Their depositional sub-environment can be described as shallow water with changing oxic and anoxic conditions, and less bioturbation, which probably lead to partial preservation of laminae.

Compared to facies **C**, facies **B** (10.0–7.5 m) shows intensely bioturbated carbonate muds (sand- to silt-size) with small gastropods (< 1 cm) and plant remains.

Facies **A** (2.0–3.0 m) is constituted by a several-cm thick peat bed and bioturbated carbonates with high contents of peat clasts formed in a subaerial swamp.

The sedimentological differentiation of the ten facies types has been verified with geochemical and sediment-physical parameters (Fig. 4.4), including palaeontological remains, ashes, and density. The lowest value for potassium ($K = 2649$ cps) has been measured at 57.62 m depth, which belongs to facies **I**. In facies **H** the TIC maximum is ca. 13 % and was reached at 43.9 m core depth. A minimal density, which tends to 1 gcm^{-3} has been detected in an interval in facies **F** at 26.88 m (a much too low value in MSCL data). The highest reflection (145.17) was shown by facies **E** at 55.14 m depth. This facies shows in general higher values for L^* . These bright coloured sediments show highest amounts of Ca (497842 cps) at 54.38 m and K (150906 cps) at 53.95 m depth.

Facies **C** shows a TOC minimum (0.5 %) at 13.3 m core depth. In general, this facies has a high Ca content, which increases to the top of these strata opposite to the trend to TIC. This indicates that above the travertine (facies **D**) the inorganic carbon has not developed as CaCO_3 . As expected, travertine shows an abrupt increase of Ca and highest densities (2.41 gcm^{-3}) of the entire sequence at 16.22 m depth. The lowest Ca content (10885 cps) has been detected, as expected, in the organic rich layers at a depth of 2.76 m (facies **A**). At 2.8 m core depth, low

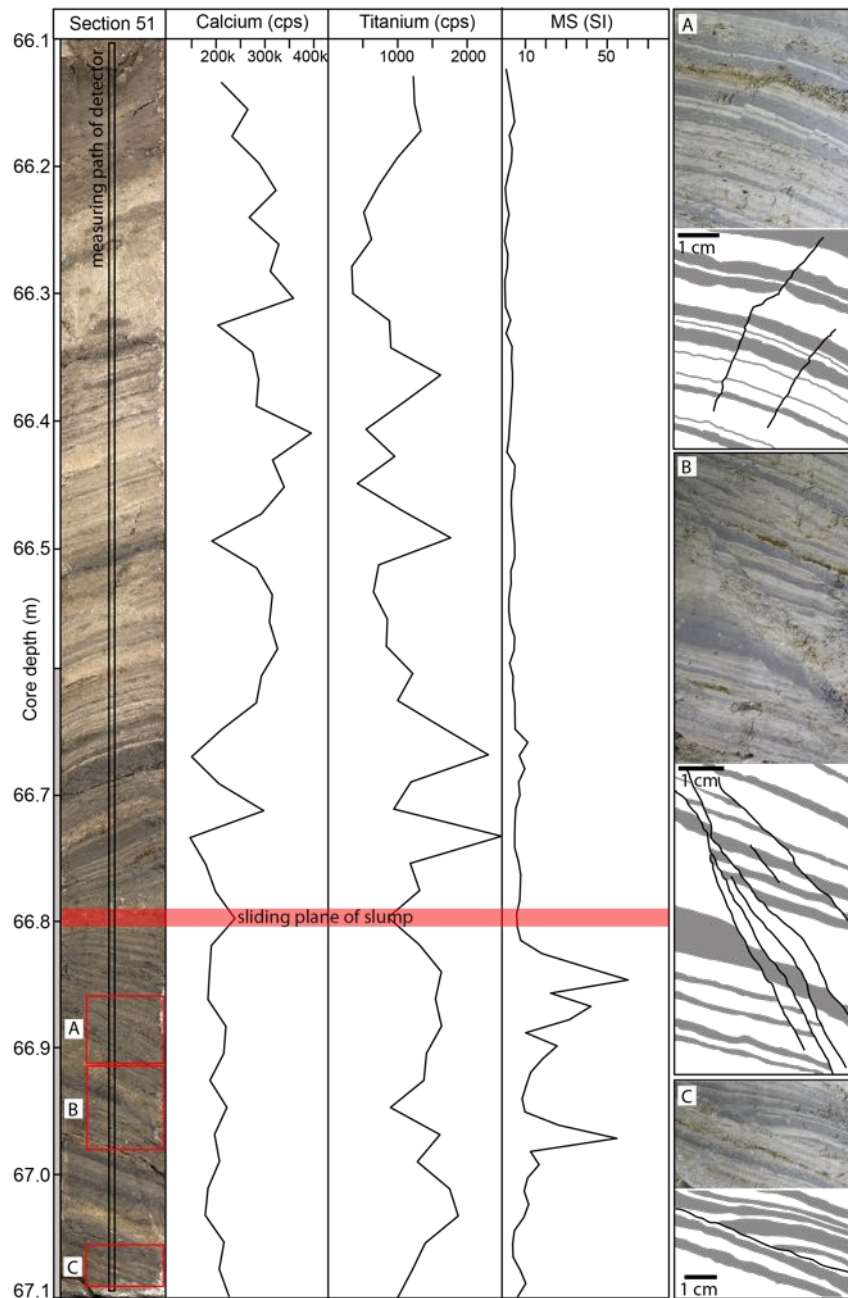


Figure 4.3.: The sedimentary sequence of facies J shows tilted and alternating laminated layers (between 66.1 and 67.1 m) probably due to a slump with a sliding plane at 66.8 m. Layers with light colors correlate with high calcium contents, whereas high titanium contents are found in dark layers in this laminated section. The magnetic susceptibility (MS) is lower above the sliding plane due to higher calcium content. The measurement path of the detector is marked with a black frame. Deformation features of the core section: A) domino-like normal faults developed below the slump deposit; B) shear bands and normal faults; C) sliding plane with folding evidencing soft-sediment deformation.

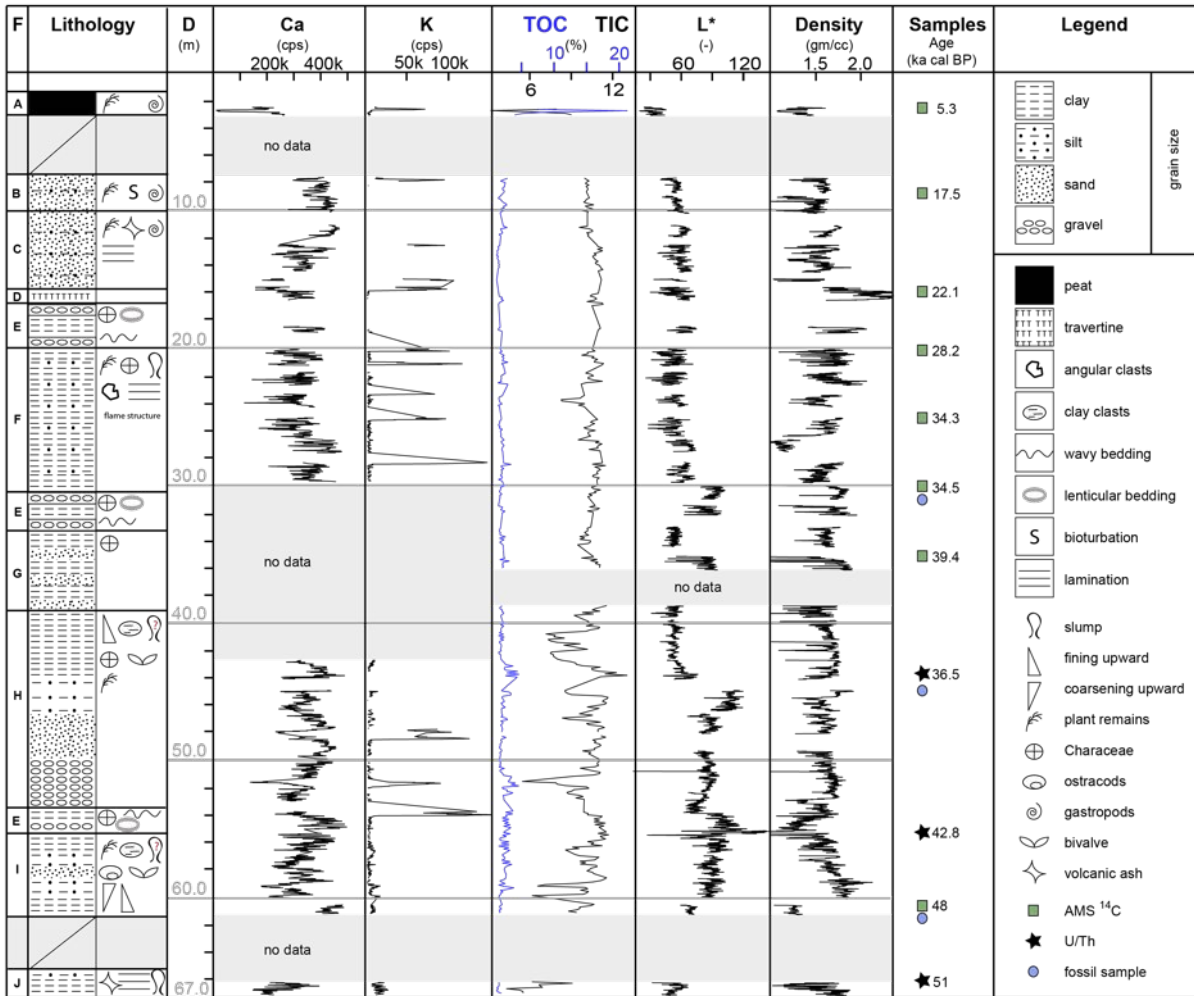


Figure 4.4.: Facies (F, see Fig. 4.2 for explanation), depth (D), lithology, sedimentary structures and fossils, calcium, potassium, total organic carbon (TOC), total inorganic carbon (TIC), L* (reflection) and bulk density results of the Banyoles Core (BAN II). Results of AMS ¹⁴C and U-series dating as well as sampling points for fossil and tephra analyses are listed.

Ca contents are accompanied by minima in TIC (3.2 %), maxima in TOC (21.5 %), and lowest reflection ($L^* = 19.48$).

In summary, the geochemical parameter Ca correlates with TIC as measured with FTIRS. Since gypsum was not detected macroscopically and FPXRF measurements yielded very low S values, Ca most likely reflects varying calcite contents of the sediments derived from precipitation. Low Ca contents may indicate periods of increased terrestrial material. This is partly indicated by concomitantly K contents, which are interpreted as tracers for terrestrial input in Lake Banyoles. Where we observe positive K excursions or peaks, Ca content diminishes.

4.3.2. Age models

To generate an age model of the Lake Banyoles sedimentary sequence, we measured eight AMS ¹⁴C and three U/Th ages. However, five samples taken for ESR dating in the uppermost 12 m of

the core did not produce reliable ESR dating results, although the sediments show remarkable fossil content. Moreover, for tephrochronology some glass shards were found in a core catcher sample between 11.04 m and 11.2 m depth which possibly correlate with the last eruption of Olot in 11.5 ka (Cebriá et al., 2000). Less and smaller glass fragments have been identified in 66.7 m core depth.

We observe a variation in ^{14}C and U/Th ages (Fig. 4.5 A), therefore we plotted conventional, calibrated and U-series ages. Whereas conventional data and U-series ages are plotted in linear interpolation (Fig. 4.5 A), the calibrated data are depicted in spline interpolation, whereby the age of sample COL1164 (Tab. 4.1) has been incorporated. COL 1164 is not considered in the linear interpolation of the conventional data (Fig. 4.5 A). All ages are given in calBP with the exception of the conventional ^{14}C data. Although calibrated ^{14}C age models are commonly used, we prefer the U-series age model, because we have no values for the correction of the lake reservoir effect in Lake Banyoles. Of course, sedimentation rates are depended on the age models and vary. The variation of the sedimentation accumulation rate is between ca. 50 cm and 250 cm per 1,000 years.

4.4. Interpretation and Discussion

For the complicated sedimentary history of core BAN II we have developed the following conceptual model of deposition. At the base of the core, facies **J** indicates laminated, partly re-deposited basinal and slope deposits. Facies **I** represents frequent low-amplitude lake-level changes, including coarsening-upward sequences indicative of re-deposition. A package of facies types (**H**, **G** and **E**) attests low to high frequent lake-level changes, interrupted by slump deposits (facies **F**). Clear terrigenous setting with sub-aerial spring activity (terrestrial conditions) is indicated by the thick travertine layer at 18 m core depth (see Fig. 4.4; facies type **D**). Facies types **C**, **B** and **A** reveal shallow-water to coastal environments with abundant bioturbation and swamp deposition.

4.4.1. Variabilities of depositional environments during the last 55 ka BP

The facies types (**A–J**) not only show several differences in their sedimentological characteristics (Valero-Garcés et al., 1998), but also include repetition of several layers, which may represent cycles of lake level changes. On the other hand, we found several indications of re-depositional events, which have not been described previously in core BAN II. We interpret those as slump

(facing page) Figure 4.5.: (A) Chronological models of the Banyoles sequence based on conventional and calibrated AMS ^{14}C and U-series dates including the chronology of Pérez-Obiol and Julià (1994), conventional AMS ^{14}C (green line) and U-series (black line) age models with linear interpolation, and calibrated AMS ^{14}C with spline interpolation (blue line). Identified volcanic glass shards and slump events are marked with shaded areas. Sediment accumulation rates (cm/ka) have been calculated for calibrated AMS ^{14}C data. Heinrich Events (H1–H5) after Hemming (2004) and Schmidt et al. (2012, for H2) are indicated in gray. (B) K/Ca ratio over time (green: conventional AMS ^{14}C age model; blue: calibrated AMS ^{14}C age model). (C) K/Ca ratio (black) and K + Ti + Fe/Ca + Sr ratio (purple) over time based on the U-series age model. See text for discussion.

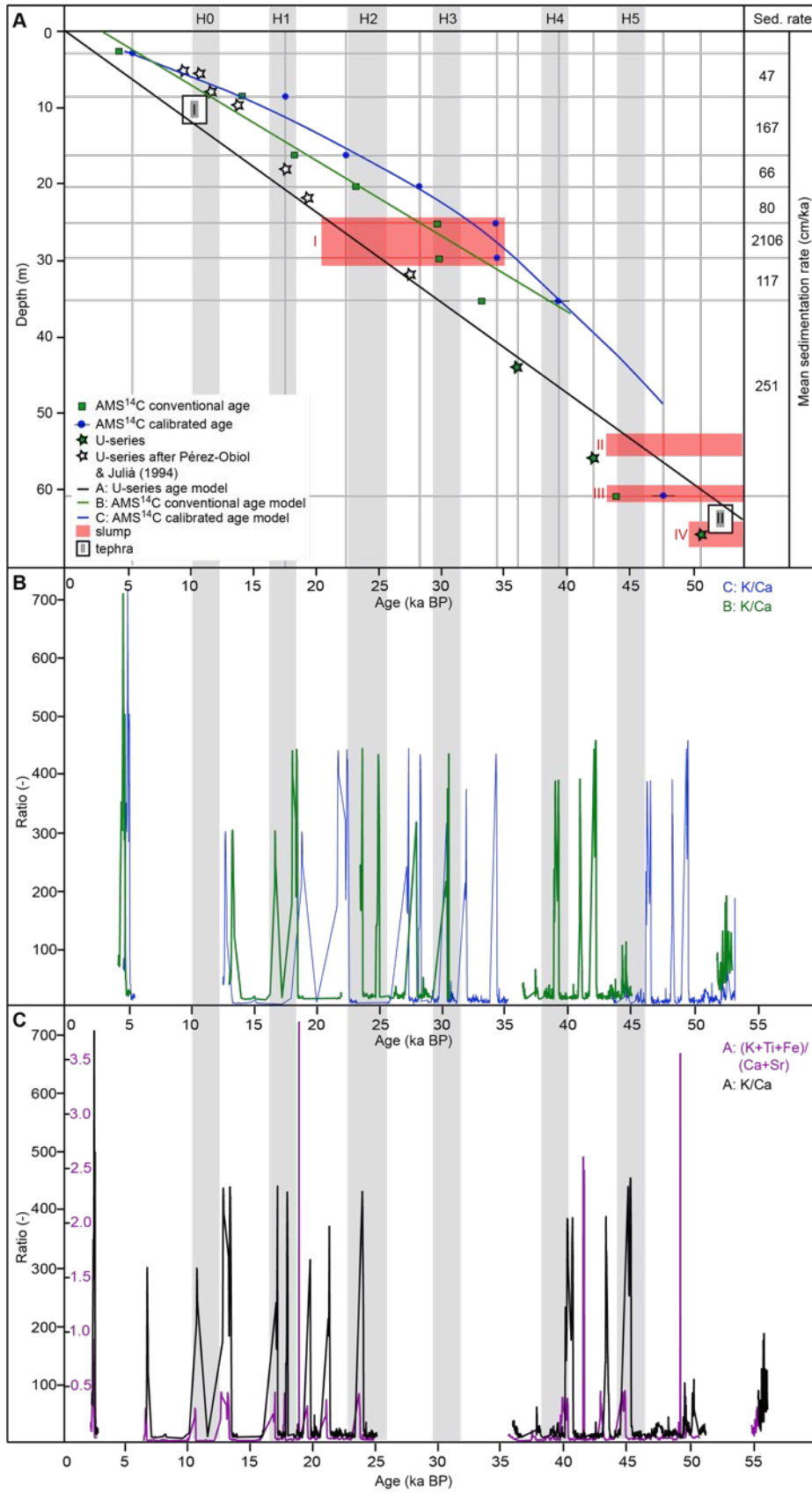


Figure 4.5.: See facing page.

deposits on the base of structural evidence such as normal faulting, folding, inversely inclined bedding planes or shear planes. It has to be noted that brittle domino-like normal faulting occurs in the lower section of the slump, which may be tentatively attributed to loading of the slump mass. But several factors could cause such movements in lakes and none of them can surely be excluded as trigger (e.g., seismogenic event; Secanell et al., 2004, or slope instability due to overload on the steep slopes). We suggest the most probable trigger involving the intense karstification and collapses during lake evolution may have caused these re-depositional events. Moreover, these slumped sediment package disturb significantly the age model and restricts the precision of Lake Banyoles as palaeoclimate archive. Compiling all available ages for core BAN II, we are able to establish an age/sedimentation rate model with average depositional rates of ca. 150 cm/ka (Fig. 4.5 A). However, depositional rates vary significantly from a minimum of ca. 50 cm/ka to approximately 250 cm/ka, whereas the rates peak in the slumped sections with ca. 2100 cm/ka. Previously published U-series ages for the upper core portion (approximately 30 m) by Pérez-Obiol and Julià (1994) revealed slightly younger ages, but with no remarkable differences in total estimated linear sedimentation rates. At around 11 m depth an ash layer of known age (ca. 11.5 ka; Cebrià et al., 2000) and provenance (Olot volcanic field) was identified and incorporated as data point in Fig. 4.5 A. For further verification of the geochemical fingerprint and origin of this material comparison with the geochemical composition of tephras from the La Garrotxa volcanic field is required. Nevertheless, taking the main wind direction into account, the source of volcanic input seems to be obvious. The process of transport and deposition is difficult to determine due to the fact that the tephra was unfortunately found in a core catcher sample. A new drilling of approximately 12 m depth would be a new chance to find a discrete layer in the sedimentary sequence.

Furthermore, we have chosen the K/Ca ratio in order to find terrigenous or lacustrine trends in the chemical analyses, where higher K-values are attributed to more terrigenous sedimentation because K is related to siliceous clay minerals or K-feldspars transported into the lake system by fluvial or aeolian processes (e.g., Haberzettl et al., 2008; Kylander et al., 2011, see also Fig. 4.4). The K/Ca ratio has been plotted against time (Fig. 4.5 B, C), as well as the $K+Ti+Fe/Ca+Sr$ ratio (Fig. 4.5 C), which reflects identical processes as the K/Ca ratio. We interpret only the peaks of relatively high ratios, so that smaller excursions are neglected. Using this ratio, we can observe a relatively good correlation with time intervals of Heinrich Events (Hemming, 2004; Schmidt et al., 2012, for H2), depending on the age models applied. Peaks or high ratio correlate with H1 to H4. H0 is slightly shifted to older ages, which may be explained in the age models. But if we take the Olot volcanic episode at 11.5 ka, also the H0 is nicely represented by the excursion of the K/Ca ratio. A major problem arises – if our assumption is correct; i.e., correlation of Heinrich Events with major peaks in the K/Ca ratio – when interpreting H5. However, that interval is intensely slumped (slumps II and III in Fig. 4.5 A), which may have led to younger ages and a shift in the excursion. On the other hand, since we observe further peaks around 4–5, 17, 27, and 52–53 ka (Fig. 4.5 B), it should be noted that many data gaps exist in these intervals (see Fig. 4.4). Applying the U-series age model we observe a shift of the peaks towards younger ages (Fig. 4.5 C), but again we find correlation with Heinrich Events. As a conclusion, the age model has to be refined, to directly link the observed peaks to different Heinrich Events.

Excursions of the K/Ca and $K+Ti+Fe/Ca+Sr$ ratios may tentatively be explained as phases of aridification (Fig. 4.6). Following Combourieu-Nebout et al. (2002) the climate in the western Mediterranean during Heinrich Events was characterized by aridification due to changes in atmospheric conditions, which affected the vegetation especially in the western Mediterranean. Hence, we suggest that the K-rich, terrigenous material was vulnerable to aeolian transport due

to periodical vegetational changes in this region, which have been primarily caused by changes in humidity identified also in other terrestrial records by several working groups (Fig. 4.6). Our hypothesis would be in agreement with the north Iberian vegetational history outlined by [Burjachs and Allué \(2003\)](#). Several phases of aridification have been described also in the Holocene ([Jalut et al., 2000](#); [Pérez-Obiol et al., 2011](#)), following the 6 ka maximum tree cover as proposed by ([Pérez-Obiol and Julià, 1994](#)). Full glacial periods and the LGM (23–19 ka after [Moreno et al., 2010](#)) are characterized by high Ca contents in sediments of core BAN II. Also, minor peaks at the very bottom of the core caused by laminated sediments of Facies J (Fig. 4.6) may fall into a “warm and cold alternating 1 ka cycles between 49.5 and 56,8.k” after [Burjachs and Julià \(1994\)](#). This deepest core interval has to be studied in more detail and with several additional proxies such as stable isotopes, which are in progress. However, the precision in the palaeoclimate reconstruction from core BAN II is restricted by processes like seismotectonic events, because the sedimentary archive is situated on an active fault, and in an area with ongoing karstification. Moreover, due to the location of the drilling site on the shore and not in the centre of the lake and identified re-depositional events, we cannot exclude a hiatus in this palaeoenvironmental record.

4.4.2. Implications for settlement patterns and cultural change in NE Iberia

The close correlation between maxima in the K/Ca -ratios and Heinrich events suggests that climate changes involving aridification and possibly cooling occurred in northeastern Iberia during the Last Glacial. These climate spells were probably accompanied by changes in vegetation cover from open forest towards mixed steppe ([Burjachs et al., 2012](#)). The question remains in how far these changes may have affected hunter-gatherer groups of Neanderthals and anatomically modern humans who were present in the area (e.g., [Grün et al., 2006](#); [Garralda, 2005](#)). There is an ongoing debate on the timing and causes of disappearance of Neanderthals in the Iberian Peninsula (e.g., [Vaquero, 2006](#); [Zilhao, 2006](#)) and also on the triggers of cultural change from the Early Upper Palaeolithic towards Solutrian techno-complexes attributed to anatomically modern humans. In northeastern Iberia different settlement patterns, possibly related to rapid climate change, are recorded in archaeological sites. Several sites contain Mousterian artifacts only, such as the cave sequences Cova del Gegant, Ermitons, Cova 120, Cova del Muricecs, Roca del Bous, Estret de Tragó, Moros de Gabasa and Fuentes de San Cristobal ([Schmidt et al., 2012](#)) or the open air site Mediona I ([Estévez et al., 1993](#)). These sites reflect a clear break in occupation between Mousterian and Early Upper Palaeolithic settlement. This kind of break was also postulated for the Cova Gran site, which includes finds from Early Upper Palaeolithic as well ([Martínez-Moreno et al., 2010](#)). Although numerical ages for most of the above mentioned sites, so far do not allow for a close correlation, this breakdown in occupation could be related to adverse climate conditions during H4. The Lake Banyoles core adds new evidence for such a dry and cold spell. At Abric Romani this probably shifted the major source of sediment towards aeolian inputs ([Courty and Vallverdu, 2001](#)). If we hypothesize that H4 went along with similar changes in vegetation cover like those documented for H 5 in the Abric Romani sequence ([Burjachs et al., 2012](#)), it would mean that an expansion of mixed steppes under cold and arid climate conditions may have been sufficient to cause, or at least promote, the disappearance of Neanderthals in northeastern Iberia.

Other archaeological sites document several technocomplexes such as Cova de l’Arbeda (Middle Palaeolithic to Magdalenian), Reclau Viver (Early Upper Palaeolithic to Solutrian), Abric Romani (Middle to Early Upper Palaeolithic) and Davant Pau (Gravettian to Solutrian). These

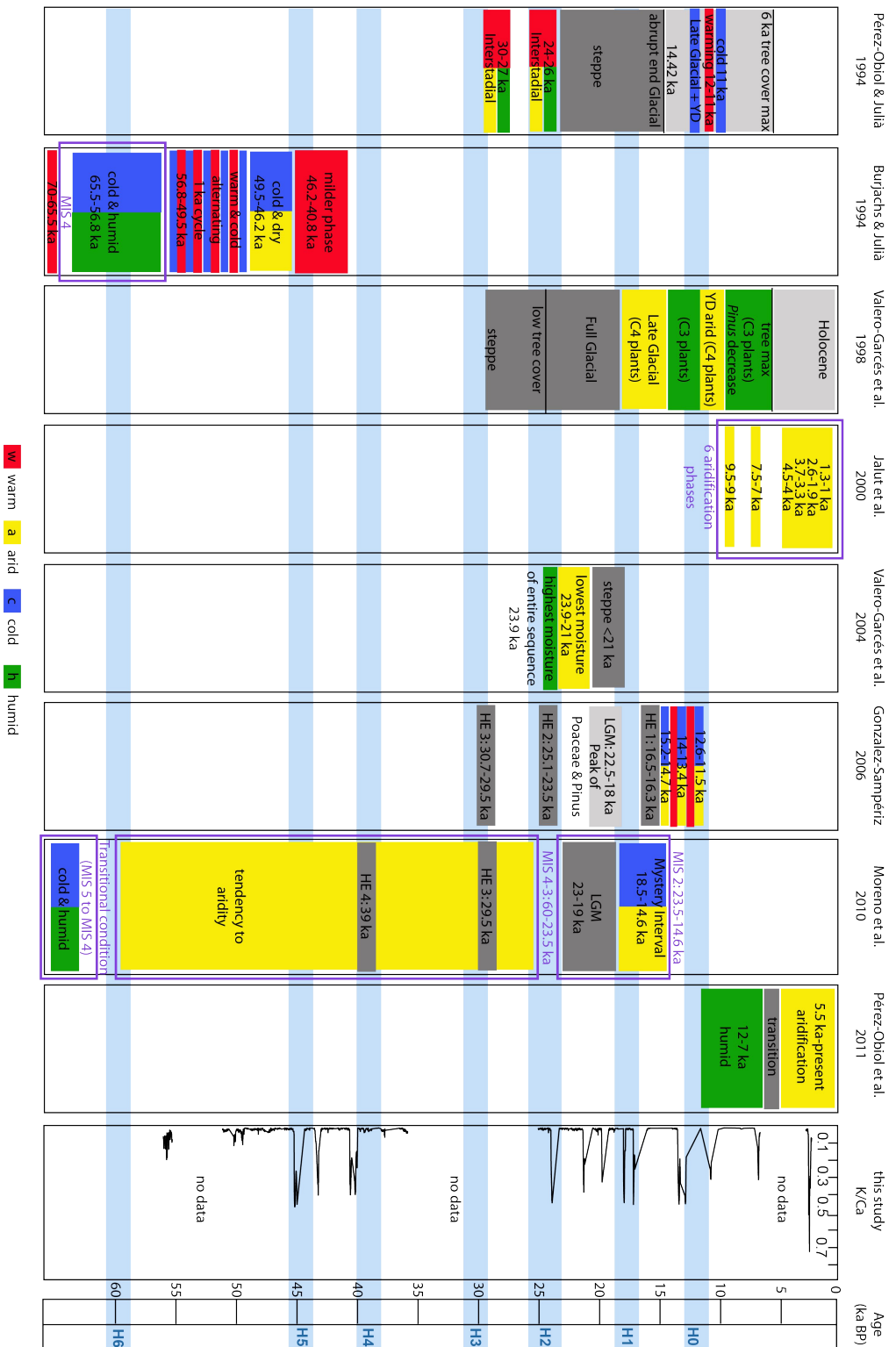


Figure 4.6.: Palaeoclimate data from several studies in Spain (Burjachs and Julià, 1994; González-Sampériz et al., 2006; Jalut et al., 2000; Moreno et al., 2010; Pérez-Obiol and Julià, 1994; Pérez-Obiol et al., 2011; Valero-Garcés et al., 1998, 2004) and the K/Ca ratio (based on the U-series age model; see Fig. 4.5 C). Heinrich Events (H1–H6) after Hemming (2004) and Schmidt et al. (2012, for H2).

sites reflect continuity of human settlement in northeastern Iberia. As based on the findings from the Lake Banyoles core the Upper Palaeolithic technocomplexes also experienced several abrupt climate changes during Heinrich Events 3, 2 and 1. If these triggered cultural changes in northeastern Iberia is difficult to say, given the comparatively low number of radiocarbon data available for the Upper Palaeolithic sequences. Besides more geochronological data, sedimentological reanalysis of the cave sequences may be of major importance for deciphering possible relationships.

4.5. Conclusions

The core BAN II from the littoral area of Lake Banyoles probably reaches down into MIS 4 covering large portions of the Last Glacial and the Holocene. We found a travertine layer in the sedimentary sequence at 17–16 m depth. This terrigenous, chemical deposit could be described as marker for the LGM (23-19 ka) due to the age model and the terrestrial origin (e.g., subaerial spring). The lithology and derived linear sedimentation rates suggest a more or less continuous accumulation of sediments, despite the identified re-deposition events, i.e. slumps. Several slumped units were detected, reflecting major reworking of lacustrine sediments. Collapses due to ongoing karstification, sediment loading or seismotectonic events would be feasible and require further investigations. Lake Banyoles in northeastern Spain serves as an archive for palaeoclimate proxies. Most of the accumulated sediments are carbonates that can be attributed to precipitation of calcite (> 95 %) from the water column, whereas higher K values are interpreted to point to more terrigenous influx into the lake. This K-rich, terrigenous material might be vulnerable to aeolian transport due to periodical vegetational changes in the region, which have been primarily caused by changes in humidity. These higher K values are tentatively interpreted as signal of individual Heinrich Events (Fig. 4.6), which are supposed to have affected the western Mediterranean. The presence of volcanic glass shards at around 11 m and ca. 67 m below surface can be attributed to the deposition of volcanic ashes. The ashes probably derive from the nearby volcanic field of Olot (Cebriá et al., 2000).

Furthermore, the Banyoles core BAN II presented can add important information on MIS 3 and MIS 4, which are partly covered both at the cave sequence at Abric Romani covering the time period from about 40 to 70 ka BP and in the earlier studies on Lake Banyoles, which provided a chronological framework down to about 31 ka BP and from 38–29 ka BP. High-resolution studies of stable isotopes of BAN II sections covering part of the MIS 3 appear to be most promising in this respect.

The new evidence on rapid climate changes in northeastern Iberia adds to the picture of a close correlation between climate change and population breakdown or cultural change during the Last Glacial. The close linking of sedimentary archives such as the one of Lake Banyoles to archaeological site sequences in Northeastern Iberia will be crucial for the interpretation of human settlement patterns in the Late Pleistocene.

4.6. Acknowledgements

This is a contribution to the CRC 806 (University of Cologne) – Our way to Europe. We would like to acknowledge Daniela Sprenk and Carsten Meyer-Jacob for FTIRS measurements and Dr. Finn Viehberg for checking the fossil content. Dr. B. Weninger (University of Cologne) helped

with the calibration of ^{14}C data and ages models. The support of Johannes Jakob during MSCL measurements and the assistance of Tabea Schröder and Daniel Kayser in laboratory work as well as Lee Clare for proof-reading are also gratefully acknowledged. Finally, we thank Juan Manuel López-García (Tarragona) and an anonymous reviewer for helpful suggestions, which significantly improved the manuscript.

4.7. A 60 ka Multi-Proxy Record from Lake Banyoles (Northeastern Spain): Extended data

This section is a slightly modified version of a published extended abstract:

Höbig, N., Weber, M. E., Kehl, M., Weniger, G.-C., Juliá, R., Melles, M., Fülöp, R. H., Vogel, H. and Reicherter, K. (2013). A 60 ka multi-proxy record from Lake Banyoles (Northeastern Spain): Extended data. In Baena, R., Fernández, J. J. and Guerrero, I., (editors): *El Cuaternario Ibérico: Investigación en el S. XXI : proceedings of the VIII Reunión del Cuaternario Ibérico*, pages 136–140, Sevilla - La Rinconada, Spain. AEQUA.

Abstract

In order to reveal evidence for rapid, short-term climate fluctuations on the Iberian Peninsula during the Late Quaternary, we performed a multi-parameter study of the 67-m long sediment core (BAN II) from Lake Banyoles (NE Spain). Our investigation included non-destructive sediment-physical, geochemical and optical methods to identify proxies which are indicative for variability in sedimentology which allude to changes in the environment. According to our age control based on AMS-¹⁴C, U- series and tephra from the La Garrotxa volcanic field our sedimentary sequence splits up into 52 m Pleistocene lacustrine deposits and approximately 15 m Holocene sediments on the top. The geochemical analyses revealed proxies (e.g., K/Ca) in the karstic system for climate variability during the Last Glacial. We attributed an increase in K/Ca to more terrigenous input into the lake. Under assumption of our U-series ages the peaks are supposed to represent the influence of Heinrich Events (HE 0-5) in northeast Iberia.

4.7.1. Introduction

Our work is part of the Collaborative Research Centre 806 (CRC 806 "Our Way to Europe") which aims at investigation of human dispersal from Africa to Europe and human-environment interaction. According to this, our study focuses on sediment records which are geographically closely related to archaeological sites and scopes on detection of rapid, short-term climatic variabilities (e.g., Heinrich Events or Dansgaard/Oeschger cycles) which might have influenced human population on the Iberian Peninsula. The Iberian Peninsula is of great interest for palaeoclimate research due to a high sensitivity to climate changes. The geographical and atmospheric conditions which are characterised on one hand by the adjacency of subpolar/subtropical latitudes and on the other hand westerly winds/N-African climate (Moreno et al., 2005) highlight Iberia for palaeoclimatic studies. High frequent climate variability is known from the last glacial period (e.g., Heinrich Events, Dansgaard/Oeschger cycles), but in order to understand the entire mechanism and impact on the environment/humans, further studies are required. Despite the large-scale records generated from marine sediments (e.g., Bond et al., 1997) and ice cores (e.g., Rasmussen et al., 2008) additional studies from terrestrial archives (e.g., lakes, peat bogs etc.) provide excellent palaeoenvironmental information. This is conditioned mainly by two properties: the rapid response of lakes to external and internal forcings and high sedimentation rates in lacustrine systems (Battarbee, 2000). These facts allow high-resolution studies concerning the impact on environment and humans on a more local scale. Although Iberia does not include typical lake countries several promising terrestrial archives for the Late Quaternary period have been investigated (e.e., Moreno et al., 2012) or are still under investigation.

Especially endorheic basins which are related to karst processes due to the all-round evaporites in Spain (e.g., [Gutiérrez et al., 2002](#)) are promising for palaeoclimate studies. The karstic Lake Banyoles (northeastern Spain) has been investigated in this study and furthermore several endorheic basins (lagunas) in the Antequera region ([Schröder et al., 2013](#)) are under investigation by our working group. For Lake Banyoles chemical proxies which might correlate with short-term climate fluctuations (here Heinrich Events) have been identified.

4.7.2. Situation

Lake Banyoles is located in Catalonia, northeastern Spain (Figure 4.1A; 42°07'N/2°45'E). The formation of the lake is attributed to intense karstification which is favoured by the regional geology and the tectonic setting. After [Goula et al. \(1999\)](#) the tectonic influence is mainly realised by two normal faults, one segment north of the lake (Albanya Fault) and the other one in the south (Olot Fault). The fault in Lake Banyoles is considered to be a minor dextral strike-slip fault between these two major normal faults. Mainly three Eocene formations are of interest concerning lake development. The Perafita Formation dated as Late Ypresian consists of 100-200 m thick dolomites which are overlain by 200-300 m thick gypsum deposits of Early Lutetian age (Beuda Formation). The uppermost units are Late Lutetian marls (Banyoles Formation) which are covered by Quaternary terrigenous deposits ([Bischoff et al., 1994](#); [Clavell, 1991](#), Figure 4.1B). The contact of dolomite and gypsum favours an intense karstification which led to the formation of multiple dolines. Due to ongoing karst processes ([Julià Brugués, 1980](#)) and the tectonic setting these dolines merged together and formed the approximately 12 km² large multi-basin lake (Figure 4.1C). The bathymetric map ([Moreno-Amich and García-Berthou, 1989](#)) shows two subbasins with several deeper depocentres. The N30E trending fault along the eastern shore of Lake Banyoles acts as a barrier for groundwater and induces upwelling ([Abellà et al., 1985](#); [Canals et al., 1990](#)). The water rechargement is mainly realised by 13 subbottom springs fed by the distant La Garrotxa volcanic area through a karst system. The lake water is supersaturated in calcite which causes precipitation. The main component of the lake sediments is endogenic calcite ([Bischoff et al., 1994](#)). In the 1990s a 67-m long sediment core (BAN II) has been drilled at the eastern shore of the lake (Figure 4.1C) and stored in 1.5 m sections in darkness at 6°C. Based on that material we generated a multi-proxy record from Lake Banyoles in high resolution. An additional benefit of this study for the CRC 806 might be achievable due to the small distance to several important archaeological sites (e.g., Cova de l'Arbreda). The correlation of various archives that have been investigated by different disciplines (e.g., geology, archaeology) is one approach of the project.

4.7.3. Methods

The sedimentary sequence of the BAN II-core was investigated continuously with non-destructive techniques and 366 equidistant samples with destructive methods, using a multi-parameter approach in order to quantify its (bio-) geochemical and sediment-physical properties (Figure 4.7). The (bio-) geochemical data contain elemental composition detected with a Field Portable X-Ray Fluorescence measurement device (FPXRF; NITON XLt 700 series). This tool was used again to close the measurement gap in the data set of the BAN II core published in [Höbig et al. \(2012\)](#). Furthermore, the total (in-) organic carbon content (TIC/TOC) has been detected by Fourier Transform Infrared Spectroscopy (FTIRS; Bruker Optics Inc. VERTEX 70; see [Vogel et al., 2008](#)). For calibration of the FTIRS-data 20 samples have been analysed with the LECO RC

412 carbon determinator. Sediment-physical properties were generated with a Multi-Sensor Core Logger (MSCL, Geotek) including gamma-ray attenuation (wet bulk density, dry bulk density, water content), p-wave velocity, magnetic susceptibility, LAB-colour and RGB-colour (Weber et al., 1997). Additional sedimentological observations (fossil, volcanic glass shard content or re-depositional events etc.) have been documented for the sequence. For detailed description see methods in section 4.2.

4.7.4. Data

The data published in Höbig et al. (2012) has been extended and the new record is presented in this abstract. The former published data has a measurement gap from around 30.00 m to 43.00 m. The geochemical data of this study includes further 10 m and only gaps from around 36.00 m to 39.00 m due to core loss during the drilling process (Figure 4.7). Age control of our

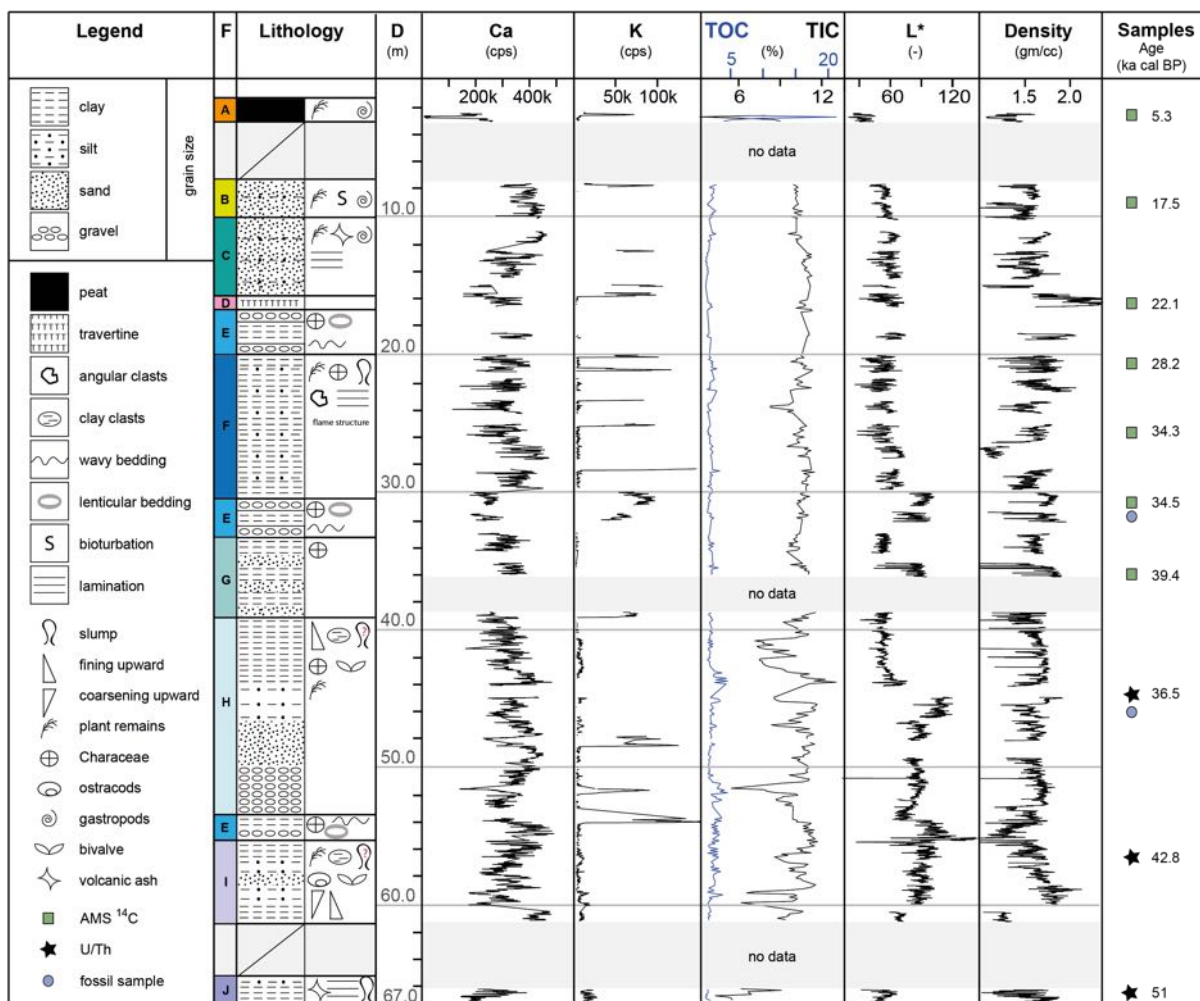


Figure 4.7.: Same proxies shown as in Figure 4.4. Geochemical data (Calcium & Potassium) has been extended for section 30–43 m.

sequence has been attempted by several techniques (e.g., Electron Spin Resonance, Radiocarbon, U-series, tephrochronology). The Accelerator Mass Spectrometry Radiocarbon ages (AMS-¹⁴C)

and U-series dating revealed good results. Furthermore, tephra from the Olot volcanic episode dated around 11.5 ka (Cebriá et al., 2000) has been included in the age control as additional indicator. Finally, we decided to use the U-series age model as most robust chronology for the record (Figure 4.8A) and to apply this model on our proxies.

4.7.5. Interpretation

Our record includes high-resolution and non-destructive sediment-physical, geochemical and optical methods to determine proxies indicative of changes in sedimentology and climate. While the absolute datings result in maximum ages of approximately 60 ka at the core base, the Last Glacial Maximum (LGM; 23–19 ka) interval ends at 16–15 m depth as indicated by a travertine layer embedded in the lacustrine sediments. The Holocene is represented by an several meter thick deposit which consists mainly of palustrine carbonates and peat on the top. Several slump events were observed in the core section, as were microtectonic structures, which constrain the movement. Evidence for palaeoclimatic variabilities have been revealed by element ratios (e.g., K/Ca; $(K+Ti+Fe)/(Ca+Sr)$) calculated from FPXRF-data. The elements Potassium (K), Titanium (Ti) and Iron (Fe) were attributed to more terrigenous input into the lake system whereas Calcium (Ca) and Strontium (Sr) were attributed to a more lacustrine trend (e.g., carbonate precipitation from lake water). The increase in terrigenous material might be realised by two processes: fluvial or aeolian (e.g., Haberzettl et al., 2008; Kylander et al., 2011). Based on the developed U-series age model these calculated ratios show several peaks which correlate relatively good with the time intervals of Heinrich Events (Hemming, 2004; Schmidt et al., 2012). Also the extended geochemical dataset supports the hypothesis of a correlation between Heinrich Events (now including HE 3) and our chosen proxies. Furthermore, one peak in our data might correlate with the Last Glacial Maximum interval (23–19 ka; Moreno et al., 2010). Hence, our ratios have been interpreted as proxy for glacial cold events, Heinrich events (HE 0–HE 5). If we consider that during Heinrich Events the Iberian climate was much colder and more arid (e.g., Combourieu-Nebout et al., 2002) the terrigenous input might be caused by deflation due to vegetational changes (e.g., Jalut et al., 2000) and intensified westerly winds which are influenced by the Northern Atlantic Oscillation (NAO; e.g., Cullen et al., 2001).

4.7.6. Conclusions

Reviewing the applied dating methods we conclude, that for Electron Spin Resonance (ESR) the signal was insufficient, for radiocarbon ages the unknown hard water effect caused uncertainty and tephra from the Late Pleistocene La Garrotxa volcanic episode was only used as additional indicator in the age control. Finally, we decided to use the U-series age model as most robust chronology for the record, due to the authigenic deposition, which makes secondary movement of Uranium unlikely. The extended geochemical data which closes the gap for Heinrich Event 3 maintains our hypothesis, that the K/Ca ratio might be a proxy for short-term climatic fluctuations on the Iberian Peninsula during the last 60 ka. Hence, northeastern Spain seems to be affected by North Atlantic abrupt cold events during the last glacial.

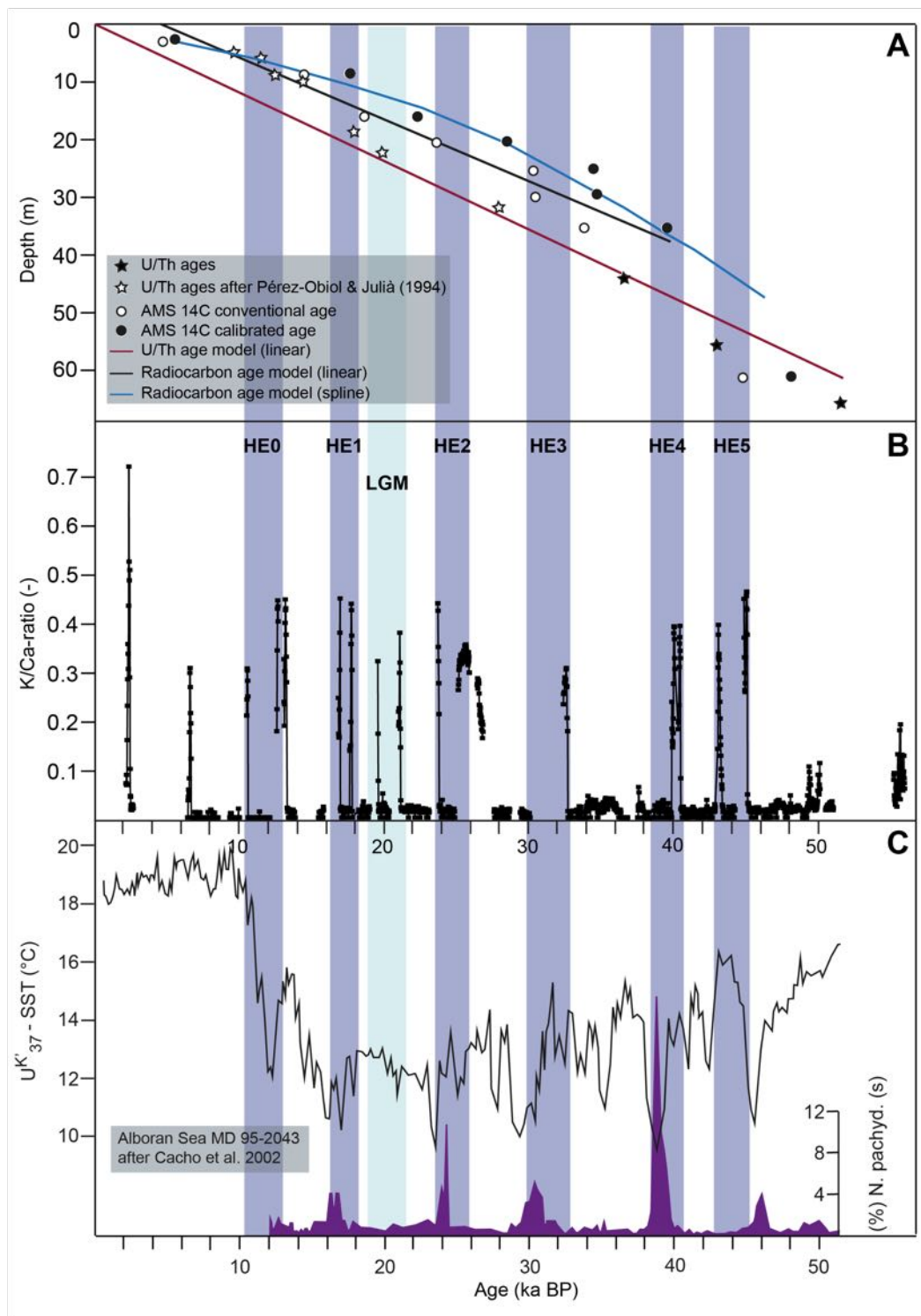


Figure 4.8.: (A) Age models as presented in Höbig *et al.* (2012, see also chapter 4, Figure 4.5). (B) extended Potassium/Calcium ratio data. (C) Proxies from Alboran Sea core (MD 95-2043; Cacho *et al.*, 2002) are plotted for reference.

5. Western Mediterranean climate and environment since Marine Isotope Stage 3: a 50,000 year record from Lake Banyoles, Spain

This chapter is a slightly modified version of a published article:

Lacey, J.H., Leng, M.J., Höbig, N., Reed, J.M., Valero-Garcés, B. and Reicherter, K. (2015). Western Mediterranean climate and environment since Marine Isotope Stage 3: a 50,000-year record from Lake Banyoles, Spain. *Journal of Paleolimnology*.

Abstract

We present new stable isotope ($\delta^{18}\text{O}_{\text{calcite}}$ and $\delta^{13}\text{C}_{\text{calcite}}$) and diatom data from a 67-m sediment core (BAN II) from Lake Banyoles, northeastern Spain. We reassessed the chronology of the sequence by correlating stable isotope data with a shorter U-series-dated record from the lake, confirming a sedimentological offset between the two cores and demonstrating that BAN II spans Marine Isotope Stages (MIS) 3 to 1. Through comparison with previous records, the multi-proxy data are used to improve understanding of palaeolimnological dynamics and, by inference, western Mediterranean climate and environmental change during the past ca. 50,000 years. Three main zones, defined by isotope and diatom data, correspond to the MIS. The basal zone (MIS 3) is characterised by fluctuating $\delta^{18}\text{O}_{\text{calcite}}$ and benthic diatom abundance, indicating a high degree of environmental and climate variability, concomitant with large lake-level changes. During the full glacial (MIS 2), relatively constant $\delta^{18}\text{O}_{\text{calcite}}$ and a poorly preserved planktonic-dominated diatom assemblage suggest stability, and intermittently, unusually high lake level. In MIS 1, $\delta^{18}\text{O}_{\text{calcite}}$ and $\delta^{13}\text{C}_{\text{calcite}}$ initially transition to lower values, recording a pattern of Late Glacial to Holocene change that is similar to other Mediterranean records. This study suggests that Lake Banyoles responds limnologically to changes in the North Atlantic ocean-atmosphere system and provides an important dataset from the Iberian Peninsula, a region in need of longer-term records that can be used to correlate between marine and terrestrial archives, and between the western and eastern Mediterranean.

5.1. Introduction

The Iberian Peninsula, located to the west of the Mediterranean basin, is a key location for understanding climate connections between the eastern and western Mediterranean ([Roberts et al., 2008](#)) and interactions with North Atlantic climate dynamics. The understanding of past climate variability across the peninsula itself has improved considerably over the last two

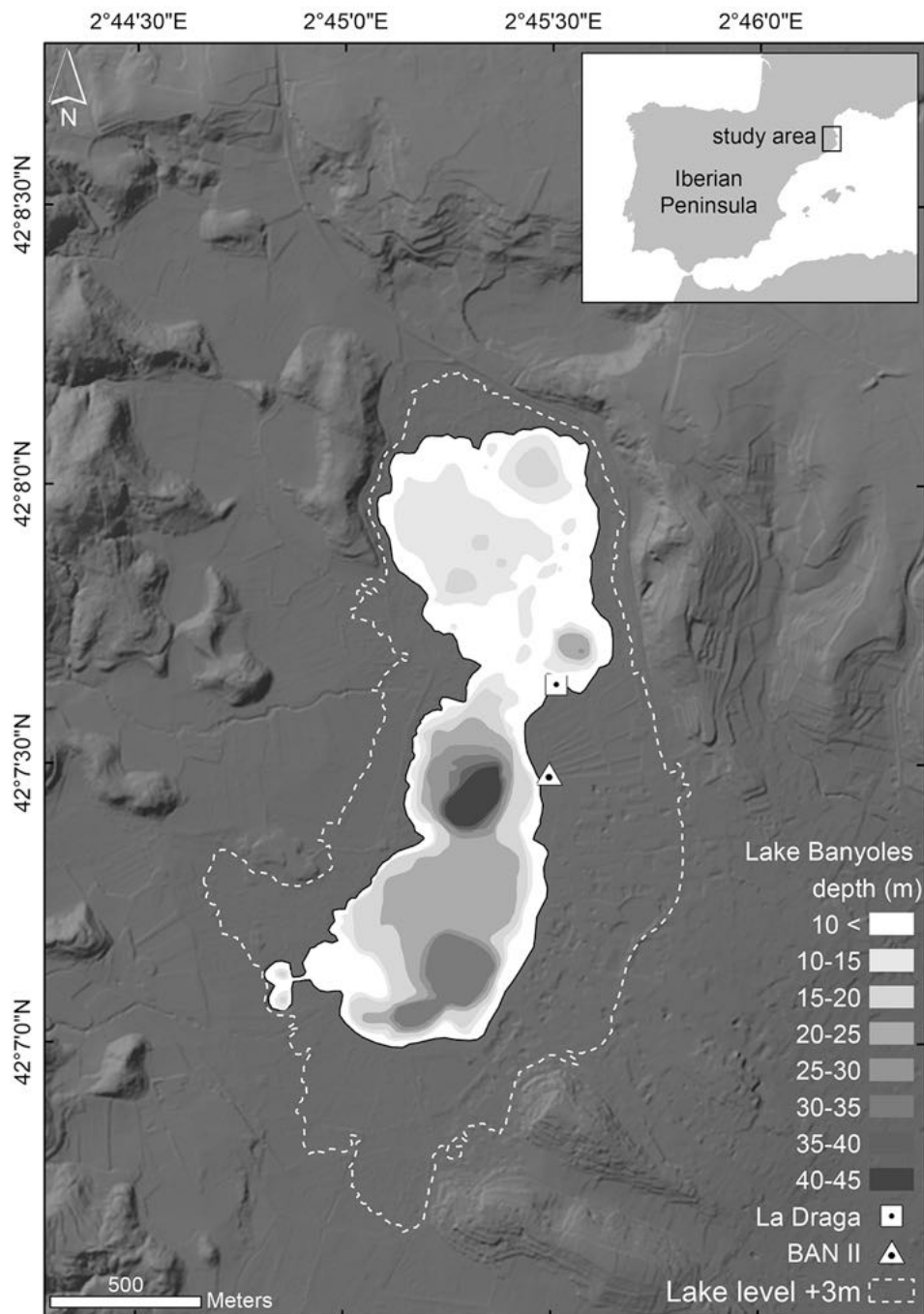


Figure 5.1.: Location of Lake Banyoles on the Iberian Peninsula (inset), and bathymetric map of the lake (modified from [Moreno-Amich and García-Berthou, 1989](#)), showing the northern and southern sub-basins comprising several smaller karstic sinks. The drill site, BAN II (this study; 42°07'29"N, 2°45'29"E), and a previous core, La Draga, are located on the eastern margin of the lake. Based on a present-day digital elevation model from 5 m LIDAR data ([CNIG, 2015, <http://centrodedescargas.cnig.es>](#)) the possible lake extent has been simulated for a lake level rise of 3 m (white dashed line), which would make the terrestrial drill sites subaqueous. The city of Banyoles is located SE of the lake.

decades, employing a range of proxy methods and sources, including sequences from peatbogs (González-Sampériz et al., 2006), speleothems (Stoll et al., 2013), cave sediment (Fernández et al., 2007), and lacustrine sediment (Reed et al., 2001; Valero-Garcés et al., 2004). Iberian palaeoclimate records show broad similarities, but many do not extend beyond the Holocene and the understanding of pre-Late Glacial in particular is still limited.

Lake Banyoles, a karst lake located to the northeast of the Iberian Peninsula (Figure 5.1), is a rare Iberian example of a relatively deep, fresh lake with a long sediment record, and is a key site for palaeoclimate research in the Western Mediterranean. Previous work on Lake Banyoles employed palynological, sedimentological and geochemical techniques for palaeoclimate reconstruction and to improve understanding of the modern physical limnology. In an early palynological study of the lake sediment core, "La Draga" (named after an adjacent Early Neolithic site excavation), Pérez-Obiol and Julià (1994) showed climatic instability during the glacial followed by a rapid transition to the Bølling/Allerød interstadial and the Younger Dryas event, suggesting that the lake responds to North Atlantic climate forcing. Valero-Garcés et al. (1998) provided the first palaeohydrological proxy data from sedimentary facies and stable isotope analysis, generating data on regional arid-phase intensity during Heinrich Events (HE; H3-H0) of the last glacial cycle. More recently, Höbig et al. (2012) used geochemistry and optical methods on core "BAN II" to identify the impact of HE (H5-H0) in the region.

5.2. Study site

Lake Banyoles (42°07'N, 02°45'E; 172 m a.s.l.) is located in the Province of Girona, Catalonia, Spain around 25 km from the Mediterranean Sea (Fig. 5.1). The region has a humid Mediterranean-type climate with an average annual rainfall of 810 mm, measured over the period 2003-2013 at the nearby town of Banyoles (Fig. 5.2a; <http://www.meteobanyoles.com/>). Minimum precipitation occurs during summer and winter months (July, 37 mm; January, 43 mm), and maximum rainfall is during autumn and spring (October, 116 mm; March, 90 mm). Relative humidity remains fairly stable throughout the year, ranging from 58% (July) to 70% (November). Average monthly temperature ranges from 8°C (January) to 25°C (July), and the annual average temperature is 16°C. The oxygen isotope composition of weighted mean annual precipitation ($\delta^{18}\text{O}_{\text{precipitation}}$) measured at Girona airport (129 m a.s.l., 25 km south of Lake Banyoles) between 2000 and 2006 was -5.7‰ (Fig. 5.2; http://www-naweb.iaea.org/napc/ih/IHS_resources_gnip.html). A correction must be applied to incorporate the altitude difference between Girona and Banyoles (-0.6‰/100 m; Fernández-Chacón et al., 2010); the offset is -0.26‰ for the 43 m altitude increase, which results in a predicted weighted mean annual $\delta^{18}\text{O}_{\text{precipitation}} \approx -5.9\text{‰}$ at Banyoles.

According to the Valero-Garcés et al. (2004) classification of Iberian karst lakes, Banyoles is a hydrologically open system with complex basin morphology and a large watershed. The lake has a maximum length of 2.15 km, a maximum width of 0.78 km and covers 1.12 km² (Moreno-Amich and García-Berthou, 1989). The average water depth is 14.8 m. The lake can be divided into two (northern and southern) sub-basins (separated by a shallow sill), which in turn consist of six isolated, subaqueous karstic sinks, which have a maximum water depth of 46.4 m (Fig. 5.1; Höbig et al., 2012). Water input to the lake is predominantly through subterranean springs (85%; Serra et al., 2005), where a fault along the eastern shore redirects groundwater flow upwards through the base of the sinks (Moreno-Amich and García-Berthou, 1989; Morellón et al., 2014). The underlying confined aquifer is recharged by rainfall from two watersheds located in the Alto-Garroxta mountain range approximately 40 km northwest of Lake Banyoles (Morellón

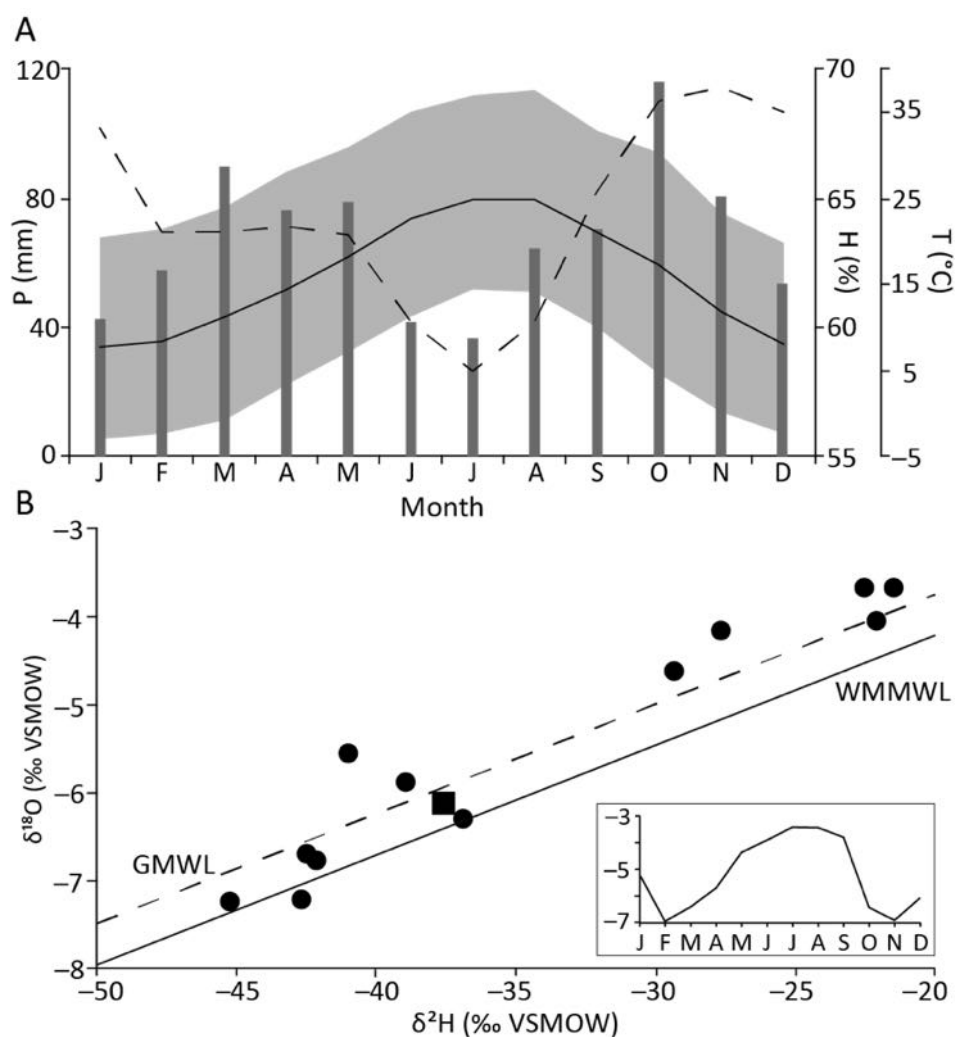


Figure 5.2.: A) Atmospheric data from Banyoles, Catalonia, Spain (Banyoles Observatory $42^{\circ}08'N$, $02^{\circ}45'E$, 175 m a.s.l.; average 2003-2013), including monthly precipitation amount (dark grey bars, P mm), temperature (average = solid line, range = light grey band; T °C) and humidity (dashed line; H %) (<http://www.meteobanyoles.com>). B) Isotope composition ($\delta^{18}O$ and δ^2H) of long-term weighted mean annual rainfall (square) and monthly mean rainfall (dots; inset: plotted by month) measured at Girona Airport (129 m a.s.l., 25 km south of Banyoles; IAEA-GNIP) between 2000 and 2006, corrected for altitude difference ($-0.6\text{‰}/100$ m; Fernández-Chacón *et al.*, 2010), also shown are the Global Meteoric Water Line (GMWL; dashed line; Craig, 1961) and the Western Mediterranean Meteoric Water Line (WMMWL; solid line; Celle-jeanton *et al.*, 2004).

et al., 2014). Five creeks situated on the western shore of the lake supply the remainder of water input (15%; Serra et al., 2005). Groundwater inputs are the dominant influence on modern sedimentation in some of the active sinkholes (Morellón et al., 2014).

The lake sediment is comprised of up to 98% CaCO₃, including inorganic (endogenic) and biogenic (gastropods, ostracods and charophytes) components, with minor quantities of clays and silt/sand-size particles of mainly quartz and feldspar (Höbig et al., 2012). The lake is therefore characterised as a marl lake, which are typical of Mediterranean karst catchments (Roberts et al., 2008; Leng and Marshall, 2004). Average sediment accumulation rate was estimated to be about 1 mm yr⁻¹ throughout the La Draga sequence (Pérez-Obiol and Julià, 1994), although this value is subject to errors inherent in the previous age model.

Here, we aimed to: 1) improve understanding of the chronology, 2) characterise the nature of palaeohydrological variability for palaeoclimate reconstruction, and 3) constrain periods of lake-level and productivity change in Lake Banyoles. We provide new data from sediment core BAN II, including oxygen ($\delta^{18}\text{O}$) and carbon ($\delta^{13}\text{C}$) isotope data from endogenic calcite, to address (1) and (2) (Leng and Marshall, 2004), and diatom data to provide an indicator of lake-level and productivity change (3) (Currás et al., 2012). Our interpretation is strengthened by multi-proxy comparison with previous work on Lake Banyoles (Höbig et al., 2012; Pérez-Obiol and Julià, 1994; Valero-Garcés et al., 1998) and with palaeoclimate reconstructions from the eastern and western Mediterranean, to improve understanding of Late Quaternary variability across this complex region.

5.3. Material and Methods

5.3.1. Core recovery and sedimentology

The 67.07-m core, BAN II, was recovered in the early 1990s from the exposed lake bed on the eastern shore of Lake Banyoles (Fig. 5.1), in 10 cm diameter PVC tubes. The core was collected as 1.5 m-long sections and since collection has been wrapped and stored in darkness at 6°C. In a previous study, the core was dated using Accelerator Mass Spectrometry (AMS ¹⁴C) and U-series (U/Th) techniques, and investigated using Multi-Sensor Core Logger, Fourier-Transform Infrared Spectroscopy and X-Ray Fluorescence (XRF) measurements on 366 equidistant samples (Höbig et al., 2012). Here, we incorporate total inorganic carbon (TIC), total organic carbon (TOC), and XRF count data (K, Ca) from this previous work (for analytical methods see Höbig et al., 2012). Ten complex facies were recognised (Höbig et al., 2012), the compositions of which are summarised here to aid multi-proxy interpretation.

The sedimentology of Lake Banyoles reflects several periods of change in the depositional environment (Höbig et al., 2012). The oldest deposits (67.07-41.00 m) are, in general, less variable, with more gradual lithological transition and an intercalated phase of a few-centimetre to decimetre-thick rhythmites (56.00-53.70 m). A major transition occurs at the boundary between facies H and G. The following sediment sequence (41.00-12.00 m) is highly variable. In the upper sequence (above ~ 12.00 m), the sedimentology indicates subtle changes in the depositional environment.

Facies J (67.07-66.10 m) at the base of the sequence comprises alternating dark- and light-coloured, laminated carbonaceous sediments. There is a gap in core recovery at the transition to facies I (61.20-56.00 m), which shows fining- or coarsening-upward sequences (< 1 m) with embedded clay clasts and intercalated layers of plant fragments, as well as sharp-bounded coarser

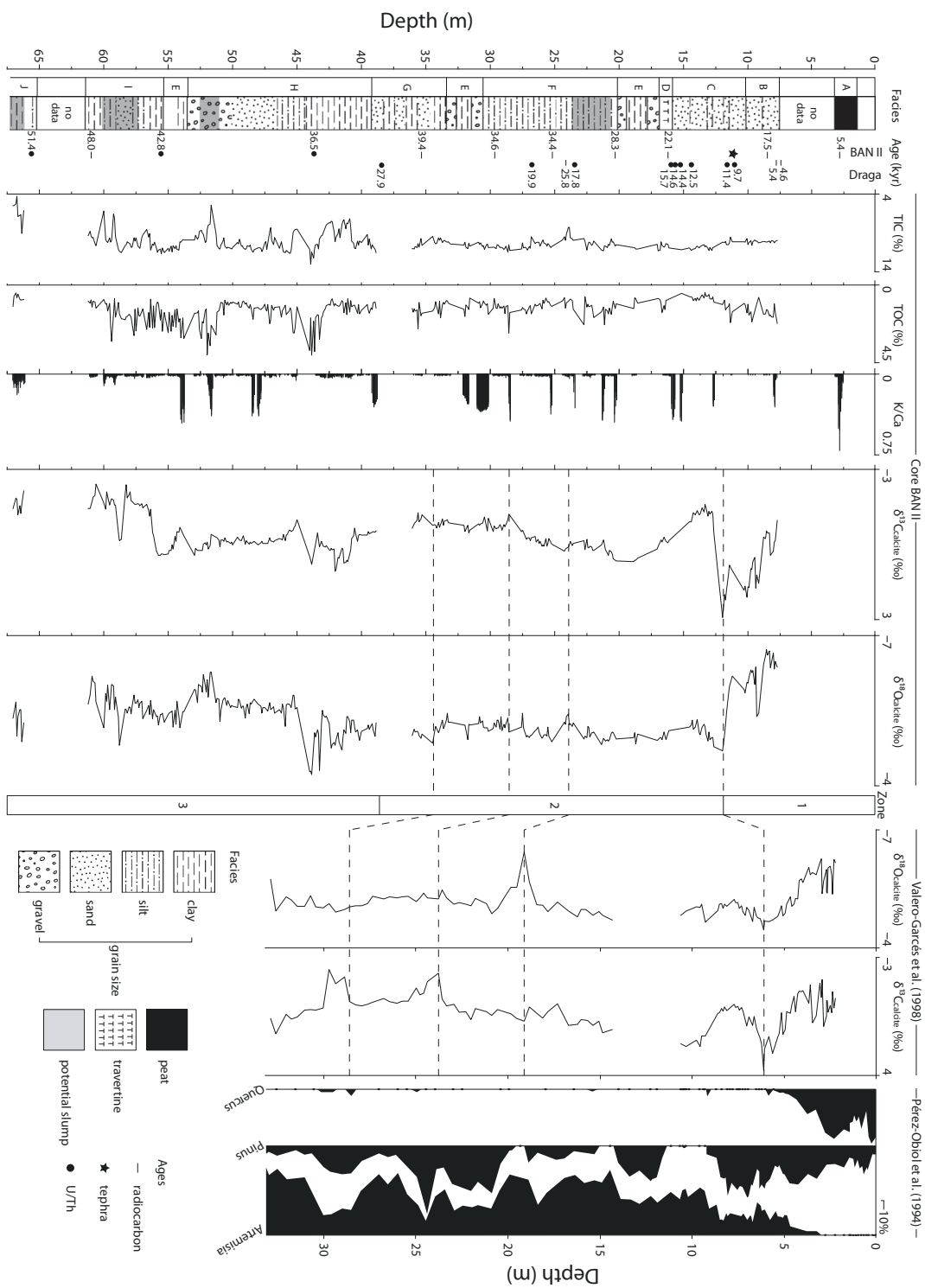


Figure 5.3: Multi-proxy data from core BAN II, including TIC, TOC, $\delta^{13}C_{calcite}$, $\delta^{18}O_{calcite}$, TIC, TOC and facies data were previously published (Höbzig et al., 2012). The data fall into three main zones (3-1; roughly corresponding to MIS 3-1), which are marked. The data from BAN II are compared with those of a previous core (selected pollen taxa, Pérez-Obiol and Julià, 1994, $\delta^{18}O_{calcite}$ and $\delta^{13}C_{calcite}$; Valero-Garcés et al., 1998), and corresponding horizons are indicated using dashed lines. Radiocarbon and U/Th ages are from Höbzig et al. (2012) and cross-correlated from Valero-Garcés et al. (1998)

layers. The overlying sequence (facies E; 56.00-53.70 m) consists mainly of two alternating components (rhythmites), consisting of wavy and/or lenticular, laminated carbonates (clay-silt size) that alternate with coarse (coarse-sand-size) calcified charophyte remains. Facies H is a large and complex unit (53.70-40.00 m), which consists of thick, fining-upward sequences (~ 2m) dominated at the base by gravel-size *Chara* remains. Further up in the sediment core (facies G; 40.00-33.00 m), thin-bedded silt- and sand-size carbonates were deposited, which have subsequently been buried by about 2 m of facies E-type rhythmites (33.00-31.00 m). The following heterogeneous facies F (31.00-20.00 m) is made of a clayey carbonate matrix, with angular carbonaceous clasts containing abundant charophytes. This is overlain by about 3 m of facies E-type rhythmites (20.00-17.00 m), which have been capped by facies D (17.00-16.00 m). Facies D contains a massive terrestrial freshwater carbonate deposit (travertine, calcareous tufa, and sinter) embedded in lacustrine carbonates. Following this (facies C; 16.00-10.00 m) the depositional environment reverts to lacustrine conditions that have preserved layered carbonate muds with gastropods and plant remains, with some evidence for bioturbation. The latter intensifies in the following facies B (10.00-7.50 m), after which the drill site became sub-aerial, indicated by palustrine carbonates and a peat deposit at the very top of the sequence (3.00-2.00 m) with no core recovery between 7.50 and 3.00 m.

5.3.2. Mineralogy

Mineralogy of the carbonate species was investigated using X-Ray Diffraction (XRD) on a Bruker D8 Advance powder diffractometer equipped with a LynxEye linear position sensitive detector and using $\text{CuK}\alpha$ radiation over the scan range $4\text{-}90^\circ 2\theta$. Phase identification was performed using Bruker DIFFRACplus EVA search/match software, interfaced with the PDF-4+ database from the International Centre for Diffraction Data (ICDD).

5.3.3. Stable isotope analysis of calcite

Oxygen and carbon isotope analysis of carbonate ($\delta^{18}\text{O}_{\text{calcite}}$ and $\delta^{13}\text{C}_{\text{calcite}}$) was performed at the same subsample intervals as those used in [Höbig et al. \(2012\)](#), comprising 10 cm resolution from the base of the core to the base of the upper peat layer at 2.70 m. For the cross-core correlation, we compared the new isotope data with isotope and palynological data from the La Draga sequence ([Pérez-Obiol and Julià, 1994](#); [Valero-Garcés et al., 1998](#)).

For isotope analysis the samples were reacted with anhydrous phosphoric acid at a constant 25°C in a vacuum overnight to evolve the CO_2 for analysis. The CO_2 was analysed using a VG Optima dual inlet mass spectrometer. The mineral-gas fractionation factor used for oxygen in calcite was 1.01025, derived from Rosenbaum and Sheppard (1986). $\delta^{18}\text{O}$ and $\delta^{13}\text{C}$ are reported as per mil (‰) deviations of the isotopic ratios ($^{18}\text{O}/^{16}\text{O}$ and $^{13}\text{C}/^{12}\text{C}$) calculated to the Vienna Pee Dee Belemnite (VPDB) scale. Within-run laboratory standards (MCS and CCS) were used, for which analytical reproducibility was $<0.1\text{‰}$ for $\delta^{18}\text{O}_{\text{calcite}}$ and $\delta^{13}\text{C}_{\text{calcite}}$.

A pilot study was carried out using 32 samples selected from throughout the core (with TOC between 0.5% and 7.0%) to assess whether reactive organic matter needed to be removed prior to isotope analysis. One aliquot was analysed using the method described above with no pre-treatment. A second aliquot was disaggregated in 100 ml of 5% sodium hypochlorite for 24 hours to oxidise any reactive organic material, rinsed three times in deionised water, dried at 40°C , ground and the analysis method was applied. The preliminary study showed the two techniques

produced similar results ($R^2 \delta^{18}\text{O} = 0.96$ and $\delta^{13}\text{C} = 0.98$, $p = <0.001$, $n = 32$), so processing to remove organic matter was not carried out on the remaining samples.

5.3.4. Diatom analysis

Diatom slides were prepared at a resolution of approximately 0.7-1.0 m intervals (53 subsamples, representing every seventh isotope subsample), using standard techniques (Battarbee *et al.*, 2001). Sediment samples of about 0.1 g were heated in 30% H_2O_2 to oxidise organic material and a few drops of concentrated HCl were added to remove carbonates. The suspension was then washed with deionised water and centrifuged several times to clean and remove clay-size particles. Microscope slides were prepared using Naphrax™. Diatoms were counted at x1000 magnification under oil immersion with a Zeiss Axioscop Plus 2 light microscope. At least 300 valves were counted where diatoms were well preserved, but fewer were enumerated in poorly preserved samples. Diatom identification was based on standard texts, with updated nomenclature (Currás *et al.*, 2012). Ryves' simple F-index (FI), comprising the ratio of pristine to partially dissolved diatom valves (Ryves *et al.*, 2001), was used to summarise preservation status. Diatom results were displayed using Tilia and TGView, and biostratigraphic zone boundaries were defined using constrained incremental sum of squares (CONISS) cluster analysis (Grimm, 2011).

5.4. Results

5.4.1. Geochemical and isotope analysis

Calcite is the dominant constituent of the BAN II sediment sequence (Fig. 5.3; average = $10.1 \pm 1.2\%$ as TIC), which was confirmed by XRD and validated by Scanning Electron Microscopy and Energy-Dispersive X-ray spectroscopy. Total organic carbon (TOC) is generally low, averaging $1.5 \pm 0.8\%$. Three main zones can be defined by eye, based on changes in the isotope data. Zone 3 (67.00-38.50 m) has the lowest average $\delta^{13}\text{C}_{\text{calcite}}$ ($-0.5 \pm 0.8\text{‰}$), intermediate $\delta^{18}\text{O}_{\text{calcite}}$ ($-5.4 \pm 0.4\text{‰}$) and lower, but variable TIC ($9.9 \pm 1.5\%$). Zone 2 (38.50-11.90 m) is defined by higher and less variable $\delta^{18}\text{O}_{\text{calcite}}$ ($-5.1 \pm 0.1\text{‰}$) and TIC ($10.6 \pm 0.5\%$). Zone 1 (11.90-7.70 m) shows high, but variable $\delta^{13}\text{C}_{\text{calcite}}$ ($0.9 \pm 1.0\text{‰}$), the lowest average $\delta^{18}\text{O}_{\text{calcite}}$ ($-6.1 \pm 0.4\text{‰}$) and moderate TIC ($10.2 \pm 0.2\%$). The isotope zones broadly correlate with the facies defined by Höbig et al. (2012), however individual lithological shifts are not generally reflected in the isotope data.

5.4.2. Diatom analysis

A total of 77 diatom taxa were identified, reflecting the diversity of benthic diatom species present at low abundance. Diatom concentration is generally low and most samples show obvious signs of dissolution in the high-alkalinity lake. No diatoms were preserved above 27.4 m depth and slides were uncountable at ≈ 53 , 50 and 43 m, and at various levels in the sequence above 40 m depth. This is reflected in very low FI values, particularly in phases of almost 100% dominance by dissolved *Cyclotella distinguenda* Hustedt, where the FI is consistently <0.2 because the majority of assemblages show strong signs of dissolution.

Six major diatom assemblage zones, DZ1 to DZ6, were defined using CONISS (Fig. 5.4). Overall, the sequence is dominated by planktonic taxa *Cyclotella distinguenda* Hustedt, an alkaliphilous freshwater diatom that can also tolerate slightly brackish water (Reed, 1998), and *Cyclotella ocellata* Pantocsek, a taxon that is probably a species complex, with very broad ecological preferences, but which is common in Mediterranean karst lakes and typically found in shallow to deep, and ultra-oligotrophic to meso-eutrophic water (Reed et al., 2010; Jones et al., 2013). The benthic flora is dominated by freshwater species within the genera *Amphora*, *Diploneis*, *Mastogloia*, *Gomphonema* and *Cymbella*, typical of epiphytic and epipelagic habitats in the littoral zone of Spanish karst lakes (Currás et al., 2012).

(facing page) Figure 5.4.: Lake Banyoles summary percentage diatom diagram showing diatom zones DZ1-DZ6, defined using CONISS and the sum total of planktonic, facultative planktonic and benthic diatoms (% plankton is taken as an approximate indicator of lake level, although intervening samples devoid of diatoms may represent fluctuations not represented in the diatom data). The F-index ($\times 100$) is also indicated, ranging from 0 (all dissolving) to 100 (pristine)

DZ1 (60.7-56.7 m)

Planktonic and benthic taxa are present in similar proportions over much of DZ1, with a peak in plankton of >80% in the mid zone corresponding to a minimum in preservation quality. Planktonic *Cyclotella distinguenda* and *C. ocellata* are co-dominant. The benthos is dominated by alkaliphilous *Cymbella leptoceros* (Ehrenberg) Kützing, *Gomphonema angustum* C.A. Agardh non Kützing nec Brébisson fide Grunow in Van Heurck, *Mastogloia lacustris* (Grunow) Grunow in Van Heurck and *Amphora pediculus* (Kützing) Grunow ex A. Schmidt, with facultative planktonic (FP) taxa present at <3% throughout. The FI average for DZ1 is low (0.24).

DZ2 (56.7-51.2 m)

The transition to DZ2 is marked by an increase in the relative abundance of plankton (mainly >85%), with dominance varying between *Cyclotella distinguenda* and *C. ocellata*, and a corresponding decrease in benthic abundance (<30%). Minor peaks in *Achnanthyidium minutissimum* (Kützing) Czarnecki and *Sellaphora bacillum* (Ehrenberg) Mann in Round et al. occur at 56.2 m (7.6%) and 52.4 m (11.3%), respectively. The FI average for DZ2 is low (0.18).

DZ3 (51.2-47.3 m)

The relative abundance of benthic taxa drops to <7% in DZ3, with the almost monospecific dominance of *C. distinguenda* (92-100%). *Mastogolia lacustris* and *G. angustum* increase in the centre of the zone (<6%). Preservation is extremely poor, with an FI average of 0.01.

DZ4 (47.3-44.1 m)

The basal sample of DZ4 is characterised by relatively high abundance of benthic taxa, mainly comprising epipelagic *Amphora* spp., a minor increase in FP *Pseudostaurosira brevisstrata* (Grunow in Van Heurck) Williams and Round to 7% and a corresponding decrease in *C. distinguenda* to 30%. *Cyclotella ocellata* reappears at low abundance (<9%). The remainder of DZ4 is poorly preserved and dominated by *C. distinguenda*, giving an FI average of 0.19.

DZ5 (44.1-41.0 m)

Zone DZ5 is the most distinct of the sequence, being dominated by the FP and benthic taxa, but without a marked shift in the range of taxa. The most notable shift is in FP, with increases in *Staurosira construens* f. *venter* (Ehrenberg) Bukhtiyarova, *P. brevisstriata* and *Staurosirella lapponica* (Grunow in Van Heurck) Williams and Round amounting to 50% abundance at the upper zone boundary, and in *A. pediculus*, which reaches peak abundance of 30%. Preservation is relatively good, with average FI values of 0.56.

DZ6 (41.0-27.4 m)

Benthic and FP taxa virtually disappear above 40 m depth, in a zone dominated by poorly preserved *C. distinguenda* and a low FI average of 0.07.

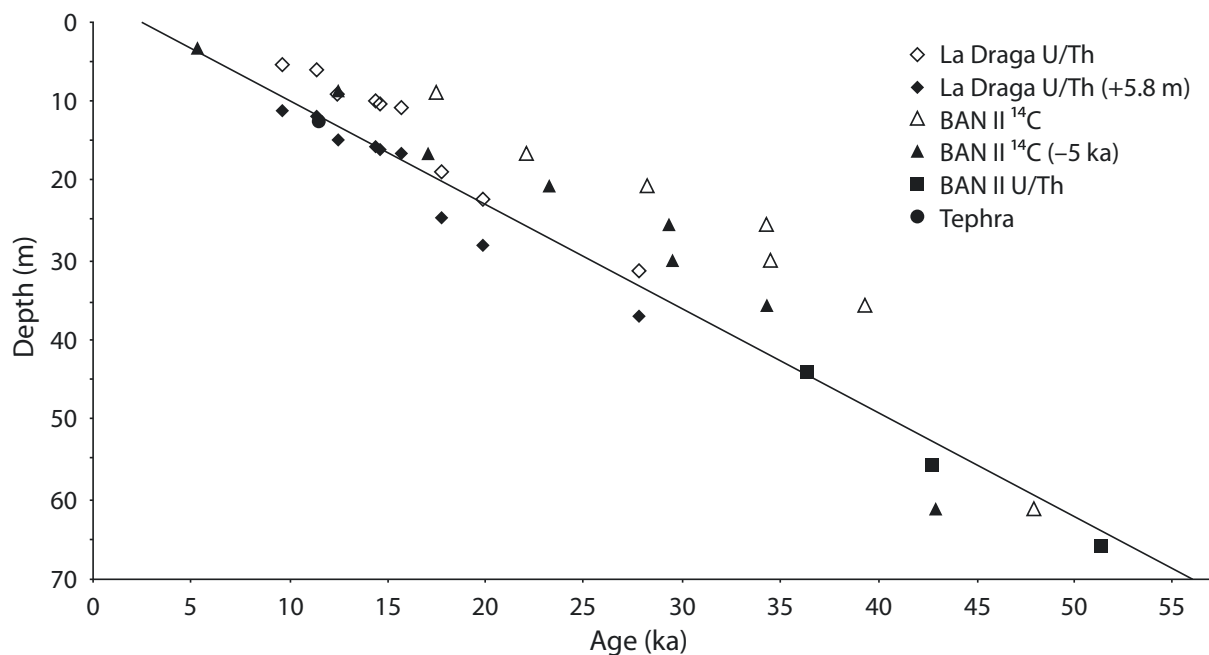


Figure 5.5.: Revised age-depth model for core BAN II, based on 8 radiocarbon ages (offset by 5 ka), 3 U/Th ages, 1 tephra, and 9 cross-correlated U/Th ages from the La Draga core (offset by 5.80 m) based comparison with new isotope data

5.5. Re-assessment of the chronology

The original chronology of BAN II was based on eight Accelerator Mass Spectrometry (AMS ^{14}C) radiocarbon age estimates and three U/Th radiometric dates (Höbig et al., 2012), with further chronological tie points inferred by cross correlation with a previously U/Th-dated core from Lake Banyoles (Pérez-Obiol and Julià, 1994). A horizon of volcanic glass shards, representing a dispersed tephra layer, was geochemically linked to the latest eruptive phase of the Olot volcanic field (ca. 11.5 ka; Höbig et al., 2012). The current age model has been modified to incorporate a radiocarbon reservoir effect (Morellón et al., 2014), and a sedimentological offset between the La Draga and BAN II cores (Fig. 5.3). The new model shows an improved correlation between radiocarbon and U/Th ages from BAN II, and ages from the La Draga record (Fig. 5.5), though age reversals are still prevalent, highlighting the complexity of chronological control.

Radiocarbon dating in karstic lacustrine environments is often subject to lake-water reservoir effects. In Lake Banyoles this generates an error of between +3.0 to +5.5 ka for central lake sediments (Morellón et al., 2014). U-series dating is considered potentially more reliable as there is no reservoir effect and contamination by the secondary migration of U is mitigated by a combination of endogenic calcite deposition with low detrital Th content, high sedimentation rates, and no evidence for sub-aerial exposure (Pérez-Obiol and Julià, 1994).

U/Th dates from bulk sediments in the lower section of the BAN II core (below 43.75 m) provide ages between 36 and 52 ka, suggesting they were deposited through MIS 3. This is inferred from a radiocarbon age (taking into account the potential reservoir effect and age limits of the radiocarbon technique) at 61.06 m of ca. 48 ka, and also suggested by pollen data,

wherein the percentage of mesophilous taxa is higher at the base of the La Draga core (Pérez-Obiol and Julià, 1994). The subsequent AMS ^{14}C ages show a linear progression through the core and, although offset, display a similar trend to U/Th ages. This suggests a relatively stable sediment accumulation rate over the past ca. 50 ka, however ^{14}C ages still offer poor overall chronological control in the BAN II sequence. The new isotope data presented here allow for more precise correlation with the previous core from Lake Banyoles, wherein maximum values of both $\delta^{18}\text{O}$ and $\delta^{13}\text{C}$ occurred at 6.10 m during the Younger Dryas in La Draga (Valero-Garcés et al., 1998). These peaks can be correlated to those at 11.90 m in BAN II, which suggests a potential 5.80 m offset between the two cores. Sediment deposition during the Holocene is indicated by a radiocarbon date taken from a peat layer (terrestrial, no reservoir effect) at 2.8 m (5367 ± 66 cal yr BP), and by increasing TOC through Zone I. Our results therefore support the previous argument that core BAN II covers MIS 3-1 (Höbig et al., 2012), but the age model is now strengthened by isotope correlation between cores. The zones (3-1) defined by isotope data broadly correlate to MIS 3-1 based on the chronological data available.

5.6. Discussions

5.6.1. Modern lake-water isotope composition and controls

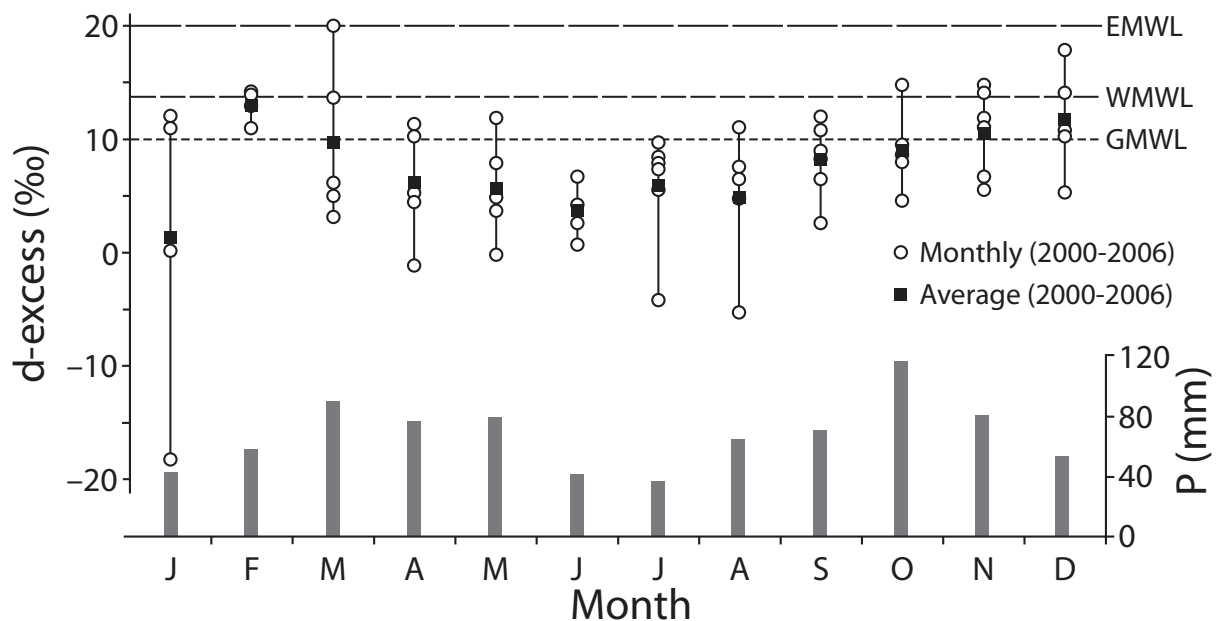


Figure 5.6.: Monthly *d-excess* values calculated from isotope data measured at Girona Airport (IAEA-GNIP) between 2000 and 2006, showing the global average *d-excess* (+10‰, GMWL; Dansgaard, 1964), and the western (+13.7‰, WMWL; Celle-Jeanton et al., 2001) and eastern (+20‰, EMWL; Dotsika et al., 2010) Mediterranean *d-excess*. Local monthly precipitation amount is shown (grey bars; P mm; <http://www.meteobanyoles.com>)

Lake Banyoles is fed by a large karst aquifer system, formed in Palaeogene limestone and gypsum, with an estimated hydrological throughput of about 1 hectometre³ per day (Pérez-Obiol and Julià, 1994). Although our modern water isotope dataset is small, it can be inferred from BAN II

data that consistently low $\delta^{18}\text{O}_{\text{calcite}}$ with relatively minimal down core variability ($-5.4 \pm 0.4\%$, 1σ , $n = 334$) reflects a hydrologically open system with a short residence time, in which the isotope composition of aquifer and lake water are similar (Valero-Garcés et al., 2004). The modern isotope composition of lake water ($\delta^{18}\text{O}_{\text{lakewater}}$) from Lake Banyoles was measured in 2011 and gave a mean $\delta^{18}\text{O}_{\text{lakewater}} = -5.4 \pm 0.5\%$ (1σ , $n = 11$; B. Valero-Garcés, unpublished data), which is generally consistent with the mean annual rainfall isotope composition ($\approx -5.9\%$; Fig. 5.2). This suggests that, in general, $\delta^{18}\text{O}_{\text{lakewater}}$ is not affected by evaporative processes, which is corroborated by low lake-water electrical conductivity (Moreno-Amich et al., 2006), indicating a water column that is deficient in total dissolved solids (Rosqvist et al., 2007). Hence, for understanding past lake water balance, $\delta^{18}\text{O}_{\text{lakewater}}$ variations are thought primarily to reflect changes in $\delta^{18}\text{O}_{\text{precipitation}}$ (i.e. temperature, source, continentality, altitude, amount, seasonality), rather than internal-lake processes, such as evaporation (Leng and Marshall, 2004).

Temperature and precipitation patterns in the North Atlantic region are dominated by the North Atlantic Oscillation (NAO; Sánchez-Goñi et al., 2002). Complex orography and other local geographical factors moderate the influence of North Atlantic atmospheric dynamics in some regions (Martin-Vide and Lopez-Bustins, 2006), however, and create strong regional differences in the seasonal timing of maximum precipitation. The majority of water delivered to the Iberian Peninsula originates from two sources: the Atlantic Ocean and Mediterranean Sea, which produce a distinct source effect on $\delta^{18}\text{O}_{\text{precipitation}}$ received at Banyoles (Moreno et al., 2014). The importance of rainfall from each individual source varies both regionally and seasonally (Gimeno et al., 2010; Moreno et al., 2014), and the extent of influence can be potentially identified using the deuterium excess (d -excess; $\delta\text{D} - 8\delta^{18}\text{O}$) of meteoric water (Fernández-Chacón et al., 2010). Following evaporation from an ocean source, d -excess does not significantly change during subsequent modification within an evolving air mass, as typically $\delta^{18}\text{O}$ and δD vary proportionately (Sharp, 2007). The global average d -excess is 10% (Dansgaard, 1964) and varies spatially because of differences in humidity, wind speed and sea surface temperatures, whereby higher humidity results in lower d -excess values (Clark and Fritz, 1997). Furthermore, seasonal variation is induced by reduced relative humidity over the oceans during winter months, and kinetic effects in arid regions under intense evaporation lead to greatly enhanced d -excess values (Sharp, 2007). In the western Mediterranean Basin d -excess is reported as 13.7% (Celle-Jeanton et al., 2001), intermediate between the global average and that for the eastern Mediterranean (20% ; Dotsika et al., 2010). The isotope composition of precipitation falling at Girona (25 km south of Lake Banyoles) was measured between 2000 and 2006 (http://www-naweb.iaea.org/napc/ih/IHS_resources_gnip.html), from which monthly values for d -excess were calculated (Fig. 5.6). The majority of average values are either below or approaching the global average d -excess ($7.4 \pm 3.5\%$, 1σ), and a lesser percentage of individual monthly values are found to exhibit higher d -excess. The higher values may well be associated with convective systems that originate from the Mediterranean (Moreno et al., 2014), however in general d -excess values are below or equal to that of the global average. This may suggest that most of the water delivered to the Banyoles area, during the periods of peak rainfall at least, is derived principally from an Atlantic source.

5.6.2. Oxygen isotope composition of calcite from Lake Banyoles

The oxygen isotope composition of the water in Lake Banyoles ($\delta^{18}\text{O}_{\text{lakewater}}$) is assumed to be captured in $\delta^{18}\text{O}_{\text{calcite}}$ produced in the surface waters at a given temperature, and $\delta^{18}\text{O}_{\text{lakewater}}$ will dominantly reflect some aspect of $\delta^{18}\text{O}_{\text{precipitation}}$ (Leng and Marshall, 2004). Variations

in $\delta^{18}\text{O}_{\text{precipitation}}$ are regulated by a number of factors including the condensation temperature, source changes, evaporation, 'amount' effects and seasonality (Leng and Marshall, 2004). Assuming the calcite was precipitated in equilibrium, the oxygen isotope composition of mean annual precipitation correlates to temperature change in the northern hemisphere by approximately $+0.6\text{‰}/\text{°C}$ (Dansgaard, 1964), which is opposed by a mineral-water isotope fractionation of $-0.24\text{‰}/\text{°C}$. Therefore, $\delta^{18}\text{O}_{\text{calcite}}$ correlates to temperature with a gradient of roughly $+0.36\text{‰}/\text{°C}$ (Leng and Marshall, 2004). This suggests that if temperature is directly driving changes in $\delta^{18}\text{O}_{\text{calcite}}$ (i.e. no change in source of precipitation), values should be lower during glacial times because of the colder climate, which is true for records from the Alpine region and central Europe (von Grafenstein et al., 1999; Schwander et al., 2000). However, in Lake Banyoles this is not the case as there is a shift from higher $\delta^{18}\text{O}_{\text{calcite}}$ in Zone 2 (MIS 2) to lower $\delta^{18}\text{O}_{\text{calcite}}$ in Zones 1 and 3 (MIS 1 and 3). This change to generally lower $\delta^{18}\text{O}$ values during wetter (and warmer) phases is seen across the majority of Mediterranean lake interglacial/interstadial records. On a glacial-interglacial timescale, temperature is considered a secondary driver of Mediterranean isotope composition compared to water balance, which is lower during cold, but highly arid glacial phases (Roberts et al., 2008).

The configuration of long-term variations in $\delta^{18}\text{O}_{\text{calcite}}$ is similar to that recorded in Greenland ice cores (NGRIP Members Andersen et al., 2004), by planktic foraminifera from the western Portuguese margin (de Abreu et al., 2003), the Alborán Sea (Cacho et al., 1999), the Ionian Sea (Allen et al., 1999) and by speleothems from Israel (Bar-Matthews et al., 1999) (Fig. 5.7). Congruence with these records means that $\delta^{18}\text{O}_{\text{calcite}}$ could be primarily driven by changes linked to the Northern Hemisphere ocean-atmosphere system during the last glacial-interglacial cycle, and suggests that a close association exists between North Atlantic and western-eastern Mediterranean climates. Furthermore, this also suggests that North Atlantic climate dynamics are most likely the primary control on the isotope composition of precipitation at Lake Banyoles, with Mediterranean sources of precipitation only of minor, secondary importance.

5.6.3. Carbon isotope composition of calcite from Lake Banyoles

We assume BAN II carbonates capture the $\delta^{13}\text{C}$ of the lake water in which they precipitated (Leng and Marshall, 2004), which will generally reflect the isotope composition of total dissolved inorganic carbon ($\delta^{13}\text{C}_{\text{TDIC}}$). This can be approximated to the isotope composition of aqueous HCO_3^- for most lakes. As only a small fractionation occurs during precipitation, $\delta^{13}\text{C}_{\text{calcite}}$ can indicate past variations in $\delta^{13}\text{C}_{\text{TDIC}}$ and carbon cycle transitions. In lakes, $\delta^{13}\text{C}_{\text{TDIC}}$ is mainly influenced by the isotope composition of inflowing waters, and by subsequent modification through kinetic processes (Leng and Marshall, 2004). Groundwater inflows typically have relatively low $\delta^{13}\text{C}_{\text{TDIC}}$ because of the incorporation of isotopically light carbon liberated from the decay of organic matter in soils, which has average $\delta^{13}\text{C} = -30$ to -16‰ , for a combination of C3 ($\delta^{13}\text{C} -32$ to -20‰) and C4 ($\delta^{13}\text{C} -17$ to -9‰) plants (Leng et al., 1999). Following decay, light carbon (CO_2) enters groundwater by dissolution, is hydrated to produce carbonic acid and dissociates to predominantly form bicarbonate (at neutral pH), which has a fractionation factor of approximately $+10\text{‰}$ when in equilibrium with CO_2 (Mook et al., 1974). Thus, $\delta^{13}\text{C}_{\text{TDIC}}$ derived solely from C3 soil- CO_2 is predicted to have $\delta^{13}\text{C}$ between -22 to -10‰ , and C4 soil- CO_2 between -7 to $+1\text{‰}$. Catchment vegetation is known to have comprised varying percentages of both arboreal and non-arboreal taxa through time (Pérez-Obiol and Julià, 1994). Therefore, the estimated values for $\delta^{13}\text{C}_{\text{TDIC}}$ are isotopically lower than both the Banyoles modern surface waters ($\delta^{13}\text{C}_{\text{DIC}} = -3.3\text{‰}$, measured in 2011; B. Valero-Garcés, unpublished data) and BAN

II core data ($\delta^{13}\text{C}_{\text{calcite}}$ range = -3.4‰ to $+2.9\text{‰}$), suggesting that organic-derived soil- CO_2 is potentially a component of $\delta^{13}\text{C}_{\text{TDIC}}$, although in addition there must be an isotopically heavier $\delta^{13}\text{C}$ source.

It is unlikely that high $\delta^{13}\text{C}_{\text{calcite}}$ is the product of equilibration with atmospheric CO_2 , which can yield $\delta^{13}\text{C}$ in excess of $+3\text{‰}$ (Leng and Marshall, 2004), a consequence of the short lake-water residence time. As the predominant water input to Lake Banyoles is through karst aquifers, it is likely that the majority of ^{13}C -enriched HCO_3^- is derived through the dissolution of aquifer carbonates, as geological sources of carbonate generally have high $\delta^{13}\text{C}$ values, between -3‰ to $+3\text{‰}$ (Leng et al., 1999). In addition, aquatic productivity may act to raise $\delta^{13}\text{C}_{\text{TDIC}}$, as during photosynthesis the preferential uptake of ^{12}C can leave TDIC isotopically heavy. In Banyoles this process may take place during restricted intervals (e.g. around 44 m), however commensurate increases in TOC would also be expected, which generally are not observed.

Excursions to lower $\delta^{13}\text{C}_{\text{calcite}}$ could be ascribed to the release of ^{12}C as a product of degradation processes following organic carbon oxidation in bottom waters, which would also likely result in low values of TOC. In Lake Banyoles this does not appear to be the case, as TOC is generally low throughout the core and shows no correlation with $\delta^{13}\text{C}_{\text{calcite}}$ ($r = -0.18$). Transitions to lower $\delta^{13}\text{C}_{\text{calcite}}$ are more probably driven by enhanced delivery of ^{12}C during times of soil development within the catchment, and associated with an increased contribution from isotopically light carbon derived from terrestrial C3 plants during warmer periods, for example as seen in the early Holocene (Fig. 5.3; Valero-Garcés et al., 1998).

Variations in $\delta^{13}\text{C}_{\text{calcite}}$ are thought to be mainly a product of the balance between the contribution from the bicarbonate ion, in addition to the concentration and constitution of soil CO_2 . During times of enhanced soil development within the catchment (e.g. within the Holocene), $\delta^{13}\text{C}_{\text{calcite}}$ is expected to be lower, as more isotopically light carbon is assumed to be incorporated into TDIC. In times of restricted soil development, commensurate with increased percentages of steppic C4 taxa, $\delta^{13}\text{C}_{\text{calcite}}$ will be higher.

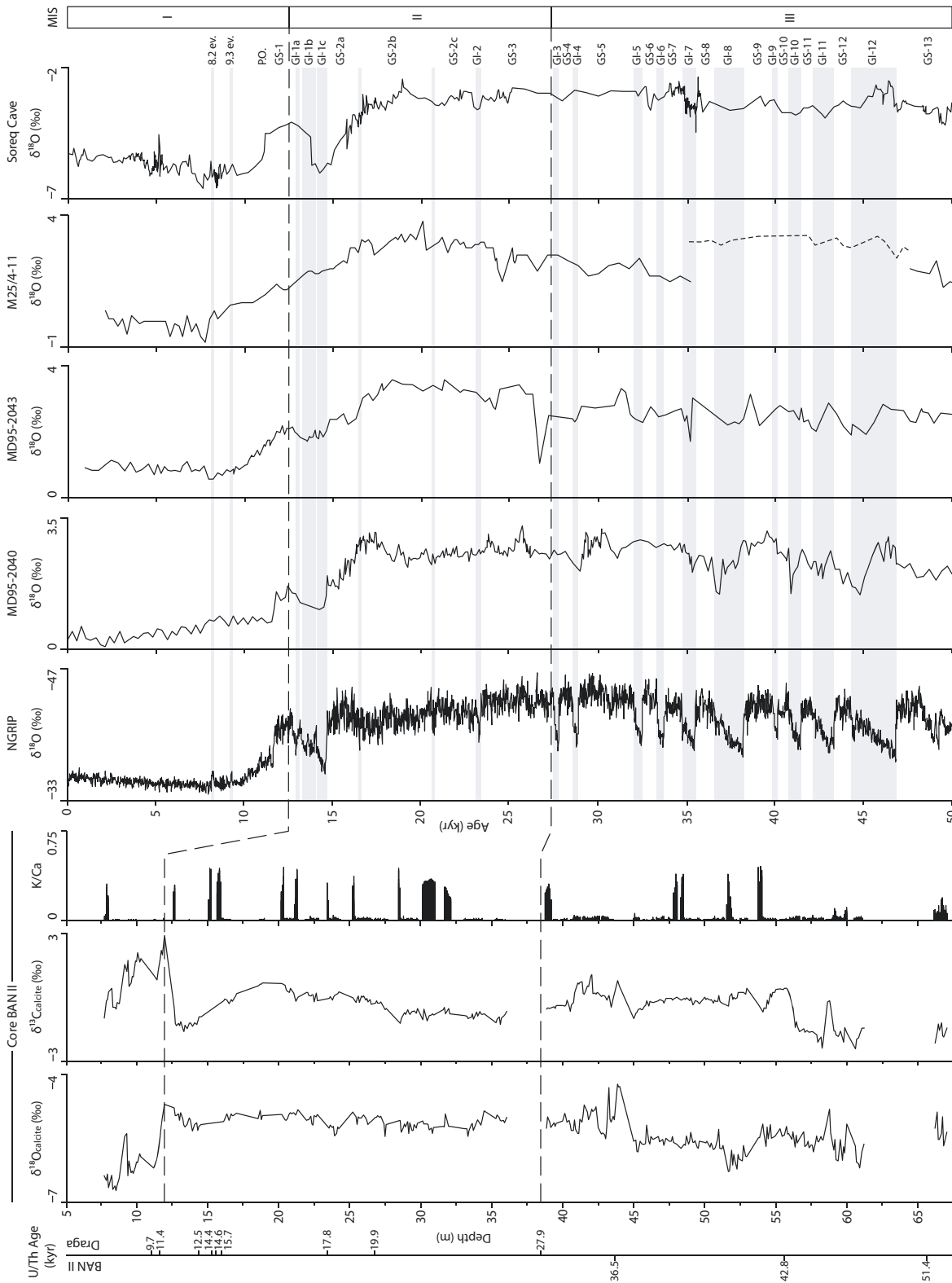


Figure 5.7.: see facing page.

5.6.4. Isotope covariance and facies variability

Carbonates produced in open lakes typically do not show covariance between $\delta^{18}\text{O}$ and $\delta^{13}\text{C}$ (Talbot, 1990), whereas in closed systems the degree of covariance depends on several factors such as atmospheric exchange, evaporation rates, and productivity (Li and Ku, 1997). Lake Banyoles displays no covariance between $\delta^{18}\text{O}_{\text{calcite}}$ and $\delta^{13}\text{C}_{\text{calcite}}$ over the whole core ($r = 0.10$), which most likely reflects its short lake-water residence time as a throughflow-dominated system. Covariance increases during certain periods when constrained time zones are considered, specifically during the Holocene ($r = 0.75$) and the $\delta^{18}\text{O}_{\text{calcite}}$ maximum toward the upper boundary of Zone III ($r = 0.88$). However, increased covariance does not necessarily relate to hydrological closure as, at least for the Holocene, there is a general transition to lower $\delta^{18}\text{O}_{\text{calcite}}$ and $\delta^{13}\text{C}_{\text{calcite}}$, most likely caused by enhanced freshwater input and the development of catchment soils. Furthermore, approaching the upper boundary of Zone III, there is a distinct parallel excursion to higher isotope values that occurs alongside a peak in TOC and TIC after 44 m. Lower lake level is indicated at that time by the preservation of benthic diatom taxa in DZ4, which suggests rapid sedimentation in a littoral zone with aquatic plants (increased TOC) during a shallow-water phase. High TIC and TOC indicate enhanced productivity at that time, which may be associated with the preferential removal of ^{12}C in the epilimnion driving increased $\delta^{13}\text{C}_{\text{calcite}}$. High $\delta^{18}\text{O}_{\text{calcite}}$ was probably a function of regional climate, related to seasonal temperature changes leading to higher $\delta^{18}\text{O}$ summer precipitation and increased aridity (Leng et al., 1999). In general, there is little correlation between $\delta^{18}\text{O}_{\text{calcite}}$ and facies variability in BAN II, suggesting that isotope values are somewhat independent of changes in lake level. This perhaps indicates that during times of reduced lake level, assumed to be related to coarser-grained facies in BAN II (Höbig et al., 2012) and regional aridity, lake water is hydrologically buffered against the effects of evaporation and kinetic fractionation. Höbig et al. (2012) suggested that four horizons have characteristics potentially attributed to slump-related processes (Fig. 5.3). The tilted nature of the basal horizon (67.07-66.10 m; facies J) suggests these sediments are indeed slumped, therefore precluding robust environmental reconstruction. However, the overlying horizons do not show the same physical appearance and appear to be undisturbed, which suggests stratigraphic variability could potentially be related to lake-level changes.

*(facing page) Figure 5.7.: Comparison of structural trends between Lake Banyoles BAN II $\delta^{18}\text{O}_{\text{calcite}}$ (plotted to depth with refined U-series chronological control as described in the text) and other North Atlantic and Mediterranean records (plotted to age). NGRIP ice core $\delta^{18}\text{O}_{\text{V-SMOW}}$ (NGRIP Members Andersen et al., 2004), Portuguese margin MD95-2040 *Globigerina bulloides* $\delta^{18}\text{O}_{\text{V-PDB}}$ (de Abreu et al., 2003), Alborán Sea MD95-2043 *Globigerina bulloides* $\delta^{18}\text{O}_{\text{V-PDB}}$ (Cacho et al., 1999), Ionian Sea M25/4-11 *Globigerinoides ruber* (solid line) and *Globigerina bulloides* (dashed line) $\delta^{18}\text{O}_{\text{V-PDB}}$ (Allen et al., 1999) and Soreq Cave, Israel speleothem $\delta^{18}\text{O}_{\text{V-PDB}}$ (Bar-Matthews et al., 1999). Grey bars indicate the INTIMATE event stratigraphy (Blockley et al., 2012) and dashed lines demarcate MIS 3-1*

5.6.5. Lake Banyoles climate and hydrology: MIS 3-1

During the last glacial period there was considerable climatic variability across the North Atlantic (Dansgaard et al., 1993), attributed to changes in thermohaline circulation and subsequent modification of ocean heat transport (Clark et al., 2002). Mediterranean marine and lacustrine records suggest that the region closely reflected the North Atlantic ocean-atmosphere system (Allen et al., 1999) and that at a millennial scale, climatic fluctuations showed a Dansgaard–Oeschger (D-O) pattern of variability (Cacho et al., 1999). During cold D-O phases, enhanced northern hemisphere atmospheric circulation is suggested by increased Saharan dust transport and incorporation in western Mediterranean Sea sediments (Moreno et al., 2002), causing higher-intensity wind systems over the Iberian Peninsula, predominantly from the west and northwest (Vegas et al., 2010). Oscillations in atmospheric moisture content during cold and arid stadial and mild and wet interstadial periods are inferred from the Alborán Sea, which shows an alternating steppe to deciduous-evergreen pollen assemblage (Sánchez-Goñi et al., 2002). This record also suggests that an extreme climate state existed during Heinrich Events (HE), which are characterised by aridity and colder conditions in the Mediterranean (Sánchez-Goñi et al., 2002). Central Spain is thought to have been colder and experienced enhanced aridity during these cold events, with widespread growth of herbaceous plant steppe taxa, suggesting a near-instantaneous transfer of climate state between the northern Atlantic to the Iberian Peninsula (Vegas et al., 2010).

In Lake Banyoles, millennial-scale $\delta^{18}\text{O}_{\text{calcite}}$ and $\delta^{13}\text{C}_{\text{calcite}}$ shifts through MIS 3 (Fig. 5.3) may be analogous to enhanced variability observed across the North Atlantic and western Mediterranean (Fig. 5.7 Cacho et al., 1999; de Abreu et al., 2003). Although the chronology could be better constrained, a response to abrupt HE has been suggested from previous reconstructions from the lake (Höbig et al., 2012; Valero-Garcés et al., 1998) and in the surrounding region (González-Sampériz et al., 2006). However, there is evidence neither for cold or arid rapid-climate-change events in $\delta^{18}\text{O}_{\text{calcite}}$ or $\delta^{13}\text{C}_{\text{calcite}}$ data (Fig. 5.3), which may be a consequence of the relative unimportance of evaporative effects on the lake water and the short residence time. Other proxies (e.g. K/Ca, Fig. 5.3) appear to be more sensitive to increased aridity and reflect local environmental conditions more closely. The abundance of *C. ocellata* in mid-MIS 3 (DZ1 to DZ2) may indicate higher productivity and, by inference, temperature, an association reported from other Mediterranean lakes, such as Lake Ohrid (Reed et al., 2010). The return to very poor diatom preservation and dominance by *C. distinguenda* above ≈ 51 m depth correlates with a lithological shift to finer-grain sediment, indicative of lake-level increase corresponding to a reduction in TOC, which suggests low, temperature-induced productivity associated with reduced evaporation, but without a strong associated isotopic signal. Towards the end of MIS 3, diatoms provide strong evidence for a shallowing trend in the proportion of benthic and FP taxa, which correlates with increased TOC and higher-quality preservation in the more organic littoral zones of Banyoles. The concomitant covariant excursion in $\delta^{18}\text{O}_{\text{calcite}}$ and $\delta^{13}\text{C}_{\text{calcite}}$ to higher values suggests this is a response to increasing aridity, and most likely related to the lake volume change indicated by the transition to a benthic-dominated diatom assemblage.

Through MIS 2 and surrounding the last glacial maximum, proxies from Lake Banyoles (notably TIC and $\delta^{18}\text{O}_{\text{calcite}}$) become less variable and the sedimentology is primarily characterised by fine-grained, clay-rich facies (Höbig et al., 2012; Valero-Garcés et al., 1998). Benthic and FP diatom taxa are essentially absent, and poorly preserved *C. distinguenda* becomes dominant, suggesting a low-productivity 'deep' lake, which is also suggested by low- $\delta^{13}\text{C}_{\text{calcite}}$, representing a decrease in productivity-driven ^{13}C enrichment. Thus, diatom data and sedimentology provide strong proxy evidence for increased lake level during MIS 2. This must be a function

mainly of low evaporative concentration with reduced temperature, as the presence of *Artemisia* steppe vegetation in the catchment (Fig. 5.3; Pérez-Obiol and Julià, 1994) provides strong proxy evidence for aridity. There is also ample pollen-based evidence that MIS 2 was extremely arid across the region as a whole (Roucoux et al., 2005). High lake levels during glacial times are also found in some Mediterranean records (Kolodny et al., 2005), but most shallow alkaline lakes are at a low level (Jones et al., 2013). Higher lake levels could be caused by a combination of lower temperatures, leading to less evaporative concentration, and a reduction in catchment vegetation cover, resulting in lower rates of evapotranspiration, which encourages aquifer throughflow and deeper lacustrine conditions.

The Late Glacial to Holocene sequence of climate and environmental change from Lake Banyoles is consistent with that of the previous studies from the lake (Valero-Garcés et al., 1998) and of other Mediterranean lacustrine records (Roberts et al., 2008). There is a shift to higher $\delta^{18}\text{O}_{\text{calcite}}$, reaching a maximum at 11.9 m in the core, which can be correlated to a similar rise in the previous isotope record at 6.1 m and a significant rise in *Artemisia* and decrease in *Pinus*, signifying the re-expansion of steppe conditions (Fig. 5.3; Pérez-Obiol and Julià, 1994; Valero-Garcés et al., 1998). The interval, dated to 12 ka (Pérez-Obiol and Julià, 1994), therefore likely corresponds to the Younger Dryas event and can be compared to similar excursions in both western and eastern Mediterranean records (Fig. 5.7). The absence of diatoms during the Holocene is consistent with their poor preservation in lake-centre sediment during maximum lake-level phases, caused by dissolution in the water column. One of the most distinct $\delta^{18}\text{O}_{\text{calcite}}$ excursions in Lake Banyoles is through the Late Glacial to Holocene transition, with a maximum change of -2‰ (-4.7‰ at 11.9 m, -6.7‰ at 8.5 m). A shift to lower $\delta^{18}\text{O}_{\text{calcite}}$ is a prominent feature that is common across most Mediterranean lakes during that time (Roberts et al., 2008), and is comparable in magnitude to the changes in the composition of western Iberian margin and Alborán Sea planktic foraminifera (de Abreu et al., 2003; Cacho et al., 1999). The subsequent excursion to higher $\delta^{18}\text{O}_{\text{calcite}}$ at 9.3 m may correspond to the 8.2 ka event, which is constrained by a U/Th date at 10.8 m (9.7 ka), assuming a 5.8-m offset between the BAN II and La Draga cores.

5.7. Conclusions

We presented new stable isotope data ($\delta^{18}\text{O}_{\text{calcite}}$ and $\delta^{13}\text{C}_{\text{calcite}}$) from Lake Banyoles, which were combined with previous data (TIC, TOC, K/Ca) from the same core (Höbig et al., 2012) and compared to a shorter core from the lake that provided isotope and pollen records (Pérez-Obiol and Julià, 1994; Valero-Garcés et al., 1998). The current age model (Höbig et al., 2012) has been modified, but we agree the core likely spans MIS 3-1, based on U/Th ages and correlation between the two sets of isotope data. U/Th ages provide the best potential age control for extended sequences recovered from Lake Banyoles, given the observed radiocarbon offset. Lake Banyoles $\delta^{18}\text{O}_{\text{calcite}}$ appears to primarily reflect a distinct source effect on $\delta^{18}\text{O}_{\text{precipitation}}$ and glacial-interglacial changes in the composition of marine source waters. Investigation of local precipitation data shows overall low d -excess and suggests that the majority of rainfall received by Lake Banyoles probably derives from Atlantic fronts rather than Mediterranean origin. The sequence from Lake Banyoles has been divided into three main zones that broadly correlate to MIS 3-1 based on the chronological information available, changes in the isotope composition of the sediments, and diatom assemblage data. Zone 3 shows a greater number of larger-amplitude excursions in $\delta^{18}\text{O}_{\text{calcite}}$, and $\delta^{13}\text{C}_{\text{calcite}}$, which are coincident with considerable millennial-scale climate fluctuations across the North Atlantic and surrounding regions. Enhanced variability in

TOC and the presence of benthic diatoms suggests MIS 3 was characterised by substantial lake level shifts and associated productivity changes. A generally more stable climate can be inferred for Zone 2, with $\delta^{18}\text{O}_{\text{calcite}}$ being higher and, along with TIC and TOC, more consistent. There may have been a high-lake-level phase at that time, suggested by a decrease in diatom preservation and a sedimentology indicative of deeper water. The transition between Zone 2 and Zone 1 shows a distinct change to lower $\delta^{18}\text{O}_{\text{calcite}}$, a pattern that is common amongst Mediterranean lake records. This study provides an important extended multi-proxy continuous record for the Iberian Peninsula, and offers a new Late Quaternary palaeoclimate archive to correlate between terrestrial and marine records from both the western and eastern Mediterranean, thus reinforcing hemispheric teleconnections.

5.8. Acknowledgements

This paper contributes to the CRC 806 (University of Cologne) – Our Way to Europe. The paper forms part of the PhD research of JHL funded by the British Geological Survey University Funding Initiative (BUFI) and also the PhD of NH at RWTH Aachen University. Thanks go to Andrea Snelling (NIGL) for assistance with the isotope work and Cheryl Haidon (University of Leicester) for providing mineralogy data.

6. Late Quaternary environmental evolution of the Como urban area (Northern Italy): A multidisciplinary tool for risk management and urban planning

This chapter is a slightly modified version of a published article:

Ferrario, M. F., Bonadeo, L., Brunamonte, F., Livio, F., Martinelli, E., Michetti, A. M., Censi Neri, P., Chiessi, V., Comerci, V. & Höbig, N. (2015). Late Quaternary environmental evolution of the Como urban area (Northern Italy). *Engineering Geology* 193: 384–401.

Abstract

The historical center of Como (Northern Italy) is prone to lake flooding and subsidence, due to the presence of unconsolidated silty sediments with poor mechanical properties. The sedimentary basin beneath the town contains over 180 m thickness of Late-Quaternary lacustrine, palustrine and alluvial deposits. The landscape evolution and the present-day environmental setting of the Como area have been reconstructed based on (i) more than 250 core logs and related geotechnical tests, (ii) detailed stratigraphic, sedimentological, paleobotanical and geotechnical analysis of several key boreholes, (iii) multi-year hydrogeological monitoring, (iv) estimation of subsidence rates and (v) integration of geomorphology, archeological findings and historical documents.

Based on our environmental analysis, we derived an integrated geological and geomorphological model of the latest Pleistocene to Holocene local landscape evolution. This model was used to help design an engineering facility to mitigate flood hazards in the Como urban area.

In 2012, we carried out investigations during a re-evaluation of the design parameters for the flood mitigation project at the Como lake-shore. The new campaign included seven boreholes, many in situ and laboratory tests, and four $\delta^{14}\text{C}$ dates. We found an organic silty unit, historical in age, with bad mechanical properties that was critical in the design of the flood mitigation project. We also obtained index properties for static and dynamic conditions, necessary for robust engineering planning. The results were used to update the project and better define future executive phases. Although the importance of acquiring independent experimental data is often overlooked, they can significantly improve the reliability of engineered systems, as demonstrated by the Como town case history.

6.1. Introduction

The landscape evolution of an area is governed by "extreme" natural events, which can potentially change the geography and stratigraphy of entire regions. Since modern landscapes are very

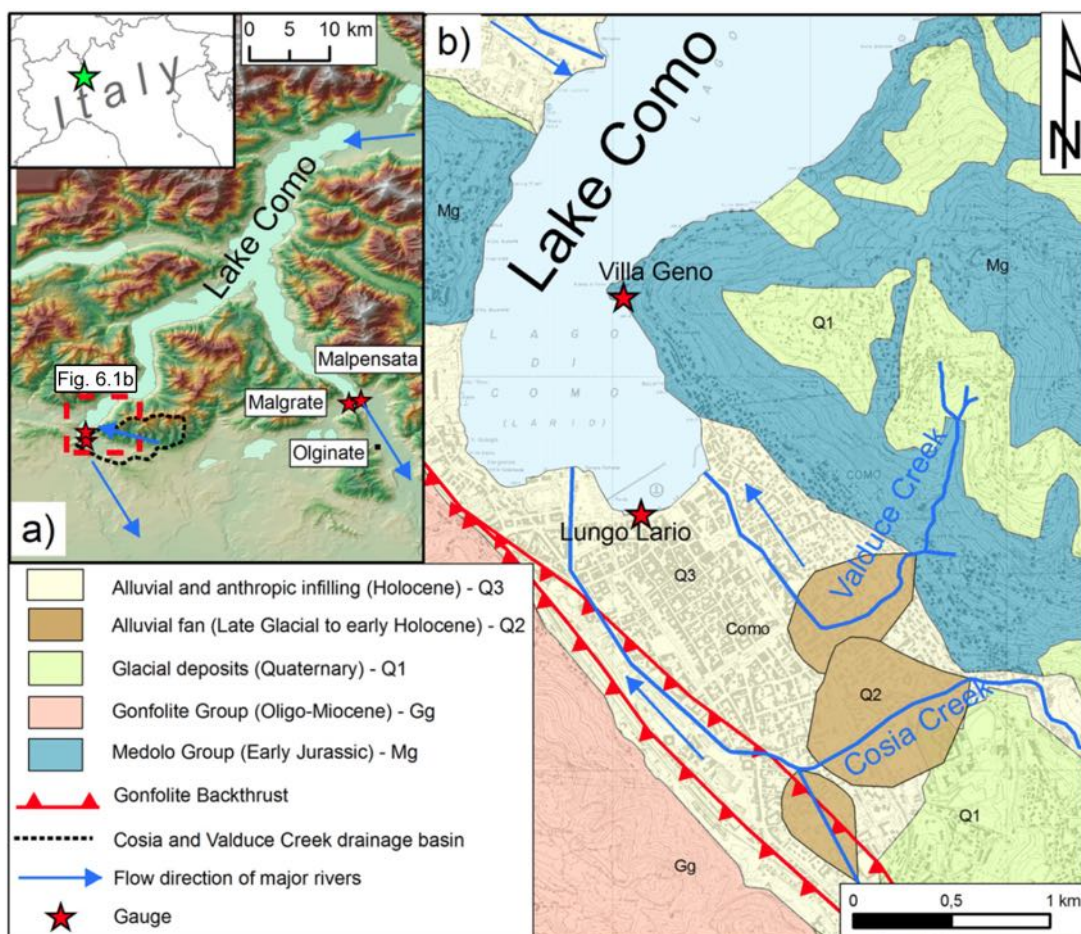


Figure 6.1.: Digital elevation model showing location of Como town, at the southern tip of Lake Como; the map shows also the Cosia and Valduce creeks drainage basin (black dotted line), the position of the hydrometer stations (gauge) and of the Olginate dam. Blue arrows indicate the flow direction of major rivers. b) Simplified geologic map of the study area, modified after Michetti et al. (2013).

often urban ones, from the societal point of view, geohazards are today among the most serious factors of environmental risk for local industrial installations and large metropolitan areas. Even if much effort has been put into characterizing the causes and dynamics of geohazards, losses are continuously increasing due to a growing population density, which can result in incautious use of the land (e.g., Smith, 2013).

The risk posed by geological hazards seems to be poorly understood, even in the highly industrialized and populated Northern Italy, as illustrated for instance by the "expected" extensive damage to modern industrial buildings during the May–June 2012 seismic sequence in the Po Plain (e.g., Cimellaro, 2014; Dolce and Di Bucci, 2014; Michetti et al., 2012), resulting in losses totaling over 13 billion euros (Daniell and Vervaeck, 2012).

Geotechnical failures of anthropic infrastructure are spread worldwide and historical failure cases have deeply shaped the engineering profession (Delatte, 2008). Lessons learnt from such disasters can help in avoiding future failures. Very few disasters occur because of lack of fundamental knowledge or technology: the main reasons for failures are human factors, such as shortcomings in the use of existing geological or geotechnical knowledge and inadequate field monitoring (Bea,

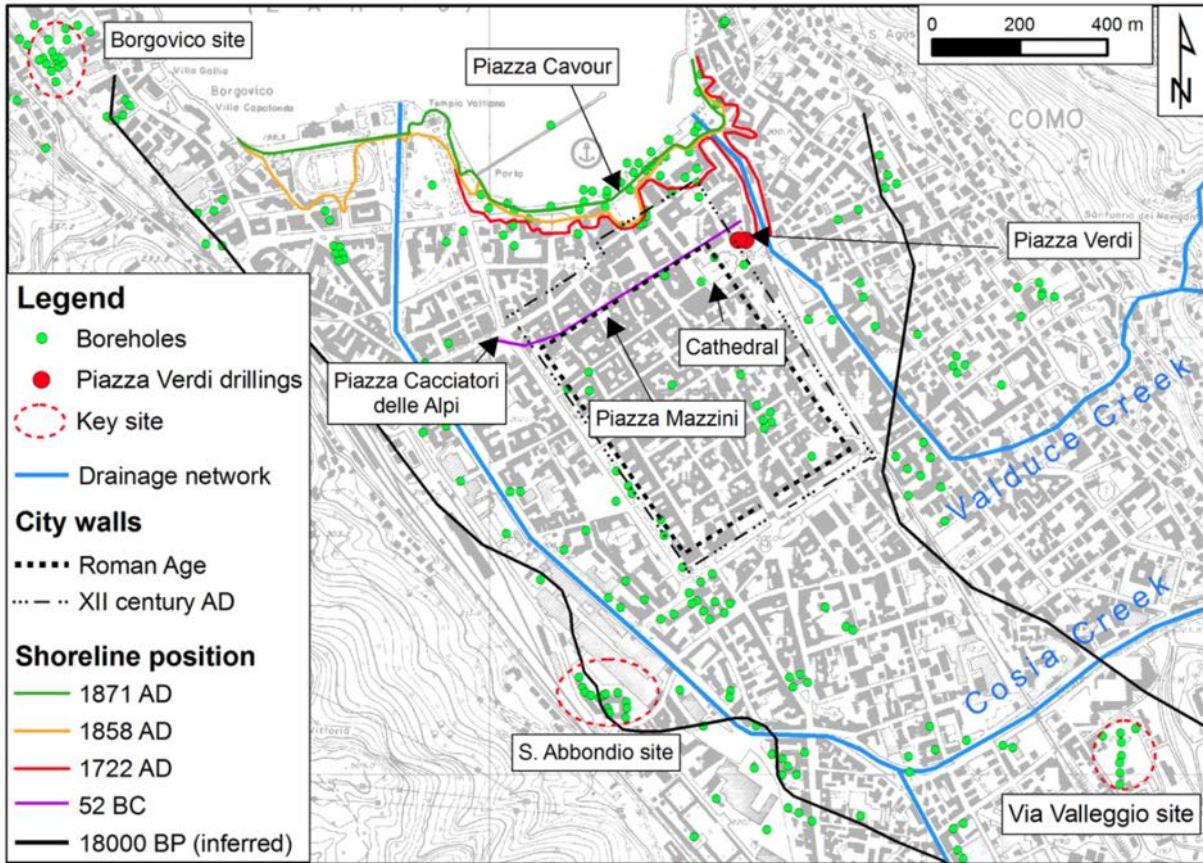


Figure 6.2.: Map of the Como urban area, based on a topographic map at a 1:10,000 scale (CTR, Carta Tecnica Regionale), showing the available borehole logs, the local drainage network, the reconstruction of the shoreline position at different times and the main archeological and urban features.

2011; Sowers, 1993). The importance of acquiring independent experimental data during the design stage of an engineering project is often overlooked, even if it applies standard-practice techniques and investment of relatively little money in respect of the total costs. A proper approach enables to identify geohazards possibly occurring during the construction and maintenance of engineering projects (e.g., Xu et al., 2009; Huang et al., 2015).

This paper illustrates how knowledge of the natural environment and the territorial setting, derived from geological analysis, can be a valuable tool in managing those risks that can affect the integrity and stability of urbanized areas, including their cultural heritage and engineering facilities. In the case of Como, losses might be caused mainly by subsidence and floods.

An engineering geological model derived from stratigraphic, geotechnical and hydrogeological data was developed and tested during the building of a facility in the Como downtown urban area, located in a lake-shore environment prone to subsidence at the northern margin of the Lombardy Po Plain (Figure 6.1a). The model provided a suitable general workflow for urban planning and furnished guidance for choosing proper operational techniques. The workflow also highlighted the need for a robust organization and control over construction works, as well as good communication with the public and proper investigation of the delicate interplay of technical and cultural matters in environmental policy (see for instance the discussion in Laborde

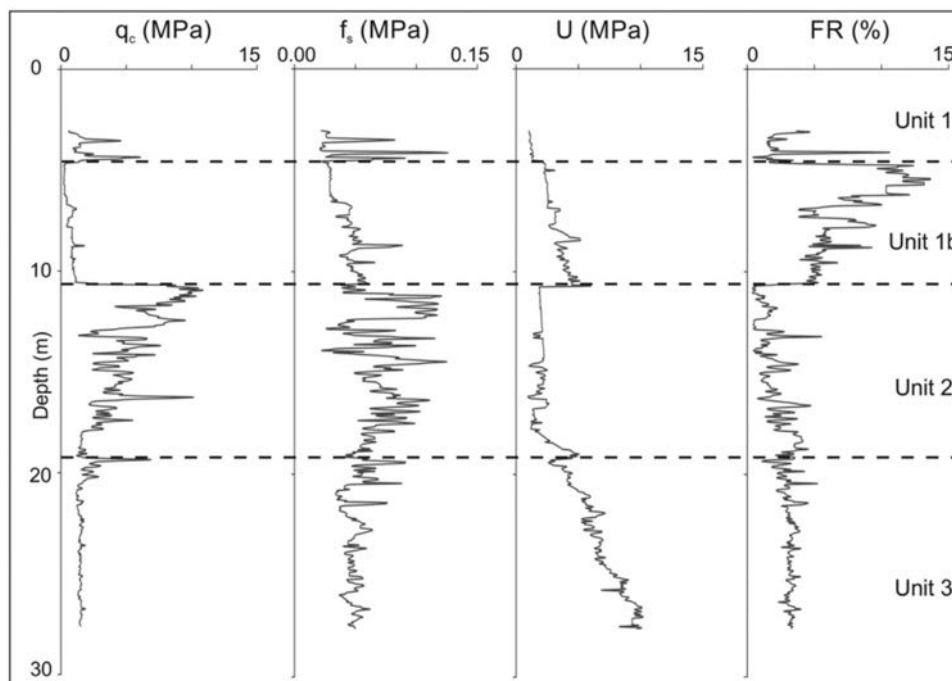


Figure 6.3.: Result of a standard piezocone test (CPTU₄), including measurements of cone resistance (q_c), sleeve friction (f_s), and pore water pressure (U) profiles. The calculated parameter FR (friction ratio) is also reported. Black dotted lines highlight the boundaries between different stratigraphic units; location of the probe is shown in Figure 6.6.

et al., 2012).

Subsidence phenomena and severe coastal and river floods can be serious threats in urban areas, as illustrated by numerous cases in Italy (e.g., Sadori et al., 2015; Comerci et al., 2015; Manunta et al., 2008; Stramondo et al., 2008, for Rome and Teatini et al., 2005; Tosi et al., 2013 for Venice) and worldwide (Amelung et al., 1999; Buckley et al., 2003; Fernández et al., 2009; Fruneau et al., 2005; Galve et al., 2009; Hu et al., 2004; Thierry et al., 2009). The methods adopted here could be applied in similar settings where risks posed by natural and anthropogenic hazards threaten cultural heritage sites. Indeed, the town of Como, like many other cities, has a history spanning millennia and thus it is possible to gather data from not only a geological or geomorphological perspective, but also from archeology and historical chronicles and documents. In particular, archeology and geomorphology in coastal areas can quantify relative topographic movements between the land and the sea or a lake (Gilli et al., 2003; Marriner, 2007; Stanley and Toscano, 2009).

Moreover, many lacustrine basins are spread at the foothills of the whole Alpine chain; these areas are highly populated and host relevant economic properties, being located in the heart of Central Europe. In this sense, the case of Como is not dissimilar in respect of many other cities located in lacustrine coastal areas at the piedmont of mountain belts, in Europe and elsewhere.

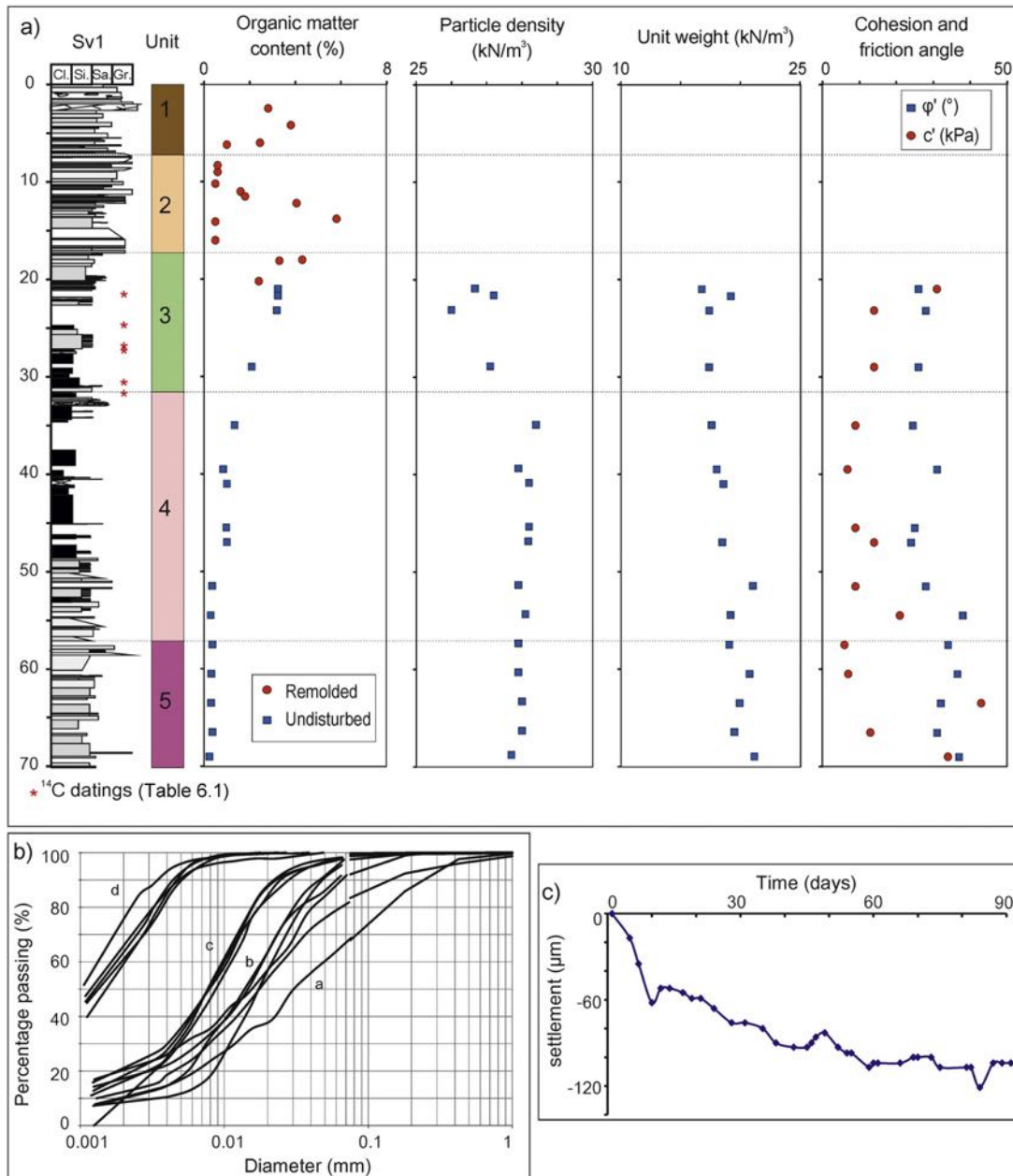


Figure 6.4.: a) Lithology of sediment core SV1 from Piazza Verdi site and related index geotechnical properties. Geotechnical tests (organic matter content, unit weight, particle density, cohesion and friction angle) were carried out at Ispra laboratories; b) grain size distribution: a–samples between 0 and 20 m, b–samples between 21 and 32 m, c–samples between 33 and 49 m, d – samples between 51 and 69 m; c) Time/settlement curve related to a long duration (90 days) oedometer test.

6.2. Geological and environmental framework

Lake Como, located at the foothills of the Southern Alps, is λ -shaped and occupies a glacial valley at an elevation of 198 m a.s.l. The Adda River is the main tributary, entering the lake in the northern sector, and is also the only outflow, at the SE termination of the lake.

The town of Como lies at the SW end of the western branch, which is hydrologically closed. A NW–SE oriented alluvial plain of ca. 5 km² and gradually rising from the lake level to 220 m a.s.l. at its southern margin, hosts the Como historical downtown. Due to its position and geomorphologic setting, the basin has collected sediment from a drainage area of more than 4500 km². The plain is drained by two small water courses, the Cosia and Valduce creeks, which are artificially forced to flow underground at their very end before flowing into the lake.

The town is built on a sedimentary basin containing a thick sequence of post-LGM (Last Glacial Maximum) lacustrine, palustrine and alluvial sediments. The basin is enclosed by two opposite-facing bedrock slopes, composed of Mesozoic pelagic carbonates (Medolo Gr. – Early Jurassic) to the NE, and deep-sea turbiditic conglomerates (Gonfolite Gr. – Oligocene-Miocene) to the SW (Figure 6.1b). A review of the regional geological framework is contained in (Michetti et al., 2013).

The Como urban area is bordered to the SW by the Gonfolite Backthrust, a major regional N-verging structure, putting the Gonfolite Group in tectonic contact with the underlying Mesozoic pelagic units (e.g., Bernoulli et al., 1989). The recent activity of this structure is indicated by deformed Pliocene-to-Quaternary deposits outcropping near Novazzano and Balerna (Ticino, Switzerland; e.g., Bini et al., 1992; Sileo et al., 2007; Zanchi et al., 1997). An outcrop in the Como urban area (“Borgovico site” after Livio et al., 2011) shows evidence of Late Pleistocene-to-Holocene reverse surface faulting along a secondary splay of the Gonfolite Backthrust, thus pointing to the need to consider local seismic potential (e.g., Michetti et al., 2012).

In 1998 the Geology Research Group at Insubria University started a systematic study of the geological, environmental and urban evolution of the Como area. Multidisciplinary data collection (section 6.3), encompassing geological disciplines (stratigraphy, hydrogeology, geotechnics), archeology and environmental sciences (¹⁴C dating, subsidence monitoring, analysis of biological proxies), have been systematically conducted since then. These observational data allowed us to draw a conceptual model of the Como basin (section 6.4). In the last three years, we have tested this model in cooperation with the Como Municipality to mitigate flood hazards (section 6.5).

6.3. Modeling the urban subsurface: multidisciplinary data collection

Land subsidence in the Como area has been studied for more than 40 years. In 1974, a municipal commission was established to study the phenomenon, which was causing severe damage to edifices. The first reconstruction of the Como town stratigraphy was based on direct investigations and the collection of more than 100 borehole logs (Comune di Como, 1980).

Subsequent research was focused on the geological framework and landscape evolution (Bini and Castelletti, 1986; Bini, 1987, 1993, 1996; Castelletti and Orombelli, 1986), hydrogeological setting (Apuani et al., 2000; Beretta et al., 1986) and archeology (Caniggia, 1968; Luraschi, 1987; Uboldi, 1993).

In recent years, studies by the Insubria University focused on the lacustrine environment and

related geohazards (Fanetti and Vezzoli, 2007; Fanetti et al., 2008), active tectonics (Livio et al., 2011) and the post-LGM evolution of the area (Capeletti, 2008; Comerci, 2004; Comerci et al., 2007; Ferrario, 2013; Martinelli, 2014). Most of the information has been integrated in local policy documents (e.g., *Comune di Como*, 2011).

6.3.1. Stratigraphy

The sedimentary infill of lake basins records past climatic changes and also extreme past events, as demonstrated by several authors (e.g., in particular for lacustrine settings of the same Alpine region, (Fanetti et al., 2008; Lauterbach et al., 2012; Strasser et al., 2013)). The sedimentary basin beneath the town of Como preserves an archive of environmental data that is almost continuous because of the high sedimentation rate and virtually no erosion.

However, the sediment architecture shows important lateral and vertical facies changes. The Como urban subsurface is composed of late glacial and Holocene loose sediments from different depositional environments; only the upper ca. 180 m of the sedimentary sequence has been directly explored by boreholes.

We conducted field surveys at 1:10,000 scale for production of the new official geological map of Italy (Michetti et al., 2013) and gathered available stratigraphic data from private and public archives. More than 250 borehole logs, covering a territory of 5 km² and including the entire urban area were collected. Most of the boreholes were a few tens of meters deep, but ca. 5% of them reach 120 to 180 m depth. Drillings were made between 1950 and 2013 for different purposes, thus the data from the logs are of heterogeneous quality. All data were therefore standardized and georeferenced on a topo map at 1:10,000 scale (*Carta Tecnica Regionale – CTR*) with meter accuracy (Figure 6.2).

The generalized stratigraphic succession of the whole urban area is based on grain-size distribution, organic and archeological content and geotechnical index properties of the sediments. The basic stratigraphy (*Comune di Como*, 1980) has gradually improved with time, with the adding of more recent data (Comerci et al., 2007; Ferrario, 2013).

Some key sites are highlighted in Figure 6.2: the most detailed stratigraphic logs are located at *Piazza Verdi* and near *Como Cathedral*. At *S. Abbondio*, several boreholes and two ¹⁴C dates are available (Castelletti and Orombelli, 1986; Comerci, 2004; Comerci et al., 2007). At *via Valleggio*, direct observation of stratigraphic sections up to 7 m high and 15 m wide was possible and two ¹⁴C dates were obtained (Comerci et al., 2007). At *Borgovico*, the Gonfolite Backthrust was observed (Livio et al., 2011).

The sedimentary sequence is composed (from the top) of 1–10 m of heterogeneous reworked material with archeological remains (Unit 1); in the lake-shore area, a silty and highly compressible sub-unit (Unit 1b) has been recognized within the anthropic sediments. Alluvial sands and gravels (Unit 2) are present down to a depth of 15–24 m. Under this sandy gravel unit are up to 30 m of palustrine organic and highly compressible silts (Unit 3); in *Piazza Verdi*, they date between 4 and 18.5 cal kyr BP. At some sites, two distinct facies have been recognized, the first one being more sandy (Unit 3a) and the second one more clayey (Unit 3b). Below 40–60 m depth, distal glaciolacustrine sediments with dropstones are present (Unit 4) and overlie coarser proximal deposits (Unit 5).

6.3.2. Geotechnical data

Lake-shore area – 1997 campaign

The lake-shore area was investigated in 1997 for a preliminary study for designing the defense system against floods ([Comune di Como, 1997](#)). Ten cores were drilled, each one 60 m deep. In situ tests included Standard Penetration Tests (SPT), Lefranc Permeability Tests (LPT) and Cone Penetration Tests with pore pressure measurements (CPTUs). Laboratory analyses were carried out on 88 undisturbed and 9 remolded samples. Inside the drilling holes, 9 piezometers and a magnet extensometer were installed.

Borehole logs were used to calibrate data of 5 CPTU tests, up to 30 m deep. Cone resistance (q_c), sleeve friction (f_s) and pore pressure (U) were recorded at 5 cm intervals; a friction ratio (FR), defined as the percentage ratio between f_s and q_c , was calculated. Sedimentary facies were recognized, based on cone resistance, vertical grading and boundary characteristics (e.g., [Amorosi and Marchi, 1999](#)).

Figure 6.3 presents the results of test CPTU4 (see (Figure 6.6 for location), between 3.05 and 27.6 m depth. The investigated sequence represents the most surficial part of the stratigraphy illustrated in subsection 6.3.1. Anthropogenic fills (Unit 1) show q_c values between 2 and 10 MPa, whereas an FR range of 2–3 % is recorded, with a single peak reaching 10%. The stratigraphic succession previously adopted for the urban planning indicated a boundary between coarse anthropic deposits and alluvial sediments. Subsequent research suggested a finer horizon, named Unit 1b, overlying the alluvial deposits of Unit 2. We identify this package because of its peculiar signature on CPTUs, defined by very low q_c values (1–2 MPa) and FR varying between 3 and 12 %; the highest FR peaks were recorded in this unit. The upper limit of Unit 1b is characterized by a sharp decrease in q_c and an increase in FR, while its lower limit is highlighted by an abrupt increase in q_c and f_s and a decrease in U and FR values.

Alluvial sediments of Unit 2 show q_c values that are higher (5–15 MPa) and FR that are lower (1–2 %) than the other units. A coarsening upward trend is generally recognizable, and wide fluctuations are due to local finer horizons. The transition to the lowermost Unit 3 is gradational and marked by a decrease in q_c and an increase in U values. The q_c range is 2–3 MPa and the FR ranges from 1 to 6 %; the unit is quite uniform, but locally a much more heterogeneous deposit related to a rhythmic alternation of organic and inorganic strata is present, as confirmed by borehole logs.

Piazza Verdi drillings

Two drillings for scientific analyses (SV1 and SV2, 70 and 65 m deep, respectively) were carried out at *Piazza Verdi* (Figure 6.2) in 2005. Sedimentological, paleomagnetic, geochemical, geophysical and paleobotanical (pollen and plant macrofossils) analyses, added to ^{14}C -AMS dating, allowed calibration of the subsurface database and placement of this site within the regional framework of the southern Alps.

Here we describe the geotechnical results obtained at *Piazza Verdi* on SV1 (tests carried out at ISPRA laboratories), while details on geochemistry and biological proxies acquired from SV2 will be the subject of a companion paper.

A number of parameters were investigated (Figure 6.4a). As soon as the sediments were collected, pocket penetrometer and shear values were recorded; resistance gradually increases from 50–150 kPa between 6 and 50 m depth to 200–300 kPa below 50 m. Inside the drilling holes,

11 standard penetration tests (ASTM D 1586) were performed. N_{spt} values range between 3 and 12 for Units 1 and 2, whereas maximum values of 39 were recorded for Unit 5. Undrained shear resistance was measured with 13 Vane-borer tests (ASTM D 2573), resulting in values of 65–110 kPa. Geotechnical laboratory tests were carried out on 15 undisturbed samples collected from depths of 20 m to 70 m and on 80 disturbed samples collected from the more surficial layers.

The grain-size distribution, determined from a sieving and sedimentation procedure based on ASTM D 422 (Figure 6.4b), the particle density and, for clayey samples, plastic and liquid limits, were measured throughout the stratigraphic column. In the first 20 m below the surface the material is predominantly detrital, with numerous anthropogenic lithics. Between 20 and 69 m the following particle size classes were identified: silts with clay between 21 and 32 m (Unit 3); clays with silt between 33 and 49 m (Unit 4); silts with clay and locally sand between 51 and 69 m (Units 4 and 5).

The organic content, measured according to ASTM D 2974, is highly variable in Units 1 and 2; values are particularly high around 20 m depth (3%; Unit 3), then decrease to 1% between 40 and 50 m (Unit 4), reaching finally 0.3% below 50 m (Unit 5; Figure 6.4a).

The particle density shows two different trends: above the depth of 30 m, values fluctuate from 26 to 27.2 kN/m³, presumably due to lithological inhomogeneity. Below that depth, values are much more constant, around 28 ± 0.2 kN/m³.

The investigated sediments all show a saturation close to 100%; the unit weight in saturated condition measured in undisturbed samples is between 17 and 19 kN/m³ down to a depth of 50 m, and between 19 and 21 kN/m³ at depths greater than 50 m (Figure 6.4a). The samples belonging to Unit 5, show higher unit weight and lower void ratio, depending on the increasing lithostatic load with depth.

Cohesion and friction angle were derived from a series of triaxial tests: cohesion generally varied between 5 and 15 kPa, although higher values were recorded locally. The friction angle ranges between 24° and 28° in the upper part of the sequence, whereas below 50 m depth values were 30° to 40°.

A series of 16 oedometer tests was carried out using the Casagrande procedure (ASTM D 2435) to evaluate the preconsolidation pressure. A few tests performed on samples cored near the lake-shore in the first 20 m show a moderate over-consolidation. *Piazza Verdi* samples show that from 20 to 35 m depth the over-consolidation ratio reduces and reaches the values of normal consolidation, characteristic of soils still consolidating under their own weight. Two different interpretations can be suggested: (i) the sediments were not loaded by the glacier because they settled after its retreat; (ii) the sediments settled in the presence of a melting glacier, but the pressure was totally or partially absorbed by a water layer below the ice.

In order to evaluate long-term compressibility, a long-duration oedometer test was carried out, applying a load of 400 kPa for about 90 days (Figure 6.4c). In such a test, the deformation is due to the viscous strain of the solid skeleton and it occurs under a constant effective pressure, and thus also (but not only) when the primary consolidation is ended. The secondary compression index (C_α) value is equal to 0.0027, which is rather low, although between ordinary limits in normally consolidated deposit. Long-duration deformability and viscous phenomena can be, therefore, a cause of subsidence in this area.

Geotechnical results were consistent with each other and highlighted a sharp discontinuity in the stratigraphy at ca. 30–33 m depth, broadly corresponding to the lithological boundary between Units 3 and 4; this fact was related to the environmental evolution of the Como basin, as discussed in subsection 6.4.2.

6.3.3. Chronological constraint: ^{14}C dates and archeology

Table 6.1.: ^{14}C ages and calibration of samples from the Como urban area. Calibration was carried out applying Oxcal software (<https://c14.arch.ox.ac.uk/oxcal/OxCal.html>, last accessed April 2014) and the IntCal13-calibration curve (Reimer et al., 2013).

Site	Lab code	Dated material	Type	Unit	Sediment core depth (m)	Elevation (m a.s.l.)	Convent. date (^{14}C yr BP)	2σ cal. (cal. yr BP)	Reference
Piazza Verdi	RC231	Charcoal	AMS	3	21.70-21.95	179.2	3959±61	4779-4183	This paper
Piazza Verdi	LTL2281A	Vegetal remains	AMS	3	25.00-25.20	175.9	4590±55	5467-5052	Capeletti (2008)
Piazza Verdi	LTL2282A	Vegetal remains	AMS	3	30.80-31.00	170.1	12,496±55	15,060-14,305	Capeletti (2008)
Piazza Verdi	GrA-30878	Bulk sediment	TOC	3	31.95	169.05	15,140±70	18,602-18,182	Capeletti (2008)
S. Abbondio		Wood		3	8.74-8.78	201	11,730±180	14,006-13,213	Castelletti and Orombelli (1986)
S. Abbondio	GrA-23357	Wood		3	5.07-5.10	204	13,230±120	16,260-15,500	Comerci (2004)
Via Valleggio	GrA-29158	Organic sed.		3	4.50-4.60	209	5100±50	5940-5725	Comerci et al. (2007)
Via Valleggio	GrA-29436	Organic sed.	AMS	3	5.00	209.5	13,880±200	17,422-16,247	Comerci et al. (2007)
Lake-shore	LTL13422A	Wood	AMS	1b	11.98	186.7	703±40	730-560	This paper (Figure 6.12d)
Lake-shore	LTL13423A	Wood	AMS	1b	16.94	181.7	1443±50	1420-1270	This paper (Figure 6.12d)
Lake-shore	LTL13424A	Wood	AMS	3	17.47	181.2	6447±45	7431-7278	This paper (Figure 6.12d)
Lake-shore	LTL13425B	Wood	AMS	3	38.40	160.3	6570±45	7570-7420	This paper (Figure 6.12d)

A number of ^{14}C dates (Table 6.1), integrated with the stratigraphic and archeological record, provide time constraints on the post-LGM evolution of the study area. Unit 3 settled out during several millennia since ca. 18.5 cal kyr BP, the minimum age for the deglaciation of the basin. The oldest archeological finds (from the Iron Age) were found on the mountain slopes surrounding the basin (Uboldi, 1993); at that time, the plain was an unhealthy, marshy area, frequently affected by debris flows and floods.

An impressive reorganization of the drainage network and related mountain catchment, including the diversion of the Cosia and Valduce creeks in the Como plain, took place immediately before *Novum Comum* was founded in 59 BC (ca. 2000 BP) under the Roman Consul Gaius Julius Caesar. Cosia stream was forced to flow at the base of the SW mountain slope, and Valduce stream on the opposite side, thus allowing the building of the town itself in the center of the plain. To the north, the town was naturally protected by the lake, whereas on the other three sides, town walls were built (Caniggia, 1968; Luraschi, 1987). Archeological evidence found at different sites indicates the migration of the coast and the town harbor towards the north. Among other findings, a Roman quay was discovered in *Piazza Cacciatori delle Alpi* (Jorio, 2004), and in *Piazza Mazzini* wooden remains were found (location in Figure 6.2). The present-day *Piazza Cavour* was the dock of the town till 1870.

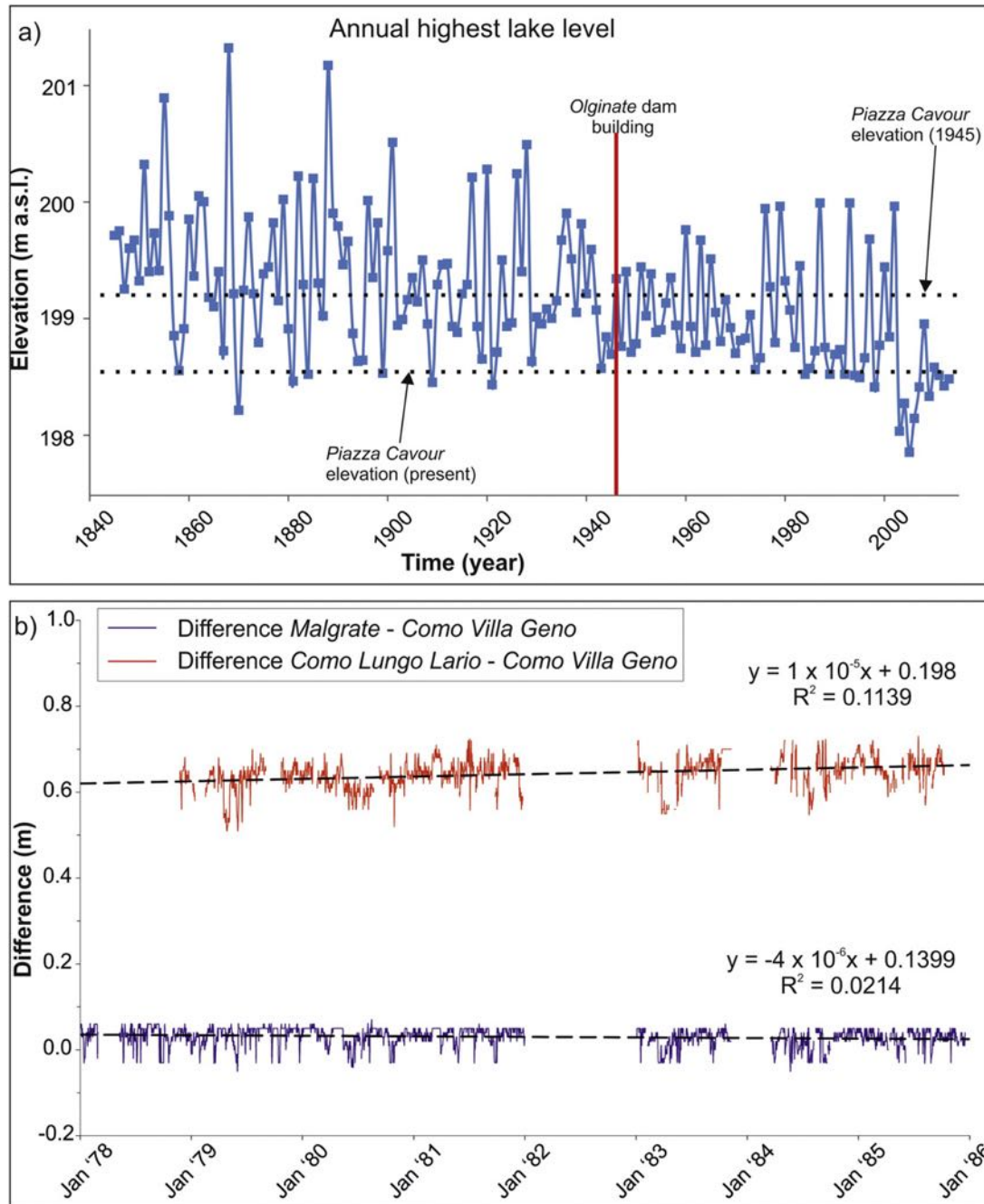


Figure 6.5.: Annual highest lake-level recorded in the Lecco branch during 1845–2013 (1845–1935: Malpensata gauge; 1936–2007: Malgrate gauge, [Moisello and Vullo, 2010](#), 2008–2013: Malgrate gauge, data courtesy Consorzio dell’Adda). Dotted lines represent Piazza Cavour elevation in 1945 (199.18 m a.s.l.) and today (198.53 m a.s.l.); the vertical red line indicates the building of Olginate dam (see Figure 6.1a). b) Lake levels daily recorded during 1977–1987 in the three measurement points; note the difference between Malgrate and Villa Geno (blue series) and between Lungo Lario and Villa Geno (red series); the first one has a horizontal trend, indicating the relative stability of the two locations; the difference between Lungo Lario and Villa Geno is increasing because Lungo Lario measurements do not reflect the real lake-level, but are equal to the lake-level plus the intervening ground subsidence; see Figure 6.1 for gauge location.

6.3.4. Lake flooding and subsidence

The hydrological regime of Lake Como has been regulated since 1946 by a dam located in *Olginate* (see Figure 6.1a). The close relation between lake-level control, flooding and subsidence is clearly illustrated in Figure 6.5a, where the annual highest lake levels recorded in the Lecco branch during 1845–2013 are shown (Moisello and Vullo, 2010). Lake-level regulation reduces but does not eliminate the flood hazard: in the last decades, major floods occurred in 1987, 1993 and 2002, and the last event of moderate intensity happened in July, 2008.

Most of the archeological finds and also building foundations in the town of Como are presently below groundwater level, thus suggesting significant variations in ground surface and groundwater level in the last centuries. This could be consistent both with ground subsidence and/or groundwater rise related to an increase in lake-level. In the whole Lake Como area, except the town of Como, Roman and Medieval settlements are always above lake-level (Luraschi, 2002), thus suggesting the absence of any significant rise in lake-level in the last two millennia. On the contrary, data in the Como area points to a strong subsidence, driven by local factors. Indeed, the sedimentary basin is characterized by a sequence of young unconsolidated silty sediments with poor mechanical properties, locally more than 30 m thick. These deposits naturally undergo differential settlement due to a decrease in the void ratio, biochemical degradation and decomposition of organic matter.

The zones experiencing higher subsidence rates are also the most valuable areas in terms of cultural heritage and local economy, namely the town's historic center and the waterfront area; thus, even if the subsiding area is spatially limited, the effects are critical to the whole town. Beyond the negative effects on the road network, tourism and the city's image, subsidence also is a significant safety and economic problem.

Surface deformation has been detected by leveling, remote sensing and gauges measurements, and archeological and geological constraints. We can discriminate between natural and anthropogenic components and quantitatively estimate subsidence rates. Here, we build on and expand previous results (Comerci, 2004; Comerci et al., 2007) with new ones and present a new estimate of the 1977–1987 subsidence rate.

Long-term subsidence rates

The boundary between Unit 3 and Unit 4 was used as a marker horizon to estimate the long-term, average subsidence rate since the late-glacial period. This limit, clearly recognizable from stratigraphic logs, is located at approximately 50 m depth near the lake, while it nearly outcrops along the inland borders of the plain, such as at the *S. Abbondio* site. Since Unit 3 does not show any vertical change of facies, the present-day stratigraphic architecture is likely due to subsidence. The limit has been dated at ca. 18.5 cal kyr BP, indicating an average subsidence rate of ca. 2.5 mm/yr in the lake-shore area (Comerci et al., 2007). Subsidence rates decrease to the south and towards the borders of the basin.

Archeological data indicate an average subsidence rate of ca. 1 mm/yr in the last two millennia, which is consistent with the long-term rate (Comerci et al., 2007).

Short-term subsidence rates

Recent subsidence rates were independently estimated from leveling, hydrometric levels and remote sensing. During the period between 1928 and 2012, ten leveling surveys were conducted;

the highest rates of subsidence, up to over 20 mm/yr, were recorded during 1950–1975. Groundwater pumping from a deep aquifer was the main cause, but other potential causes include land reclamation, ground overloading and road traffic ([Comune di Como, 1980](#)). After that period, subsidence decreased because of the suspension of aquifer exploitation in the Como valley; between 1980 and 1997 there was even a slight increase in elevation of several benchmarks. Ground sinking can be estimated from hydrometric data, comparing instrumental values of gauges located on stable bedrock and others located on compressible sediments. Three measurement devices are considered here. The gauge located in *Malgrate* (Lecco branch, SE end of Lake Como, see Figure 6.1a) gives the "official" lake level and is the one used by institutions responsible for lake-level management. In the Como branch (SW end of Lake Como) two gauges are present, one founded directly on bedrock northeast of Como town (*Villa Geno*, see Figure 6.1a,b), and the other is located on the lake-shore deposits (*Lungo Lario*, see Figure 6.1a,b). The first two instruments were built in 1936 on stable rock, whereas the latter is located on very young (ca. 120-yr old) highly compressible sediments.

A subsidence rate of 10^{-5} m/day (ca. 3.65mm/yr) has been calculated; this is an order-of-magnitude value and is consistent with rates estimated with other methods. Data demonstrate the relative stability between Villa Geno and Malgrate and the progressive lowering of the instrument located at Lungo Lario.

During the last 20 years, ground movements have been surveyed both by geodetic leveling ([Barzagli et al., 2011](#); [Bonci et al., 2004](#); [Giussani, 1997](#)) and radar persistent scatterer interferometry PSInSAR ([Ferretti et al., 2000](#)). Analysis of ERS2 data (for the 1992–2003 time interval) shows that results are in good agreement ([Comerci, 2004](#)). In the absence of external triggering factors, the present-day subsidence rate is comparable to the long-term one, i.e., on the order of a few mm/yr near the lake-shore. In contrast, an uplift trend of up to 2 mm/yr is recorded on the higher relief areas that border the plain, consistent with the regional uplift characterizing the whole pre-Alpine chain ([Arca and Beretta, 1985](#)). Since 2008, relevant engineering works have been carried out on the lake-shore area. Interferometric data acquired for the 2003–2012 period ([TRE Europe, 2012](#)) show a cumulative sinking of 4 m (ca. 5 mm/yr) in the working area, most of which occurred between 2008 and 2009. In contrast, elsewhere in the town a constant rate of 1–2 mm/yr of sinking was recorded.

6.3.5. Hydrogeology

In the Como urban area, a shallow aquifer is present down to ca. 25 m depth, within anthropic and alluvial deposits (Units 1 and 2); a deeper aquifer, subdivided into several lenses or layers due to lateral heterogeneity, is located in the proximal glaciolacustrine deposits (Unit 5). The confining unit is the sequence of clays and silts of Units 3 and 4 ([Apuani et al., 2000](#); [Beretta et al., 1986](#)). The deep aquifer was intensively exploited for civil and industrial supply until 1980, when water extraction was forbidden ([Comune di Como, 1980](#)).

Figure 6.6a shows the isopiezometric curves related to the mean level of the surficial aquifer in the absence of human-induced alterations: groundwater flows from SE to NW, towards the lake, which is the local base level. This interpretation is derived from multi-year monitoring of the urban instrumental network (Figure 6.6b), which consists of ca. 30 piezometers in total, 18 of which are located in the center of the town ([Comune di Como, 1997](#); [RCR s n c, 2010](#)). The first systematic measurements were made in 1975–1977, whereas during 1980–2005 only sparse readings were taken; since 2006, monthly measurements have been taken by the Insubria

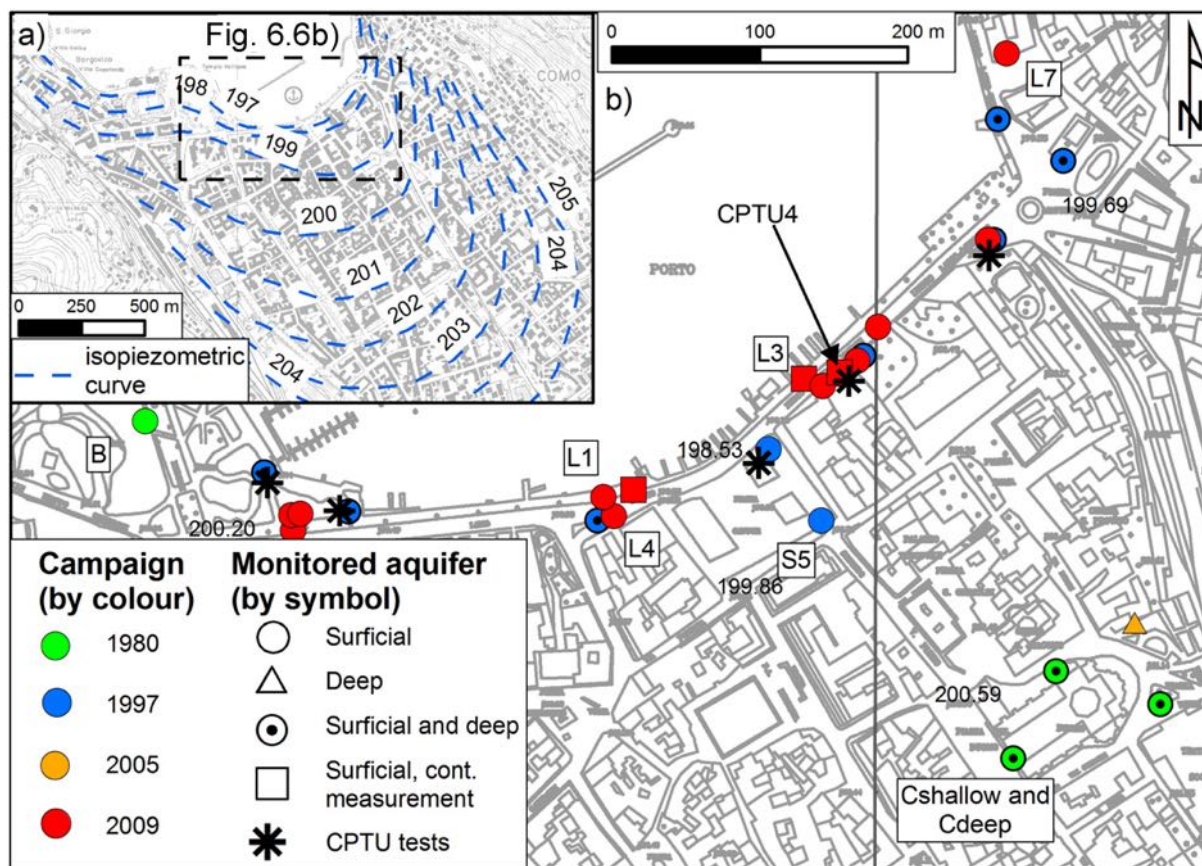


Figure 6.6.: Schematic reconstruction of curves of equal piezometric level of the phreatic aquifer (values expressed in m a.s.l.). b) Location of the instrumental network for groundwater monitoring and of CPTU tests.

University.

Figure 6.7a shows a comparison between lake and groundwater level, for seven selected measurement points, during January 2006–December 2012. All instruments excepted C_{deep} are in the shallow aquifer – the L series is located at the lake-shore, S5 at *Piazza Cavour* and C near the cathedral. The piezometric level in the shallow aquifer near the lake is closely related to the lake-level, and strongly follows its trend, although with fewer high-frequency oscillations and with a short delay. *Piazza Cavour* was partially inundated in July, 2008 (Figure 6.7a). Inland, farther from the lake, the lake-level influence is less pronounced and variability decreases.

In natural conditions, seasonal variability ranges between 1 and 1.5 m; however, human activities can significantly lower the water level, as happened between June 2009 and June 2010 due to the ongoing engineering works. A lowering of 3–4 m and the subsequent recovery of groundwater level are clearly evident (Figure 6.7b).

The few measurement points in the deep aquifer are flowing artesian wells, except for the piezometer named C_{deep} , located just in front of the cathedral together with C_{shallow} (Figure 6.6b). C_{shallow} has a screen depth at 5 m below the ground surface, and C_{deep} at 21 m. The level in C_{shallow} is always ca. 1 m lower than the one in C_{deep} and thus the wells are definitely monitoring two distinct water bodies – the shallow aquifer for C_{shallow} and a deeper aquifer for C_{deep} . A geochemical investigation is currently underway to better understand the hydrogeological setting of the area.

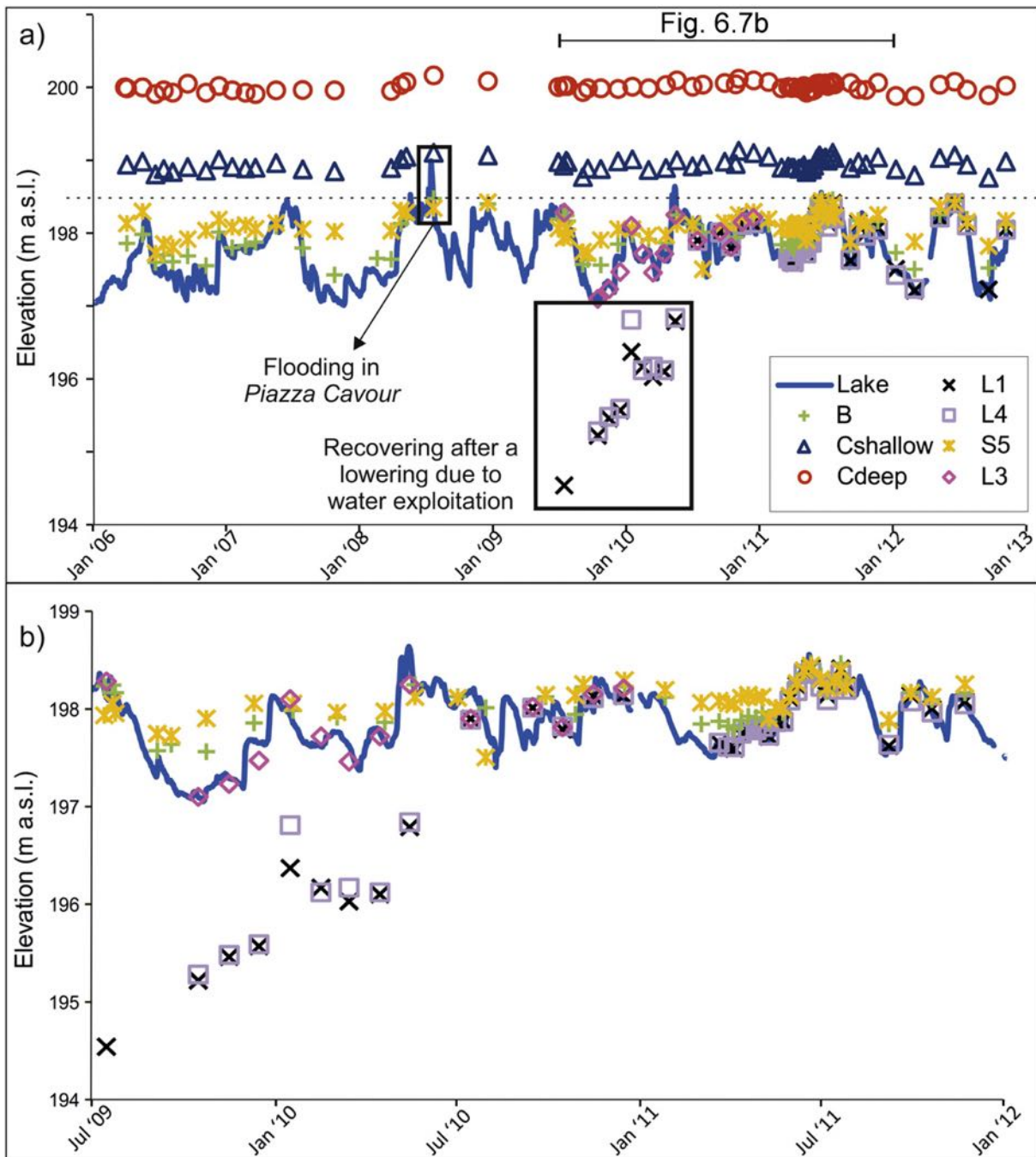


Figure 6.7.: a) Comparison between lake-level (Malgrate station; Figure 6.1a) and groundwater level detected at seven selected measurement points (see Figure 6.6b) during January 2006–December 2012. L series is located on the lake shore, S5 at Piazza Cavour and C near the cathedral; all instruments excepted C_{deep} refer to the shallow aquifer. The dashed horizontal line represents the elevation at which Piazza Cavour is inundated (198.53 m a.s.l.). b) Focus on the coastal area, where engineering works caused a lowering of the water table.

6.4. Modeling the urban subsurface: results

Safe urban planning has to be based on the forecast of sediment behavior under stresses (overloading, possible ground shaking, etc.). For Como, this issue is not trivial, because the present-day landscape surrounding the town is the product of many different geologic processes. Firstly, we correlate stratigraphic data in order to draw two geological cross-sections (subsection 6.4.1) and subsequently we reconstruct the landscape evolution since late-glacial times (subsection 6.4.2).

6.4.1. Stratigraphic correlations

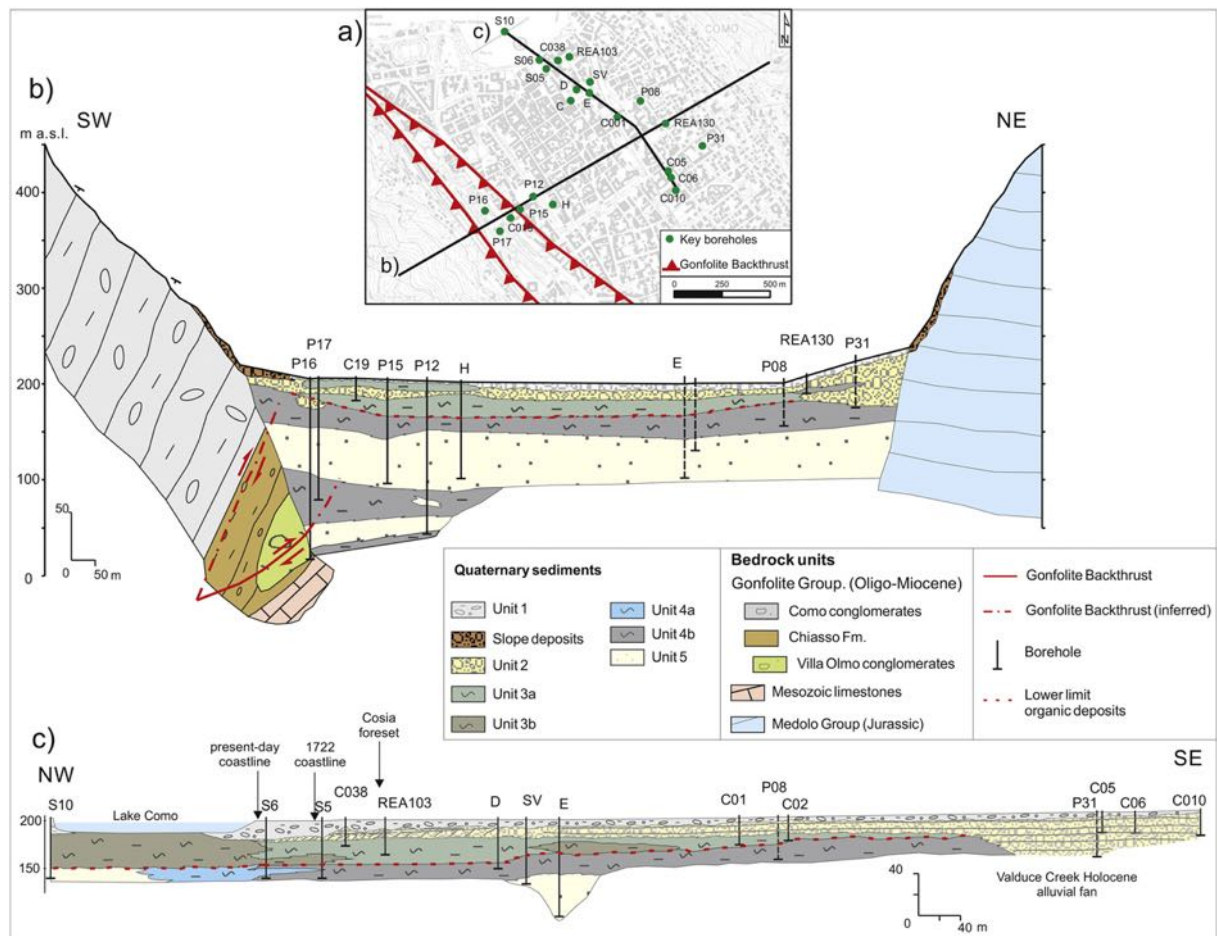


Figure 6.8.: a) Trace of the sections and position of the stratigraphic logs. b) Geological cross-section SW–NE oriented, perpendicular to the sedimentary basin; vertical exaggeration 2. c) Section NW–SE oriented, from Lake Como towards the town. Sections redrawn after Ferrario (2013).

Two cross-sections (Figure 6.8a), nearly perpendicular to each other, were drawn based on borehole logs and geotechnical data; stratigraphic units were defined based on those of subsection 6.3.1 but some adjustments were made to take local features into account. Unit 1b is found only in the lake-shore area and not elsewhere; while slope deposits are common on the borders

of the plain, thus a specific unit was added.

Figure 6.8b shows a SW–NE oriented section, broadly perpendicular to the axis of the sedimentary basin. The section is based on 11 stratigraphic logs, some more than 130 m long (P12, P16, P17), but their stratigraphic detail is low. In this section, only the main units have been recognized, without distinguishing different facies. Well data highlight that the basin, repeatedly occupied by a huge glacier during the Quaternary, is a valley overdeepened by glacial erosion, like many others both on the northern and southern side of the Alps (e.g., [Preusser et al., 2010](#)). On the western side of the basin, well P16 reaches the bedrock (Gonfolite Gr.) at 181 m below ground surface (ca. 35 m a.s.l.); bedrock absolute elevation rises to ca. 200 m a.s.l. a few km to the south ([Comune di Como, 2011](#)), along the axis of the former ice tongue, thus implying a rise in the valley floor of more than 150 m. Valley sides are characterized by a dip of ca. 45°; a significant increase in dip is recorded in the buried sectors, where it has been estimated at ca. 60°. The increase of valley side dip can be explained, besides selective erosion of less resistant lithologies, as possibly due to structural control from recent activity of the Gonfolite Backthrust. Figure 6.8c shows a NW–SE oriented profile, from the lake towards Como town. The section is based on 15 highly detailed stratigraphic logs and highlights the different lake coastline positions and a Cosia Creek foreset located between the lake-shore and the cathedral ([Bini and Castelletti, 1986](#)). The southern part of the section crosses an old alluvial fan attributed to Valduce Creek ([Bini, 1993](#)).

6.4.2. Landscape evolution

Late-glacial

During the LGM, in the Alps dated at ca. 21–19 cal kyr BP (e.g., [Ivy-Ochs et al., 2006](#); [Ravazzi et al., 2007](#)), the top of the Adda Glacier reached about 825 m of elevation on the mountain slopes around Como and spread in the piedmont area as far as the town of Cantù, ca. 10 km south of Como (Figure 6.9a). Basin deglaciation of several overdeepened foreland piedmont lakes on southern and northern sides of the Alps, including Lake Como, appears to be synchronous at millennial scale ([Ravazzi et al., 2014](#)). With glacier retreat, a proglacial lake formed at 270 m a.s.l. between the glacier front and the *Camerlata* sill (Figure 6.9b) when the *Camerlata* threshold acted as a spillway, and waters flowed to the south in the present-day Seveso River valley. Another proglacial lake was present at the end of the Lecco branch, at an elevation of ca. 220 m a.s.l. ([Nangeroni, 1972](#)). During this phase, coarse proximal sediments (Unit 5) and finer deposits with dropstones (Unit 4) settled in the Como plain, suggesting the presence of a relatively wide and deep glaciolacustrine basin and a cold and arid climate.

When glacier retreat reached the Bellagio sill, the local lake-level dropped from 270 to 220 m a.s.l. ([Bini, 1993](#)), and the Como branch joined the Lecco branch, generating the modern Lake Como. The Como branch became a closed basin, a sediment trap with a spillway located in the Lecco branch (Figure 6.9c). The drainage network around Como town underwent a complete inversion, flowing north now towards the newly born lake.

With the inception of a more temperate and humid climate, organic remains started to be deposited in the lake, locally consisting of marshes and surrounded by vegetated slopes. We dated the first appearance of organic matter in the stratigraphic sequence at several sites; at the *Piazza Verdi* and via *Valleggio* sites ages of ca. 18.5 and 17 cal kyr BP were obtained,

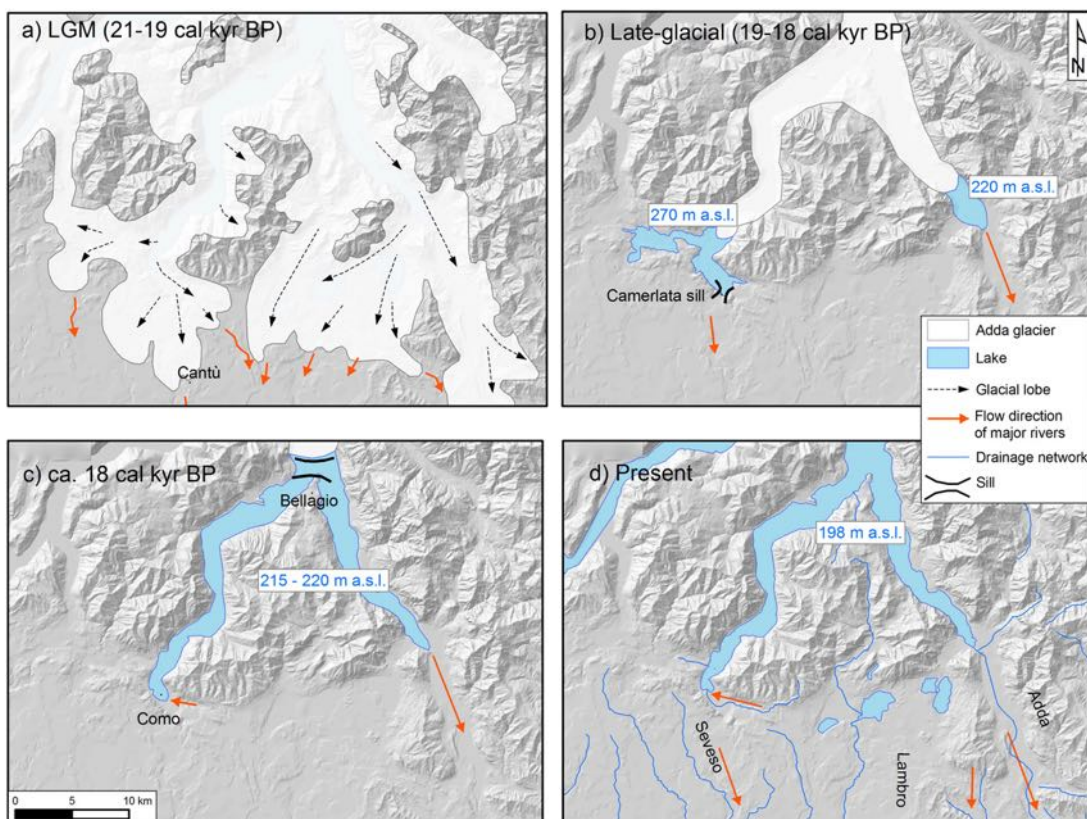


Figure 6.9.: Simplified landscape evolution of the Como basin since LGM(a), Late-glacial (b), 18 cal kyr BP (c) up to present (d); glacial cover, proglacial lakes and the main drainage systems are shown (modified after [Bini, 1993](#)).

respectively (Table 6.1). At that time, the entire Como plain was deglaciated.

The stratigraphic database was examined using spatial analysis GIS functions. Unit 3 was divided into six classes of different thicknesses (see Figure 6.10; 0 m; 1–2 m; 3–5 m; 6–10 m; 11–15 m; > 15 m) and plotted on the topographic map. A maximum thickness (> 30 m) was found in the lake-shore area and gradually decreased towards the borders of the basin. The elevation field of the base of Unit 3 was calculated by means of a kriging interpolator; this boundary is well-documented by core logs, geophysical and geotechnical parameters, and by biological proxies. This paleo-surface is dated at ca. 18.5 cal kyr BP and its 3D architecture is clearly deformed by the long-term subsidence (Figure 6.10).

Unit 3 did not cover the whole Como urban area: in the outer part of the basin (e.g., *Borgovico* site) Unit 2 directly overlies Unit 4. The spatial extension of Holocene organic silts runs at an elevation of ca. 215–220 m a.s.l., which we interpreted as the paleo-lake level when the two branches of Como and Lecco were connected due to deglaciation and organic material started to accumulate on the lake bottom. We suggest that while on higher areas (*Borgovico*) a subaerial environment developed, on peripheral areas (e.g., *S. Abbondio*) a shore environment was present, and the inner part of the basin (e.g., *via Valleggio*) was occupied by shallow waters ([Comerci et al., 2007](#)). By that time, the glacier had retreated north of the Bellagio sill, otherwise the lake-level would have been at 270 m a.s.l.

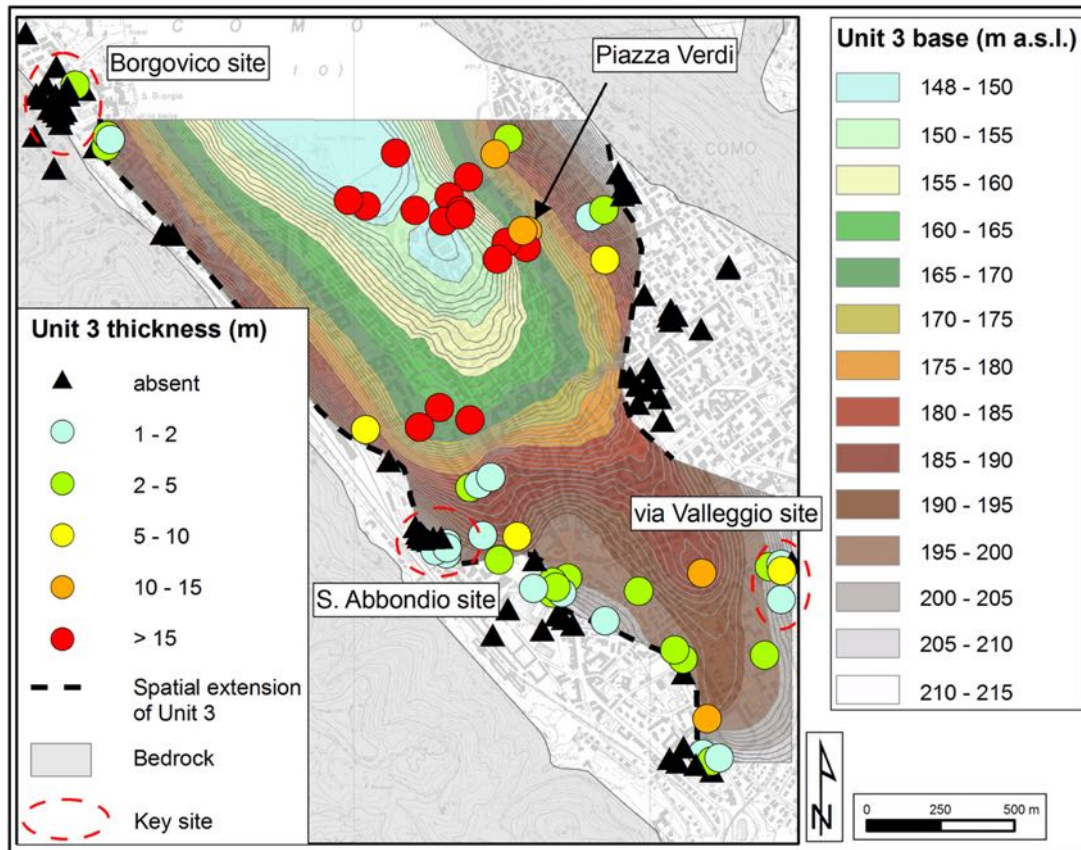


Figure 6.10.: Thickness of Unit 3 (round symbols) and elevation of Unit 3 base.

Post-glacial to Holocene

The sedimentation of Unit 3 in the center of the Como basin continued up to Early Holocene in a stable lacustrine environment, with no glacial influence. The supply of coarse material was very low, because the local drainage network consisted of small tributaries. Only along the edge of the plain did slope and fan deposits contribute to the filling of the basin. The Cosia Creek drainage basin was limited to its lower part: the upper and intermediate basins were tributaries of the Lambro and Seveso River basins (Figure 6.11a), probably due to glacial deposits damming the paleo-Cosia course. With the erosion of these deposits, the drainage basin of Cosia Creek extended to the east through at least two piracy events, reaching its present-day configuration (Ascheri, 1972; Orombelli, 1976). The last piracy event probably occurred just before 6 cal kyr BP, when the drainage basin expanded from 7 km² to approximately 20 km². This expansion occurred in an area rich in glacial deposits, which were rapidly eroded and transported into the lake.

Stratigraphic logs and ¹⁴C dates (Table 6.1) helped in identifying the position and the adjustments of the local drainage courses. The Cosia alluvial fan reached the areas of *via Valleggio* (ca. 5.8 kyr BP) and *Piazza Verdi* (ca. 4.5 cal kyr BP), which points to a fast progradation of the Cosia Creek delta over the palustrine basin (Figure 6.11b). This was promoted both by natural and anthropogenic components and resulted in the deposition of 10 to 25 m of gravels and sands. A strong increase in microscopic charcoal influx occurred about 5.6 cal kyr BP (Martinelli, 2014) and reflects human influence, in particular the use of fire in deforestation. The fast

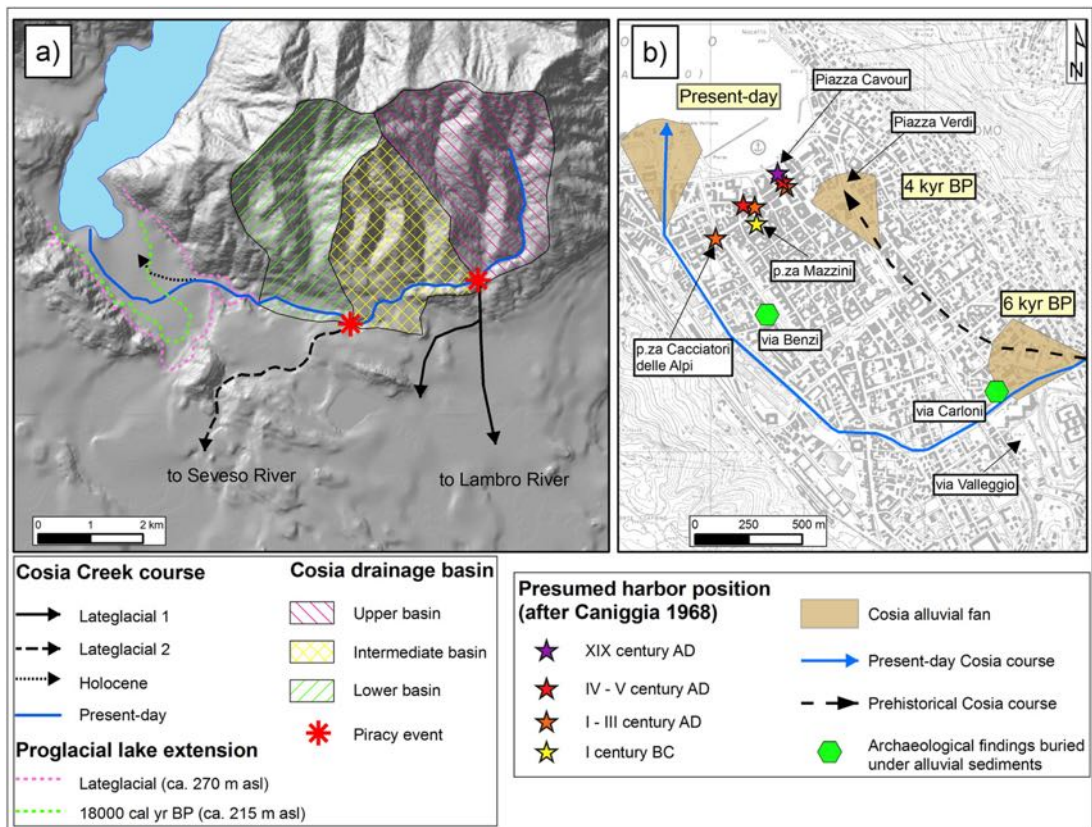


Figure 6.11.: a) Cosia Creek probable courses during Early Holocene and their drainage basin, which has been subdivided into upper, intermediate and lower basins; b) Stratigraphic and archeological findings that helped to identify the Holocene position of the Cosia alluvial fan and the evolution in the position of the town harbor.

progradation of the Cosia Creek delta abruptly ceased ca. 4 cal kyr BP; in this case, natural (e.g., lack of source material, lake-level oscillations) or human factors (e.g., better human control of the territory) may have contributed.

The lake-shore position was stable up to ca. 2 cal kyr BP, when Roman colonization occurred. The settlement of the town involved surface-water control and diversion of Cosia and Valduce Creeks. The subsequent historical evolution deals with several expansions and the migration of the harbor towards the North (Figure 6.11b). Locally, archeological evidence is buried below alluvial deposits, pointing to Cosia Creek floods (e.g., *via Carloni* and *via Benzi* sites; [Uboldi, 1993](#)). Our research substantially confirms the model based on the archeological studies ([Caniggia, 1968](#); [Jorio, 2004](#), see section 6.3.2). Over the last three centuries ca. 200 m of lake margin progradation has occurred, due to land reclamation and anthropic fill in lake-shore areas.

6.5. Applying the model: lake-shore area

In order to avoid, or at least minimize, economic loss due to lake-shore flooding, a new integrated defense system against floods is under construction on the Como lake-shore. It consists of rows of mobile gates intended to protect the town during events causing very high lake levels. This

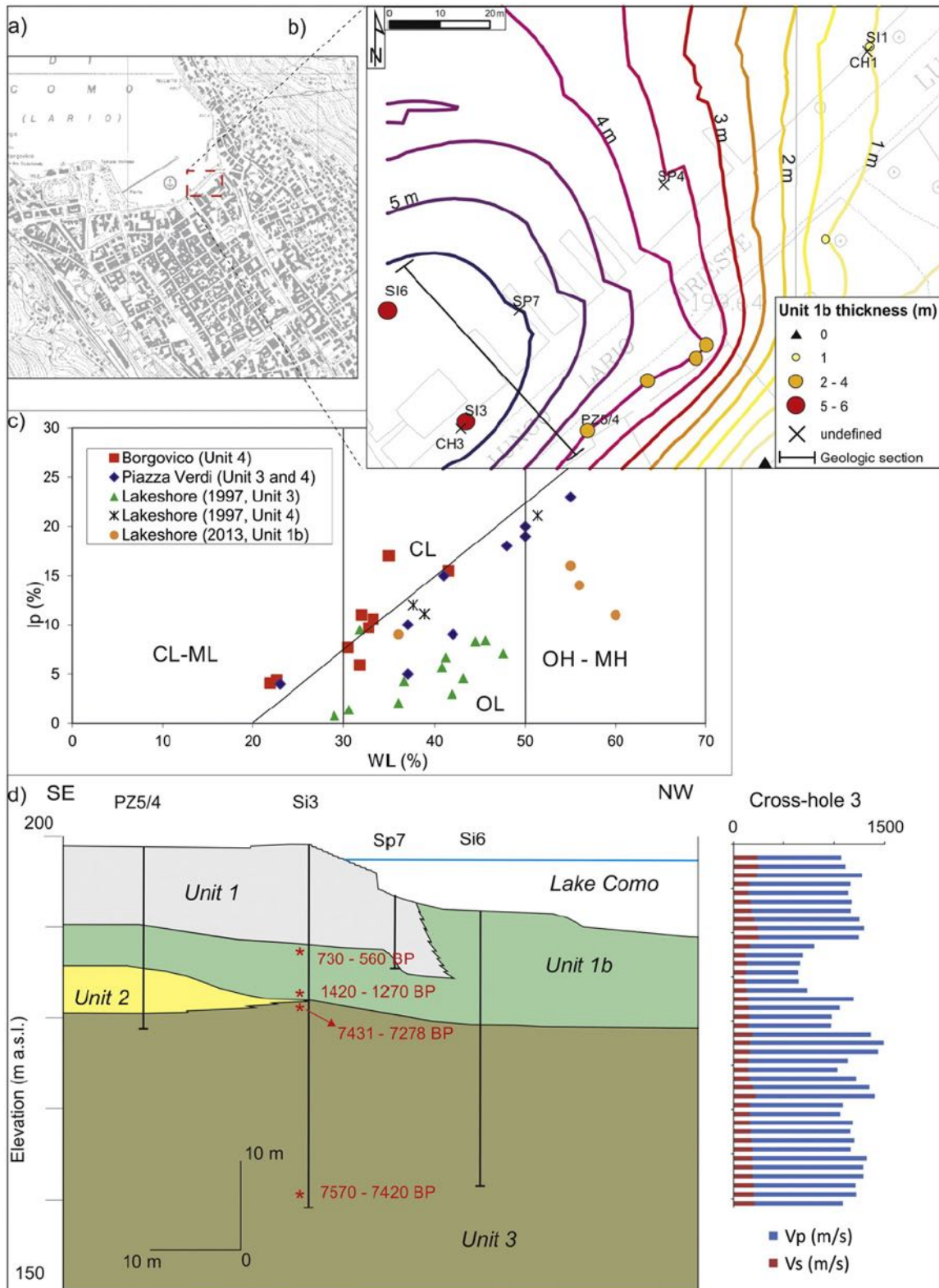


Figure 6.12.: a) Location of the supplementary coring campaign performed in 2013; b) Isopachmap of Unit 1b including location of the geological section shown in d); c) Casagrande plasticity chart for samples of Units 1b, 3 and 4; d) SE-NW oriented geologic section, ^{14}C dating and results of the cross-hole test CH3.

facility is critical for urban management in the next decades. During a revision of the project for this facility in 2012–2013, we had an opportunity to apply our model to characterize the interactions between the facility, the physical environment and the local urban setting. We anticipated that the most critical location for engineering works would have been in the eastern part of the lake-shore, where thicker sediments with very poor mechanical properties (Unit 1b) were expected. Our model suggested that Unit 1b settled after the course of Cosia Creek was altered by the Romans, so we presumed a very young (approximately < 2 kyr) age for these deposits. Even if only a few meters thick, Unit 1b was the most critical unit but its role in engineering and environmental characterization had never been highlighted. Therefore, we planned and carried out a new drilling campaign in order to (i) characterize in detail subsoil properties, both in static and dynamic terms, as prescribed by current national laws and (ii) identify possible submerged structures, that could influence project design, choice of operative techniques and related economic costs.

6.5.1. In situ and laboratory tests

The supplementary investigations were conducted in 2013: two continuous core drillings 40-m deep (SI1 and SI3) were made, and three cores (SI6, SP4, SP7), 10- to 30-m deep were extracted on the promenade and on the lake bottom, respectively. Two other cores (CH1, CH3) were drilled adjacent to SI1 and SI3 for cross-hole surveys, without recovering the sediments (Figure 6.12b).

For the first time, deposits of Unit 1b were fully investigated. The unit consists of organic silts, very rich in archeological remains and brick fragments, and is up to 6 m thick. ^{14}C dates yielded an age of a few centuries AD (upper to lower Middle Ages; Table 6.1). AGIS-based model allowed us to estimate isopachs of the unit (Ferrario et al., 2013, Figure 6.12b).

Drillings and SPT allowed us to identify an anthropic fill placed to protect lake-shore infrastructure. Using DPSH (Dynamic Probing Super Heavy) penetration tests, the wedge shape of this fill, which is 3-m thick near the lake and becomes thinner to the north, was assessed. Cross-hole seismic tests allowed us to map the variation in P- and S-seismic wave velocities with depth, to define the seismic category of the sedimentary sequence and to evaluate its elastic parameters (Young's modulus, Poisson's coefficient) under dynamic conditions.

Laboratory tests were primarily focused on defining index properties of Unit 1b. Water content, plasticity, triaxial and oedometric tests were conducted. Figure 6.12c shows the Casagrande plasticity chart, comparing previous data on Units 3 and 4 and the new results. Finally, a geologic section perpendicular to the lake-shore was drawn (Ferrario et al., 2015, Figure 6.12d) and a stability analysis was conducted.

6.5.2. Geotechnical stratigraphy

The integration of stratigraphic data and geotechnical parameters enabled us to formulate a geotechnical stratigraphy. The main geotechnical parameters are listed in Table 6.2. Some units were combined, due to the similarity in their index properties; however, the facies distinction had a clear role for landscape reconstruction.

- *Unit 1: Recent anthropic fill (< 200 years)*

Anthropic fill, reworked materials and recent deposits; medium-coarse sands and fine gravels with silty matrix and sparse pebbles; bricks and vegetal remains are widespread.

Table 6.2.: Physical and mechanical parameters of the stratigraphic units. Data derives from the integration of new drillings performed on the lake-shore with Piazza Verdi and other available probes.

	Units 1-2	Unit 1b	Units 3-4	Unit 5
N-value (SPT)	"5-30; > 100 (coarse sediments)"			40-50
Tip resistance (pocket penetrometer) (kPa)		25-50	40-150	
Cone resistance Qc (MPa)	1-10	0.2-0.5	1.6-2.4	
Unit weight (kN/m ³)	19.0	13.5-14.4	18.0	20.0
Permeability coefficient k (m/s)	10 ⁻⁵ -10 ⁻⁶ (Unit 1) 10 ⁻² -10 ⁻⁸ (Unit 2)	10 ⁻⁶ -10 ⁻⁸	10 ⁻⁶ -10 ⁻⁸	
Friction angle (°)	34	21	24	32
Cohesion c' (kPa)	0	0	0	0
Undrained cohesion Cu (kPa)	0	10	50	0
"Young modulus E (MPa; from CPTU tests)"	12-15			
"Confined modulus Mo (MPa; from CPTUs & oedometric tests)"		0.6-1.3	1.6-2.6 (depth 15-40 m) 3.7-4.0 (40-55 m)	

Locally, protective fill for coastal infrastructure and archeological materials (pottery, leather tiers) are present; in the *Piazza Cavour* area, thickness reaches 15 m. Low to medium permeability (10⁻⁵ to 10⁻⁶ m/s).

– *Unit 1b: Organic silts (Roman to Middle Ages)*

Plastic silts very rich in organic matter and water; locally sand, clay and peat are present, vegetal remains are widespread. The unit reaches a maximum thickness of 6 m and settled in a low-energy depositional environment, presumably a sheltered harbor or a dock; sparse reworked brick fragments were found up to 14 m below ground surface and suggest a historical age for the deposits, as confirmed by ¹⁴C dates. Low to very low permeability (10⁻⁶ to 10⁻⁸ m/s); water content = 60–90%, Liquid limit LL = 60%, plasticity chart group OH.

Confined modulus derived from CPTUs and oedometric probes (e.g., [Mitchell and Gardner, 1975](#)) ranges between 0.6 and 1.3 MPa. Undrained cohesion from triaxial and compression tests ranges between 6 and 15 kPa.

– *Unit 2: Alluvial deposits (Holocene)*

Coarse sands and fine gravels, sparse pebbles; locally finer horizons are present. This fluvial facies is related to the local drainage network and hosts groundwater circulation due to medium to high relative permeability (10⁻² to 10⁻⁵ m/s). The thickness rapidly decreases from the south towards the lake. Geotechnical parameters are similar to those of Unit 1.

– *Unit 3: Organic silts (Late Pleistocene–Holocene)*

Clayey silts (OL group in the plasticity chart), with coarser horizons and vivianite; on the western side of the lake-shore, sandy silts predominate (Unit 3a), while on the eastern side, the unit is richer in clay (Unit 3b). Decomposed vegetal fragments are dispersed or organized in aggregates or lenses. A laminated structure, with alternating thin organic and thicker inorganic strata is present; the laminations are generally sub-horizontal, but sometime inclinations of up to 40° or flame-structures are recorded, the latter interpreted as gas-emission features. The unit represents a lacustrine–palustrine depositional enviro-

onment and has low permeability (10^{-6} to 10^{-8} m/s). Grain-size analysis of 18 samples taken in the lake-shore area gave a mean value of 6.9ϕ , a sorting of 1.84 and a skewness of -0.23 ; sediments can thus be defined as poorly sorted, coarse-skewed fine silts.

The unit thickens from E to W, ranging from ca. 15 m to more than 40 m in *Piazza Cavour*. Water content ranges between 40 and 70%, close to the liquid limit. The unit is widespread in the entire urban area and is largely responsible for the subsidence, due to its high compressibility.

– *Unit 4: Inorganic silts (Late Pleistocene)*

Clayey silts (CL-ML group in plasticity chart), widespread in the whole urban area below ca. 40–60 m depth; locally a sandy facies has been recognized (Unit 4a), but the unit is typically composed of finer material (Unit 4b). Dropstones are widely distributed, suggesting a glaciolacustrine depositional environment; index parameters are similar to those of Unit 3.

– *Unit 5: Glaciolacustrine sands (Late Pleistocene)*

Medium to coarse sands, locally silts or gravels are present. On the lake-shore, the boundary with the uppermost unit generally lies at a depth of ca. 50–60 m, but on the eastern side it reaches a depth of 30 m. The unit is at least 50 m thick and hosts the deep aquifer; the few tests carried out at *Piazza Verdi* suggest a high shear resistance and low compressibility.

6.5.3. Model reliability and insights on the historical evolution of the town

The results from our investigations broadly confirmed our hypothesis and thus the reliability of the model itself. Indeed, in the eastern part of the lake-shore, we found both recent organic silts (Unit 1b) and submerged anthropic structures. These finds enable us to follow different phases of the historical evolution of the area: during the Roman age, it was a shallow-waterlake-margin environment, where fine sediment very rich in organic matter, wood and archeological remains settled. Then, the evolution of the city was a general expansion towards the north, obtained through several phases of land reclamation, that caused lake-shore migration (see Figure 6.2) and harbor relocation (see Figure 6.11).

6.6. Conclusions

This study analyzes the Late Quaternary environmental evolution and ongoing hazard challenges to the town of Como, addressing the interaction between engineering construction and the geoenvironment. The conceptual flow leading to the applied approach (Figure 6.13) is derived mainly from the one developed for siting nuclear power plants and codified in a series of Safety Guides (e.g., IAEA, 2011). Safety requirements for nuclear installations are very strict, but the method is valid for planning every kind of infrastructure or industrial plant; therefore, we adapted those criteria for the Como case study.

As a summary of our study, we provide a general workflow (Figure 6.13) in which the importance of a robust organization and control over construction works is highlighted, as well as a proper communication to people. The workflow is intended to be used not only by geologist or engineers, but also by people without technical expertise, such as politicians, decision makers,

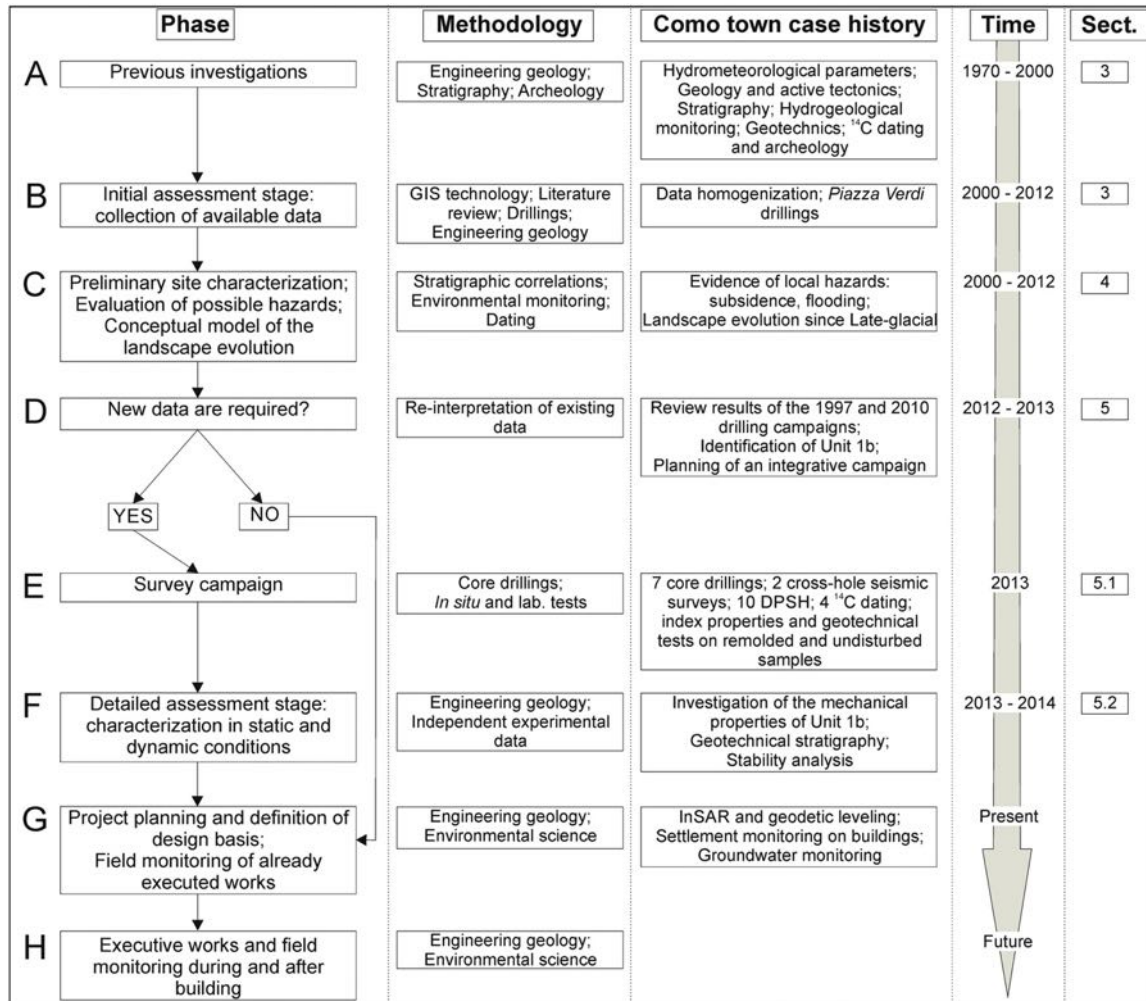


Figure 6.13.: Conceptual flow of the research; we apply this model to the town of Como during the planning for a project for protecting the town from the flood hazard. The column Sect. refers to the section in the present paper in which every phase is discussed.

architects, planners and the general public.

The environmental framework and the historical evolution of the area have been investigated since 1970 (Phase A). The initial assessment stage of our study was based on a thorough revision of available data, systematic monitoring and new data acquisition, including the drilling of two scientific boreholes in *Piazza Verdi* (Phase B). The collection of ca. 250 core logs and geotechnical data allowed us to define the stratigraphic architecture and mechanical properties of the sedimentary basin beneath the town. The hydrogeological setting was defined by means of long-term groundwater monitoring. The recent evolution of the town was reconstructed by integration of geomorphology, archeological finds and historical documents. We analyzed lake flood records and estimate long-term subsidence rates (2–4 mm/yr since Late-glacial) and human-induced ones (ca. 2 cm/yr during 1950–1975).

The reconstruction of a history of landscape evolution allowed us to identify local geological hazards that threaten Como town, mainly lake flooding and subsidence (Phase C). In 2012, we revised the engineering planning of a strategic facility for the mitigation of the flood haz-

ard, using our model to evaluate possible interactions between the facility and the local urban environment. Reinterpretation of existing data indicated the existence of a sedimentary package (Unit 1b) with very poor mechanical properties that had previously not been investigated (Phase D). In our opinion, existing data were not sufficient for a complete site characterization, therefore we planned several new studies. Investigations in 2013 include drill of seven cores and the execution of several geological and geotechnical probes (Phase E). These further investigations allowed us to make a detailed assessment of the site, defining the index properties suitable for engineering planning in both static and dynamic conditions (Phase F).

Our results are at present being used as input data for revising the project and choosing better operative techniques. The possible modifications induced by the facility or by the related engineering works are currently being evaluated through integrated monitoring, including remote sensing and geodetic leveling, clinometric measuring on buildings and hydrogeological monitoring (Phase G). New executive phases will start in the near future for the facility completion; measurements will continue, both during and after completion of the proposed works (Phase H). The facility is planned for protecting the town against floods with a recurrence frequency of 50 years, so an appropriate survey of the local setting has to continue at least for several decades.

This paper presents a case history that had immediate consequences for territorial management; however, we believe that the same approach has wide applications and can be used well beyond this single case. The methodological framework summarized in Figure 6.13 highlights the primary role that multidisciplinary environmental research should play in understanding natural hazards and their relations with human infrastructure, especially in densely inhabited regions. The adopted techniques are easy to access and generally of low-cost and they can significantly improve the quality and reliability of engineering projects. Case histories of failures of geotechnical engineered systems clearly demonstrate that a proper understanding of the geological setting is not always achieved. Our work highlights that data obtained by different methods complement and reinforce each other because various spatial and temporal scales are investigated. The integration of the archeological record helps in filling the gap between geological and historical studies in cases where written records are missing or incomplete. This kind of research necessarily requires cooperation among different specialists in earth science. Our work can also unfold new perspectives at the local scale, for instance for archeological studies aimed at revealing the migration of the harbor position since Roman times.

Urban planning and heritage management are both themes of worldwide relevance, in which a proper geological and engineering practice has a clear role. This is particularly true in urban environments, where poor or unknown ground conditions and vulnerable existing urban fabric are challenging tasks that have to be addressed during design and construction works. Thus, the ability to distinguish between natural and human-driven components of the local landscape is of crucial importance.

6.7. Acknowledgements

The authors would like to thank the Como Municipality; Georicerche s.r.l. is greatly acknowledged for the field investigations and for supporting ^{14}C dating and Consorzio dell'Adda for lake-level data. Two anonymous reviewers contributed significantly to the improvement of the manuscript. Part of this research was realized within the project of Italian-Swiss cooperation SITINET "Censimento, valorizzazione e messa in rete di siti geologici e archeologici". Topographic maps and Digital Elevation Models were provided by Regione Lombardia.

7. Lithofacies and geochemical characterization of post-LGM sediments at Lake Como, North Italy

7.1. Introduction

The Late Glacial climate is characterized by strong variability and intense landscape modification (e.g., Southern Alps: [Finsinger et al., 2008](#)). Advance and retreat of glaciers control melt water occurrence. Melting is responsible for runoff events and increased transport capacities. Flooding activity as indicator of palaeohydrological conditions and thus palaeoclimatic changes in the Alps has been studied in the past (e.g., [Simonneau et al., 2013](#); [Wirth, 2013](#)). The Alpine region in general is prone to flood events, caused by heavy rainfall, which is supposed to be controlled by North Atlantic atmospheric circulation ([Florineth and Schlüchter, 2000](#); [Wirth, 2013](#)). During phases of more positive North Atlantic Oscillation (NAO), flood activity decreases, whereas negative NAO conditions favour floodings in the Southern Alps ([Wirth, 2013](#)). Long continuous lacustrine records are supposed to give valuable archives for palaeorecords. Sudden changes in depositional conditions, like increase in allochthonous material may be remnants of extreme palaeoenvironmental conditions. Thus, besides information on flood event recurrence, reconstruction of any natural hazard will be beneficial for future awareness/preparedness and risk assessment (e.g., [Lauterbach et al., 2012](#)). At Lake Como flood events occur frequently and have been reported for the last centuries ([Ferrario et al., 2015](#), see also chapter 6). Here, we present a record covering approx. 4–16 ka BP, which comprises lithofacies characterisation and high-resolution geochemical core-log data, of Como basin sediments. This record provides evidences for post-LGM climate variability, controlled by atmospheric circulation patterns. Extreme hydrological events have been correlated with global climatic events at the transition of MIS 2 and MIS 1.

7.2. Setting

The Como basin is of fluvial origin, deeply incised during the Messinian. This steep valley has been overprinted by glacier activity during the Pleistocene ([Riva, 1957](#); [Castelletti and Orombelli, 1986](#)). Since the deglaciation a lake occupies the basin, with the present-day lake level at 198 m asl. Main tributaries are the Mera and Adda river in the North. The only outlet is located in the SE branch of the lake (Lecco branch see Figure 7.1) and the study site is located in the hydrologically closed SW Como-branch of the lake. In the vicinity of the Como basin carbonates of the South Alpine Nappes (Mesozoic-Tertiary sequence) build up the slopes. Conglomerates of the Gonfolite Formation are cropping out at the SW shore (see geological map; [Michetti et al., 2013](#)). Furthermore, moraines have been mapped in the south, remnants of

13 glacial advances (Bini, 1987). Former studies revealed a more than 180 m thick sedimentary infill below the city of Como, where the drill core Sv2 has been recovered (Ferrario et al., 2015, see also chapter 6).

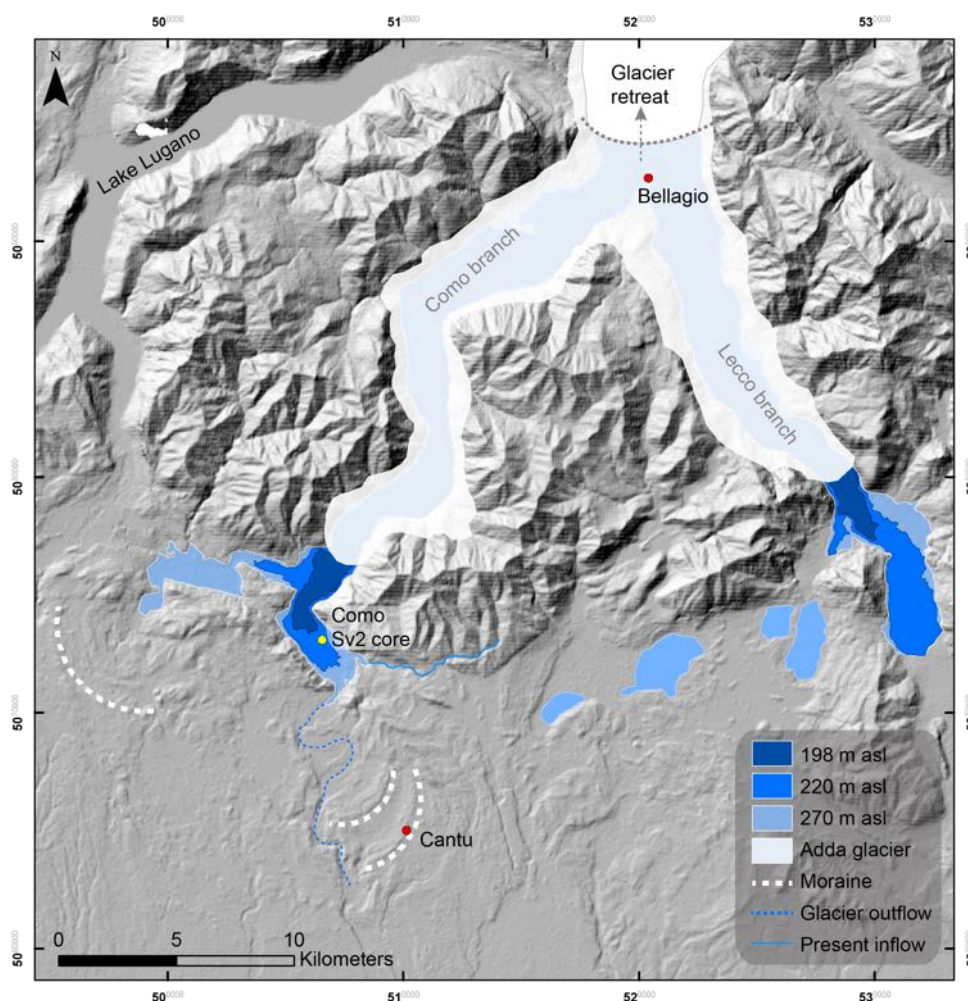


Figure 7.1.: Lake Como palaeoenvironmental evolution since the Late Glacial (post-LGM) modified after *Comerci et al. (2007)*; *Ferrario et al. (2015)*. Coring location of Sv2 core in the city of Como and results of a GIS-based morphological analysis based on SRTM-1 data (30 m cell size, USGS, 2015). Lake level changes since the LGM and glacier retreat after *Ferrario et al. (2015)* (see also chapter 6).

7.3. Materials and methods

A 70 m-long sediment core (Sv1) and a 65 m-long sediment core (Sv2) have been recovered from the present-day lakeshore, in the city centre of Como, during a drilling in 2005 by the Insubria University. A geotechnical study including the Sv1 core has been published recently (Ferrario et al., 2015, see also chapter 6). The other core, Sv2 is presented here. The analyses include optical description of the sediment core for lithofacies characterization, geochemical data by X-Ray Fluorescence scanning (XRF; V. Wennrich, University Cologne), sediment-physical

properties by Multi-Sensor Core Logging (MSCL; A.Gilli, ETH Zurich, Switzerland). From MSCL we revealed magnetic susceptibility (MS) and density data. Nine radiocarbon datings provided age control for ca. 18–33 m interval of the Sv2 core. Calibration of conventional ages has been performed by using *OxCal v. 4.2* (Ramsey, 2009) with the *IntCal 13* curve (Reimer et al., 2013).

7.4. Results and interpretation

7.4.1. Lithofacies characterization

The sediments are primarily of detrital origin, whereas authigenic and endogenic content like carbonates and diatoms varies. Organic matter content shows a clear break around 30 m sub-bottom depth (Martinelli, 2014). At the transition from glaciolacustrine (Unit 4) to palustrine deposits (Unit 3) organic content increases significantly.

Five depositional subenvironments (Unit 1-5) are described in a previously published geotechnical study and is based on parallel drill core (Sv1), recovered a few meters off Sv2 (see Comerci et al., 2007; Ferrario et al., 2015, see also chapter 6). The same described units build up the Sv2 core and are composed of the nine identified lithofacies (see Figure 7.2). Here, the palaeoenvironmental aspect is discussed in more detail with implications for climate variability. **Lithofacies 1** contains an anthropogenically affected top layer with archaeological remains (is equal to Unit 1, Figure 7.2). **Lithofacies 2** is composed of gravels and sands, which are of fluvial origin. Most likely transported by the Cosia River (is equal to Unit 2, Figure 7.2). **Lithofacies 3** shows laminated silty carbonate-bearing mud, with abundant biological remains (plant remains, pollen, spores, charcoal, etc.). The lithofacies 3 has been deposited in a lacustrine-palustrine environment. A swampy setting with low water depth and low hydrologic energy has been established. **Lithofacies 4** consist of mostly silty sediments showing convolute bedding, indicative for post-sedimentary deformation processes. This lithofacies may evolve from lithofacies 3 after deposition. **Lithofacies 5a** is composed of poorly sorted material with angular clasts, indicating a disturbed sediment layer, probably related to a re-depositional event, like landslides/debris flows. **Lithofacies 5b** shows a basal coarse layer and subtle change to finer sediments (fining upwards) with a clay layer on top. This is characteristic for a re-depositional event, like subaqueous turbidites. In this case the deposit is more than 3 m thick, which would be rather a megaturbidite than a turbidite (Fanetti et al., 2008). **Lithofacies 6** consists of fine and coarse alternations of lacustrine muds with intercalated sand-sized layers of variable thickness (mm to dm-thickness) and dropstones are present as well. Seasonal flood events might be responsible for the intercalated sand layers in a distal glaciolacustrine setting. Furthermore, turbidites with a characteristic coarse basal layers and clay cap on top, have been observed as well. **Lithofacies 7** deposits are composed of mottled, convolute bedded, dark and light grey fine (clay) sediments, which indicate a distal glaciolacustrine depositional environment. **Lithofacies 8** consists of massive coarse (sand) detrital sediments. Those deposits are pointing to undisturbed proximal glaciolacustrine deposits. **Lithofacies 9** is composed of massive occurrence of dropstones in grey clayey sands, which are supposed to be deposited in a lake of glacial origin. Those dropstones are proxies for ice floating on the lake.





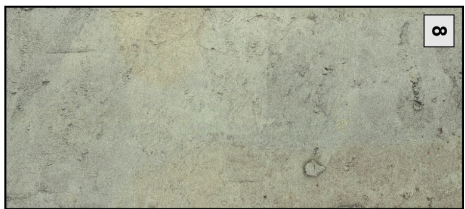
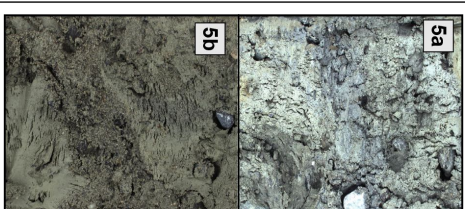
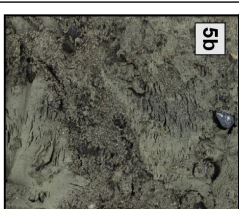


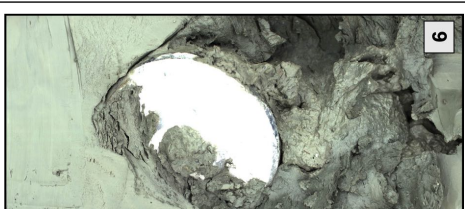
 <p>1</p> <p>Top layer</p> <p>Mixed material, containing archaeological remains</p> <p>Anthropogenic layer</p>	 <p>2</p> <p>Coarse clastics</p> <p>Alluvial sands and gravels, different sorting and rounding</p> <p>Fluvial deposits</p>	 <p>3</p> <p>Laminations</p> <p>Dark and light grey alternation of silty clay (carbonates and siliciclastics), contains abundant biological remains, vivianite is present</p> <p>Undisturbed sediments</p> <p>Palustrine-lacustrine sediments</p>	 <p>4</p> <p>Convolute layering (silt)</p> <p>Mottled dark and light grey (partly light brownish/yellowish) laminations</p> <p>Postdepositional deformation (creeping etc.)</p> <p>Disturbed sediments</p> <p>Palustrine-lacustrine sediments</p>	 <p>8</p> <p>Massive deposit (coarse)</p> <p>Detrital grey sands (carbonates and siliciclastics)</p> <p>Undisturbed deposits</p> <p>Glaciolacustrine sediments (proximal)</p>	 <p>5a</p> <p>Event layer</p> <p>Poorly sorted light grey deposit (clay to gravel), angular clasts, dropstones and clay clasts are present</p>  <p>5b</p> <p>Disturbed sediments</p> <p>Mass wasting deposit</p>	 <p>6</p> <p>Corase-fine alternation</p> <p>Grey carbonate mud with intercalated coarse (fine sand-medium sand size) layers (turbidites), and dropstones are possible. Sections of massive sands (> 1m) are present at the base of the core.</p> <p>Undisturbed + turbidites</p> <p>Glaciolacustrine sediments</p>	 <p>7</p> <p>Convolute layering (clay)</p> <p>Mottled dark and light grey laminations</p> <p>Postdepositional deformation, e.g., mass flow</p> <p>Disturbed deposits</p> <p>Glaciolacustrine sediments (distal)</p>	 <p>9</p> <p>Dropstone-bearing layer</p> <p>Dropstones are abundant (< 10 cm grain size) within a grey, massive, silty-sandy glacio-lacustrine deposit</p> <p>Undisturbed deposit</p> <p>Dropstone event</p>
---	--	--	--	---	--	---	---	---

Figure 7.2.: Nine lithofacies identified in the S02 core, with a short description and depositional subenvironments.

7.4.2. Lithostratigraphy

Recently, [Ferrario et al. \(2015\)](#) stated that the sedimentary sequence Sv1 has not been compressed by ice/glacier, due to lacking overconsolidation of the sediments. Thus, we conclude that the close-by parallel Sv2 record is of post-LGM age either, which dates 20-18 cal ka BP in the Alps ([Florineth and Schlüchter, 2000](#)). The study of biological proxies (pollen, non-pollen palynomorphs, diatoms, ostracods, plant remains etc.) of the Sv2 sediments (18-33 m) revealed a noticeably increased occurrence of vegetation remains from 33 m upwards ([Martinelli, 2014](#)). Below (at least down to 36 m; [Martinelli, 2014](#)), biological remains are almost absent.

The optically observed transition from glaciolacustrine (Unit 4/5) to palustrine-lacustrine (Unit 3) conditions correlates with variability in the core-log data. Sediment-physical properties (MS, density), elemental composition (K, Ca, Si, P), and their ratios (see Figure 7.3) show significant changes at around 32 m depth. Data for Unit 3 deposits is more noisy and siliciclastic content as well as Phosphorus increases in those sediments. Siliciclastic material is present in the vicinity of the Como basin (North branch and south tip), and increased runoff may be responsible for higher influx into the basin. Phosphorus, although often mobile in sediments, seem to be a palaeo-productivity proxy, as those values increase with supposed intensified run-off. Unit 4 sediments appear less noisy and the MS is variable for several layers. In particular the two described Event Layers (lithofacies 5a and 5b), are striking with respect to the palaeoenvironmental history.

Possible explanations for this significant drop in biological remains can be either an increase in sedimentation rates or reworking of glacial deposits. Anyway the low content of bio-proxies point to glacial climatic conditions (probably Marine Isotope Stage 2; MIS 2). Radiocarbon dating of the Sv2 core verified Holocene age for Unit 3 deposits (see Table 7.1 and Figure 7.3). Taking the chronologically ordered dates no.01-06 into account a mean linear sedimentation rate (LSR = 2.6 mm/a) for Unit 3 has been determined. Two samples have to be considered carefully (no. 07 and 08), as they originate from the chaotic lithofacies 5 (Event Layers), which has probably been reworked. Deepest probably reliable sample from the transition of lithofacies 9 to lithofacies 5 revealed 8487 cal a BP at ca. 33 m. But further datings would give clearance and make the age model more robust. At this stage two age models are supposed for the Sv2 sequence (Sv2-a, Sv2-b see Figure 7.4). For both models further verification is eligible, as no datings below 32m have been obtained. The Sv2-a model supposes either almost no sedimentation during the 8-18 ka, or even a 10 ka hiatus. Sv2-bage-depth model assumes a more

Table 7.1.: Results of radiocarbon dating from Sv2 samples. Conventional ages from [Martinelli \(2014\)](#). Calibration of conventional ages by *OxCal v. 4.2* (after [Ramsey, 2009](#), *IntCal 13* calibration curve after [Reimer et al., 2013](#)).

No.	Laboratory	Depth (m)	Material	Conv. Age (a BP)	Mean cal. Age (a BP)	2 σ (cal. a BP)
01	CIRCE, Napoli	18.26	wood	3722 \pm 38	4068	4149-3986
02	Beta Analytics	22.84	bulk sed	4420 \pm 40	5117	5125-5108
03	CIRCE, Napoli	23.92	bulk sed	4554 \pm 36	5267	5320-5213
04	Beta Analytics	24.96	bulk sed	5100 \pm 40	5834	5922-5746
05	CIRCE, Napoli	27.70	wood	6347 \pm 38	7253	7333-7173
06	CIRCE, Napoli	29.42	wood	7351 \pm 37	8125	8218-8031
07	CIRCE, Napoli	30.98	wood	11172 \pm 49	13020	13139-12901
08	CIRCE, Caserta	32.55	bulk sed	9751 \pm 53	11170	11255-11084
09	CIRCE, Caserta	32.90	bulk sed	7681 \pm 69	8487	8592-8382

continuous sedimentation rate and two event layers can be explained by significant climate periods dating post-LGM. Layer 5a as indicated by the chronology is supposed to be the transition

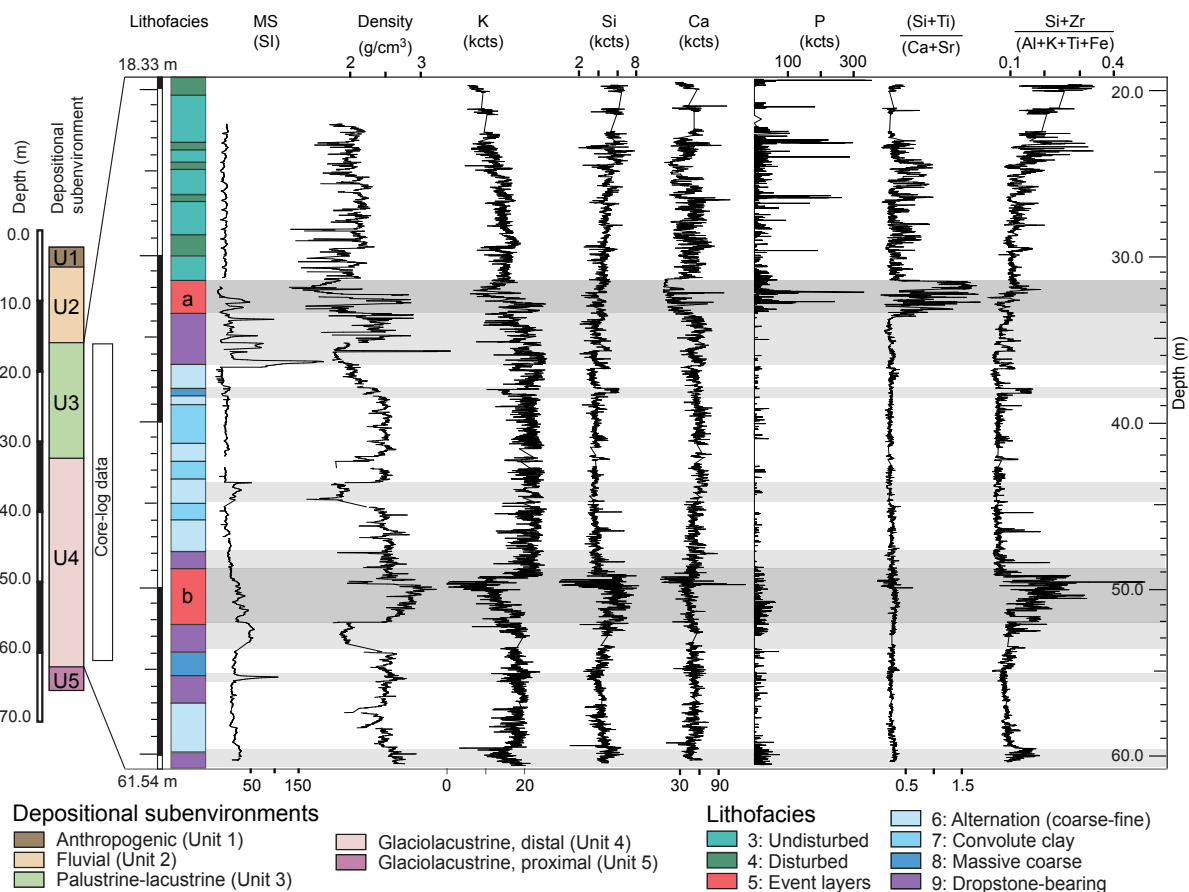


Figure 7.3.: Core-log data of Sv2 (from left to right) Depositional subenvironment (U1 to U5) according to Sv1 after Ferrario et al. (2015); identified lithofacies (3-9) in the sedimentary section (18.33 m-61.54 m). Magnetic susceptibility (MS), density, elemental composition (K, Si, Ca, P), and ratios are plotted next to linear sedimentation rates (LSR) and radiocarbon ages.

from the Late Glacial to Holocene or probably Early Holocene. The 5b deposits should date between 18 ka BP (post-LGM) and onset of the Holocene (ca. 12 ka BP). The lithofacies 5 is composed of sediments with a striking increase in grain-size, pointing to a major change in sedimentation processes. Such deposits require a high transport capacity, which can be achieved by mass-wasting events, which can occur subaerial and subaqueous, like debris flows, landslides or turbidites. This process might also be responsible for the low content in biological remains, due to reworking of glacial deposits. If Sv2-b is taken into account the glaciolacustrine deposits between 5a and 5b dates back to 12.85-11.65 ka BP, the Adda glacier is supposed to be at a similar position like today, which is contradictory to the deposited sediments (personal communication by Franz Livio, 2015). A higher content in organic remains would be expected.

7.5. Discussion

Major changes in the depositional conditions are documented by event layers 5a and 5b, which indicate phases of high energetic transportation. Allochthonous sediments with larger grainsizes

interrupt (i) 5b: the glaciolacustrine deposits (Unit 4) and, (ii) 5a: mark the transition of the glaciolacustrine to palustrine-lacustrine setting (Unit 3). Such intensified influx processes of allothonous material can be related to various processes. In the Como case or deep Alpine lakes in general, those deposits are supposed to be either triggered by (i) loading effects of the slopes (overloading) (ii) seismic events, (iii) lake level fluctuations (Fanetti et al., 2008), (iv) exceptional precipitation or ice melting events (Lauterbach et al., 2012). Furthermore, from submarine turbidites (v) wind-driven wave activity as an additional trigger mechanism has been proposed (Hampton et al., 1996), which may have played a role at Como either.

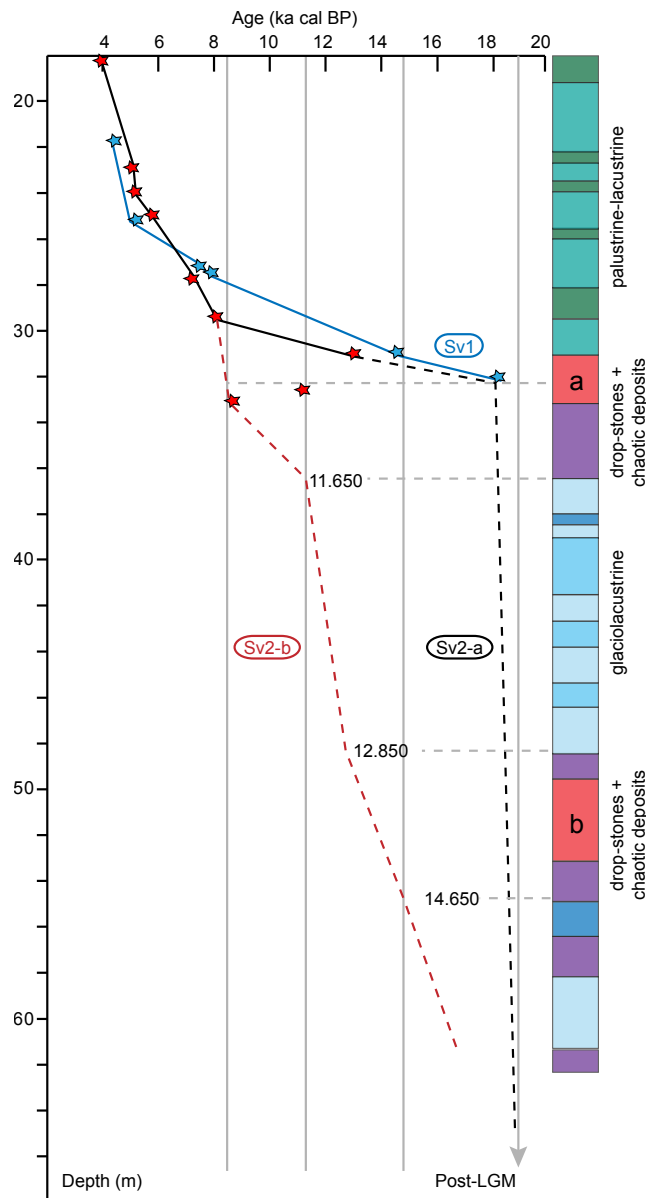


Figure 7.4.: Two proposed age-depth models for the Sv2 core (Sv2-a; Sv2-b). For correlation Sv1 core datings are plotted as well (blue asterix). Below 32.9 m no age control by datings has been achieved (dashed lines).

7.5.1. Slope overloading

Particularly steep slopes and high sedimentation rates favour slope failures due to sediment overloading. Under present-day conditions the slopes of the Bellagio plateau, where hemipelagic sediments accumulate quickly, have been identified as prone to failure (see [Fanetti et al., 2008](#)). But with respect to the location of the Sv2 sediments, it seems to be unlikely that coarse material from such mass-wasting events could reach the southern tip of the branch and settle out.

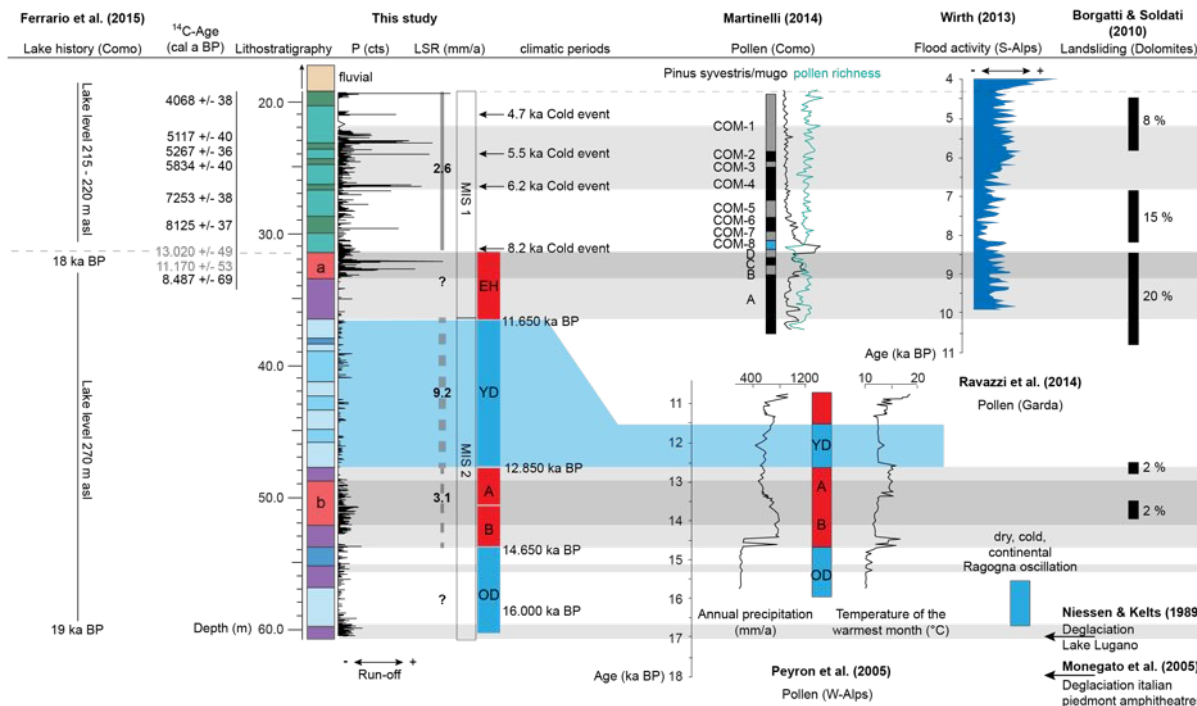


Figure 7.5.: Comparison of the Como Sv2 record with other studies from Como (geotechnical [Ferrario et al., 2015](#), pollen: [Martinelli, 2014](#)), a flood activity study from Southern Alpine lakes ([Wirth, 2013](#)), a pollen-based reconstruction from a W-Alpine lake ([Peyron et al., 2005](#)), and a pollen study from Lake Garda (S-Alps; [Ravazzi et al., 2014](#)). EH: Early Holocene; YD: Younger Dryas; A: Allerød; B: Bølling; OD: Oldest Dryas

7.5.2. Seismic events

Earthquake-triggered mass-wasting events are recorded in lacustrine sediments and have been studied at many sites (Alpine region e.g., [Schnellmann et al., 2006](#); [Strasser et al., 2007](#)). Mostly aiming on hazard assessment long continuous records are pursued, which give long palaeoseismological records. Several studies on the palaeoseismological history of Lake Zürich and Central Switzerland reaching back to the Late Glacial (approx. 15 ka BP) have been performed (e.g., [Monecke et al., 2004](#); [Strasser et al., 2013](#)). For a correlation with the Sv2 core, the large distance might cause uncertainties and low magnitude earthquakes might not have had affected the Como area. Holocene palaeoseismological records have been compiled from the Southern Alps at Lake Iseo ([Lauterbach et al., 2012](#)) and Lake Como ([Fanetti et al., 2008](#)). Anyway, both studies conclude, that local earthquakes are potential triggers for mass-wasting events in

the Southern Alps. As magnitude 6.0 to 6.5 earthquakes have been reconstructed for the Po Plain (Michetti, 2005). Nevertheless, further palaeoseismological work is required in the region to make sound correlations for the Como area.

7.5.3. Lake level fluctuations

In the Como branch of the lake seismic studies revealed megaturbidite deposits of Holocene age that are potentially triggered by lake level changes, induced by glacier fluctuations (Fanetti et al., 2008). From various former studies major lake level changes during the last deglaciation at Lake Como have been proposed (e.g., Comerci et al., 2007; Ferrario et al., 2015). The glacier retreat beyond the Bellagio plateau caused the hydraulic connection between the Lecco and Como branch. As consequence the lake level lowered about 50-55 m in the Como branch, with a lake level at 215-220 m asl. Such relatively rapid lake level changes might cause significant changes in hydrodynamics and slope instabilities (Fanetti et al., 2008; Hampton et al., 1996). From Sv2 core Event layer 5a may coincide with this lake level drop, as above 5a the subenvironment changed to a marshy palustrine setting, characterized by a low water depth.

7.5.4. Wind action

As wind is controlled by the atmospheric circulation major changes in the direction, intensity and frequency are expected since the Late Glacial. Wind can have an impact on lake currents, especially in deep lakes, which affect the distribution and depocentres of suspended sediments. Palaeocurrent conditions have been reconstructed at, Lake Geneva (Switzerland) for the Late Glacial to Holocene (Girardclos et al., 2003). Recent wind conditions were studied by Laborde et al. (2012) at Lake Como.

7.5.5. Run-off peaks

Remobilization and transport of terrigenous material from the catchment to the lake by extreme run-off events has been recorded in Alpine lakes (e.g., Simonneau et al., 2013) and Lake Iseo, particularly for the Southern Alps (Lauterbach et al., 2012). Reconstruction of the Holocene flood activity in the Southern Alps from lacustrine archives revealed a connection to North Atlantic circulation patterns (Wirth, 2013). Therefore, palaeoclimatic information like insolation variations should be recorded in palaeoflood records. Both event layers from Sv2 (5a and 5b) are accompanied by an increased occurrence of dropstones (lithofacies 9). Those dropstones can be either indicators of glacier retreat or small readvances (Strasser et al., 2007), but the combined signal of intensified runoff activity and dropstone occurrence point to intense ice melting phases during lithofacies 5 and 9 deposition. Assuming a continuous record and taking the ¹⁴C-chronology (see Figs.7.4 and 7.5) into account those event layers date back to 14,650 – 12,850 a BP (5b) and 11,650 – 8,300 a BP (5a), which are supposed to be warming phases. From a work dealing with landslide enhancement in the SE-Alps, those indicators are supposed to be geomorphological evidence of climatic changes (Borgatti and Soldati, 2010). They correlate with the event layer 5a (see Figure 7.5).

7.5.6. Implications for palaeoclimate

Two phases of intense warming affected the Como Basin during the last Deglaciation. Event Layer 5b has been estimated to correlate with the rapid warming at the onset of the Bølling/Allerød interstadial (BA). This has already been shown by isotopic signatures from ostracods in Southern Alpine lakes (Finsinger et al., 2008). During approx. 14,650 – 12,850 a BP massive melt water occurrence transported terrigenous material to the Como basin, which induces an increase in phosphorous (P). Phosphorous is mainly present as iron- or calciumphosphate originated from bacterial organic matter decay (Fagel et al., 2005). Furthermore, the magnetic susceptibility points to increased influx of magnetisable material, most probable related to soil erosion from the catchment. The following glaciolacustrine succession, implying a cooling event, is assumed to record the Younger Dryas stadial (YD). This intense cold period is documented in ostracod isotopes either (Finsinger et al., 2008). At the onset of the Holocene a strong temperature increase is expected (ice core; Rasmussen et al., 2006). Intensification of flood events in the Southern Alps (Wirth, 2013) coincide with the observations at Lake Como during approx. 11,650 – 8,300 a BP. The transition of the glaciolacustrine to the palustrine lacustrine environment indicates an almost deglaciated Como basin. The following 8.2 ka event (Bond et al., 1997), although expected to be a cold phase, shows increased P-values at Como. But from Lake Ledro an enhanced grassland soil erosion has been observed, which leads the authors to a cold and wet phase (Magny et al., 2012; Simonneau et al., 2013). After a period of climatic stability during the Mid Holocene, the flood intensity increases around 5.9 ka BP and finally the depositional environment evolved into a fluvial setting at approx. 4.2 – 4.0 ka BP.

7.6. Conclusions

1. From lithostratigraphic and geochemical analyses of a 65m-long post-LGM sedimentary record major changes of the depositional subenvironment haven been deduced.
2. Two Event Layers (5a/5b), indicating a major change in sediment transportation processes have been identified.
3. Two age-depth models (Sv2-a, Sv2-b) are discussed and one has been applied for palaeoenvironmental reconstruction.
4. As palaeoproductivity proxy, phosphorous has been proposed, which seem to correlate with phases of increased run-off activity, thus most likely due to intensified insolation.
5. Based on the Sv2-b age model, forces responsible for the events 5a and 5b have been interpreted as climatically induced, although seismic triggers can not be fully excluded.
6. As main forcing of the local palaeohydrology, climatic variations, which are most probable driven by the North Atlantic Oscillation, have been proposed.

8. Resume

8.1. Re-evaluation and synthesis

From three lacustrine sites, palaeorecords of the Western Mediterranean climate history have been acquired (Figure 8.1). Type and origin of the studied lakes, which are aligned on a NE-SW axis, are particularly different. Our multi-proxy studies indicate various strengths and weaknesses of each setting for palaeoreconstructions. Each lake has been exposed to individual climatic patterns, controlled by mutual atmospheric circulation patterns (Figure 8.2).

Individual proxy data sets

The multi-proxy data from **Laguna de Fuente de Piedra** were useful to identify different lithofacies, which indirectly indicated palaeohydrological changes, as showed in a conceptual model for the margin of the lake. The water table oscillations recorded in facies result from changes in the ratio between the water inputs and losses. The changes in the long term trend in Ti, Ca, Sr and S can be related to variations in the insolation resulting in changes in the seasonality that affected the hydrology of the basin. Titanium (Ti) and calcium (Ca) data show an opposing trend. In contrast sulphur (S) and strontium (Sr) show both a different behaviour, as controlled by different minerals. Due to minor chemical contrast between surrounding mineralogy and authigenic lacustrine deposits, the distinction of allogenic, authigenic and early-diagenetic origin plays a key role to understand depositional conditions at LFP. Therefore crystal habit characterization is essential for palaeoreconstruction. Dolomite is pointing to diagenetic alteration of calcite to dolomite and/or sulfate reduction by bacteria, causing spheric dolomite crystal morphologies.

Lake Banyoles sediments, which are mainly composed of endogenic carbonates, seem to be highly sensitive to terrigenous influx. This material can be either of fluvial or aeolian origin. Potassium (K), respectively iron (Fe), and titanium (Ti) content, which are related to clay minerals in this setting, increase during phases of intensified terrigenous influx. Thus the ratio of those elements to calcium (Ca) indicate peaks of erosion in the catchment or influx of deflated material transported to the lake. The isotopic signal is difficult to interpret, due to the open nature of the lake system, which causes no covariance of carbon and oxygen isotopes. Anyway, by using stable isotopes this study revealed that Lake Banyoles primarily receives water from the Atlantic rather than the Mediterranean. A high lake level phase has been proposed for zone 2 (higher ^{18}O), which broadly represents the Marine Isotope Stage 2 (MIS 2). The warmer phases (zone 3, zone 1 respectively MIS 3, MIS 1) show lower values for ^{18}O in Lake Banyoles and other Mediterranean lakes, in contrast to central European lakes.

At **Lake Como** optical description and geochemical data allowed to define proxies, which have been most probably controlled by palaeoproductivity. This does not necessarily refer to lake internal production, but can be related to intensified erosion from the catchment. Increased run-off, either by more precipitation or melt water occurrence, might be responsible. A proxy,

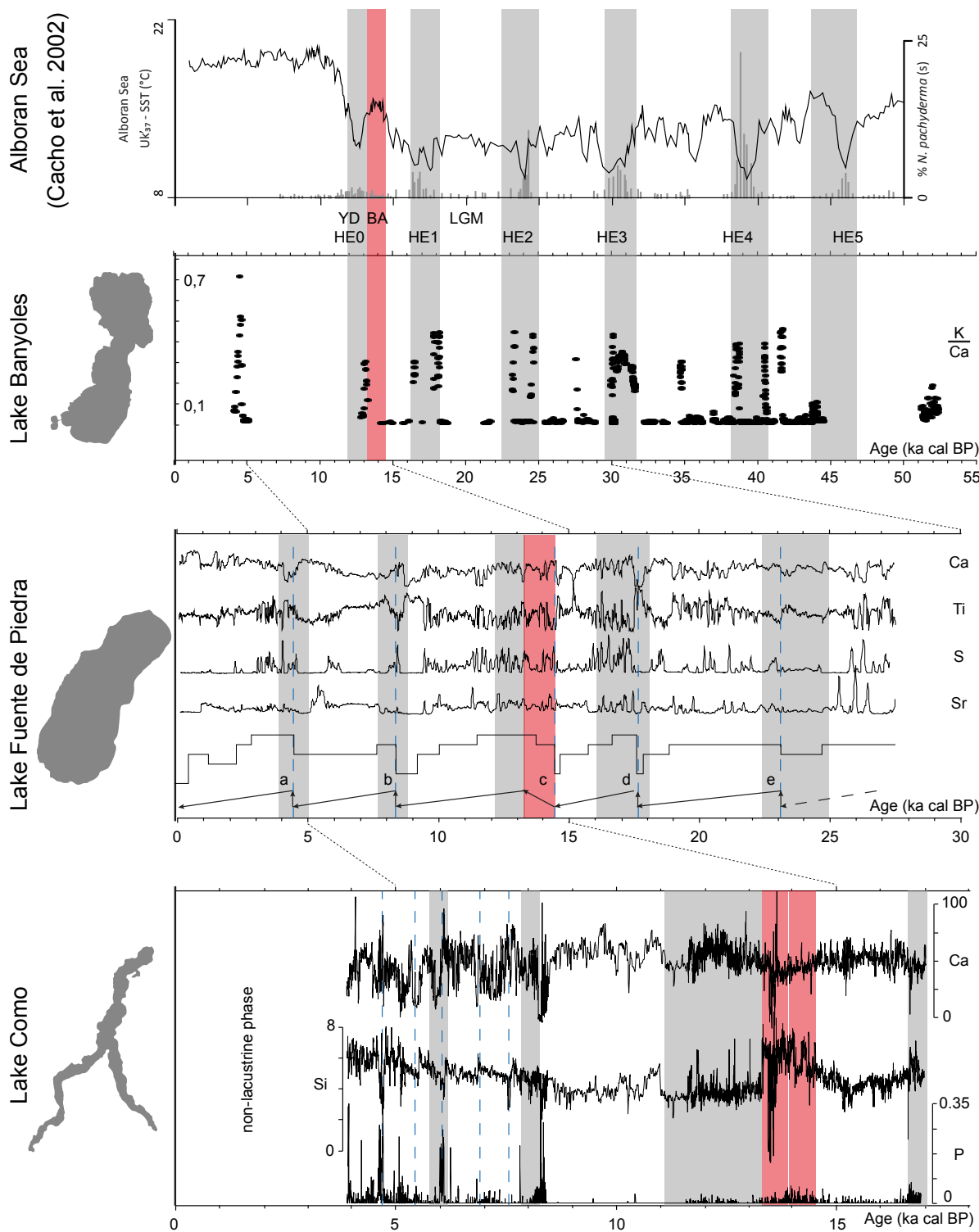


Figure 8.1.: Correlation of the studied lakes and further correlation with records from other archives (Alborán Sea; Cacho et al., 2002). Note the records have been re-ordered and are arranged with respect to the covered timespan, from long (Lake Banyoles) to short (Lake Como) from top to bottom. Grey bars: Heinrich Events (HE 0–5); red bar: Bölling/Allerød interstadial (BA); blue-dashed lines separate fluctuations; LGM: Last Glacial Maximum; YD: Younger Dryas

reflecting grain size supports this hypothesis. A change in Al, K, Ti, and Fe content, due to their relation to clay minerals, indicates less fine fraction deposited during the described event layers. These sediments are related to intense run-off or landsliding processes.

Closing the gap

The compiled palaeorecords encompass different time ranges, of which Lake Banyoles covers the longest timespan. According to the age model, the studied sedimentary sequence comprises 55 ka BP. Due to problems during the coring process two sections have not been recovered (65.0-61.5 m; 7.5-3.0 m). A continuous sedimentary sequence from Laguna de Fuente de Piedra dates back to approximately 28 ka BP. The lacustrine sediments from Como, although the longest sedimentary sequence, are of post-Last Glacial Maximum age, approximately 17.0 – 4.0 ka BP.

Site Comparison

All basins contain a considerable sediment fill, which allows a look into the past. The resolution in time is mostly controlled by the sedimentation rates, which vary strongly. Oversimplified mean linear sedimentation rates, revealed for LFP 0.5 mm/a (14 m in 28 ka), for Lake Banyoles 1.4 mm/a (66 m in 47 ka), and for Lake Como 3.4 mm/a (44 m in 13 ka; lacustrine phase). In this assumption constant linear deposition is considered, but re-depositional events are very likely in these lake settings. But as a rough estimator for the inherent temporal resolution it can be consulted cautiously. In particular, Lake Como contains turbiditic deposits that cause rapid deposition of sediment packages in single events. Time control in order to quantify this effect would be eligible, but challenging. The low content of organic carbon in all three sites is the major issue causing limitations in age modelling by radiocarbon dating. Though at Lake Banyoles, U-Th dating of endogenic carbonates revealed robust chronologies in addition to the ^{14}C results. A mutual temporal overlap of all three sites spans the Bølling/Allerød interstadial (B/A) and the Younger Dryas (respectively Heinrich Event 0; HE0).

Inter-archive correlation and forcings

A direct correlation with other archives (Figure 8.2) of the compiled records highlights differences of each lake as palaeoclimatic archive and the effect of Quaternary short-term climatic changes (e.g., North Atlantic Cold Events). North Atlantic cold events are recorded in all three studied sites. The two spatial endmembers, located at the Mediterranean borders (Lake Como and LFP) are in particular sensitive to atmospheric variability (Finsinger et al., 2008). The Lake Como record correlates with the flood occurrence study in the Southern Alps (see chapter 7). At least for the Holocene changes in atmospheric circulation have been proposed to cause increased flood occurrence in the Alps during cold phases and subtropical dry conditions during warm phases (see Figure 8.2; Wirth, 2013). This has been linked to the North Atlantic Oscillation (NAO), as the flooding peaks coincide with Bond events (Bond et al., 1997). During more negative NAO states, low solar activity induces a southward movement of the Intertropical Convergence Zone (ITCZ). Cool, weak westerlies cross Iberia and cold air reaches further south across the Alps. Thus Lake Como is supposed to be affected, as observed in the Holocene sedimentary sequence (Figure 8.2). At LFP rapid lake level rises coincide with Bond events either, which

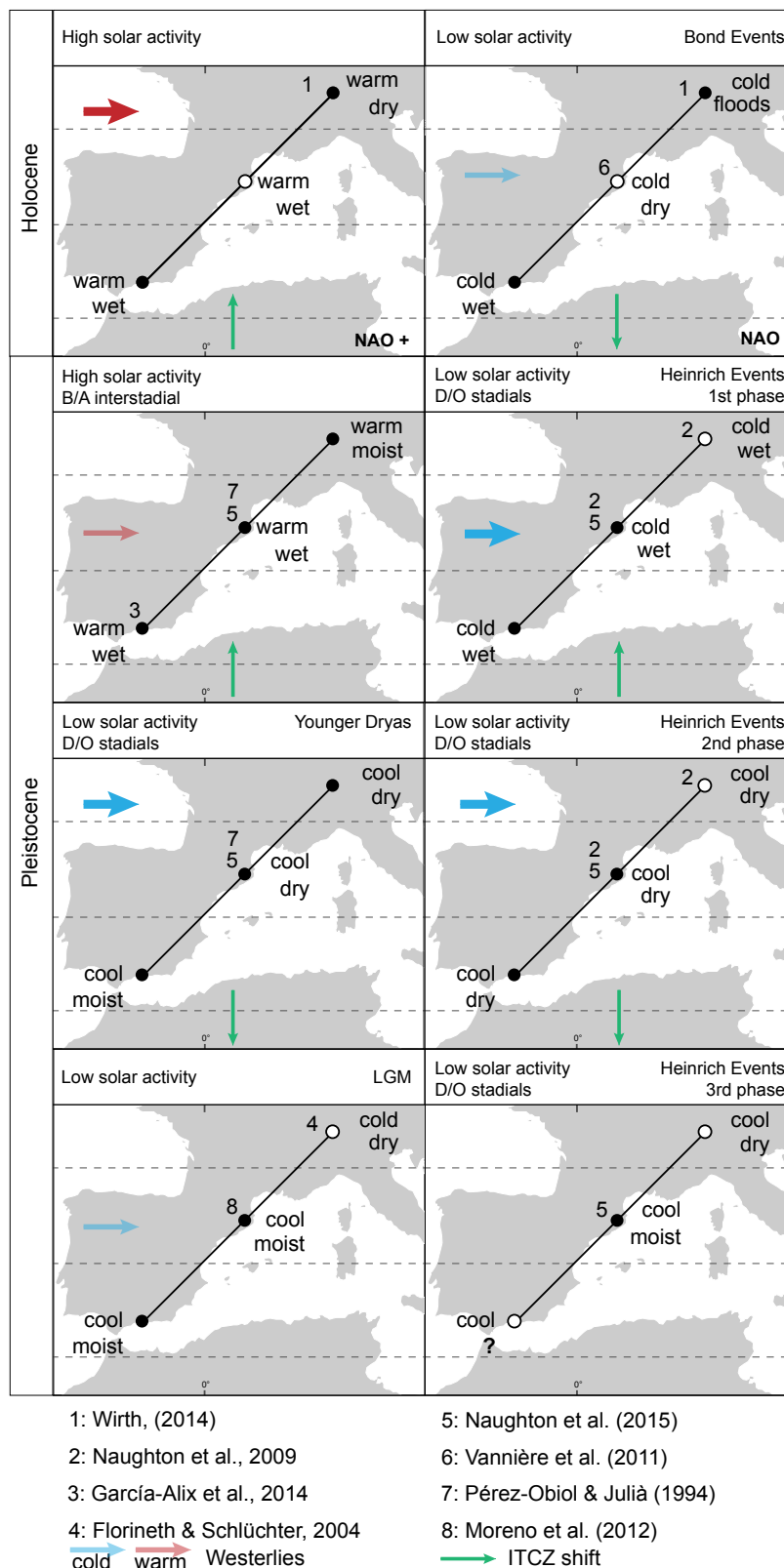


Figure 8.2.: Snapshot of different climatic settings at the Pleistocene/Holocene transition. Black icons: observed in this study; white icons: not observed in this study (atmospheric circulation modified from Moreno et al., 2005; Rodrigo-Gámiz et al., 2011; Vannièrè et al., 2011; Wirth, 2013; Wanner et al., 2001, and references therein). Note: arrow size and opacity indicate intensity westerly wind intensity.

probably have set up regional cold and wet conditions. The core from Lake Banyoles did not reveal continuous data for the Holocene, thus no robust conclusions for correlations with Bond Events are possible. In contrast Holocene warm phases have stronger pressure gradients that cause northwards shifted and intensified westerlies. At Lake Como less precipitation is present, whereas at the same time North Africa is characterised by wet climate, which might have been present at Laguna de Fuente de Piedra either. According to [Vanni re et al. \(2011\)](#) in Northern Spain (Lake Banyoles) warm and wet conditions should be present.

For the Pleistocene climatic events (Dansgaard-Oeschger stadials and interstadials) forcings are supposed to be different as already described by other studies (e.g., [Moreno et al., 2005](#); [Naughton et al., 2009](#)).

At Lake Como an intensified run-off transporting coarse material to the lake has been proposed for the B lling/Aller d interstadial (B/A). In South Spain a warm and wet period has been identified from a palaeolake ([Garc a-Alix et al., 2014](#)). The same has been furthermore proposed for North Africa ([Rodrigo-G miz et al., 2011](#)). An increase in lake level is confirmed in LFP. This high lake stage has been preserved during the Younger Dryas (HE 0), which points most probable to moist and less evaporative conditions (cool temperatures). In Northern Spain there seems to be a different impact of the YD (e.g., pollen at Banyoles, [P rez-Obiol and Juli , 1994](#)), with a more obvious signal in the Atlantic-NW and minor in the Mediterranean-NE. The climatic pattern of HE 0 (YD) seems to be different from other HEs. According to [Naughton et al. \(2015\)](#) HE 1, HE 2, and HE 4 are characterized by three phases of variable climate. The initial two phases might be recorded at LFP, where a significant lake level rise at the onset of these HEs have been described. This high lake level has either been preserved or gradually lowered in the following third phase. This points to a slightly negative water balance in LFP (e.g., cool and dry/less wet). The overall signature of HEs, in Iberia and at the Iberian realm, is drier than the LGM climatic conditions ([Moreno et al., 2012](#)). A relatively moist signal has been detected in various archives (e.g., [Morell n et al., 2009](#)) and has been recorded in LFP as well. At least stable hydrological conditions with decreasing summer insolation were present during the LGM in Iberia, probably responsible for moist signals ([Moreno et al., 2012](#)). However, during the LGM the NAO system, which is often considered for present-day climate variability, is supposed to be significantly different during the Glacial and needs further investigations ([Naughton et al., 2015](#)). As many open questions and uncertainties remain in climate reconstruction of the Pleistocene/Holocene transition, further investigations are necessary for verification and some strategies are addressed in section 8.2.

Extreme climate events

Abrupt major changes in the depositional setting coincide with North Atlantic Cold Events. Although dating uncertainties are present, the observations correlate with reconstructed climate history from other studies. In the present-day thermo-/meso-mediterranean zone (southern Spain), the hydro-sensitive LFP recorded high amplitude lake level changes, which are characterized by rapid increases and gentle decreases. Those repeating sequences point to drastic hydrological changes. In the meso-/supra-mediterranean zone, Lake Banyoles indicated sharp peaks of terrigenous influx. If this points to wet or rather dry conditions needs further investigations, because Heinrich Events are supposed to cause both depending on the phase. The sub-mediterranean, represented by Lake Como, comprises sensitivity to flood events, which are continuously recorded for the Holocene. But two event layers probably of (a) Early Holocene age and (b) B lling/Aller d might be remnants of intense run-off events or landslides. As regional

tectonic activity has been described, seismic triggers cannot be fully excluded, for this increased transport of allogenic material to the lake.

8.2. Outlook

Based on the results obtained within this work, open research questions and several ideas to improve the records emerged. The marginal lake model from **Laguna de Fuente de Piedra** revealed evidence for past lake level changes. But the longest drill core investigated here, did not encompass the entire lacustrine basin fill. Thus, another coring in the southwest basin or towards the lake centre, to recover the complete lake sequence would be eligible. This would be helpful to develop a model for the entire lake basin and reach farther back in time. Ideally this will be supported by a geophysical survey across the present-day lake. Seismic data or electrical resistivity data may give further insights into the basin morphology and formation processes. In particular subsidence processes at Laguna de Fuente de Piedra are of interest especially with respect to the surrounding and higher elevated lake deposits. Time control of this material is difficult, radiocarbon might reach the detection limit, but OSL dating might be a prosperous alternative. Sampling for OSL should be performed towards the northern tip of the basin, due to the stream inlet bringing siliciclastic material. If the terrace is younger than 40 ka, radiocarbon dating of leaf waxes should be additionally taken into account. Based on the material already acquired during the drilling campaigns, the reconstruction of the lake evaporation history by the Hydroxygen Index (HI) and C/N ratio might reveal another proxy, for correlation with the achieved palaeohydrological record (e.g., [Hepp et al., 2015](#)). This could be accompanied by palynological studies. Furthermore, from Lake Ohrid for example lipid biomarkers turned out to be a valuable proxy for hydrological changes, which induces modifications in the biome ([Holtvoeth et al., 2015](#)). It may also contain valuable information for the hydro-sensitive LFP.

At **Lake Banyoles** an extension of the already existing palynological record ([Pérez-Obiol and Julià, 1994](#)) is strongly recommend from the still available material of the BANII core. A detailed study of the sections comprising the Heinrich Events, in particular mineralogical data could highlight the origin of the potassium peaks by determination of the responsible clay minerals. Furthermore, for micro tephra analysis 20 m continuous samples in u-channels have already been sent to Emma Tomlinson (Trinity College Dublin). Another idea on the Lake Banyoles sediments aims on improving U/Th dating of endogenic lacustrine carbonates with the state of the art analytic instruments ([personal communications Denis Scholz](#)).

The **Lake Como** record could be improved by total organic carbon analyses (TOC) along the entire sedimentary sequence. Depending on the amount of organic carbon, additional radiocarbon datings could be performed, in order to reveal robust age control for the lower part of the sediment succession. Furthermore palynological data below 38 m, in particular of the section between 53.0 to 48.0 m subbottom depth would be beneficial to evaluate a potential warm phase responsible for the increased allogenic influx. As discussed, those deposits are related to mass movements, which can be explained by (delta-) slope failure (intense run-off or lake level changes) or even seismically induced. Both processes are common in the Alps (slope failures: e.g., [Girardclos et al., 2007](#); earthquakes: e.g., [Strasser et al., 2007](#)). Detailed mineralogical characterization of those deposits would clarify potential source areas of the material, which can be supported by regional palaeoseismological studies of the lake's vicinity or further palaeolimnological studies also of proximal lakes.

Due to the scarcity of lakes in Southern Spain and the necessity to expand the understanding of palaeoclimate history in the Western Mediterranean, further archives like speleothems would be a chance to get additional insights into southern Iberian climate history. Those recorders could build a bridge between lacustrine records, marine records as well as archaeological data sets. This inter-disciplinary approach is demonstrated in the Collaborative Research Centre 806 and therefore, speleothems from the Ardales Cave are already under investigation (Denis Scholz, Mainz University, Germany). This cave is in close neighbourhood to Laguna de Fuente de Piedra and the records will be excellent for correlation and integration with archaeological data from the Ardales Cave.

References

- Abellà, C., Montesinos, E., and Turet, J. (1985). Colonization and dynamics of phototrophic bacteria in a recently formed lagoon in Banyoles karstic area (Girona, Spain). *Scientia gerundensis*, 1:33–49.
- Alasset, P.-J. and Meghraoui, M. (2005). Active faulting in the western Pyrénées (France): Paleoseismic evidence for late Holocene ruptures. *Tectonophysics*, 409(1-4):39–54.
- Allen, J. R., Brandt, U., Brauer, A., Hubberten, H.-W., Huntley, B., Keller, J., Kraml, M., Mackensen, A., Mingram, J., Negendank, J. F., et al. (1999). Rapid environmental changes in southern Europe during the last glacial period. *Nature*, 400(6746):740–743.
- Alonso, M. (1998). Las lagunas de la España peninsular. *Limnetica*, 18:1–176.
- Amelung, F., Galloway, D. I., Bell, J. W., Zebker, H. A., and Laczniak, R. J. (1999). Sensing the ups and downs of Las Vegas: InSAR reveals structural control of land subsidence and aquifer-system deformation. *Geology*, 27(6):483–486.
- Amorosi, A. and Marchi, N. (1999). High-resolution stratigraphy piezocone test: an example of the Late Quaternary deposits of the Southeastern Po Plain. *Sedimentary Geology*, 128:67–81.
- Andersen, K. K., Azuma, N., Barnola, J.-M., Bigler, M., Biscaye, P., Caillon, N., Chappellaz, J., Clausen, H. B., Dahl-Jensen, D., Fischer, H., et al. (2004). High-resolution record of northern hemisphere climate extending into the last interglacial period. *Nature*, 431(7005):147–151.
- Apuani, T., Cancelli, A., and Cancelli, P. (2000). Hydrogeological and geotechnical investigations along the shoreline of the town of Como, Italy. In Moore, D. P. and Hungr, O., editors, *Engineering Geology and Environment*.
- Arca, S. and Beretta, G. P. (1985). Prima sintesi geodetico-geologica sui movimenti verticali del suolo nell'Italia Settentrionale (1897-1957). *Boll. Soc. Geol. It.*, XLIV(2):125–156.
- Ascheri, A. (1972). Studio geologico sui fenomeni di subsidenza nell'area urbana della città di Como. Technical Report 1, Comune di Como.
- Aubry, T., Dimuccio, L. A., Almeida, M., Neves, M. J., Angelucci, D. E., and Cunha, L. (2011). Palaeoenvironmental forcing during the Middle-Upper Palaeolithic transition in central-western Portugal. *Quaternary Research*, 75(1):66–79.
- Bar-Matthews, M., Ayalon, A., Kaufman, A., and Wasserburg, G. J. (1999). The Eastern Mediterranean paleoclimate as a reflection of regional events: Soreq cave, Israel. *Earth and Planetary Science Letters*, 166(1):85–95.
- Bárcena, M. A., Cacho, I., Abrantes, F., Sierro, F. J., and Grimalt, J. O. (2001). Paleoproductivity variations related to climatic conditions in the Alboran Sea (western Mediterranean) during the last glacial-interglacial transition: the diatom record. *Palaeogeography, Palaeoclimatology, Palaeoecology*, 167:337–357.

- Barnolas, A. (1987–1989). Geological Map, 1:50,000 Sheet Banyoles 295. Madrid, Spain.
- Barzaghi, R., Passoni, D., Pinto, L., and Sansò, F. (2011). Livellazione di alta precisione e misurazione di rete GNSS di controllo per l'analisi della subsidenza della sponda meridionale del lago di Como. Technical report.
- Battarbee, R. W. (2000). Palaeolimnological approaches to climate change, with special regard to the biological record. *Quaternary Science Reviews*, 19(1–5):107–124.
- Battarbee, R. W., Jones, V. J., Flower, R. J., Cameron, N. G., Bennion, H., Carvalho, L., and Juggins, S. (2001). Diatoms. In Smol, J., Birks, H., Last, W., Bradley, R., and Alverson, K., editors, *Tracking Environmental Change Using Lake Sediments*, volume 3 of *Developments in Paleoenvironmental Research*, pages 155–202. Springer Netherlands.
- Bea, R. (2011). Reliability and human factors in geotechnical engineering. *Journal of Geotechnics and Geoenvironment*, 132(5):631–643.
- Beretta, G. P., Denti, E., Fumagalli, L., and Sala, P. (1986). Note sull'idrogeologia delle città di Como e Lecco. *Geological Society of Italy*, 32:235–251.
- Berger, A. and Loutre, M. (1991). Insolation values for the climate of the last 10 million years. *Quaternary Science Reviews*, 10(4):297 – 317.
- Bernoulli, D., Bertotti, G., and Zingg, A. (1989). Nothward thrusting of the Gonfolite Lombarda (“South-Alpine Molasse”) onto the Mesozoic sequence of the Lombardian Alps; implications for the deformation history of the Southern Alps. *Eclogae Geol. Helv.*, 82(3):841–856.
- Bini, A. (1987). *L'apparato glaciale wurmiano di Como*. PhD thesis, Università degli studi di Milano.
- Bini, A. (1993). Geologia del Quaternario e geomorfologia della Piana di Como . In Ubaldi, M., editor, *Carta archeologica della Lombardia*, pages 59–63. Franco Cosimo Panini.
- Bini, A. (1996). La regolazione del Lago di Como: problemi e proposte. In *Atti del convegno. Villa Olmo, Como, Italy*. Kiwanis International Europe.
- Bini, A. and Castelletti, L. L. (1986). Geologia e paleobotanica di un sedimento olocenico nel sottosuolo di piazza Roma a Como. *Natura bresciana*, (23):357–363.
- Bini, A., Quinif, Y., Sules, O., and Uggeri, S. (1992). Les mouvements tectoniques récents dans les grottes du Monte campo dei Fiori (Lombardie, Italie). *Karstologia*, 19(1):23–30.
- Birks, H. H., Gelorini, V., Robinson, E., and Hoek, W. Z. (2015). Impacts of palaeoclimate change 60000-8000 years ago on humans and their environments in Europe: Intergrating palaeoenvironmental and archaeological data. *Quaternary International*, 378:4–13.
- Bischoff, J. L., Julià, R., Shanks, W. C., and Rosenbauer, R. J. (1994). Karstification without carbonic acid: Bedrock dissolution by gypsum-driven dedolomitization. *Geology*, 22:995–998.
- Bischoff, J. L. and Rosenbauer, R. J. (1988). A test of uranium-series dating of fossil tooth enamel: results from Tournal Cave, France. *Applied Geochemistry*, 3:145–151.

- Blockley, S. P., Lane, C. S., Hardiman, M., Rasmussen, S. O., Seierstad, I. K., Steffensen, J. P., Svensson, A., Lotter, A. F., Turney, C. S., and Ramsey, C. B. (2012). Synchronisation of palaeoenvironmental records over the last 60,000 years, and an extended INTIMATE1 event stratigraphy to 48,000 b2k. *Quaternary Science Reviews*, 36:2–10. The INTegration of Ice core, Marine and TERrestrial records of the last termination (INTIMATE) 60,000 to 8000 BP.
- Bonci, L., Cametti, A., Comerci, V., Matarazzo, D., Michetti, A. M., Vittori, E., and Vullo, F. (2004). Città di Como - Livellazione di Alta Precisione. Technical report.
- Bond, G., Showers, W., Cheseby, M., Lotti, R., Almasi, P., deMenocal, P., Priore, P., Cullen, H., Hajdas, I., and Bonani, G. (1997). A Pervasive Millennial-Scale Cycle in North Atlantic Holocene and Glacial Climates. *Science*, 278(5341):1257–1266.
- Borgatti, L. and Soldati, M. (2010). Landslides as a geomorphological proxy for climate change: A record from the Dolomites (northern Italy). *Geomorphology*, 120(1-2):56–64.
- Bout-Roumazeilles, V., Combourieu-Nebout, N., Peyron, O., Cortijo, E., Landais, A., and Masson-Delmotte, V. (2007). Connection between South Mediterranean climate and North African atmospheric circulation during the last 50,000yrBP North Atlantic cold events. *Quaternary Science Reviews*, 26(25-28):3197–3215.
- Bown, T. M. and Kraus, M. J. (1981). Lower Eocene alluvial paleosols (Willwood Formation, Northwest Wyoming, U.S.A.) and their significance for paleoecology, paleoclimatology, and basin analysis. *Palaeogeography, Palaeoclimatology, Palaeoecology*, 34:1–30.
- Bradley, R. and Eddy, J. (1991). Records of past global changes. *Global changes of the past*, pages 5–9.
- Bradley, R. S. (1999). *Paleoclimatology: Reconstructing Climates of the Quaternary*, volume 68 of *International Geophysics Series*. Academic Press, second edition.
- Bradtmöller, M., Pastoors, A., Weninger, B., and Weniger, G.-C. (2012). The repeated replacement model – Rapid climate change and population dynamics in Late Pleistocene Europe. *Quaternary International*, 247:38–49.
- Brayshaw, D. J., Rambeau, C. M., and Smith, S. J. (2011). Changes in Mediterranean climate during the Holocene: Insights from global and regional climate modelling. *The Holocene*, 21(1):15–31.
- Buckley, S. M., Rosen, P. A., Hensley, S., and Tapley, B. D. (2003). Land subsidence in Houston, Texas, measured by radar interferometry and constrained by extensometers. *Journal of Geophysical Research*, 108(B11):2542.
- Burjachs, F. and Allué, E. (2003). Paleoclimatic evolution during the last glacial cycle at the NE of the Iberian Peninsula. In Ruiz-Zapata, M. B., Dorado, M., Valdeomillos, A., Gil, M. J., Bardaji, T., Bustamante, I., and Martínez, I., editors, *Quaternary climatic changes and environmental crisis in the Mediterranean Region*, pages 191–200. Universidad de Alcalá de Henares, Madrid.
- Burjachs, F. and Julià, R. (1994). Abrupt climatic changes during the last glaciation based on pollen analysis of the Abric Romani, Catalonia, Spain. *Quaternary Research*, 42:308–315.

- Burjachs, F., López-García, J. M., Allué, E., Blain, H.-A., Rivals, F., Bennàsar, M., and Expósito, I. (2012). Palaeoecology of Neanderthals during Dansgaard–Oeschger cycles in northeastern Iberia (Abric Romani): From regional to global scale. *Quaternary International*, 247(0):26–37.
- Burjachs, F. and Renault-Miskovsky, J. (1992). Paléoenvironnement et paléoclimatologie de la Catalogne durant près de 30 000 ans (du Würmien ancien au début de l’Holocène) d’après la palynologie du site de l’Arbreda (Gérone, Catalogne). *Quaternaire*, 3(2):75–85.
- Cacho, I., Grimalt, J., and Canals, M. (2002). Response of the Western Mediterranean Sea to rapid climatic variability during the last 50,000 years: a molecular biomarker approach. *Journal of Marine Systems*, 33–34(0):253–272.
- Cacho, I., Grimalt, J. O., Canals, M., Sbaffi, L., Shackleton, N. J., Schönfeld, J., and Zahn, R. (2001). Variability of the western Mediterranean Sea surface temperature during the last 25,000 years and its connection with the Northern Hemisphere climatic changes. *Paleoceanography*, 16:40–52.
- Cacho, I., Grimalt, J. O., Pelejero, C., Canals, M., Sierro, F. J., Flores, J. A., and Shackleton, N. (1999). Dansgaard-Oeschger and Heinrich event imprints in Alboran Sea paleotemperatures. *Paleoceanography*, 14:698–705.
- Canals, M., Got, H., Julià, R., and Serra, J. (1990). Solution-collapse depression and suspensates in the limnogenic lake of Banyoles (NE Spain). *Earth Surface Processes and Landforms*, 15:243–254.
- Caniggia, G. (1968). Lettura di una città: Como. 46p.
- Capeletti, S. (2008). *Studio dei sedimenti recenti della città di Como: analisi multidisciplinari ed implicazioni per l’evoluzione ambientale del bacino idrografico lariano*. PhD thesis, Università degli studi dell’Insubria, Como, Italy.
- Carrión, J. S. (2002). Patterns and processes of Late Quaternary environmental change in a montane region of southwestern Europe. *Quaternary Science Reviews*, 21(18):2047–2066.
- Carrión, J. S., Fernández, S., González-Sampériz, P., Gil-Romera, G., Badal, E., Carrión-Marco, Y., López-Merino, L., López-Sáez, J. A., Fierro, E., and Burjachs, F. (2010). Expected trends and surprises in the Lateglacial and Holocene vegetation history of the Iberian Peninsula and Balearic Islands. *Review of Palaeobotany and Palynology*, 162(3):458–475.
- Carrión, J. S., Finlayson, C., Fernández, S., Finlayson, G., Allué, E., López-Sáez, J. A., López-García, P., Gil-Romera, G., Bailey, G., and González-Sampériz, P. (2008). A coastal reservoir of biodiversity for Upper Pleistocene human populations: palaeoecological investigations in Gorham’s Cave (Gibraltar) in the context of the Iberian Peninsula. *Quaternary Science Reviews*, 27(23-24):2118–2135.
- Carrión, J. S., Yll, E. I., Willis, K. J., and Sánchez, P. (2004). Holocene forest history of the eastern plateaux in the Segura Mountains (Murcia, southeastern Spain). *Review of Palaeobotany and Palynology*, 132(3):219–236.
- Casamitjana, X., Colomer, J., Roget, E., and Serra, T. (2006). Physical Limnology in Lake Banyoles. *Limnetica*, 25:181–188.

- Casas, E. and Lowenstein, T. K. (1989). Diagenesis of saline pan halite: comparison of petrographic features of modern, quaternary and permian halites. *Journal of Sedimentary Petrology*, 59:724–739.
- Castelletti, L. and Orombelli, G. (1986). Una nuova data ^{14}C per la storia della deglaciazione del bacino del Lago di Como. *Geogr. Fis. Din. Quat.*, 9:56–58.
- Cebriá, J. M., López-Ruiz, J., Doblas, M., Hertogen, J., and Benito, R. (2000). Geochemistry of the Quaternary alkali basalts of Garrotxa (NE Volcanic Province, Spain): a case of double enrichment of the mantle lithosphere. *Journal of Volcanology and Geothermal Research*, 102:217–235.
- Celle-Jeanton, H., Gonfiantini, R., Travi, Y., and Sol, B. (2004). Oxygen-18 variations of rainwater during precipitation: application of the Rayleigh model to selected rainfalls in Southern France. *Journal of Hydrology*, 289(1):165–177.
- Celle-Jeanton, H., Travi, Y., and Blavoux, B. (2001). Isotopic typology of the precipitation in the Western Mediterranean region at three different time scales. *Geophysical Research Letters*, 28(7):1215–1218.
- Cimellaro, G. P. (2014). Seismic performance in industrial sheds and liquefaction effects during May 2012 Emilia earthquakes sequence in Northern Italy. *Journal of Earthquake and Tsunami*, 8(2).
- Clark, I. and Fritz, P. (1997). *Environmental Isotopes in Hydrogeology*. CRC Press.
- Clark, P. U., Pisias, N. G., Stocker, T. F., and Weaver, A. J. (2002). The role of the thermohaline circulation in abrupt climate change. *Nature*, 415(6874):863–869.
- Clavell, E. (1991). *Geologia del petrol de les conques Terciaries de Catalunya*. Phd thesis, University of Barcelona, Barcelona, Spain.
- CNIG (2015). Digital elevation model, 5 m resolution, MDT05 dataset 20123.
- Cody, R. D. and Cody, A. M. (1988). Gypsum nucleation and crystal morphology in analog saline terrestrial environments. *Journal of Sedimentary Petrology*, 58:247–255.
- Cohen, A. S. (2003). *Paleolimnology: The History and Evolution of Lake Systems*. Oxford University Press, New York.
- Comboureu-Nebout, N., Turon, J. L., Zahn, R., Capotondi, L., Londeix, L., and Pahnke, K. (2002). Enhanced aridity and atmospheric high-pressure stability over the western Mediterranean during the North Atlantic cold events of the past 50 k.y. *Geological Society of America*, 30(10):863–866.
- Comerci, V. (2004). *Evoluzione geologica e ambientale recente in aree subsidenti, esempio di studio nella città di Como*. Università degli Studi dell'Insubria. PhD thesis, Università degli Studi dell'Insubria.
- Comerci, V., Capelletti, S., Michetti, A. M., Rossi, S., Serva, L., and Vittori, E. (2007). Land subsidence and Late Glacial environmental evolution of the Como urban area (Northern Italy). *Quaternary International*, 173-174:67–86.

- Comerci, V., Vittori, E., Cipolloni, C., Di Manna, P., Guerrieri, L., Nisio, S., Succhiarelli, C., Ciuffreda, M., and Bertolotti, E. (2015). Geohazards monitoring in Rome from InSAR and in-situ data: outcomes of the PanGeo Project. *Pure Applied Geophysics*.
- Comín, F. A. and Alonso, M. (1988). Spanish salt lakes: Their chemistry and biota. *Hydrobiologia*, 158:237–245.
- Comune di Como (1980). Relazione di sintesi della Commissione per lo Studio dei fenomeni di Subsidenza. Technical report, 34p, Como, Italy.
- Comune di Como (1997). Indagini geognostiche per la caratterizzazione geologica e geotecnica del sottosuolo finalizzata alla progettazione delle opere per la difesa dalle esondazioni della passeggiata a lago. Technical report, Como, Italy.
- Comune di Como (2011). Documento di Piano del Piano di Governo del Territorio. Technical report, Como, Italy.
- Cortés-Sánchez, M., Morales-Muñiz, A., Simón-Vallejo, M. D., Bergadà-Zapata, M. M., Delgado-Huertas, A., López-García, P., López-Sáez, J. A., Lozano-Francisco, M. C., Riquelme-Cantal, J. A., Roselló-Izquierdo, E., Sánchez-Marco, A., and Vera-Peláez, J. L. (2008). Palaeoenvironmental and cultural dynamics of the coast of Málaga (Andalusia, Spain) during the Upper Pleistocene and early Holocene. *Quaternary Science Reviews*, 27(23-24):2176–2193.
- Courty, M.-A. and Vallverdú, J. (2001). The microstratigraphic record of abrupt climate changes in cave sediments of the Western Mediterranean. *Geoarchaeology*, 16(5):467–499.
- Craig, H. (1961). Isotopic variations in meteoric waters. *Science*, 133(3465):1702–1703.
- Cullen, H. M., D’Arrigo, R. D., Cook, E. R., and Mann, M. E. (2001). Multiproxy reconstructions of the North Atlantic Oscillation. *Paleoceanography*, 16(1):27–39.
- Currás, A., Zamora, L., Reed, J., García-Soto, E., Ferrero, S., Armengol, X., Mezquita-Joanes, F., Marqués, M., Riera, S., and Julià, R. (2012). Climate change and human impact in central Spain during Roman times: High-resolution multi-proxy analysis of a tufa lake record (Somolinos, 1280 m asl). *Catena*, 89(1):31–53.
- Daniell, J. and Vervaeck, A. (2012). Damaging Earthquakes Database 2011 - The Year in Review. Technical report, Centre for Disaster Management and Risk Reduction Technology. www.earthquake-report.com, Karlsruhe, Germany.
- Dansgaard, W. (1964). Stable isotopes in precipitation. *Tellus A*, 16(4).
- Dansgaard, W., Johnsen, S. J., Clausen, H. B., Dahl-Jensen, D., Gundestrup, N. S., Hammer, C. U., Hvidberg, C. S., Steffensen, J. P., Sveinbjornsdottir, A. E., Jouzel, J., and Bond, G. (1993). Evidence for general instability of past climate from a 250-kyr ice-core record. *Nature*, 364(6434):218–220.
- Danzeglocke, U., Jöris, O., and Weninger, B. (2008). Calpal-2007. Software.
- de Abreu, L., Shackleton, N. J., Schönfeld, J., Hall, M., and Chapman, M. (2003). Millennial-scale oceanic climate variability off the Western Iberian margin during the last two glacial periods. *Marine Geology*, 196(1):1–20.

- Dearing, J. (1994). Environmental magnetic susceptibility. *Using the Bartington MS2 system. Kenilworth, Chi Publ.*
- Delatte, N. J. (2008). *Beyond Failure: Forensic Case Studies for Civil Engineers*. American Society of Civil Engineers.
- d’Errico, F. and Sánchez-Goñi, M. F. (2003). Neanderthal extinction and the millennial scale climatic variability of OIS 3. *Quaternary Science Reviews*, 22(8-9):769–788.
- Desprat, S., Combourieu-Nebout, N., Essallami, L., Sicre, M., Dormoy, I., Peyron, O., Siani, G., Bout Roumazeilles, V., and Turon, J. (2013). Deglacial and Holocene vegetation and climatic changes in the southern Central Mediterranean from a direct land–sea correlation. *Climate of the Past*, 9(2):767–787.
- Dolce, M. and Di Bucci, D. (2014). National Civil Protection Organization and technical activities in the 2012 Emilia earthquakes (Italy). *Bulletin of Earthquake Engineering*, 12(5):2231–2253.
- Dotsika, E., Lykoudis, S., and Poutoukis, D. (2010). Spatial distribution of the isotopic composition of precipitation and spring water in Greece. *Global and Planetary Change*, 71(3):141–149.
- Dutkiewicz, A., Herczeg, A., and Dighton, J. (2000). Past changes to isotopic and solute balances in a continental playa: clues from stable isotopes of lacustrine carbonates. *Chemical Geology*, 165(3–4):309 – 329.
- Esper, J., Frank, D. C., Timonen, M., Zorita, E., Wilson, R. J. S., Luterbacher, J., Holzkämper, S., Fischer, N., Wagner, S., Nievergelt, D., Verstege, A., and Büntgen, U. (2012). Orbital forcing of tree-ring data. *Nature Climate Change*, 2(7):1–5.
- Estévez, J., Piqué, R., Villa, A., Taulé, M., Weniger, G., Bonet, A., and Clemente, I. (1993). El poblamiento prehistorico en la cuenca del Mediona (Alt Penedes, Barcelona). In *1. Congresso de Arqueologia Peninsular: Trabalhos de Antropologie e Etnologia*, pages 119–136.
- Fagel, N., Alleman, L., Granina, L., Hatert, F., Thamo-Bozso, E., Cloots, R., and André, L. (2005). Vivianite formation and distribution in Lake Baikal sediments. *Global and Planetary Change*, 46(1):315–336.
- Fanetti, D., Anselmetti, F. S., Chapron, E., Sturm, M., and Vezzoli, L. (2008). Megaturbidite deposits in the Holocene basin fill of Lake Como (Southern Alps, Italy). *Palaeogeography, Palaeoclimatology, Palaeoecology*, 259(2-3):323–340.
- Fanetti, D. and Vezzoli, L. (2007). Sediment input and evolution of lacustrine deltas: The Breggia and Greggio rivers case study (Lake Como, Italy). *Quaternary International*, 173-174:113–124.
- Fernández, P., Irigaray, C., Jimenez, J., El Hamdouni, R., Crosetto, M., Monserrat, O., and Chacon, J. (2009). First delimitation of areas affected by ground deformations in the Guadalfeo River Valley and Granada metropolitan area (Spain) using the DInSAR technique. *Engineering Geology*, 105(1):84–101.
- Fernández, S., Fuentes, N., Carrión, J. S., González-Sampériz, P., Montoya, E., Gil, G., Vega-Toscano, G., and Riquelme, J. A. (2007). The Holocene and Upper Pleistocene pollen sequence of Carihuela Cave, southern Spain. *Geobios*, 40(1):75–90.

- Fernández-Chacón, F., Benavente, J., Rubio-Campos, J., Kohfahl, C., Jiménez, J., Meyer, H., Hubberten, H., and Pekdeger, A. (2010). Isotopic composition ($\delta^{18}\text{O}$ and δD) of precipitation and groundwater in a semi-arid, mountainous area (Guadiana Menor basin, Southeast Spain). *Hydrological processes*, 24(10):1343–1356.
- Ferrario, M., Bonadeo, L., Brunamonte, F., Livio, F., Martinelli, E., Michetti, A., Neri, P. C., Chiessi, V., Comerci, V., and Hóbig, N. (2015). Late Quaternary environmental evolution of the Como urban area (Northern Italy): A multidisciplinary tool for risk management and urban planning. *Engineering Geology*, 193:384 – 401.
- Ferrario, M. F. (2013). *Analisi e modellazione dei fattori geologico-ambientali nella localizzazione dei siti industriali: il caso del bacino padano*. PhD thesis, Università degli Studi dell’Insubria.
- Ferrario, M. F., Brunamonte, F., Castelletti, L., Livio, F., Martinelli, E., Michetti, A. M., and Motella, S. (2013). Historical shoreline evolution and the Roman Harbour in the Como urban area: results from stratigraphic and geotechnical analyses. *MapPapers*, I-III:72–76.
- Ferretti, A., Prati, C., and Rocca, F. (2000). Measuring subsidence with SAR interferometry: applications of the Permanent Scatterers technique. In *Proceedings of the Sixth International Symposium on Land Subsidence*, Ravenna.
- Finsinger, W., Belis, C., Blockley, S. P. E., Eicher, U., Leuenberger, M., Lotter, A. F., and Ammann, B. (2008). Temporal patterns in lacustrine stable isotopes as evidence for climate change during the late glacial in the Southern European Alps. *Journal of Paleolimnology*, 40(3):885–895.
- Fletcher, W. J. and Goñi, M. F. S. (2008). Orbital- and sub-orbital-scale climate impacts on vegetation of the western Mediterranean basin over the last 48,000 yr. *Quaternary Research*, 70(3):451–464.
- Florineth, D. and Schlüchter, C. (2000). Alpine Evidence for Atmospheric Circulation Patterns in Europe during the Last Glacial Maximum. *Quaternary Research*, 54(3):295–308.
- Fort, R., Calvo, J. P., and Ordonez, S. (1982). Contribución al conocimiento de la geología del borde oriental de la Cuenca de Madrid (sector Pastrana-Illana). *Tecniterrae*, 9(49):23–40.
- Freytet, P. and Plaziat, J.-C. (1982). *Continental Carbonate Sedimentation and Pedogenesis - Late Cretaceous and Early Tertiary of Southern France*. Schweizerbart Science Publishers, Stuttgart, Germany.
- Frigola, J., Moreno, A., CAcho, I., Canals, M., Sierro, F. J., Flores, J. A., Grimalt, J. O., Hodell, D. A., and Curtis, J. H. (2007). Holocene climate variability in the western Mediterranean region from a deepwater sediment record. *Paleoceanography*, 22(PA2209):1–16.
- Fruneau, B., Deffontaines, B., Rudant, J., and Le Parmentier, A. (2005). Monitoring vertical deformation due to water pumping in the city of Paris (France) with differential interferometry. *Comptes Rendus Geoscience*, 337:1173–1183.
- Fuller, I. C., Macklin, M. G., Passmore, D. G., Brewer, P. A., Lewin, J., and Wintle, A. G. (1996). Geochronologies and environmental records of Quaternary fluvial sequences in the Guadalope basin, northeast Spain, based on luminescence dating. *Geological Society Special Publication*, 115(1):99–120.

- Galve, J. P., Gutiérrez, F., Lucha, P., Bonachea, J., Remondo, J., Cendrero, A., Gutiérrez, M., Gimeno, M. J., Pardo, G., and Sánchez, J. A. (2009). Sinkholes in the salt-bearing evaporite karst of the Ebro River valley upstream of Zaragoza city (NE Spain): geomorphological mapping and analysis as a basis for risk management. *Geomorphology*, 108(3):145–158.
- García-Alix, A., Jiménez-Moreno, G., Jiménez-Espejo, F. J., García-García, F., and Huertas, A. D. (2014). An environmental snapshot of the Bølling interstadial in Southern Iberia. *Quaternary Research*, 81(2):284–294.
- Garralda, M. D. (2005). Los Neandertales en la Península Ibérica. *Munibe (Antropología-Arkeología)*, 57 (Homenaje a Jesús Altuna):289–314.
- Geotek (2011). MSCL Software Version 7.96.2.
- Geyh, M. A., Grosjean, M., Núñez, L., and Schotterer, U. (1999). Radiocarbon Reservoir Effect and the Timing of the Late-Glacial/ Early Holocene Humid Phase in the Atacama Desert (Northern Chile). *Quaternary Research*, 52:143–153.
- Gibert, L. (2015). unpublished data. personal communication.
- Gibert, L., Ortí, F., and Rosell, L. (2007). Plio-Pleistocene lacustrine evaporites of the Baza Basin (Betic Chain, SE Spain). *Sedimentary Geology*, 200(1-2):89–116.
- Gibert, L., Rosell, L., Inglès, M., and Scott, M. (2011). Endogenic sedimentary products in the evaporitic Baza Basin (SE Spain). In *5th International Limnogeology Congress, Abstracts*, Konstanz, Germany.
- Gilli, A., Anselmetti, F. S., Ariztegui, D., and McKenzie, J. A. (2003). *A 600-year sedimentary record of flood events from two sub-alpine lakes (Schwendiseen, Northeastern Switzerland)*. Lake Systems from the Ice Age to Industrial Time. Birkhäuser, Basel.
- Gimeno, L., Nieto, R., Trigo, R. M., Vicente-Serrano, S. M., and López-Moreno, J. I. (2010). Where does the Iberian Peninsula moisture come from? An answer based on a Lagrangian approach. *Journal of Hydrometeorology*, 11(2):421–436.
- Giralt, S., Burjachs, F., Roca, J. R., and Julia, R. (1999). Late Glacial to Early Holocene environmental adjustment in the Mediterranean semi-arid zone of the Salines playa-lake (Alacante, Spain). *Journal of Paleolimnology*, 21:449–460.
- Giralt, S. and Julia, R. (2003). Water level reconstruction in closed lakes based on the mineral composition of sediments. In Valero-Garcés, B. L., editor, *Limnology of Spain: A tribute to Kerry Kelts*. CSIC, Madrid.
- Giralt, S., Rico-Herrero, M. T., Vega, J. C., and Valero-Garcés, B. L. (2011). Quantitative climate reconstruction linking meteorological, limnological and XRF core scanner datasets: the Lake Sanabria case study, NW Spain. *Journal of Paleolimnology*, 46(3):487–502.
- Girardclos, S., Baster, I., Wildi, W., Pugin, A., and Rachoud-Schneider, A.-M. (2003). Bottom-current and wind-pattern changes as indicated by Late Glacial and Holocene sediments from western Lake Geneva (Switzerland). In *Lake Systems from the Ice Age to Industrial Time*, pages 39–48. Springer.

- Girardclos, S., Schmidt, O. T., Sturm, M., Ariztegui, D., Pugin, A., and Anselmetti, F. S. (2007). The 1996 AD delta collapse and large turbidite in Lake Brienz. *Marine Geology*, 241(1):137–154.
- Giussani, A. (1997). Studio dei fenomeni di subsidenza del territorio del Comune di Como. Technical report.
- González-Donoso, J. M., Serrano, F., and Linares, D. (2000). Sea surface temperature during the Quaternary at ODP Sites 976 and 975 (western Mediterranean). *Palaeogeography, Palaeoclimatology, Palaeoecology*, 162:17–44.
- González-Sampériz, P., Valero-Garcés, B. L., Moreno, A., Jalut, G., García-Ruiz, J. M., Martí-Bono, C., Delgado-Huertas, A., Navas, A., Otto, T., and Dedoubat, J. J. (2006). Climate variability in the Spanish Pyrenees during the last 30,000 yr revealed by the El Portalet sequence. *Quaternary Research*, 66(1):38–52.
- González-Sampériz, P., Valero-Garcés, B. L., Moreno, A., Morellón, M., Navas, A., Machín, J., and Delgado-Huertas, A. (2008). Vegetation changes and hydrological fluctuations in the Central Ebro Basin (NE Spain) since the Late Glacial period: Saline lake records. *Palaeogeography, Palaeoclimatology, Palaeoecology*, 259:157–181.
- Goula, X., Olivera, C., Fleta, J., Grellet, B., Lindo, R., Rivera, L. A., Cisternas, A., and Carbon, D. (1999). Present and recent stress regime in the eastern part of the Pyrenees. *Tectonophysics*, 308:487–502.
- Grimm, E. (2011). Tilia, Tilia-Graph, and TGView. Illinois State Museum. Springfield, Illinois.
- Grün, R., Maroto, J., Eggins, S., Stringer, C., Robertson, S., Taylor, L., Mortimer, G., and McCulloch, M. (2006). ESR and U-series analyses of enamel and dentine fragments of the Banyoles mandible. *Journal of Human Evolution*, 50:347–358.
- Günster, N., Eck, P., Skowronek, A., and Zöller, L. (2001). Late Pleistocene loess and their paleosols in the Granada Basin, Southern Spain. *Quaternary International*, 76/77:241–245.
- Gutiérrez, F., Ortí, F., Gutiérrez, M., Pérez-Gonzalez, A., Benito, G., Gracia, F. J., and Durán, J. J. (2002). Paleosubsidence and active subsidence due to evaporite dissolution in Spain. *Carbonates and Evaporites*, 17(2):121–133.
- Gutiérrez-Santolalla, F., Acosta, E., Ríos, S., Guerrero, J., and Lucha, P. (2005). Geomorphology and geochronology of sackung features (uphill-facing scarps) in the Central Spanish Pyrenees. *Geomorphology*, 69(1-4):298–314.
- Haberzettl, T., Kück, B., Wulf, S., Anselmetti, F. S., Ariztegui, D., Corbella, H., Fey, M., Janssen, S., Lücke, A., Mayr, C., Ohlendorf, C., Schäbitz, F., Schleser, G. H., Wille, M., and Zolitschka, B. (2008). Hydrological variability in southeastern Patagonia and explosive volcanic activity in the southern Andean Cordillera during Oxygen Isotope Stage 3 and the Holocene inferred from lake sediments of Laguna Potrok Aike, Argentina. *Palaeogeography, Palaeoclimatology, Palaeoecology*, 259(2-3):213–229.
- Hampton, M. A., Lee, H. J., and Locat, J. (1996). Submarine Landslides. *Reviews of Geophysics*, 34:33–59.

- Heinrich, H. (1988). Origin and Consequences of Cyclic Ice Rafting in the Northeast Atlantic Ocean during the Past 130,000 Years. *Quaternary Research*, 29:142–152.
- Hemming, S. R. (2004). Heinrich events: Massive late Pleistocene detritus layers of the North Atlantic and their global climate imprint. *Reviews of Geophysics*, 42(1):RG1005.
- Hepp, J., Tuthorn, M., Zech, R., Mügler, I., Schlütz, F., Zech, W., and Zech, M. (2015). Reconstructing lake evaporation history and the isotopic composition of precipitation by a coupled $\delta^{18}\text{O}$ – $\delta^2\text{H}$ biomarker approach. *Journal of Hydrology*, 529:622–631.
- Heredia, J., Araguás-Araguás, L., and Ruiz, J. M. (2004). Use of environmental tracers to characterize a complex hydrogeological system under variable density conditions: case of the subsurface brine of Fuente de Piedra (SW Spain). *Cartagena*, 18:679–692.
- Heredia, J., Ruiz, J. M., and García de Domingo, A. (2009). Caracterización de un sistema hidrogeológico complejo con variabilidad extrema de la densidad: Laguna de Fuente de Piedra (Málaga). Vinculación con un sistema kárstico regional hipersalino. *Boletín Geológico y Minero*, 120(3):423–442.
- Higham, T., Douka, K., Wood, R., Ramsey, C. B., Brock, F., Basell, L., Camps, M., Arrizabalaga, Á., Baena, J., Barroso-Ruiz, C., Bergman, C., Boitard, C., Boscato, P., Caparrós, M., Conard, N. J., Draily, C., Froment, A., Galván, B., Gambassini, P., Garcia-Moreno, A., Grimaldi, S., Haesaerts, P., Holt, B., Iriarte-Chiapusso, M.-J., Jelinek, A., Pardo, J. F. J., Maíllo-Fernández, J.-M., Marom, A., Maroto, J., Menéndez, M., Metz, L., Morin, E., Moroni, A., Negrino, F., Panagopoulou, E., Peresani, M., Pirson, S., de la Rasilla, M., Riel-Salvatore, J., Ronchitelli, A., Santamaria, D., Semal, P., Slimak, L., Soler, J., Soler, N., Villaluenga, A., Pinhasi, R., and Jacobi, R. (2014). The timing and spatiotemporal patterning of Neanderthal disappearance. *Nature*, 512(7514):306–309.
- Höbig, N., Mediavilla, R., Gibert, L., Santisteban, J. I., Cendón, D. I., Ibáñez, J., and Reicherter, K. (2016). Palaeohydrological evolution and implications for palaeoclimate since the Late Glacial at Laguna de Fuente de Piedra, southern Spain Palaeohydrological evolution and implications for palaeoclimate since the Late Glacial at Laguna de Fuente de Piedra, southern Spain. *Quaternary International*, 407(Part A):29–46.
- Höbig, N., Weber, M. E., Kehl, M., Weniger, G. C., Julià, R., Melles, M., Fülöp, R.-H., Vogel, H., and Reicherter, K. (2012). Lake Banyoles (northeastern Spain): A Last Glacial to Holocene multi-proxy study with regard to environmental variability and human occupation. *Quaternary International*, 274:205–218.
- Höbig, N., Weber, M. E., Kehl, M., Weniger, G.-C., Julià, R., Melles, M., Fülöp, R. H., Vogel, H., and Reicherter, K. R. (2013). A 60 ka multi-proxy record from Lake Banyoles (northeastern Spain): Extended data. In Baena, R., Fernández, J. J., and Guerrero, I., editors, *El Cuaternario Ibérico: Investigación en el S. XXI : proceedings of the VIII Reunión del Cuaternario Ibérico*, pages 136–140, Sevilla - La Rinconada, Spain. AEQUA.
- Hodell, D., Crowhurst, S., Skinner, L., Tzedakis, P. C., Margari, V., Channell, J. E. T., Kamenov, G., Maclachlan, S., and Rothwell, G. (2013). Response of Iberian Margin sediments to orbital and suborbital forcing over the past 420ka. *Paleoceanography*, 28(1):185–199.
- Holtvoeth, J., Rushworth, D., Imeri, A., Cara, M., Vogel, H., Wagner, T., and Wolff, G. A. (2015). Improved end-member characterization of modern organic matter pools in

- the Ohrid Basin (Albania, Macedonia) and evaluation of new palaeoenvironmental proxies. *Biogeosciences Discussions*, 12(15):12975–13039.
- Hovorka, S. D. (1992). Halite pseudomorphs after gypsum in bedded anhydrite - clue to gypsum-anhydrite relationships. *Journal of Sedimentary Petrology*, 62:1098–1111.
- Hu, R. L., Yue, Z. Q., Wang, L. C., and Wang, S. J. (2004). Review on current status and challenging issues of land subsidence in China. *Engineering Geology*, 76:65–77.
- Huang, N. E., Shen, Z., Long, S. R., Wu, M. C., Shih, H. H., Zheng, Q., Yen, N. C., Tung, C. C., and Liu, H. H. (1998). The empirical mode decomposition and the Hilbert spectrum for nonlinear and non-stationary time series analysis. *Proceedings of the Royal Society A: Mathematical, Physical and Engineering Sciences*, 454(1971):903–995.
- Huang, Y., Bao, Y., and Wang, Y. (2015). Analysis of geoenvironmental hazards in urban underground space development in Shanghai. *Natural Hazards*, 75:2067–2079.
- Huerta, P., Armenteros, I., Recio, C., and Blanco, J. A. (2010). Palaeogroundwater evolution in playa-lake environments: Sedimentary facies and stable isotope record (Palaeogene, Almazán basin, Spain). *Palaeogeography, Palaeoclimatology, Palaeoecology*, 286(3–4):135 – 148.
- IAEA (2011). Meteorological and hydrological hazards in site evaluation for nuclear installations.
- Ivy-Ochs, S., Kerschner, H., Reuther, A., Maisch, M., Sailer, R., Schaefer, J., Kubik, P. W., Synal, H., and Schlüchter, C. (2006). The timing of glacier advances in the northern European Alps based on surface exposure dating with cosmogenic ^{10}Be , ^{26}Al , ^{36}Cl , and ^{21}Ne . *Special Papers Geological Society of America*, 415:43–60.
- Jalut, G., Amat, A. E., Bonnet, L., Gauquelin, T., and Fontugne, M. (2000). Holocene climatic changes in the Western Mediterranean, from south-east France to south-east Spain. *Palaeogeography, Palaeoclimatology, Palaeoecology*, 160:255–290.
- Jones, T. D., Lawson, I. T., Reed, J. M., Wilson, G. P., Leng, M. J., Gierga, M., Bernasconi, S. M., Smittenberg, R. H., Hajdas, I., Bryant, C. L., et al. (2013). Diatom-inferred late Pleistocene and Holocene palaeolimnological changes in the Ioannina basin, northwest Greece. *Journal of Paleolimnology*, 49(2):185–204.
- Jorio, S. (2004). Una nuova proposta di localizzazione per il porto di Como: i risultati dello scavo in Piazza Cacciatori delle Alpi – via Gallio. *Rivista Archeologica dell’antica provincia e Diocesi di Como*, 186:231–244.
- Julià Brugués, R. (1977). Nuevos datos sobre la posición cronoestratigráfica de los materiales cuaternarios de la cuenca lacustre de Banyoles-Besalú (Girona). *Acta Geológica Hispánica*, 12(1):55–59.
- Julià Brugués, R. (1980). *La conca lacustre de Banyoles-Besalú*. Monografies del Centre d’Estudis comarcals de Banyoles. Centre d’Estudis Comarcals de Banyoles, Banyoles, Spain.
- Kaland, P. E., Krzywinski, K., and Stabell, B. (1984). Radiocarbon-dating of transitions between marine and lacustrine sediments and their relation to the development of lakes. *Boreas*, 13(2):243–258.

- Kalnicky, D. J. and Singhvi, R. (2001). Field portable XRF analysis of environmental samples. *Journal of Hazardous Materials*, 83:93–122.
- Kohfahl, C., Rodriguez, M., Fenk, C., Menz, C., Benavente, J., Hubberten, H., Meyer, H., Paul, L., Knappe, A., López-Geta, J. A., and Pekdeger, A. (2008). Characterising flow regime and interrelation between surface-water and ground-water in the Fuente de Piedra salt lake basin by means of stable isotopes, hydrogeochemical and hydraulic data. *Journal of Hydrology*, 351(1-2):170–187.
- Kolodny, Y., Stein, M., and Machlus, M. (2005). Sea-rain-lake relation in the Last Glacial East Mediterranean revealed by $\delta^{18}\text{O}$ - $\delta^{13}\text{C}$ in Lake Lisan aragonites. *Geochimica et Cosmochimica Acta*, 69(16):4045–4060.
- Kraus, M. J. and Aslan, A. (1993). Eocene hydromorphic paleosols; significance for interpreting ancient floodplain processes. *Journal of Sedimentary Research*, 63(3):453–463.
- Kylander, M. E., Ampel, L., Wohlfarth, B., and Veres, D. (2011). High-resolution X-ray fluorescence core scanning analysis of Les Echets (France) sedimentary sequence: new insights from chemical proxies. *Journal of Quaternary Science*, 26:109–117.
- Laborde, S., Imberger, J., and Toussaint, S. (2012). A wall out of place: a hydrological and sociocultural analysis of physical changes to the lakeshore of Como, Italy. *Ecology and Society*, 17(1).
- Lacey, J., Leng, M., Höbig, N., Reed, J., Valero-Garcés, B., and Reicherter, K. (2015). Western Mediterranean climate and environment since Marine Isotope Stage 3: a 50,000-year record from Lake Banyoles, Spain. *Journal of Paleolimnology*, pages 1–16.
- Lauterbach, S., Chapron, E., Brauer, A., Huls, M., Gilli, A., Arnaud, F., Piccin, A., Nomade, J., Desmet, M., von Grafenstein, U., and Participants, D. (2012). A sedimentary record of Holocene surface runoff events and earthquake activity from Lake Iseo (Southern Alps, Italy). *The Holocene*, 22(7):749–760.
- Leng, M. J. and Marshall, J. D. (2004). Palaeoclimate interpretation of stable isotope data from lake sediment archives. *Quaternary Science Reviews*, 23(7):811–831.
- Leng, M. J., Roberts, N., Reed, J. M., and Sloane, H. J. (1999). Late Quaternary palaeohydrology of the Konya Basin, Turkey, based on isotope studies of modern hydrology and lacustrine carbonates. *Journal of Paleolimnology*, 22(2):187–204.
- Leroy, S. A. G. (2008). Vegetation cycles in a disturbed sequence around the Cobb-Mountain subchron in Catalonia (Spain). *Journal of Paleolimnology*, 40(3):851–868.
- Li, H.-C. and Ku, T.-L. (1997). $\delta^{13}\text{C}$ - $\delta^{18}\text{O}$ covariance as a paleohydrological indicator for closed-basin lakes. *Palaeogeography, Palaeoclimatology, Palaeoecology*, 133(1-2):69–80.
- Linares, L. (1990). Hidrogeología de le laguna de Fuente de Piedra (Málaga). Tesis doctoral, Universidad de Granada.
- Lionello, P., Malanotte-Rizzoli, P., and Boscolo, R. (2006). *Mediterranean climate variability*, volume 4. Elsevier.

- Livio, F., Berlusconi, A., Chunga, K., Michetti, A. M., and Sileo, G. (2011). New stratigraphic and structural evidence for Late Pleistocene surface faulting along the Monte Olimpino Back-thrust (Lombardia, N Italy). *Boll. Soc. Geol. It.*, 14:17–25.
- López-García, J. M. and Cuenca-Bescós, G. (2010). Evolution climatique durant le Pléistocène Supérieur en Catalogne (Nord-est de l’Espagne) d’après l’étude des micromammifères. *Quaternaire*, 21/3:249–257.
- Lowenstein, T. K. and Hardie, L. A. (1985). Criteria for the recognition of salt-pan evaporites. *Sedimentology*, 32(5):627–644.
- Luraschi, G. (1987). Como romana: le mura. *Soc. Arch. Com.*, pages 103–112.
- Luraschi, G. (2002). Storia di Como romana e del suo territorio. Technical report, Como.
- Luzón, A., Mayayo, M., and Pérez, A. (2009). Stable isotope characterisation of co-existing carbonates from the Holocene Gallocanta lake (NE Spain): palaeolimnological implications. *International Journal of Earth Sciences*, 98(5):1129–1150.
- Mack, G. H., James, W. C., and Monger, H. C. (1993). Classification of paleosols. *Geological Society of America Bulletin*, 105(2):129–136.
- Magee, J. W. (1991). Late Quaternary lacustrine, groundwater, aeolian and pedogenic gypsum in the Prungle Lakes, southeastern Australia. *Palaeogeography, Palaeoclimatology, Palaeoecology*, 84:3–42.
- Magee, J. W., Bowler, J. M., Miller, G. H., and Williams, D. L. G. (1995). Stratigraphy, sedimentology, chronology and palaeohydrology of Quaternary lacustrine deposits at Madigan Gulf, Lake Eyre, South Australia. *Palaeogeography, Palaeoclimatology, Palaeoecology*, 113:3–42.
- Magny, M., Joannin, S., Galop, D., Vanniere, B., Haas, J. N., Bassetti, M., Bellintani, P., Scandolari, R., and Desmet, M. (2012). Holocene palaeohydrological changes in the northern Mediterranean borderlands as reflected by the lake-level record of Lake Ledro, northeastern Italy. *Quaternary Research*, 77:382–396.
- Manunta, M., Marsella, M., Zeni, G., Sciotti, M., Atzori, S., and Lanari, R. (2008). Two-scale surface deformation analysis using SBAS-DInSAR technique: a case study of the city of Rome, Italy. *International Journal of Remote Sensing*, 29:1665–1684.
- Maroto, J., Soler, N., and Fullola, J. M. (1996). Cultural change between Middle and Upper Paleolithic in Catalonia. In Carbonell, E. and Vaquero, M., editors, *The Last Neandertals, the first anatomically modern humans : a tale about the human diversity*, pages 219–250, Tarragona, Spain. Universitat Rovira i Virgili.
- Marriner, E. (2007). Geoscience of ancient Mediterranean harbours. *Earth Science Reviews*, 80(3):137–194.
- Martin-Puertas, C., Valero-Garcés, B. L., Pilar Mata, M., González-Sampériz, P., Bao, R., Moreno, A., and Stefanova, V. (2008). Arid and humid phases in southern Spain during the last 4000 years: the Zoñar Lake record, Córdoba. *The Holocene*, 18(6):907–921.

- Martin-Serrano García, A. (1982). Geological map, 1:50,000 Sheet Antequera 1023. Instituto Geológico y Minero de España (IGME), Madrid.
- Martin-Vide, J. and Lopez-Bustins, J.-A. (2006). The Western Mediterranean Oscillation and rainfall in the Iberian Peninsula. *International Journal of Climatology*, 26(11):1455–1475.
- Martinelli, E. (2014). *Analisi palinologiche e geofisiche per la ricostruzione delle trasformazioni ambientali nella regione lariana tra Tardiglaciale e Olocene: nuovi dati dal sondaggio di Piazza Verdi a Como*. PhD thesis, Università degli Studi dell'Insubria.
- Martínez, A., Rivero, L., and Casas, A. (1997). Integrated gravity and seismic interpretation of duplex structures and imbricate thrust systems in the southeastern Pyrenees (NE Spain). *Tectonophysics*, 282:303–329.
- Martinez, K., Garcia, J., Carbonell, E., Agusti, J., Bahain, J. J., Blain, H. A., Burjachs, F., Cáceres, I., Duval, M., Falgueres, C., Gomez, M., and Huguet, R. (2010). A new Lower Pleistocene archeological site in Europe (Vallparadis, Barcelona, Spain). *Proceedings of the National Academy of Sciences*, 107(13):5762–5767.
- Martínez-Moreno, J., Mora, R., and de la Torre, I. (2010). The Middle-to-Upper Palaeolithic transition in Cova Gran (Catalunya, Spain) and the extinction of Neanderthals in the Iberian Peninsula. *Journal of Human Evolution*, 58:211–226.
- Martínez-Ruiz, F., Kastner, M., Gallego-Torres, D., Rodrigo-Gámiz, M., Nieto-Moreno, V., and Ortega-Huertas, M. (2015). Paleoclimate and paleoceanography over the past 20,000 yr in the Mediterranean Sea Basins as indicated by sediment elemental proxies. *Quaternary Science Reviews*, 107:25–46.
- Martrat, B., Jimenez-Amat, P., Zahn, R., and Grimalt, J. O. (2014). Similarities and dissimilarities between the last two deglaciations and interglaciations in the North Atlantic region. *Quaternary Science Reviews*, 99:122–134.
- Mayayo, M. J., Luzón, A., Soria, A. R., Roca, A. C., Sánchez, J. A., and Pérez, A. (2003). Sedimentological, hydrochemical and mineralogical evolution of the Holocene Gallocanta Lake, NE Spain. In Valero-Garcés, B. L., editor, *Limnogeology in Spain: a tribute to Kerry R. Kelts*, pages 359–384, Madrid, Spain. Consejo Superior de Investigaciones Científicas.
- Mayewski, P. A., Rohling, E. E., Curt Stager, J., Karlén, W., Maasch, K. A., David Meeker, L., Meyerson, E. A., Gasse, F., van Kreveland, S., Holmgren, K., Lee-Thorp, J., Rosqvist, G., Rack, F., Staubwasser, M., Schneider, R. R., and Steig, E. J. (2004). Holocene climate variability. *Quaternary Research*, 62(3):243–255.
- Mediavilla, R. (2001). *Estratigrafía y sedimentología del Neógeno del sector central de la Cuenca del Duero (provincia de Palencia)*. PhD thesis, Complutense University of Madrid, Madrid, Spain.
- Mediavilla, R., Santisteban, J. I., and Dabrio, C. J. (2003). Mixed siliciclastic-carbonate sedimentation in shallow, low gradient, wave-dominated lakes. A case study from the Miocene Duero Basin. In Valero-Garcés, B. L., editor, *Limnogeology in Spain: a tribute to Kerry R. Kelts*, pages 99–118, Madrid, Spain. Consejo Superior de Investigaciones Científicas.

- Mees, F., Casteneda, C., Herrero, J., and Van Ranst, E. (2012). The Nature and Significance of Variations In Gypsum Crystal Morphology In Dry Lake Basins. *Journal of Sedimentary Research*, 82(1):37–52.
- Menz, C. and Fenk, C. (2007). Interaction between salt lake and groundwater - a hydrochemical, isotopegeochemical and sedimentological study in Fuente de Piedra basin, Spain. Diploma thesis and geological mapping, Freie Universität Berlin.
- Michetti, A. M. (2005). Dark Nature and paleoseismology: understanding the seismic landscape off he Southern Alps, Italy. In *Dark Nature-Rapid Natural Change and Human Resources*, Como, pages 6–10.
- Michetti, A. M., Giardina, F., Livio, F., Mueller, K., Serva, L., Sileo, G., Vittori, E., Devoti, R., Riguzzi, F., Carcano, C., Rogledi, S., Bonadeo, L., Brunamonte, F., and Fiorasco, G. (2012). Active compressional tectonics, Quaternary capable faults, and the seismic landscape of the Po Plain (N Italy). *Annals of Geophysics*, 55(5):969–1001.
- Michetti, A. M., Livio, F., Pasquarè, L. A., Vezzoli, L., Bini, A., Bernoulli, D., and Sciun-nach, D. (2013). Note Illustrative della Carta Geologica d’Italia. Foglio 075 Como. http://www.isprambiente.it/Media/carg/note_illustrative/75_Como.pdf. ISPRA - Istituto Superiore per la Protezione e la Ricerca Ambientale.
- Mitchell, J. K. and Gardner, W. S. (1975). In situ measurement of volume change characteristics. In *ASCE Conf. on “In situ measurement of soil properties”*.
- Moisello, U. and Vullo, F. (2010). I massimi annuali di portata dell’Adda a Lecco in diversi regimi di deflusso. Technical Report 13.
- Monecke, K., Anselmetti, F. S., Becker, A., Sturm, M., and Giardini, D. (2004). The record of historic earthquakes in lake sediments of Central Switzerland. *Tectonophysics*, 394(1-2):21–40.
- Mook, W., Bommerson, J., and Staverman, W. (1974). Carbon isotope fractionation between dissolved bicarbonate and gaseous carbon dioxide. *Earth and Planetary Science Letters*, 22(2):169–176.
- Morellón, M., Anselmetti, F. S., Valero-Garcés, B., Giralt, S., Ariztegui, D., Sáez, A., Mata, M. P., Barreiro-Lostres, F., Rico, M., and Moreno, A. (2014). The influence of subaquatic springs in lacustrine sedimentation: Origin and paleoenvironmental significance of homogen-ites in karstic Lake Banyoles (NE Spain). *Sedimentary Geology*, 311:96–111.
- Morellón, M., Valero-Garcés, B., Anselmetti, F., Ariztegui, D., Schnellmann, M., Moreno, A., Mata, P., Rico, M., and Corella, J. P. (2009). Late Quaternary deposition and facies model for karstic Lake Estanya (North-eastern Spain). *Sedimentology*, 56(5):1505–1534.
- Moreno, A., Cacho, I., Canals, M., Grimalt, J. O., Sánchez-Goñi, M. F., Shackleton, N., and Sierro, F. J. (2005). Links between marine and atmospheric processes oscillating on a mil-lennial time-scale. A multi-proxy study of the last 50,000 yr from the Alboran Sea (Western Mediterranean Sea). *Quaternary Science Reviews*, 24(14-15):1623–1636.
- Moreno, A., González-Sampériz, P., Morellón, M., Valero-Garcés, B. L., and Fletcher, W. J. (2012). Northern Iberian abrupt climate change dynamics during the last glacial cycle: A view from lacustrine sediments. *Quaternary Science Reviews*, 36:139–153.

- Moreno, A., Sancho, C., Bartolomé, M., Oliva-Urcia, B., Delgado-Huertas, A., Estrela, M. J., Corell, D., López-Moreno, J. I., and Cacho, I. (2014). Climate controls on rainfall isotopes and their effects on cave drip water and speleothem growth: the case of Molinos cave (Teruel, NE Spain). *Climate dynamics*, 43(1-2):221–241.
- Moreno, A., Stoll, H., Canals, M., Prins, M. A., Sánchez-Goñi, M. F., Grimalt, J. O., and Weltje, G. J. (2002). Saharan dust transport and high-latitude Glacial climatic variability: The Alboran Sea record. *Quaternary Research*, 58:318–328.
- Moreno, A., Stoll, H., Jiménez-Sánchez, M., Cacho, I., Valero-Garcés, B., Ito, E., and Edwards, R. L. (2010). A speleothem record of glacial (25–11.6kyr BP) rapid climatic changes from northern Iberian Peninsula. *Global and Planetary Change*, 71:218–231.
- Moreno-Amich, R. and García-Berthou, E. (1989). A new bathymetric map based on echosounding and morphometrical characterization of the Lake of Banyoles (NE-Spain). *Hydrobiologia*, 85:83–90.
- Moreno-Amich, R., Pou-Rovira, Q., Vila-Gispert, A., Zamora, L., and García-Berthou, E. (2006). Fish ecology in Lake Banyoles (NE Spain): a tribute to Ramon Margalef. *Limnetica*, 25(1-2):321–334.
- Münnich, K.-O. (1975). Messung des ^{14}C -Gehaltes von hartem Grundwasser. *Naturwissenschaften*, 34:32–33.
- Murray, R. C. (1964). Origin and diagenesis of gypsum and anhydrite. *Journal of Sedimentary Research*, 34(3):512–523.
- Nangeroni, G. (1972). Il monte Barro (Prealpi Lombarde): note di geomorfologia. *Atti Società Italiana Scienze Naturali e Museo Civico Storia Naturale Milano*, 108(2):159–196.
- Naughton, F., Goñi, M. F. S., Kageyama, M., Bard, E., Duprat, J., Cortijo, E., Desprat, S., Malaizé, B., Joly, C., Rostek, F., and Turon, J. L. (2009). Wet to dry climatic trend in north-western Iberia within Heinrich events. *Earth Science Reviews*, 284(3-4):329–342.
- Naughton, F., Goñi, M. F. S., Rodrigues, T., Salgueiro, E., Costas, S., Desprat, S., Duprat, J., Michel, E., Rossignol, L., Zaragosi, S., Voelker, A. H. L., and Abrantes, F. (2015). Climate variability across the last deglaciation in NW Iberia and its margin. *Quaternary International*, pages 1–14.
- Olivera, C., Redondo, E., Lambert, J., Riera Melis, A., and Roca, A. (2006). *Els terratrèmols dels segles XIV i XV a Catalunya*. Institut Cartogràfic de Catalunya, Barcelona.
- Olivera, C., Riera, A., Lambert, J., Banda, E., and Alexandre, P. (1994). *Els Terratrèmols de l'any 1373 al Pirineu: Efectes a Espanya i França*. Servei Geològic de Catalunya, Barcelona, Spain.
- Olsson, I. U. (1979). A warning against radiocarbon dating of samples containing little carbon. *Boreas*, 8(2):203–207.
- Orombelli, G. (1976). Indizi di deformazioni tettoniche Quaternarie al margine meridionale delle Prealpi Comasche. *Quaderno Gruppo di studio del Quaternario padano*, 3:25–37.

- Ortí, F., Pérez-López, A., García-Veigas, J., Rosell, L., Cendón, D. I., and Pérez-Valera, F. (2014). Sulfate isotope composition (^{34}S , ^{18}O) and Strontium isotopic ratios ($^{87}\text{Sr}/^{86}\text{Sr}$) of Triassic evaporites in the Betic Cordillera (SE Spain). *Revista de la Sociedad Geológica de España*, 27(1):79–89.
- Ortí, F., Rosell, L., and Anadón, P. (2003). Deep to shallow lacustrine evaporites in the Libros Gypsum (southern Teruel Basin, Miocene, NE Spain): an occurrence of pelletal gypsum rhythmites. *Sedimentology*, 50(2):361–386.
- Peñalba, M. C. (1994). The history of the Holocene vegetation in northern Spain from pollen analysis. *Journal of Ecology*, 82:815–832.
- Pérez, A., Luzón, A., Roc, A. C., Soria, A. R., Mayayo, M. J., and Sánchez, J. A. (2002). Sedimentary facies distribution and genesis of a recent carbonate-rich saline lake: Gallocanta Lake, Iberian Chain, NE Spain. *Sedimentary Geology*, 148:185–202.
- Pérez-Obiol, R., Jalut, G., Julià, R., Pelachs, A., Iriarte, M. J., Otto, T., and Hernandez-Beloqui, B. (2011). Mid-Holocene vegetation and climatic history of the Iberian Peninsula. *The Holocene*, 21(1):75–93.
- Pérez-Obiol, R. and Julià, R. (1994). Climatic Change on the Iberian Peninsula Recorded in a 30,000-Yr Pollen Record from Lake Banyoles. *Quaternary Research*, 41:91–98.
- Peyron, O., Bégeot, C., Brewer, S., Heiri, O., Magny, M., Millet, L., Ruffaldi, P., Van Campo, E., and Yu, G. (2005). Late-Glacial climatic changes in Eastern France (Lake Lautrey) from pollen, lake-levels, and chironomids. *Quaternary Research*, 64(2):197–211.
- Plummer, L. N., Prestemon, E. C., and Parckhurst, D. L. (1994). User's Guide to NETPATH – A Computer Program for Mass-balance Calculations: An Interactive Code (NETPATH) for Modelling NET Geochemical Reactions along a Flow PATH-Version 2.0. Water res. invest. report, USGS.
- Pons, A. and Reille, M. (1988). The Holocene and Upper Pleistocene pollen record from Padul (Granada, Spain): a new study. *Palaeogeography, Palaeoclimatology, Palaeoecology*, 66:243–263.
- Preusser, F., Reitner, J. M., and Schlüchter, C. (2010). Distribution, geometry, age and origin of overdeepened valleys and basins in the Alps and their foreland. *Swiss Journal of Geosciences*, 103(3):407–426.
- Quézel, P. and Médail, F. (2003). *Ecologie et biogéographie des forêts du bassin méditerranéen*, volume 572. Elsevier Paris.
- Ramsey, C. B. (2009). Bayesian analysis of radiocarbon dates. *Radiocarbon*, 51(1).
- Rasmussen, S., Seierstad, I., Andersen, K., Bigler, M., Dahl-Jensen, D., and Johnsen, S. (2008). Synchronization of the NGRIP, GRIP, and GISP2 ice cores across MIS 2 and palaeoclimatic implications. *Quaternary Science Reviews*, 27(1–2):18–28. INTEgration of Ice-core, Marine and Terrestrial records (INTIMATE): Refining the record of the Last Glacial-Interglacial Transition.

- Rasmussen, S. O., Andersen, K. K., Svensson, A., Steffensen, J. P., Vinther, B. M., Clausen, H. B., Siggaard-Andersen, M.-L., Johnsen, S. J., Larsen, L. B., Dahl-Jensen, D., et al. (2006). A new Greenland ice core chronology for the last glacial termination. *Journal of Geophysical Research: Atmospheres (1984–2012)*, 111(D6).
- Ravazzi, C., Peresani, M., Pini, R., and Vescovi, E. (2007). Il Tardoglaciale nelle Alpi italiane e in Pianura Padana. Evoluzione stratigrafica, storia della vegetazione e del popolamento antropico. *Il Quaternario*, 20(2).
- Ravazzi, C., Pini, R., Badino, F., De Amicis, M., Londeix, L., and Reimer, P. J. (2014). The latest LGM culmination of the Garda Glacier (Italian Alps) and the onset of glacial termination. Age of glacial collapse and vegetation chronosequence. *Quaternary Science Reviews*, 105:26–47.
- RCR s n c (2010). Esecuzione di sondaggi e installazione di strumentazione piezometrica ad integrazione della rete di monitoraggio comunale esistente. Technical report.
- Reed, J. (1998). Diatom preservation in the recent sediment record of Spanish saline lakes: implications for palaeoclimate study. *Journal of Paleolimnology*, 19(2):129–137.
- Reed, J. M., Cvetkoska, A., Levkov, Z., Vogel, H., and Wagner, B. (2010). The last glacial-interglacial cycle in Lake Ohrid (Macedonia/Albania): testing diatom response to climate. *Biogeosciences*, 7(10):3083–3094.
- Reed, J. M., Stevenson, A. C., and Juggins, S. (2001). A multi-proxy record of Holocene climatic change in southwestern Spain: the Laguna de Medina, Cádiz. *The Holocene*, 11(6):707–719.
- Reeves, C. C. (1968). *Introduction to paleolimnology, by C.C. Reeves, Jr.* Elsevier Pub. Co Amsterdam, New York.
- Reimer, P. J., Bard, E., Bayliss, A., Warren Beck, J., Blackwell, P. G., Ramsey, C. B., Buck, C. E., Cheng, H., Edwards, R. L., Friedrich, M., Grootes, P. M., Guilderson, T. P., Haffidason, H., Hajdas, I., Hatté, C., Heaton, T. J., Hoffmann, D. L., Hogg, A. G., Hughen, K. A., Kaiser, K. F., Kromer, B., Manning, S. W., Niu, M., Reimer, R. W., Richards, D. A., Scott, E. M., Southon, J. R., Staff, R. A., Turney, C. S. M., and Van Der Plicht, J. (2013). INTCAL13 and MARINE13 radiocarbon age calibration curves 0-50,000 years cal BP. *Radiocarbon*, 55(4):1869–1887.
- Rendón, M. A., Garrido, A., Rendón Martos, M., Ramirez, J. M., and Amat, J. A. (2014). Assessing sex-related chick provisioning in greater flamingo *Phoenicopterus roseus* parents using capture-recapture models. *Journal of Animal Ecology*, 83(2):479–490.
- Retallack, G. J. (1988). Field recognition of paleosols. *Geological Society of America Special Papers*, 216:1–20.
- Rethemeyer, J., Fülöp, R.-H., Höfle, S., Wacker, L., Heinze, S., Hajdas, I., Patt, U., König, S., Stapper, B., and Dewald, A. (2013). Status report on sample preparation facilities for ^{14}C analysis at the new CologneAMS center. *Nuclear Instruments and Methods in Physics Research Section B: Beam Interactions with Materials and Atoms*, 294:168–172. Proceedings of the Twelfth International Conference on Accelerator Mass Spectrometry, Wellington, New Zealand, 20–25 March 2011.

- Riva, A. (1957). Gli anfiteatri morenici a sud del lario e le pianure diluviali tra adda e olona. *Atti Ist. Geol. Univ. Pavia*, 7:5–95.
- Roberts, D., McMinn, A., Cremer, H., Gore, D. B., and Melles, M. (2004). The Holocene evolution and palaeosalinity history of Beall Lake, Windmill Islands (East Antarctica) using an expanded diatom-based weighted averaging model. *Palaeogeography, Palaeoclimatology, Palaeoecology*, 208(1-2):121–140.
- Roberts, N., Jones, M. D., Benkaddour, A., Eastwood, W. J., Filippi, M. L., Frogley, M. R., Lamb, H. F., Leng, M. J., Reed, J. M., Stein, M., Stevens, L., Valero-Garcés, B., and Zanchetta, G. (2008). Stable isotope records of Late Quaternary climate and hydrology from Mediterranean lakes: the ISOMED synthesis. *Quaternary Science Reviews*, 27(25-26):2426–2441.
- Rodó, X., Giralt, S., Burjachs, F., Comin, F. A., Tenorio, R. G., and Julià, R. (2002). High-resolution saline lake sediments as enhanced tools for relating proxy paleolake records to recent climatic data series. *Sedimentary Geology*, 148:203–220.
- Rodrigo-Gámiz, M., Martínez-Ruiz, F., Jiménez-Espejo, F. J., Gallego-Torres, D., Nieto-Moreno, V., Romero, O., and Ariztegui, D. (2011). Impact of climate variability in the western Mediterranean during the last 20,000 years: oceanic and atmospheric responses. *Quaternary Science Reviews*, 30(15-16):2018–2034.
- Rodríguez-Jiménez, P., Carrasco, F., Benavente, J., and Almecija, C. (1993). Mineralogía de los sedimentos de la Laguna de Fuente de Piedra (provincia de Málaga). *Geogaceta*, 14:1–3.
- Rodríguez-Rodríguez, M. (2002). Contribución hidrogeológica a la caracterización ambiental de zonas húmedas de Andalucía. Tesis doctoral, Universidad de Granada.
- Rodríguez-Rodríguez, M., Benavente, J., Cruz-San Julián, J. J., and Moral Martos, F. (2006). Estimation of ground-water exchange with semi-arid playa lakes (Antequera region, southern Spain). *Journal of Arid Environments*, 66(2):272–289.
- Rodríguez-Rodríguez, M., Benavente Herrera, J., and Moral Martos, F. (2005). High Density Groundwater Flow, Major-ion Chemistry and Field Experiments in a Closed Basin: Fuente de Piedra Playa Lake (Spain). *American Journal of Environmental Sciences*, 1(2):164–171.
- Rosen, M. R., Miser, D. E., Starcher, M. A., and Warren, J. K. (1989). Formation of dolomite in the Coorong region, South Australia. *Geochimica et Cosmochimica Acta*, 53:661–669.
- Rosén, P., Vogel, H., Cunningham, L., Hahn, A., Hausmann, S., Pienitz, R., Zolitschka, B., Wagner, B., and Persson, P. (2011). Universally applicable model for the quantitative determination of lake sediment composition using Fourier transform infrared spectroscopy. *Environmental Science & Technology*, 45:8858–8865.
- Rosén, P., Vogel, H., Cunningham, L., Reuss, N., Conley, D., and Persson, P. (2010). Fourier transform infrared spectroscopy, a new method for rapid determination of total organic and inorganic carbon and biogenic silica concentration in lake sediments. *Journal of Paleolimnology*, 43(2):247–259.
- Rosén, P., Vogel, H., Cunningham, L., Reuss, N., Conley, D., Persson, P., et al. (2009). Fourier transform infrared spectroscopy: rapid, quantitative analysis of biogeochemical properties of lake sediments. *PAGES (Past Global Changes) News*, 17(3):98–100.

- Rosqvist, G. C., Leng, M. J., and Jonsson, C. (2007). North Atlantic region atmospheric circulation dynamics inferred from a late-Holocene lacustrine carbonate isotope record, northern Swedish Lapland. *The Holocene*, 17(7):867–873.
- Roucoux, K., De Abreu, L., Shackleton, N., and Tzedakis, P. (2005). The response of NW Iberian vegetation to North Atlantic climate oscillations during the last 65 kyr. *Quaternary Science Reviews*, 24(14):1637–1653.
- Rull, V. and Abbott, M. B. (2010). Paleoenvironmental trends in Venezuela during the last glacial cycle. In Vegas-Vilarrúbia, T., Bezada, M., Montoya, E., Nogué, S., and González, C., editors, *Urumaco and Venezuelan Paleontology: The Fossil Record of the Northern Neotropics*, pages 52–83. Indiana University Press.
- Ryves, D., Juggins, S., Fritz, S. C., and Battarbee, R. (2001). Experimental diatom dissolution and the quantification of microfossil preservation in sediments. *Palaeogeography, Palaeoclimatology, Palaeoecology*, 172(1):99–113.
- Sadori, L., Allevato, E., Bellini, C., Bertacchi, A., Boetto, G., Di Pasquale, G., Giachi, G., Giardini, M., Masi, A., Pepe, C., Russo Ermolli, E., and Lippi, M. (2015). Archaeobotany in Italian ancient Roman harbours. *Review of Palaeobotany and Palynology*, in press.
- Saladié, P., Vallverdú, J., Bennasar, M., Cabanes, D., Mancha, E., Menéndez, L., Blain, H. A., Ollé, A., Mosquera, M., Vilalta, J., Cáceres, I., Exposito, I., Esteban, M., Huguet, R., Rosas, A., Solé, A., López-Polín, L., García, A. B., Martínez, B., Carbonell, E., and Capdevil, R. (2008). Resultats preliminars del nivell 2 del sondeig al Centre de Convencions del barranc de la Boella. *Cota Zero*, 23:13–19.
- Sánchez-Goñi, M. F., Cacho, I., Turon, J.-L., Guiot, J., Sierro, F., Peyrouquet, J., Grimalt, J., and Shackleton, N. (2002). Synchronicity between marine and terrestrial responses to millennial scale climatic variability during the last glacial period in the Mediterranean region. *Climate dynamics*, 19(1):95–105.
- Sánchez-Goñi, M. F., Landais, A., Fletcher, W. J., Naughton, F., Desprat, S., and Duprat, J. (2008). Contrasting impacts of Dansgaard–Oeschger events over a western European latitudinal transect modulated by orbital parameters. *Quaternary Science Reviews*, 27(11-12):1136–1151.
- Santisteban, J. I., Mediavilla, R., Celis, A., Castaño, S., and de la Losa, A. (2016). Millennial-scale cycles of aridity as a driver of human occupancy in central Spain? *Quaternary International*, 407:96–109.
- Sanz, M. (1981). *El sistema hidrologico de Banyoles – La Garrotxa*. Unpubl. PhD thesis. PhD thesis, Universitat Autònoma de Barcelona, Barcelona, Spain.
- Sanz, M. E., Rodríguez-Aranda, J. P., Calvo, J. P., and Ordonez, S. (1994). Tertiary Detrital Gypsum in the Madrid Basin, Spain. In Renault, R. W. and Last, W. M., editors, *Sedimentology and Geochemistry of Modern and Ancient Saline Lakes Models*, volume 50, pages 217–228. SEPM Society for Sedimentary Geology.
- Scheiber, L., Ayora, C., Vázquez-Suñé, E., Cendón, D. I., Soler, A., Custodio, E., and Baquero, J. C. (2015). Recent and old groundwater in the Niebla-Posadas regional aquifer (southern Spain): Implications for its management. *Journal of Hydrology*, 523:624–635.

- Schmidt, I., Bradtmöller, M., Kehl, M., Pastoors, A., Tafelmaier, Y., Weninger, B., and Weniger, G.-C. (2012). Rapid climate change and variability of settlement patterns in Iberia during the Late Pleistocene. *Quaternary International*, 274(1):179–204.
- Schnellmann, M., Anselmetti, F. S., Giardini, D., and McKenzie, J. A. (2006). 15,000 Years of mass-movement history in Lake Lucerne: Implications for seismic and tsunami hazards. *Eclogae Geologicae Helvetiae*, 99(3):409–428.
- Schreiber, B. C. (1987). Environments of subaqueous gypsum deposition. In Dean, W. E., editor, *Marine Evaporites*, pages 43–73. SEPM Society for Sedimentary Geology.
- Schröder, T., Hoebig, N., and Reicherter, K. R. (2013). Multi-proxy studies from endorheic salt basins in the Antequera region (Andalusia) for paleoenvironmental reconstruction. In Baena, R., Fernández, J. J., and Guerrero, I., editors, *El Cuaternario Ibérico: Investigación en el S. XXI : proceedings of the VIII Reunión del Cuaternario Ibérico*, pages 226–229, Sevilla - La Rinconada, Spain. AEQUA.
- Schubel, K. A. and Lowenstein, T. K. (1997). Criteria for the recognition of shallow-perennial-saline-lake halites based on recent sediments from the Qaidam basin, Western China. *Journal of Sedimentary Research*, 67(1):74–87.
- Schulte, L. (2002). Climatic and human influence on river systems and glacier fluctuations in southeast Spain since the Last Glacial Maximum. *Quaternary International*, 93-94:85–100.
- Schulte, L. and Julià, R. (2001). A Quaternary soil chronosequence of Southeastern Spain. *Zeitschrift für Geomorphologie, NF*, 45(2):145–158.
- Schwander, J., Eicher, U., and Ammann, B. (2000). Oxygen isotopes of lake marl at Gerzensee and Leysin (Switzerland), covering the Younger Dryas and two minor oscillations, and their correlation to the GRIP ice core. *Palaeogeography, Palaeoclimatology, Palaeoecology*, 159(3):203–214.
- Secanell, R., Goula, X., Sousagna, T., Fleta, J., and Roca, A. (2004). Seismic hazard zonation of Catalonia, Spain, integrating random uncertainties. *Journal of Seismology*, 8(1):25–40.
- Sepulchre, P., Ramstein, G., Kageyama, M., Vanhaeren, M., Krinner, G., Sánchez-Goñi, M. F., and d’Errico, F. (2007). H4 abrupt event and late Neanderthal presence in Iberia. *Earth and Planetary Science Letters*, 258:283–292.
- Serra, T., Soler, M., Julià, R., Casamitjana, X., and Colomer, J. (2005). Behaviour and dynamics of a hydrothermal plume in Lake Banyoles, Catalonia, NE Spain. *Sedimentology*, 52(4):795–808.
- Sharp, Z. (2007). *Principles of stable isotope geochemistry*. Pearson Prentice Hall, New Jersey.
- Shearman, D. J. (1966). Origin of marine evaporites by diagenesis. *Transactions of the Institution of Mining and Metallurgy, Section B, Applied Earth Science*, B57:202–215.
- Sierro, F. J., Hodell, D. A., Curtis, J. H., Flores, J. A., Reguera, I., Colmenero-Hidalgo, E., Bárcena, M. A., Grimalt, J. O., Cacho, I., Frigola, J., and Canals, M. (2005). Impact of iceberg melting on Mediterranean thermohaline circulation during Heinrich events. *Paleoceanography*, 20:PA2019.

- Sileo, G., Giardina, F., Livi, F., Michetti, A. M., Mueller, K., and Vittori, E. (2007). Remarks on the Quaternary tectonics of the Insubria Region (Lombardia, NW Italy and Ticino, SE Switzerland). *Boll. Soc. Geol. It.*, 126(2):411–425.
- Simonneau, A., Chapron, E., Vanniere, B., Wirth, S., Gilli, A., Giovanni, C. D., Anselmetti, F., Desmet, M., and Magny, M. (2013). Mass-movement and flood-induced deposits in Lake Ledro, southern Alps, Italy: implications for Holocene palaeohydrology and natural hazards. *Climate of the Past*, 9(2):825–840.
- Smith, K. (2013). *Environmental Hazards – Assessing risk and reducing disaster*. Routledge, New York, 6 edition.
- Solé, J., Turiel, A., and Llebot, J. E. (2007). Using empirical mode decomposition to correlate paleoclimatic time-series. *Natural Hazards and Earth System Sciences*, 7(2):299–307.
- Soler Subils, J., Soler Masferrer, N., and Maroto, J. (2009). L’Arbreda’s Archaic Aurignacian dates clarified. *Eurasian Prehistory*, 5(2):45–55.
- Sowers, G. F. (1993). Human factors in civil and geotechnical engineering failures. *Journal of Geotechnical Engineering*, 119(2):238–256.
- Stanley, J. D. and Toscano, M. A. (2009). Ancient archaeological sites buried and submerged along Egypt’s Nile delta coast: gauges of Holocene delta margin subsidence. *Journal of Coastal Research*, 25(1):158–170.
- Stoll, H. M., Moreno, A., Mendez-Vicente, A., Gonzalez-Lemos, S., Jimenez-Sanchez, M., Dominguez-Cuesta, M. J., Edwards, R. L., Cheng, H., and Wang, X. (2013). Paleoclimate and growth rates of speleothems in the northwestern Iberian Peninsula over the last two glacial cycles. *Quaternary Research*, 80(2):284–290.
- Stramondo, S., Bozzano, F., Marra, F., Wegmüller, U., Cinti, F. R., Moro, M., and Saroli, M. (2008). Subsidence induced by urbanisation in the city of Rome detected by advanced InSAR technique and geotechnical investigations. *Remote Sensing of Environment*, 112(6):3160–3172.
- Strasser, M., Monecke, K., Schnellmann, M., and Anselmetti, F. S. (2013). Lake sediments as natural seismographs: A compiled record of Late Quaternary earthquakes in Central Switzerland and its implication for Alpine deformation. *Sedimentology*, 60(1):319–341.
- Strasser, M., Stegmann, S., Bussmann, F., Anselmetti, F. S., Rick, B., and Kopf, A. (2007). Quantifying subaqueous slope stability during seismic shaking: Lake Lucerne as model for ocean margins. *Marine Geology*, 240(1-4):77–97.
- Stuiver, M. and Polach, H. A. (1977). Discussion: Reporting of ^{14}C Data. *Radiocarbon*, 19(3):355–363.
- Stuiver, M. and Reimer, P. J. (1986). A computer programme for radiocarbon age calibration. *Radiocarbon*, 28(2B):1022–1030.
- Sutherland, D. (1980). Problems of radiocarbon dating deposits from newly deglaciated terrain: examples from the Scottish Lateglacial. In Sutherland, D. G., Lowe, J. J., Gray, J. M., and Robinson, J. E., editors, *Studies in the Lateglacial of North-West Europe*, pages 139–149. Quaternary Research Association (Great Britain), Pergamon Press, Oxford.

- Talbot, M. R. (1990). A review of the palaeohydrological interpretation of carbon and oxygen isotopic ratios in primary lacustrine carbonates. *Chemical Geology*, 80:261–279.
- Tarrús, J. (2008). La Draga (Banyoles, Catalonia), an Early Neolithic Lakeside Village in Mediterranean Europe. *Catalan History Review*, 1:17–33.
- Teatini, P., Tosi, L., Strozzi, T., Carbognin, L., Wegmüller, U., and Rizzetto, F. (2005). Mapping regional land displacements in the Venice coastland by an integrated monitoring system. *Remote Sensing of Environment*, 98(4):403–413.
- Thierry, P., Prunier-Leparmentier, A. M., Lembezat, C., Vanoudheusden, E., and Vernoux, J. F. (2009). 3D geological modelling at urban scale and mapping of ground movement susceptibility from gypsum dissolution: The Paris example (France). *Engineering Geology*, 105(1):51–64.
- Tosi, L., Teatini, P., and Strozzi, T. (2013). Natural versus anthropogenic subsidence of Venice. *Scientific Reports*, 3(2710).
- TRE Europe (2012). SqueeSARTM data, Satellite Analysis City of Como. preliminary results technical report.
- Truc, G. (1978). Lacustrine sedimentation in an evaporitic environment: the Ludian (Paleogene) of the Mormoiron basin, southeastern France. In Matter, A. and Tucker, M. E., editors, *Modern and Ancient Lake Sediments*, volume 2 of *Special Publication*, pages 189–203, Oxford, UK. International Association of Sedimentologists, Blackwell Publishing Ltd.
- Uboldi, M. (1993). Carta Archeologica della Lombardia, III. *Como. La città murata e la convalle*, 1.
- USGS Earth Explorer (2012). Landsat 7 ETM+ Scene LE72010342012108ASN00. USGS Earth Resources Observation and Science (EROS) Center. <http://earthexplorer.usgs.gov>.
- USGS Earth Explorer (2013). Landsat 8 OLI Scene LC82010342013246LGN00. USGS Earth Resources Observation and Science (EROS) Center. <http://earthexplorer.usgs.gov>.
- Valero-Garcés, B., Zeroual, E., and Kelts, K. (1998). Arid Phase in the Western Mediterranean region during the Last Glacial Cycle reconstructed from lacustrine records. In Benito, G., Baker, V. R., and Gregory, K. J., editors, *Paleohydrology and environmental change*, pages 67–80. John Wiley & Sons Ltd.
- Valero-Garcés, B. L., Delgado-Huertas, A., Navas, A., Machín, J., González-Sampérez, P., and Kelts, K. (2000a). Quaternary palaeohydrological evolution of a playa lake: Salada Mediana, central Ebro Basin, Spain. *Sedimentology*, 47(6):1135–1156.
- Valero-Garcés, B. L., González-Sampérez, P., Delgado-Huertas, A., Navas, A., Machin, J., and Kelts, K. (2000b). Lateglacial and Late Holocene environmental and vegetational change in Salada Mediana, central Ebro Basin, Spain. *Quaternary International*, 73/74:29–46.
- Valero-Garcés, B. L., González-Sampérez, P., Navas, A., Machn, J., Delgado-Huertas, A., Peña-Monné, J. L., Sancho-Marcén, C., Stevenson, T., and Davis, B. (2004). Paleohydrological fluctuations and steppe vegetation during the last glacial maximum in the central Ebro valley (NE Spain). *Quaternary International*, 122:43–55.

- Valero-Garcés, B. L. and Moreno, A. (2011). Iberian lacustrine sediment records: responses to past and recent global changes in the Mediterranean region. *Journal of Paleolimnology*, 46(3):319–325.
- Valero-Garcés, B. L., Moreno, A., Navas, A., Mata, P., Machin, J., Delgado-Huertas, A., González-Sampériz, P., Schwalb, A., Morellón, M., Cheng, H., and Edwards, R. L. (2008). The Taravilla lake and tufa deposits (Central Iberian Range, Spain) as palaeohydrological and palaeoclimatic indicators. *Palaeogeography, Palaeoclimatology, Palaeoecology*, 259:107–129.
- Valiño, M. D., Rodríguez, A. V., Zapata, M. B. R., Garcia, M. J. G., and de Bustamante Gutiérrez, I. (2002). Climatic changes since the Late-glacial/Holocene transition in La Mancha Plain (South-central Iberian Peninsula, Spain) and their incidence on Las Tablas de Daimiel marshlands. *Quaternary International*, 93:73–84.
- Vannièrè, B., Power, M., Roberts, N., Tinner, W., Carrión, J., Magny, M., Bartlein, P., Colombaroli, D., Danianu, A., Finsinger, W., Gil-Romera, G., Kaltenrieder, P., Pini, R., Sadori, L., Turner, R., Valsecchi, V., and Vescovi, E. (2011). Circum-Mediterranean fire activity and climate changes during the mid-Holocene environmental transition (8500–2500 cal. BP). *The Holocene*, 21(1):53–73.
- Vaquero, M. (2006). El tránsito Paleolítico Medio/Superior en la Península Ibérica y la Frontera del Ebro. Comentario a Zilhao (2006). *Pyreneae*, pages 107–129.
- Vasconcelos, C. and McKenzie, J. A. (1997). Microbial mediation of modern dolomite precipitation and diagenesis under anoxic conditions (Lagoa Vermelha, Rio de Janeiro, Brazil). *Journal of Sedimentary Research*, 67:378–390.
- Vegas, J., Ruiz-Zapata, B., Ortiz, J. E., Galán, L., Torres, T., García-Cortés, Á., Gil-García, M. J., Pérez-González, A., and Gallardo-Millán, J. L. (2010). Identification of arid phases during the last 50 cal. ka BP from the Fuentillejo maar-lacustrine record (Campo de Calatrava Volcanic Field, Spain). *Journal of Quaternary Science*, 25(7):1051–1062.
- Vogel, H., Rosén, P., Wagner, B., Melles, M., and Persson, P. (2008). Fourier transform infrared spectroscopy, a new cost-effective tool for quantitative analysis of biogeochemical properties in long sediment records. *Journal of Paleolimnology*, 40(2):689–702.
- von Grafenstein, U., Erlenkeuser, H., Brauer, A., Jouzel, J., and Johnsen, S. J. (1999). A mid-European decadal isotope-climate record from 15,500 to 5000 years BP. *Science*, 284(5420):1654–1657.
- Wacker, L., Fülöp, R.-H., Molnár, M., and Rethemeyer, J. (2010a). Preparation of carbonates with age. Technical report, Ion Beam Physics, ETH Zürich, Zürich, Switzerland.
- Wacker, L., Némec, M., and Bourquin, J. (2010b). A revolutionary graphitisation system: Fully automated, compact and simple. *Nuclear Instruments and Methods in Physics Research Section B: Beam Interactions with Materials and Atoms*, 268(7–8):931 – 934. Proceedings of the Eleventh International Conference on Accelerator Mass Spectrometry.
- Wanner, H., Brönnimann, S., Casty, C., Gyalistras, D., Luterbacher, J., Schmutz, C., Stephenson, D. B., and Xoplaki, E. (2001). North Atlantic Oscillation - Concepts and Studies. *Surveys in Geophysics*, 22:321–382.

- Warren, J. (2000). Dolomite: occurrence, evolution and economically important associations. *Earth Science Reviews*, 52:1–81.
- Weber, M. E., Niessen, F., Kuhn, G., and Wiedicke, M. (1997). Calibration and application of marine sedimentary physical properties using a multi-sensor core logger. *Marine Geology*, 136:151–172.
- Wetzel, R. G. (1981). *Limnología*. Ediciones Omega.
- Wirth, S. (2013). *The Holocene flood history of the Central Alps reconstructed from lacustrine sediments: Frequency, intensity and controlling climate factors*. Phd thesis, ETH Zürich, Zürich, Switzerland.
- Wohlfarth, B., Skog, G., Possnert, G., and Holmquist, B. (1998). Pitfalls in the AMS radiocarbon-dating of terrestrial macrofossils. *Journal of Quaternary Science*, 13(2):137–145.
- Wolf, D. and Faust, D. (2015). Western Mediterranean environmental changes: Evidences from fluvial archives. *Quaternary Science Reviews*, 122:30–50.
- Xu, Y. S., Shen, S. L., and Du, Y. J. (2009). Geological and hydrogeological environment in Shanghai with geohazards to construction and maintenance of infrastructures. *Engineering Geology*, 109:241–254.
- Young, R. A., editor (1993). *The Rietveld method*. Number 5 in IUCr Monograph on Crystallography. International Union of Crystallography/Oxford University Press, Oxford.
- Zanchi, A., Bini, A., Felber, M., Rigamonti, I., and Uggeri, A. (1997). Neotectonic evidences along the Lombardian foothills of the Southern Alps. *Geologia Insubrica*, 2(2):99–112.
- Zielhofer, C., Faust, D., Escudero, R. B., del Olmo, F. D., Kadereit, A., Moldenhauer, K.-M., and Porras, A. (2004). Centennial-scale late-Pleistocene to mid-Holocene synthetic profile of the Medjerda Valley, northern Tunisia. *The Holocene*, 14(6):851–861.
- Zilhao, J. (2006). Chronostratigraphy of the Middle-to-Upper Paleolithic Transition in the Iberian Peninsula. *Pyreneas*, 1:7–84.

A. Appendix

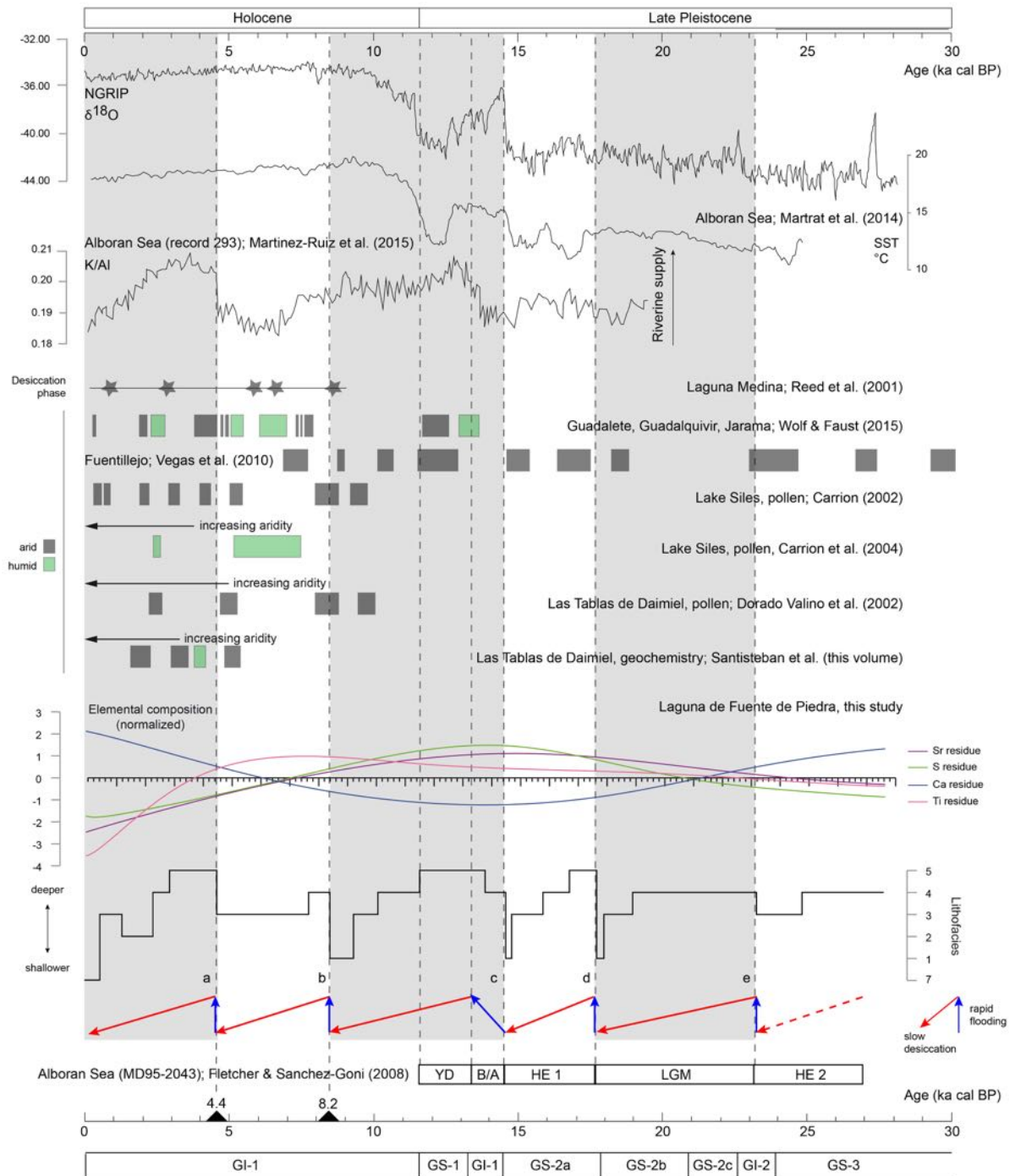


Figure A.1.: See facing page.

(facing page) Figure A.1.: Correlation of the Laguna de Fuente de Piedra palaeorecord with records from other studies from the western Mediterranean (see Fig. 3.1 for location) and NGRIP oxygen isotope data is plotted for reference (Andersen et al., 2004). From Alboran Sea seasurface temperature (Martrat et al., 2014) and riverine input from K/Al ratio (Martínez-Ruiz et al., 2015) are shown. Desiccation events at Laguna Medina (Reed et al., 2001), arid/humid phases from fluvial dynamics (Wolf and Faust, 2015), major arid/humid phases at Fuentillejo maar (Vegas et al., 2010), pollen records from lacustrine sites (Lake Siles, pollen, Carrión, 2002; Carrión et al., 2004) and aridity trends from the Las Tablas de Daimiel wetlands are illustrated (pollen, Valiño et al., 2002; elemental composition, Santisteban et al., 2016). Normalized residues of the elemental composition (Ti, Ca, Sr, S) and lithofacies indicative for palaeolakelevel at LFP, are plotted for correlation. For reference climatic events like Heinrich Events (HE), Last Glacial Maximum (LGM), Bølling/Allerød (B/A), Younger Dryas (YD), etc. are indicated (pollen, Fletcher and Goñi, 2008).

